ADSORPTION AND REACTION ON PROMOTED ZINC OXIDE CATALYSTS IN RELATION TO HIGHER ALCOHOL SYNTHESIS

by

Peter John Robert O'Malley, B.E. (Hons)

January, 1987

A thesis submitted for the degree of Doctor of Philosophy of the University of London and for the Diploma of Membership of the Imperial College.

Department of Chemical Engineering and Chemical Technology
Imperial College
London, S.W.7.

ABSTRACT

This study has investigated the effect of alkali promotion on the reactivity of ZnO in relation to higher alcohol decomposition and synthesis. The techniques of temperature programmed desorption and decomposition (TPD) have been used to characterise the products and surface intermediates involved. A well characterised low surface area ZnO was used as a catalyst and K_2CO_3 as promoter.

The investigation of higher alcohol synthesis was of interest in view of the predicted increase in the use of oxygenates as gasoline octane boosters. Although alkali promotion of methanol synthesis catalysts is an established method for increasing higher alcohol yields, relatively little is understood regarding the quantitative aspects of alkali promotion and of the mechanism of higher alcohol synthesis on ZnO containing catalysts. Of particular interest in this thesis were the adsorption characteristics of the reactants and products of the higher alcohol synthesis.

The adsorption and TPD of CO_2, H_2 and water were investigated for ZnO and promoted ZnO. The Zn (0001) polar surface of unpromoted ZnO was found to strongly adsorb hydroxyl species with a heat of adsorption of 151 ± 10 kJ/mol. Consequently, dehydroxylation was very important in determining the behaviour of the catalyst, and temperatures of up to 750 K were required. Potassium promotion was found to preferentially suppress hydroxyl adsorption on this surface. Promotion also suppressed the formation of surface formate after coadsorption of CO_2 and H_2.

The decomposition of 1-propanol, 2-propanol and acetone was investigated in detail. The alcohol desorption products from

unpromoted ZnO corresponded to reversible desorption of the parent alcohol at low temperature (400 K), and to dehydrogenation, dehydration and oxidation surface decomposition reactions at progressively higher temperatures. 2-Propanol decomposition was selective toward dehydration while 1-propanol was selective to oxidation via a surface carboxylate species. A mechanism has been proposed based on these results.

Selective site poisoning, through coadsorption of water with the alcohol, and by chlorine treatment of ZnO, was used to establish the crystal face dependency of the alcohol decomposition reactions. In particular, a site equivalence was established between the 2-propanol dehydration and hydroxyl adsorption sites proposed to be associated with the Zn (0001) polar surface.

Potassium promotion was found to suppress reaction on both polar surfaces and, to a significant extent, dehydration and oxidation on the non-polar $(10\bar{1}0)$ surface. The dehydrogenation yield was enhanced by alkali promotion. Promotion effects of potassium with respect to higher alcohol synthesis are also considered.

ACKNOWLEDGEMENTS

I would like to thank the National Research Advisory Council of New Zealand for the granting of the study award that has enabled me to carry out this research work. I am particularly grateful to my supervisor Dr Dave Chadwick for his guidance, interest and advice that kept me headed in the right direction throughout this project, and also to my wife Sue for equally important support (of a less technical nature!). In addition I would like to thank:- Dr's K.C. Waugh and M. Bowker of ICI New Science Group, and their technicians Bill Petts and Danny Vandervell, for their interest in this project, for the supply of catalyst samples and for the use of their facilities at Runcorn, Dr M. Spencer of ICI Agricultural Division for the supply of high surface area catalyst, Prof D.A. Dowden for useful advise and discussion in relation to alkali promoters of ZnO, George Cambanis for his help with the XPS measurements and Dick Wood of the Chem Eng Department for the construction of the temperature controller and for his advice on computer interfacing.

CONTENTS

LIST OF TABLES

LIST OF FIGURES

Page

Chapter 8

Page

Chapter 9

CHAPTER 1

INTRODUCTION

(1.1) The Use of Oxygenates in Relation to Transport Fuels

Until recently, developments in the fuel alcohol industry were largely concerned with the utilisation of alcohols as blending stocks or substitutes for petroleum derived transportation fuels[1,2,3]. Alcohols were seen as attractive alternatives to the petroleum based fuels in the face of rising crude oil prices and the prospect of diminishing oil supplies[3]. In particular, the use of C_2-C_6 higher alcohol/methanol or ethanol blends offered a number of advantages over straight-run methanol or ethanol as gasoline blending stock that included improved volatility and driveability, improved hydrocarbon solubility, improved water tolerance and higher volumetric heat of combustion[2]. However, these goals have largely been put aside in view of the current world surplus and falling price of crude oil. Recent developments, such as the introduction of regulations phasing out the use of lead compounds as octane boosters in gasoline, are likely to have significant effects on the use production of oxygenates in the near future.

Certain lead compounds, such as tetraethyl lead and tetramethyl lead, are employed for raising the octane number of gasoline[4]. These lead compounds are ideal for use as additives to gasoline, since they essentially effect only the octane number for all practical purposes while other physical properties remain practically unchanged. Their decisive drawback, however, is their detrimental effect on the environment and on human health[4]. As a consequence, the lead

content in gasoline is being progressively reduced in both Europe and the United States, while lead-free gasoline is also available in the United States and Japan[5]. Further impetus for the removal of lead has come from the increased use of exhaust catalyst units in motor vehicles, because lead acts as a catalyst inhibitor[4].

The United States is expected to essentially eliminate allowable lead usage by the early 1990's, while increasing the percent of unleaded premium[5]. Western Europe also plans to eliminate the use of lead, although the timing is uncertain[5]. An estimated 55% of the worlds gasoline market will be lead free by 1990[6]. In the US demand for premium unleaded gasoline is projected to grow from the 15% of the total gasoline pool in 1984 to an estimated figure of 20% for 1986 and to 30% by 1990[7].

The sharp rise in demand is also related to the way costs of gasoline production have changed and to an increased demand for premium grade gasoline, instead of regular grade, as prices have dropped[1]. Increased engine performance requirements are also predicted to result in an increase in the pool average octane number from 86.8 to 88.3 (R+M/2) in the US and 92.2/82.1 to 94.6/84.7 (RON/MON) in Europe. Japan, which uses no lead at present, is expected to increase pool octane from 91 to 92 RON[5]. Although in the short term, the slide in crude price will also encourage the conversion of hydrocarbons for octane, in the long term, increased gasoline demand due to lower crude oil prices will cause refiners to back off on process severity and produce maximum product at lower octane quality to meet this demand[1].

A number of possibilities are available for providing additional octane to the gasoline pool in view of the developments described

above[5]. A first option is for the restructuring of refineries for the conversion of components with a low octane number to components with a high octane number[4]. Alternatives here include the raised severity upgrading of reformate, FCC gasoline and alkylate gasoline to increase octane. While significant octane improvements can be gained by these steps, higher operating costs can make these options unattractive[5]. However, even at present, the production cost of the increased octane has not been found to be offset by the fall in oil prices[7]. Limitations can also result because of the way refinery flexibility is directly related to the operation of several interacting units. For example, to increase reformate octane may cause a penalty on volume and increased Reid vapour pressure of the final end product, while refinery operation to maximise gasoline production to meet rising volume demands would leave less flexibility for process generated octanes[1].

The use of additives, and in particular oxygenates, as gasoline octane enhancers is an attractive option[4,5,6,8]. An increased demand for such additives to augment the octane number as the lead content of petrol is lowered is projected. Table 1.1 outlines one projection made in 1985, although this is considered to be out of date due to uncertainty in predicting future US lead phasedown regulations and crude oil prices[1]. Oxygenated octane enhancement is forecast to account for 3.0 to 3.7% of the US gasoline pool by 1990, while in Europe the oxygenate content of gasoline is estimated to grow to 4%[9].

Table 1.1: A projection of U.S. fuel-oxygenate use (1985 projection) (MM gal/yr), from reference (1).

year	ethanol	methanol	TBA[a]	MTBE[b]	total
1980	80	20	40	70	210
1985	590	130	90	370	1190
1990	1000	420	250	550	2220
1995	1250	750	300	650	2980

(a)= tertiary butanol

(b)= methyl tertiary butyl ether

Methyl tertiary butyl ether (MTBE) is one of the most attractive oxygenate octane boosters currently employed in the US and Europe. Although MTBE synthesis from refinery isobutene is cost attractive, its production potential is extremely limited by the availability of such streams[5]. The present total US capacity for MTBE from isobutene is only 70,000 bpsd[5]. Butane offers alternative source for isobutene synthesis, but MTBE produced in this way is unlikely to be economically viable[4].

Alcohols are excellent potential octane improvers as shown by their individual mixed octane ratings given in table 1.2. If only the octane number is considered, methanol appears to be an ideal additive, especially since it is currently available in sufficient quantity and at a low price[4]. Unfortunately methanol is unfavourable as an additive with respect to both the Reid vapour pressure and phase separation in presence of water[2,3,4] and must be blended with higher alcohols such as 2-propanol and tertiary butanol (TBA)[5] to

Table 1.2: The mixed octane number of alcohols measured as an engine octane number (MON) in a mixture with petrol (MON= 83, aromatics= 25 vol%), from reference (4).

alcohol	engine octane number at given vol %	
	5%	10%
methanol	98	100
ethanol	100	104
2-propanol	96	96
1-propanol	92	90
tert-butanol	94	93
n-butanol	80	78
n-hexanol	41	46
n-octanol	21	27

overcome these problems. Ethanol requires no higher alcohol cosolvents, but production costs at present make it unattractive[5], and when added to gasoline, also aggrevates volatility problems[1]. A mixture of 50% methanol and 50% TBA, distributed under the trade name Oxinol, has been found to be an ideal additive for gasoline[4] and gasoline containing 6% Oxinol is presently sold at many service stations in West Germany.

TBA is obtained as a by-product of propylene oxide synthesis[4] or can be synthesised from isobutene. Severe limitations also exist in the supply of propylene oxide[5]. The current production of TBA in Europe of about 450,000 tpa is not sufficient even to provide the 24×10^6 tpa of petrol consumed in West Germany with an admixture of 6% Oxinol[4]. Production of TBA from isobutene also suffers from supply

limitations as described for MTBE.

To meet the increasing demand for the supply of alcohol octane improvers, new processes that produce methanol/higher alcohol mixtures (known as fuel methanol), suitable for use as gasoline octane enhancers, are being developed. Table 1.3 describes several of these that are potential commercial possibilities. The table serves to illustrate the variety of the types of catalyst that can be used to produce fuel methanol, and also the degree of flexibility of product composition that can be obtained.

(1.2) The Synthesis of Higher Alcohols by Alkali Promoted Methanol Catalysts

The synthesis of higher alcohol mixtures by CO hydrogenation, using processes based on methanol catalysts modified by alkali promotion has been known for the past 60 years[12]. The addition of small amounts of alkali promoters to methanol synthesis catalysts increases the yield of higher alcohols in the range of C_2 to C_6. Characteristically there is a high ratio of branched to linear alcohols formed. Within the C_{2+} fraction the main products are generally i-butanol, 1-propanol and ethanol. The yield of 2-propanol is low, while little or no tertiary alcohols are produced. The synthesis also produces a complex range of other minor oxygenates including esters, ketones and aldehydes. The high branched to linear ratio contrasts with the largely straight chained oxygenate and hydrocarbon products obtained from the Fischer-Tropsch synthesis, showing a different reaction mechanism to be operative[12]. The product composition is also found not to depend critically on the type of catalyst used; similar results have been recently obtained for modern high activity Cu/ZnO methanol

Table 1.3: Recent process developments for the synthesis of fuel methanol

process description	catalyst type	product description	references
I.F.P Higher Alcohol Process -developed by the Institût Français du Petrole -operated under low pressure methanol synthesis conditions (60-100 bar, 270-320°C)	Alkalised Co-Cu based mixed oxides, including other metallic elements such as Cr, Al and Zn	mainly linear alcohols: methanol= 50-70 wt% ethanol= 16-23 wt% 1-propanol= 8-14 wt% n-butanol= 4-7 wt% n-pentanol= 2-3 wt% C_{6}^{+}= 1.5-3 wt%	8,10
Lurgi Fuel Methanol Process -developed by Lurgi GmbH -operated under low pressure methanol synthesis conditions (290°C,50-100 bar)	modified Lurgi low pressure Cu-based methanol synthesis catalyst	methanol= 53.5 wt% ethanol= 3.9 wt% propanol= 3.1 wt% butanol= 6.2 wt% pentanol= 3.8 wt% hexanol^{+}= 14.8 wt% other oxygenates= 10.1 wt% C_5 hydrocarb.= 4.3 wt% water= 0.3 wt%	4

..continued on following page

Table 1.3 continued:

process description	catalyst type	product description	references
Texaco Alcohol-Ester Process -developed by Texaco Chemical Company -uses patented Ru "melt" catalysts -operating conditions 220°C, 430 bar	Ru oxide dispersed in a molten, quarternary phosphonium or ammonium salt	methanol= 12.9 wt% ethanol= 59.5 wt% propanol= 3.7 wt % acetate esters= 10.3 wt%	6
Dow Higher Alcohol Process -developed by Dow Chemical Company	agglomerated molybdenum sulphides (alkali promoted)	methanol= 0-90% (variable) mixed alcohol octane= 120	11

catalysts[13,14] as were found in early studies (1920-1930's) based on ZnO or low activity Zn-Cr-Mn oxide methanol catalysts[12]. The selectivity toward higher alcohol formation increases according to[12,13]:

$$Li < Na < K < Rb < Cs$$

i.e. in order of increasing promoter basicity. Therefore, it would appear that it is the base catalysed reactions that are promoted by the alkali[13].

The synthesis of higher alcohols from CO can be summarised by the reactions[12]:

$$2n\ H_2 + n\ CO \rightarrow C_nH_{2n+1}OH + (n-1)\ H_2O$$

$$(n+1)\ H_2 + (2n-1)\ CO \rightarrow C_nH_{2n+1}OH + (n-1)\ CO_2$$

The formation of higher alcohols via the hydrogenation of CO presents a thermodynamically favourable pathway[12], so at a given temperature the stability of the alcohols increases with carbon number. Although the synthesis of the higher alcohols would appear then to be a favourable mechanistic route for the CO hydrogenation reaction, in actual practice the product distribution obtained is determined by kinetic, rather than these thermodynamic factors[12]. As a consequence, the reaction pathway is limited and the lowest alcohol, methanol, is the predominant product. It is generally found that the higher alcohol yield is maximised at operating temperatures and reactor contact times higher than normally used for methanol synthesis[12,14], while the required H_2:CO ratio is lower.

Early studies into higher alcohol synthesis were based on low activity catalysts that contained non-reducible oxides such as ZnO, Cr_2O_3 and MnO[12,15-17]. The extreme operating conditions required by these catalysts makes their use unattractive today[13] and recent

research has generally concentrated on studying the effect of promotion on the behaviour of higher activity low pressure Cu/ZnO based methanol synthesis catalysts[12,13,18]. The early research into the higher alcohol synthesis was largely qualitative in its treatment of results, and as such, provided little insight into the more quantitative aspects of reaction kinetics and selectivity. The relative complexity of the synthesis product distribution hampered efforts in this direction and work to produce more selective alcohol catalysts was concentrated on methanol synthesis. The development of high intrinsic activity low pressure methanol synthesis catalysts based on Cu/ZnO has allowed the higher alcohol synthesis to be carried out under milder operating conditions[12,13]. However, the mechanistic details of the higher alcohol synthesis are still not well understood, and in particular, the nature of the influence of alkali promotion on the synthesis has not been determined.

The use of alkali promoters in catalysis is not confined to higher alcohol synthesis and they are also used in a number of other catalytic processes. The promoter action can be manifest in several ways[19]:

-an increase in reaction selectivity or specificity

-an increase in catalytic activity

-prolonged effect on catalyst life

The effect of potassium promotion on the Fischer-Tropsch synthesis has, for example, been more extensively studied than the effect of promotion on the higher alcohol synthesis, and although a different composition product is produced, there are several elements in common with the alkali promoted higher alcohol synthesis that are worthy of note. Potassium is one of the key promoters of the Fischer-Tropsch

reaction that is used to change the selectivity and activity of the synthesis[20]. Potassium promotion causes a shift in the product spectrum toward longer chain molecules, and increases both the selectivity toward oxygenates and the olefinity of the hydrocarbon products. Electronic interpretations of the promoter action have been presented[20], although the role of the promoter has also been attributed to be one of a selective poison[21-23] that suppresses the hydrocarbon, but not the oxygenate forming, reaction steps.

(1.3) Scope of the Thesis

Section 1.1 has presented aspects of trends in the predicted use of methanol/higher alcohol mixtures, while section 1.2 has introduced the alkali promoted higher alcohol synthesis as a catalytic process for the production of such fuel methanol mixtures. Although the effect of alkali promotion in higher alcohol synthesis has been known for some some years, its mechanistic details are not fully understood. The aim of the present study has been to elucidate details of the effect of alkali promotion, and to relate this to a higher alcohol synthesis mechanism.

The mechanism of alcohol synthesis on the Cu/ZnO low pressure type of methanol catalyst is a complex process. Rather than attempt to establish the influence of alkali promotion using such a catalyst, this study has concentrated on the behaviour of a single component (ZnO). As part of a future more wide ranging study, it is important to establish the effect of alkali promotion on the individual catalyst components in this manner before the behaviour of the catalyst as a whole can be quantified. ZnO itself, however, is a poor industrial

alcohol catalyst since it has poor stability and low activity[12].

Potassium promotion has been investigated since, although the order of activity for higher alcohol synthesis decreases in the order of Cs, Rb and K[12-14], the high cost of Rb and Cs make them less attractive on an industrial scale[12,14], and K is generally considered to be the most practical promoter.

The study has been primarily concerned with the effects of potassium promotion of an AnalaR grade ZnO on the decomposition of 1-propanol and 2-propanol, determined using the technique of temperature programmed desorption[24]. The two C_3 alcohols are of particular interest with respect to the alkali promoted higher alcohol synthesis since typically only 1-propanol is produced in any significant amount [12,14]. By injection of each alcohol into a synthesis gas feed stream it has been demonstrated that 1-propanol and 2-propanol appear to be derived from different surface reaction intermediates[13,14]. The adsorption and decomposition of reactants (CO, CO_2 and H_2) and other products (acetone, propene and water) have also been investigated in order to fully characterise the adsorption and decomposition behaviour of ZnO and potassium promoted ZnO.

By this method, temperature programmed desorption provides information about the nature of the surface intermediates present in the decomposition process, and hence, on the decomposition reaction mechanism. However, the "principle of microscopic reversibility", which assumes the character of the surface intermediates will be similar in the forward alcohol synthesis direction, allows this information to be used in formulating possible synthesis mechanisms. As an illustration of this technique, studies using temperature programmed decomposition and infra-red spectroscopy, have shown that methanol decomposes on ZnO

through a formate intermediate[25,26,27]. The same formate intermediate has been identified after CO_2 and hydrogen coadsorption on ZnO[25], as well as during methanol synthesis itself[28,29] by infrared spectroscopy. Although the synthesis of higher alcohols is more complex and involves reactions generally considered to be consecutive to that of methanol synthesis[12,14], the study of the decomposition of the reaction products, in a manner similar to methanol, can provide important information regarding possible surface intermediates present during the synthesis of higher alcohols. This technique then has provided the basis for the experimental programme and for the conclusions of this thesis.

CHAPTER 2

SURVEY OF THE RELEVANT LITERATURE

(2.1) Introduction

The survey of the relevant literature has been divided into four main sections. Section 2.2 presents a summary of research into the synthesis of higher alcohols using modified methanol catalysts. This consists of two parts; section 2.2.1 reviews the period from around the late 1920's to the date of the extensive review on the subject by Natta[1] (1957), while section 2.2.2 covers the period from this date up to the present. Each part presents a general description of the catalysts used, the alcohol product distributions obtained, the effect of operating conditions and mechanistic proposals. Section 2.3 describes aspects of the structure of zinc oxide in relation to its properties as an adsorption and reaction surface, while section 2.4 reviews the literature concerned with the behaviour of zinc oxide toward the adsorption of hydrogen, CO, CO_2 and water and as a surface for the adsorption and catalytic decomposition of C_1 to C_3 alcohols and related compounds. Although the experimental work for the present study was concerned specifically with an investigation of the C_3 alcohols, details have also been presented for methanol and ethanol as the behaviour of these alcohols is of direct relevance to the consideration of the C_3 alcohols decomposition characteristics.

(2.2) Higher Alcohol Synthesis

(2.2.1) Early Research

The first highly selective catalysts for methanol synthesis were developed in the early 1920's[12,30]. Most practical industrial forms of catalyst were based on mixtures of two or more oxides, with ZnO as the most widely used oxide as a catalyst base in combination with a promoter in the form of a another irrreducible oxide. A commonly used promoter was Cr_2O_3, although a wide variety and large number of other catalyst compositions were also formulated[30]. These catalysts had a low intrinsic activity, so as a general rule, the required methanol and higher alcohol synthesis reaction conditions were quite severe (approximately 300-450°C and 200-250 atm pressure).

Early studies demonstrated that CO hydrogenation over alkalised iron (synthol) catalysts[31,32] could produce a variety of oxygenates, although the catalysts also had a marked tendency to form methane. In contrast, metal oxide catalysts were found to produce little methane and to give a liquid product that consisted mainly of aliphatic alcohols[32]. It was observed[12,15] that metal oxide methanol catalysts produced under basic conditions (e.g. precipitation from basic solution) gave an increased yield of higher alcohols compared to similar catalysts prepared under non-basic conditions (e.g. by the ignition of metal nitrates). This was attributed[12] to the promoting action of traces of alkali ions adsorbed on the catalyst surface not removed during the filtration and washing stages of catalyst preparation. These observations led to quantitative investigations of the influence of the addition of various alkali promoters (Li, Na, K, Rb, Cs) to Cr-Mn mixed oxide[15,33] and ZnO[12] catalysts on the higher alcohol

yield. The formation of higher alcohols was found to increase with increasing basic strength of the added promoter according to:

$$Cs > Rb > K > Na > Li$$

Impregnation with Li, Na or K reduced the rate of catalyst activity by an amount proportional to the amount of added alkali, while Rb and Cs were found to have little influence on the output of liquid product [15]. Although Rb and Cs were the most favourable promoters in terms of alcohol yield[12,33], cost was felt to prohibit their use on an industrial scale[12]. The average composition of the reaction product was found not to substantially depend on the kind of anion used with the alkali during impregnation, while the relative promoting action of the added alkalis (and the product compositions obtained) was also not dependent of the exact nature of the catalyst[12]. The promotion effects were attributed[12] to the alkali basic strength and independent to a large extent of interaction with the base catalyst.

The product distribution from the higher alcohol synthesis was characterised by high branched to linear alcohol ratios. Table 2.1 presents a representative alcohol product distribution obtained from a Rb impregnated Cr-Mn oxide catalyst[33]. In particular, within the C_{2+} higher alcohol fraction, the main alcohol was i-butanol, followed in smaller amounts by 1-propanol and ethanol. For this catalyst approximately 85% of the higher alcohol fraction consisted of i-butanol and 1-propanol.

A more complete analysis of the products obtained from potassium impregnated ZnO was published by Natta et al[12], with the following alcohols identified, demonstrating the complexity of the product distribution:

Table 2.1: Quantitative analysis of alcohols from the higher alcohol synthesis over a Rb promoted Cr-Mn oxide catalyst.

(9.8% Rb/Cr-Mn, 200 atm, 400°C, SV= 53000 hr^{-1}), from reference (33)

alcohol	total alcohol fraction (wt%)	higher alcohol fraction (wt%)
methanol	76	-
ethanol	2	8.3
1-propanol	8	33.3
i-butanol	12.5	52
n-butanol	-	-
β-methylbutanol	1.5	6.3

normal alcohols: methanol, ethanol, 1-propanol, 1-amyl alcohol,

branched alcohols: iso-butanol, 2-methylbutanol, 2-methylpentanol, 3-methylpentanol, iso-amyl alcohol, 2-3-dimethylbutanol,

secondary alcohols:iso-propanol, ethyl-iso-propylmethanol, di-iso-propyl-butanol, propyl-iso-propylcarbinol,

tertiary alcohols: tertiary butyric and amyl alcohols.

A breakdown of the main alcohol products in the C_{2+} fraction is presented in table 2.2. Again, the major higher alcohol was i-butanol at nearly 47% of the C_{2+} fraction, followed in lesser amounts by 1-propanol, ethanol and 2-methyl-butanol. Iso-butanol and 1-propanol together accounted for nearly 60% of the C_{2+} alcohols. The similarity of this product distribution with that given in the previous table

Table 2.2: Quantitative analysis of alcohols in the C_{2+} fraction from the higher alcohol synthesis over K promoted ZnO.

(9.3% K_2O/ZnO, $CO:H_2=4$, 400-420°C, 400 atm, SV= 1700 hr^{-1}), from reference (12).

alcohol	fraction of C_{2+} (wt%)
ethanol	4.2
1-propanol	11.6
2-propanol	3.7
n-butanol	2.0
i-butanol	46.7
2-methylbutanol	4.8
higher alcohols BP > 107°C	4.3
higher alcohols 107°C < BP > 180°C	15.1
higher alcohols BP > 180°C	7.8

further demonstrates the independence of the distribution to the exact nature of the catalyst or promoter as noted previously.

Temperature was noted to be the most important operating parameter in higher alcohol synthesis over alkali promoted oxide catalysts[32], with higher alcohol formation occurring to an appreciable extent only when the reaction was operated at temperatures of 400°C and higher[12,32]. There appeared to be critical temperature below which the reaction led primarily to methanol and above which there was found to be a sharp increase in the selectivity to higher alcohols [12,32].

High space velocities were employed for methanol synthesis to

increase the purity of the final product through decreasing the reaction time for possible unwanted reactions producing side products[12]. Since higher alcohols appear to be produced by reactions consecutive to that of the methanol synthesis, lower reactor space velocities were found to be needed than for the corresponding methanol synthesis reaction[17]. The effect of contact time on the higher alcohol yield from K promoted Zn-Mn-Cr oxide catalyst is shown in figure 2.1[16]. Considerable methanol in the final product can be seen to be produced even at low space velocities where thermodynamically the amount of methanol (at the 400°C reaction temperature) in equilibrium with the higher alcohols should have been be neglible[12]. This indicated the reaction product distribution to be kinetically, rather than equilibrium, limited.

The best yields of higher alcohols were obtained[12] when the $CO:H_2$ ratio was higher than the stoichiometric ratio of 0.5 required by the reaction:

$$n\,CO + 2n\,H_2 \rightarrow C_nH_{2n+1}OH + (n+1)\,H_2O$$

Water vapour appeared to act as an inhibitor for the formation of higher alcohols[16] by being selectively adsorbed on the catalyst surface and blocking active sites for alcohol synthesis and it was suggested[16] that excess CO promoted the higher alcohol synthesis by removal from the catalyst of any water formed by alcohol condensation through the reverse water gas shift reaction. A reactant feed composed of only CO_2 and H_2 yielded only methanol and no higher alcohols, although Natta[12] has noted that higher alcohols can be formed from CO_2/H_2 feeds in contradiction to this, citing Russian publications as evidence for this.

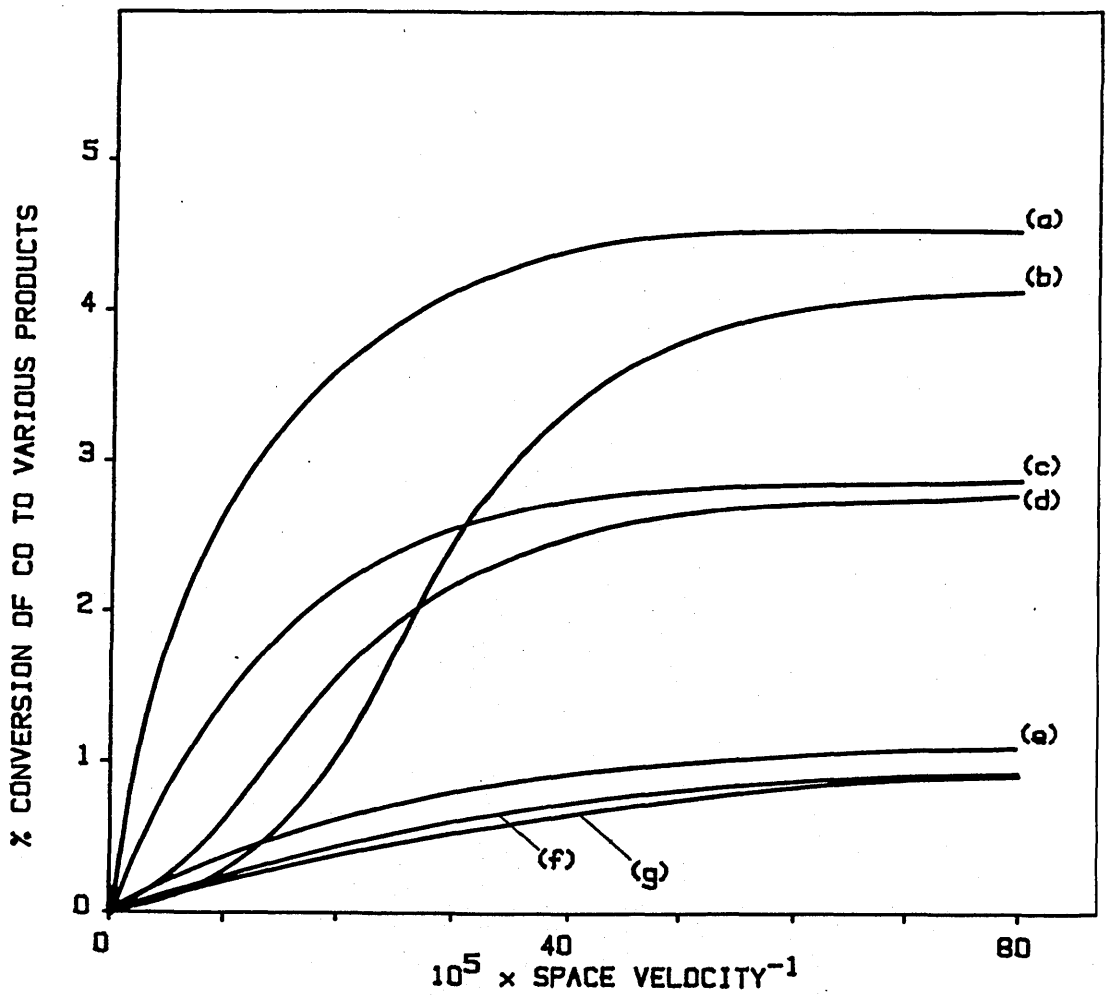

Figure 2.1: Plot of the effect of contact time on the alcohol yield over a potassium promoted Zn-Mn-Cr catalyst. (a)= methanol; (b)= alcohols higher than butanol; (c)= propanol; (d)= butanol; (e)= ethanol; (f)= acids; (g)= aldehydes. From references (16).

It was noted that the high branched content of the product alcohols showed the mechanism of the higher alcohol synthesis to be drastically different to that of the Fischer-Tropsch synthesis where only linear alcohols were obtained[17]. Several early higher alcohol synthesis mechanisms were proposed to explain this. In a scheme proposed by Fischer[31] higher alcohols were produced by the direct addition of CO to methanol to form acids, which were reduced to aldehydes and alcohols or decomposed to ketones. Morgan et al[15] proposed an alternative mechanism based on the aldolic condensation of formaldehyde, while Frolich et al[16] and Graves[34] suggested that higher alcohols were produced by the successive condensation of lower alcohols according to simple addition rules.

Natta[12] proposed a mechanism that accounted for the promoting effect of the alkali by including the formation of alkali salts of fatty acids into the reaction scheme. According to this hypothesis the higher alcohol synthesis took place with the following consecutive steps:

(i) synthesis of methanol, catalysed by ZnO:

$CO + 2H_2 \rightarrow CH_3OH$

(ii) formation of potassium methylate by reaction of the methanol with the alkali or with alkali zincate:

$CH_3OH + KOH \rightarrow CH_3OK + H_2O$ or

$CH_3OH + K_2ZnO_2 \rightarrow CH_3OK + Zn(OH)OK$

(the formation of alkali zincate according to Natta could take place in the temperature range of the alcohol synthesis by the reaction:

$ZnO + 2KOH \rightarrow K_2ZnO_2 + H_2O$)

(iii) reaction of alkali methylate and CO to form alkali acetate:

$CH_3OK + CO \rightarrow CH_3COOK$

(iv) hydrogenation of alkali acetate to alkali ethylate:

$$CH_3COOK + 2H_2 \rightarrow H_2O + C_2H_5OK$$

The water formed in the above reactions provoked the hydrolysis of the alcoholates thus regenerating the KOH and forming ethanol:

$$C_2H_5OK + H_2O \rightarrow C_2H_5OH + KOH$$

The portion of C_2H_5OK not hydrolysed could react with CO to form alkali propionate which in turn was easily reduced to alkali propylate:

$$C_2H_5OK + CO \xrightarrow{H_2} C_2H_5COOK \rightarrow C_3H_7OK + H_2O$$

The C_3H_7OK was hydrolysed as before to give the corresponding alcohol plus KOH. The formation of 2-propanol was explained by inclusion of the possibility of thermal decomposition of CH_3COOK to acetone and reduction to the alcohol. Primary linear higher alcohols could be formed by the direct hydrogenation of the salts of the corresponding fatty acids or by the thermal decomposition of mixtures of alkali formate and alkali salts on fatty acids:

$$HCOOK + CH_3CO \rightarrow CH_3CHO + K_2CO_3$$

$$CH_3CHO + H_2 \rightarrow CH_3CH_2OH$$

Natta pointed out that the mechanism of formation of higher alcohols through the direct reduction of fatty acid salts was unable to explain the fact that in the higher alcohol synthesis only a small amount of ethanol was produced. The high yields of i-butanol and 1-propanol were suggested by Natta to be due to the acids from which these alcohols were formed being adsorbed more readily than those for the formation of other branched or primary alcohols. He also proposed the possibility that 2-propanol, formed by the reduction of acetone, reacted promptly with CO to give i-butyric acid, which in turn underwent reaction with alkali formate to yield i-butanol.

(2.2.2) Recent Research

Recent studies of the alkali promoted higher alcohol synthesis have generally been based on high activity Cu/ZnO methanol catalyst formulations. These catalysts allow the use of much less severe operating conditions than those reported by the early higher alcohol synthesis studies (section 2.2.1), a significant improvement since a lower temperature favours the equilibrium yield of higher alcohols [14]. Alkali promotion of these catalysts results in a similar change of product selectivity as found by the early catalyst studies (section 2.2.1). Smith and Anderson[14] investigating the effects of adding a K_2CO_3 promoter to a commercial $Cu/ZnO/Al_2O_3$ based methanol catalyst in a laboratory differential flow reactor found alkali promotion led to an increase in the selectivity for higher alcohols, giving a product distribution similar to that reported by the early studies described in the previous section (table 2.3). Methanol was found to be the predominant product, with the higher alcohols 2-methyl-1-butanol (iso-butanol), ethanol, 1-propanol and pentanol occurring in significant quantity in the C_2+ fraction. A maximum in butanol (i- plus n-butanol) selectivity was obtained for a 0.5% K_2CO_3 promoted catalyst.

Klier et al[13,18] conducted a study based on a similar Cu/ZnO methanol synthesis catalyst (30/70 composition) and found alkali promotion to cause three effects: (i) an increase in activity of the Cu/ZnO catalyst toward methanol synthesis, (ii) a change of the CO_2 dependence of the methanol conversion, and (iii) a change in selectivity in favour of C_2-C_4 alcohols and esters. The main effect of the alkali promotion was the increase in the methanol synthesis rate at lower temperatures and higher H_2:CO feed gas ratios. The most

significant enhancement was given by the strongest base studied, CsOH, indicating that it was the base catalysed reactions that were promoted by the system. The promotional effects of the alkalis with respect to the methanol synthesis rate were found to be in the order:

$$Cs > Rb > K > Ba = \text{undoped} > Na > Li$$

The main mechanistic function of the Cs in relation to these promotion effects was proposed by Klier et al[18] to be the activation of the CO by the formation of a surface formate according to:

$$Cs^+OH^- + CO \rightleftharpoons HCOO^-Cs^+$$

which was further reduced by hydrogen to C_1 surface precursor intermediates of methanol. The hydrogenation was accompanied by a parallel decomposition to carbon dioxide and hydrogen, thus completing the shift reaction and rapidly removing the surface hydroxyls which retard the activation of hydrogen in water rich syn-gas. The promoting role of the Cs ions was proposed to be due to their removal of this water, thus enhancing the methanol synthesis rate[18]. At higher temperatures and lower H_2:CO ratios, the base-catalysed carbon-carbon bond forming reactions were found to be promoted, increasing the higher alcohol yield[18]. Within the higher alcohol fraction (from a Ba promoted catalyst) the main alcohols produced were reported by Klier et al[13] to be 1-propanol, ethanol and 2-methyl-1-propanol.

A study of a K promoted Zn-Cr mixed oxide catalyst by Di Conca et al[35], with respect to higher alcohol synthesis, found the potassium to be present essentially only on the surface of the catalyst in a free form rather than form any special compounds. An increase in the selectivity for higher alcohols was found for temperatures greater than 653 K, with i-butanol the main alcohol obtained. It was concluded that the potassium did not appear to modify the nature of the

Table 2.3: Quantitative analysis of alcohols from the higher alcohol synthesis over potassium promoted $Cu/ZnO/Al_2O_3$. From reference (14)

alcohol	alcohol selectivity[(a)]	
	total alcohols	higher alcohols
methanol	61.4	-
ethanol	4.8	12.4
2-propanol	1.8	4.7
1-propanol	9.2	23.8
1-butanol	2.5	6.5
2-butanol	1.7	4.4
2-methyl-1-propanol	13.8	35.8
pentanols	4.8	12.4

(a)= (C atoms in alcohol)/(C in total alcohols) x100%

hydrogenating centres on the catalyst surface and its role as a promoter for higher alcohol synthesis was attributed to its basic character. This conclusion favoured the condensation of formaldehyde and/or formiate in agreement with the mechanism proposed earlier by Natta[12] (see section 2.2.1).

The addition of alkali promoters has been found to cause a decrease in catalyst surface area[13,14,18,35]. Klier[18] reported the addition of alkaline earth and Li hydroxides to the Cu/ZnO catalyst described above resulted in a 10-23% decrease in area, while other alkaline compounds caused a more dramatic 40-50% reduction; Cs concentrations as small as 0.1% were found to cause a significant area loss[18]. This was attributed to a lowering of the surface energy of

the catalyst particles that removed the driving force for particle growth[18], resulting in the formation of larger catalyst particles during the catalyst precipitation stage[13,18,35] or to the formation of $K_2Cr_2O_7$[35].

Smith and Anderson[14] found a strong temperature dependence for the higher alcohol product distribution over the range 533 to 558 K, based on a 0.5% K_2CO_3 promoted Cu/ZnO catalyst (table 2.4). At 533 K there was neglible selectivity toward butanol, while at 558 K up to 7.2% butanols (mainly 2-methyl-1-propanol) were obtained.

Butanol selectivity is also favoured by high $CO:H_2$ feed gas ratios[13,14]. At a ratio of 0.5, Smith et al[14] found the butanol selectivity to be almost independent of the conversion, while at a ratio of 2 selectivity was found to be a strong function of reactant conversion. These results suggested that decreasing the CO to H_2 concentration decreased the relative rate of hydrogenation of the methanol precursor and inhibited methanol formation. Decreased $CO:H_2$ ratios were also found by Klier et al[13] to suppress the formation rate of branched primary alcohols in favour of linear alcohols.

Correlation of the effects of CO and H_2 partial pressures on the alcohol production rate to an emperical rate law by Smith et al[14] has shown the production rate of 2-methyl-1-propanol to vary approximately with the square of the CO partial pressure, while being almost independent of the H_2 partial pressure. The selectivity for 2-methyl-1-propanol relative to methanol also showed that CO rich syn-gas inhibited methanol production.

For methanol synthesis normally a small amount of CO_2 in the syn-gas feed enhances the methanol production rate[13]. However, Klier et al[13] found alkali promoted Cu/ZnO showed a reversal of this

Table 2.4: The effect of operating temperature on the higher alcohol selectivity over potassium promoted Cu/ZnO catalyst.

(inlet space velocity= 2100 hr^{-1}, H_2:CO=0.89, catalyst= 0.5% K_2CO_3/Cu/ZnO). From reference (14).

alcohol	reactor temperature (K)		
	533	548	558
methanol	96.5(a)	83.6	73.7
ethanol	2.2	7.1	6.9
2-propanol	0.1	0.9	0.5
1-propanol	1.0	4.4	5.4
1-butanol	0.1	1.0	2.3
2-butanol	0.0	1.0	0.9
2-methyl-1-propanol	0.1	1.6	4.0
pentanols	-	0.3	0.4

(a)= (C atoms in alcohol)/(C in total alcohols) x100%

behaviour with the addition of CO_2 to the feed syn-gas inhibiting the methanol production rate[13]. This was attributed to the possible formation of a surface carbonate species obtained by the reaction of the CO_2 with alkali hydroxide. This carbonate was proposed to be inert in the alcohol synthesis, causing blockage of the active sites and resulting in the observed inhibition of the alcohol synthesis rate[13].

A modified condensation chain growth scheme for the higher alcohol synthesis, similar to the earlier mechanism of Graves[34], was proposed by Smith et al[36]. The model extended Graves' simple chain

growth scheme according to the following rules:

(i) higher alcohol formation results from the reaction of two intermediates of lower carbon number, with at least one of these having a carbon number of one or two, so that chain growth is by one or two carbon addition only.

(ii) addition occurs at the α or β carbon (with respect to the hydroxylated carbon atom) of the reaction intermediate (with the latter being the fast step). Two carbon addition does not occur at an α carbon.

(iii) it is assumed that all of the reaction rates are first order with respect to the concentration of the growing surface intermediate (including desorption of this intermediate), the rate constants are independent of the carbon number and that all steps are reversible.

Estimates of the distribution parameters were obtained by Smith et al[14], from experimental results, by non-linear square estimation, with carbon addition to an adsorbed species assumed to stop following β addition to an α substituted intermediate or α addition to a β substituted intermediate (the latter case allowing for the relatively large amounts of 2-methyl-1-propanol formed[14]). For a general adsorbed intermediate the possible reactions predicted by this mechanism are:

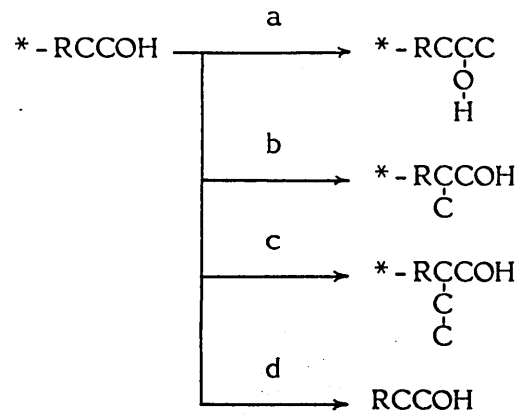

where *-RCCOH is the adsorbed surface species, a and b the first order rate constants for one carbon addition at the α and β positions respectively, c the first order rate constant for two carbon β addition and d the desorption rate constant.

Smith et al used this model to successfully predict experimentally observed[14] product distributions. For the major alcohol components ethanol, 1-propanol, 2-methyl-1-propanol and pentanol, the predicted values were found to agree to within 10% of the experimentally measured values. The high methanol selectivity was shown to be a result of a slow initial growth step, while the large 2-methyl-1-propanol selectivity was due to α addition being the only growth step of the 2-methyl-1-propanol intermediate. The probability of the initial growth step was found to have the most significant effect on the alcohol selectivity; for greater higher alcohol selectivities this probability must be large (i.e. the rate of one carbon α addition relative to desorption must be high) to allow the methanol precursor to react and not to desorb as methanol.

Klier et al[13] have proposed a mechanism for the higher alcohol synthesis based on the stepwise addition of a general C_1 intermediate to a reacting alcohol chain:

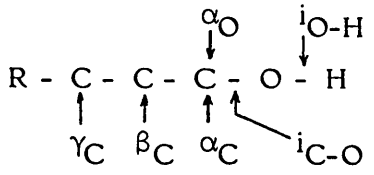

where α_C, β_C, and γ_C are defined as attachment of the intermediate by its C end onto the α, β and γ carbons of the reacting chain, α_O attachment of the intermediate by its oxygen at the α carbon, and i_{C-O} and i_{O-H} insertions of the C_1 intermediate at the α carbon into the C-O and O-H bonds of the growing alcohol chain.

The possible reactions and types of products allowed by this scheme are:-

α_C giving: RCC(C)-OH (secondary alcohols)

β_C giving: RCC(C)C-OH (branched primary alcohols)

γ_C giving: RCCC(C)-OH (branched primary alcohols)

α_O giving: RCC(=O)-OH (methyl esters)

i_{C-O} giving: RCCC-C-OH (linear alcohols)

i_{O-H} giving: RCCC-O-C(=O)H (formate esters)

The experimental results of Klier et al[13] showed the rates of the α_C, γ_C and i_{O-H} additions to be neglible, α_O to be more effective than i_{O-H} for ester formation and that β_C addition dominated the synthesis of the C_{3+} products. At high $CO:H_2$ ratios, and in the presence of alkali promoters, the efficiency of β_C addition was dominant, while at low ratios, and on unpromoted Cu/ZnO catalyst, the addition was suppressed in favour of the i_{C-O} linear growth insertion.

An aldol synthesis involving aldehyde precursors or products of alcohol dehydrogenation was proposed to account for the influence of the alkali and feed gas composition:

$$RCH_2CH_2CH_2OH \rightleftharpoons RCH_2CH_2CHO + H_2$$

$$RCH_2CH_2CHO + CsOH \rightleftharpoons RCH_2\bar{C}HCHO + H_2O \quad (Cs^+)$$

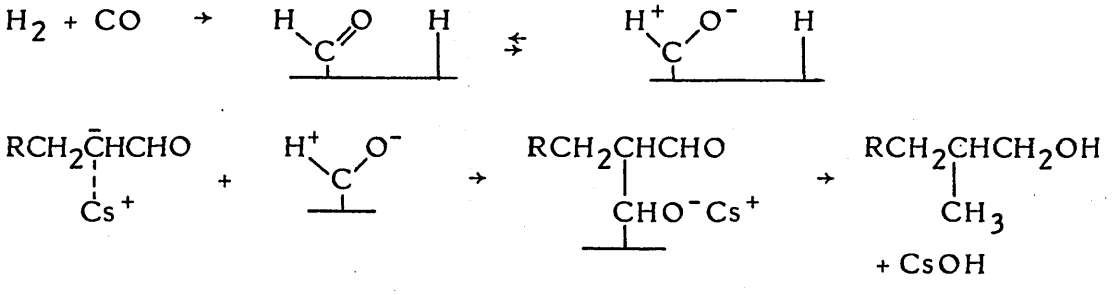

Since only primary or secondary, but not tertiary, β carbons are attacked in this scheme, the promotional effect for branched higher alcohols would be greatest in the presence of stronger bases (found experimentally[13]).

The formation of surface alkoxide and acetate species was proposed as a likely route for the i_{CO} process, similar that the earlier mechanism of Natta[12] (see section 2.2.1):

$$RCH_2O^- + CO \rightarrow RCH_2COO^-$$

$$RCH_2COO^- + 2H_2 \rightarrow RCH_2CH_2OH + HO^-$$

Since this reaction requires hydrogen, it would be favoured by a low $CO:H_2$ ratio as was observed experimentally.

Manazec[37] has presented a further mechanism for higher alcohol synthesis in order to explain the high branched to linear ratio of the alcohol products. In this scheme, the chain initiation step is proposed to be the formation of a bound formyl species, produced either

by the interaction of hydrogen and CO on the metal oxide surface, or by the reduction of surface formate species by hydrogen. The primary mechanism for chain growth is a CO insertion into the metal-carbon bond of the formyl to make a cyclic acyl. Through an isomer intermediate the acyl rearranges to form an enediolate, via a 1,2 hydrogen shift:

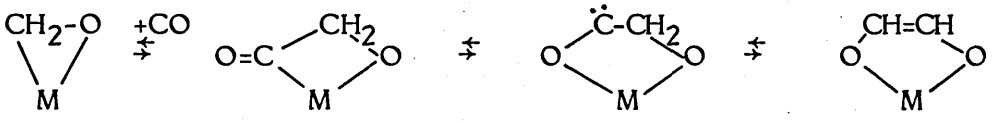

Hydrogenation of the enediolate is rapid in the presence of excess hydrogen forming a coordinated diol, which dehydrates to form a coordinated enol:

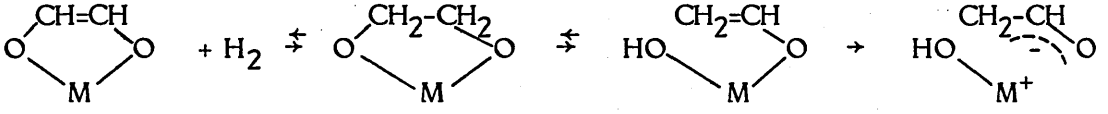

Protonation of the enol then leads to the formation of a bound aldehyde containing one more carbon atom, thus completing the chain growth cycle:

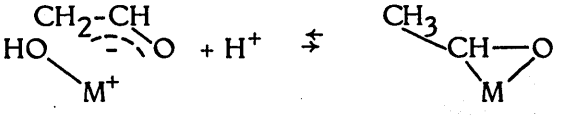

Chain growth continues by subsequent CO insertions that follow the same steps. For growth involving 3 carbon atoms the coordinated 1,2 propanediolate intermediate can dehydrate to give two possible enol structures:

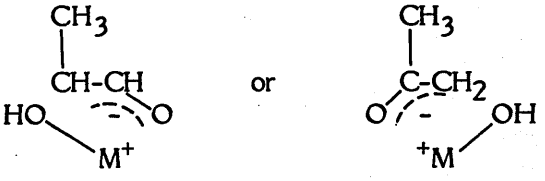

Manazec proposes formation of the enol with the central methyl group to be favoured since it is less sterically hindered and because of electronic factors which would favour the electron donating methyl

group to be situated on the less electron rich central carbon atom. As a result, the reservoir of surface enol species would favour the branched, rather than the linear, enol. The enols are protonated to their respective aldehyde structures according to the mechanism given above, and the cycle is continued via a third CO insertion step to form the acyl species. The acyls are then available to undergo a 1,2 hydrogen shift. In the case of the branched enol, there are only methyl species available for participation in the shift, and since the migratory aptitude of methyl is much lower than that of hydrogen, the branched acyl would undergo competing reactions such as hydrogenation to the alcohol (i-butanol) which can be desorbed from the surface. The desorption of this alcohol serves as a kinetic drain of alcohols from the system. In comparison, the acyl derived from the linear enol has hydrogen available for the 1,2 shift so can be transformed into the enediol and undergo further chain growth. Hydrogenation is still a competing reaction but, because the 1,2 shift is rapid, chain growth is favoured over alcohol formation.

Manazec[37] proposes the differences in stabilities of the two enolates, and the different reactivities of the acyls formed by CO insertion into the enolates, to explain the tendency for branched alcohol formation in the higher alcohol synthesis.

(2.3) Zinc Oxide Crystal Structure

Since the catalytic activity of ZnO has been shown not only to be affected by the chemical composition, but also by the detailed atomic arrangement of the surface[28], it is first necessary to consider in detail the structural nature of ZnO before its properties as an adsorbate are described.

ZnO has a hexagonal wurtzite crystallite structure where the zinc and oxygen ions are in tetrahedral coordination within the lattice [38]. The bonding in the lattice is intermediate between completely ionic and completely covalent, with both ions being more polarizable than in a perfect crystal and carrying an effective charge of only $\pm$ 0.5e[38]. Cleavage of the idealised crystal structure along the plane normals forms the three low index surfaces as shown in figure 2.2; the polar Zn (0001) and O ($000\bar{1}$) and the non-polar ($10\bar{1}0$) crystal faces. The structural environments of the Zn and oxide ions in each of the three surface types are different hence each plane can be expected to possess different adsorbent and catalytic properties.

(i) Zn (0001) Polar Surface

The Zn (0001) polar surface carries an outwardly situated layer of zinc ions. Each cation is coordinated to three underlying lattice oxygens with a fourth coordinatively unsaturated ("dangling") bond normal to the surface[39]. It has been predicted[40] that surface reconstruction will occur so that the Zn ions will settle toward the trigonal holes of the underlying oxide layer. The Zn (0001) surface is pictured as being a layer of Zn ions, still uppermost, but closer to the underlying oxide layer than they are in the idealised structure. Some relaxation of Zn ions into the oxide layer has been measured by LEED studies[39].

In order to satisfy the charge compensation criterion[41,42], it is predicted that every fourth Zn cation will be lost from the freshly prepared surface, thus creating a surface with Zn vacancies each surrounded by three saturatively uncoordinated oxide ions.

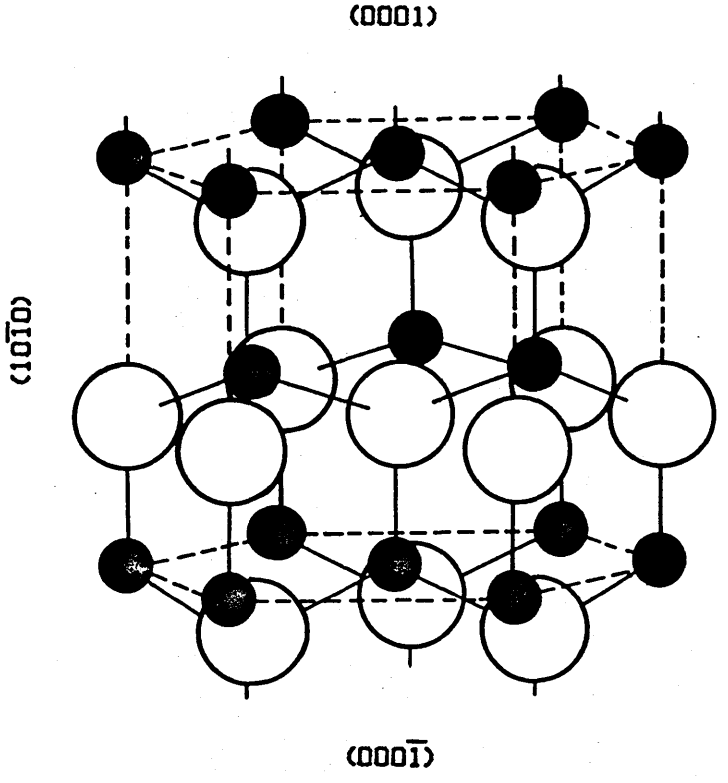

Figure 2.2: The crystalline structure of zinc oxide.
● = zinc; ○ =oxygen.

(ii) O $(000\bar{1})$ Polar Surface

The O $(000\bar{1})$ surface has a structure complementary to that of the Zn (0001) plane, consisting of a layer of oxide ions with underlying lattice Zn ions[39,40]. Atherton et al[43] and Morimoto[44] have also predicted a surface reconstruction where the Zn cations occupy the trigonal sites formed by surface oxygens to give a three fold oxygen coordination. This reconstruction however initially leads to each of the surface oxygens having a distorted octahedral coordination and to the cations being at a shorter distance from the second layer Zn than the distances present in the crystal bulk. By "expanding" the surface layers so to leave the surface oxygens in a regular octahedral co-ordination, the first-to-second layer Zn-Zn distances are relaxed so they become virtually the same as those existing in the crystal bulk[43].

An alternative cleavage line to produce the $(000\bar{1})$ plane has also been considered by Atherton et al[43] and Morimoto et al[44] where the O $(000\bar{1})$ face was defined as consisting of an outermost layer of Zn ions singly coordinated to lattice oxygens. Surface reconstruction was proposed to occur by migration of the Zn ions toward the lattice to occupy the trigonal sites formed by the lattice oxygens.

More recent LEED studies[38,45] have provided conflicting evidence for any $(000\bar{1})$ surface reconstruction where it has been shown that for freshly cleaved crystals in vacuo, surface reconstruction did not occur but the charge compensation criterion was satisfied by the loss of every fourth oxygen ion (per Zn ion). Bocuzzi at al[46] and Griffin and Yates[41] have also favoured such an interpretation in which the charge compensation criterion was satisfied by the removal of every fourth oxide ion. In correspondence with each oxygen vacancy

there is formed a triplet of uncoordinated Zn ions surrounded by a two-dimensional hexagonal structure of oxide ions.

(iii) $(10\bar{1}0)$ Non-Polar Surface

The $(10\bar{1}0)$ prism surface plane, unlike the polar surfaces, is charge balanced and therefore electrically neutral since it contains equal numbers of oxygen and Zn ions. The centres of the Zn and oxygen atoms are coplanar and each of them coordinates three counter ions[44]. No surface reconstruction is predicted to occur[40], a result also confirmed by LEED studies[38,45]. The relative electrical neutrality of the $(10\bar{1}0)$ face has been reflected in the results of Gopel and Lampe[47] who found the ZnO prism surface to be an almost ideal semi-conductor compound surface for systematic studies of reversible solid/gas interactions, exhibiting well defined and stable surface geometry.

In general ZnO catalysts are subjected to high temperature (approximately 673 K) calcination treatment in order to be catalytically activated[38]. This activation is likely to be related to the formation of a defective crystal structure that deviates considerably from the ideal low index cleavage surfaces described above. The formation of defects has been shown to be a strong function of both the method of ZnO sample preparation and pretreatment conditions employed[47]. Esser et al[48] felt that a consequence of this was a possible reason for the irreproducible and sometimes contradictory results that have been obtained for ZnO in the past.

Gopel and co-workers[47,53,54] have shown surface oxygen vacancies are readily formed and become experimentally measurable at temperatures above 700 K, and at these temperatures exist in thermodynamic

equilibrium with the ZnO lattice. The equilibrium concentration of defects can be modified by the presence of oxygen gas during the sample heating. Further exposure of a ZnO single crystal surface to oxygen at room temperature was found to remove surface vacancies. Such oxygen vacancies have been found to act as specific sites for strong CO_2 chemisorption[48], reflecting the important role that such defects play in determination of the catalytic characteristics of ZnO.

Heating a Zn (0001) single crystal surface to 570-670 K in vacuo has been shown[50] to result in a LEED pattern that indicated regular step formation of one unit cell height, corresponding to steps of $(10\bar{1}0)$ surface separated by terraces of (0001) structure. In addition, "real" ZnO may contain high index planes. These high index planes will contain a high density of steps and kinks, although it has been proposed that they can be regarded as being analogous to a highly defective low index surfaces[49]. The existance of point and line defects associated with real surface has been shown by a number of studies to considerably modify the surface properties of ZnO (see also section 2.4). The higher reactivity of anion vacancy sites is due to the exposure of three Zn cations around the defect site with 'dangling' bonds[50], while the atoms existing along the edges of the steps have immediate surroundings which are different in number and configuration of nearest neighbours and in the number and type of dangling bonds compared to those of surface atoms in the 'flat' portions[51]. It has been noted that adsorption and reaction on stepped surfaces can be enhanced because of the special sites provided by the step edges. Work has shown[50] that surface step sites are analogous to anion vacancy sites since they expose two Zn cations with a similar bonding environment i.e. can be considered as a line of point defects.

Thermal desorption studies[50] have found step sites to possess similar adsorbent characteristics as anion vacancy point defects, indicating the local environment of a step site to be closer to that of an anion vacancy than a site on a terrace structure.

(2.4) Adsorption and Decomposition on Zinc Oxide

(2.4.1) Hydrogen Adsorption on Zinc Oxide

Although the chemisorption of hydrogen onto the surface of zinc oxide has been the subject of many investigations, the exact nature of the adsorption process is still being debated among the workers in the field. At room temperature two main forms of adsorbed hydrogen on ZnO have been identified[40], designated Types I and II. Type I adsorption is characterised as being fast and reversible, occurring only on sites that constitute approximately 5-10% of the total ZnO surface [40,55]. The equilibrium for Type I adsorption has been found to be 90% complete in 30 minutes, with full equilibrium reached in 1 hour. It is generally agreed that Type I adsorption is in the form of hydride/hydroxyl pairs on the ZnO surface[41,55,56,46,57] on the basis of spectroscopy studies. Type II adsorption is strong and irreversible, and although initially fast, continues at a very slow rate for several days[40]. More recently[57] Type II adsorption has been shown to consist of two stages; adsorption onto the non-polar $(10\bar{1}0)$ face to form a stable bridged hydrogen complex, followed by a very slow diffusion into the crystal bulk. The Type I and II adsorption species have been found to be independent of each other indicating separate adsorption sites are involved[58].

Temperature programmed desorption studies have further revealed

up to 7 different adsorption forms for hydrogen[59,60,61], although some correspond to low temperature states that are not populated at room temperature[61,62]. High temperature adsorption states have also been identified whose presence is a function of the non-stoichiometry of the ZnO sample investigated[60].

Types I and II adsorption have been shown to have different catalytic activities. Type I hydrogen has been identified as responsible for catalytic hydrogen activation[62] and with the active sites for hydrogenation and exchange reactions[58,62]. However, a recently published study by Roberts and Griffen[27] has shown Type I sites are not essential for methanol synthesis. Although Type II hydrogen has been found to be unreactive in the ethylene hydrogenation reaction, it was noticed that the presence of Type II hydrogen was found to exhibit a promoting effect on the reaction rate[40].

The effect of oxygen treatment both at room and high temperatures was negligible for Type I and only slight for Type II adsorption [40,63], indicating the adsorption sites to be independent of the electronic state of the ZnO surface i.e. degree of surface reduction. An apparent oxygen poisoning effect for hydrogen adsorption appeared to be caused by hydrogen remaining on the surface during oxygen treatment reacting to form adsorbed surface hydroxyls that inhibit hydrogen adsorption[27,40].

Early proposals[40,46] for the active sites responsible for hydrogen Type I chemisorption were based on the Zn ions situated in the trigonal holes of a close-packed layer of oxide ions formed by the reconstruction of the $(000\bar{1})$ polar face. These sites would only occupy a fraction of the surface. Corresponding to each oxygen vacancy is formed a triplet of uncoordinated Zn ions surrounded by a

hexagon of oxide ions in the outermost layer. Hydrogen adsorption occurs through heterogeneous dissociation to form hydride and hydroxyl pairs on one of the Zn ions in the triplet and on an adjacent oxide ion in the surrounding hexagon[46]. A similar active site geometry has also been proposed involving the reconstructed Zn (0001) polar surface[27,41]. The Zn polar face was favoured over the O polar since the adsorption of hydrogen was found to not produce surface OH bands consistent with adsorption on the oxygen rich O polar surface [41]. Reconstruction of this surface (by the loss of every fourth cation) forms a hexagonal array of Zn cations surrounding oxygen anions. The clusters of adjacent exposed Zn cations, adjacent to the cation, were proposed to be the Zn-O pair sites of Type I adsorption, subject to the constraint that not more than one hydrogen adsorption site existed for each missing cation[41]. The Type I sites have been further associated with sites on stepped or pyramidal low index surfaces[64] that present two rows of face-to-face uncoordinated Zn cations with different orientation dangling bonds with respect to the surface. The hydrogen molecule is strongly polarised by these cations and, as a result, undergoes dissociation.

The nature of the active sites for Type II adsorption has been less well defined. Dent and Kokes[40] felt this form of adsorption involved partial penetration into the ZnO bulk structure along octahedral channels between the Zn and O lattice atoms, while Boccuzzi et al[46] proposed Type II adsorption involved the following hydrogen bonded and bridged structures:

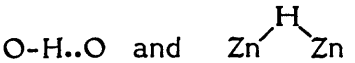

Such an active centre was more complex than proposed for Type I adsorption, implying the extended interaction of a hydrogen atom with greater that one oxygen and zinc atom and that this type of adsorbed hydrogen is located in subsurface cavities of the ZnO lattice[46].

(2.4.2) Carbon Monoxide Adsorption on Zinc Oxide

The adsorption of CO is sensitive to the surface condition of the ZnO employed[48] and as a consequence, some inconsistancies in its behaviour have been reported in the literature. Early research has identified two CO adsorption forms on ZnO[65,66,67]; one non-activated reversible form predominant at room temperatures, and an activated strongly bonded form occurring at high temperatures[67]. The high temperature form was found to be removed as CO_2 on heating[65] by surface reduction of lattice oxygen, leaving an oxygen vacancy in the ZnO surface that appeared to be stable at room temperatures[68]. The activation energy for the CO derived CO_2 desorption was found to be identical, within experimental error, to that obtained for CO_2 desorption[69], in further confirmation that its formation was through chemical reduction of the surface[69] by CO reacting with lattice oxygen to yield chemisorbed CO_2^- and oxygen vacancies $V(O_s^+)$. This irreversibly bound form of CO is found to cover only a fraction (5-10%) of the total ZnO surface[40,70].

Temperature programmed investigations[50] of the behaviour of the $(10\bar{1}0)$ single crystal ZnO surface have shown that while CO desorbed as CO_2 from a stoichiometric surface (little CO desorption was observed), only CO desorption was detected after adsorption onto a reduced $(10\bar{1}0)$ surface that contained anion vacancies. This suggested that surface reduction of the ZnO occurred to form the CO_2, rather than a

disproportionation of CO to CO_2 and C[50].

Esser et al[48] proposed two mechanisms for the catalytic oxidation of CO; a high temperature one (T> 600 K) characterised by extremely short mean residence times of adsorbing or interacting molecules, and a low temperature one (T< 450 K), where the chemisorbed complexes were thermodynamically stable on the ZnO surface. Both mechanisms involved the adsorption of CO as a CO_2 surface complex associated with lattice oxygen forming a surface oxygen vacancy. The rate of CO oxidation had the same temperature dependence for both the polycrystalline powder and single crystal ZnO samples and it was concluded the CO oxidation reaction was face specific to the $(10\bar{1}0)$ surface.

Various proposals have been made as to the nature of the CO adsorption sites. Studies of the room temperature interaction of H_2 and CO on ZnO found that CO appeared to be adsorbed onto exposed Zn cations associated mainly with a reconstructed O polar surface[46,71]. The active sites for CO adsorption were proposed to be the "triplet" of Zn cations formed by the loss of one in every four oxide ions from this surface (due to surface charge stabilisation), with one Zn cation the site for dissociative adsorption of hydrogen (in association with an adjacent oxide- see previous section), and the remaining two uncoordinated Zn cations, the CO adsorption sites[46]. The active sites have also been proposed to be associated with a reconstructed Zn (0001) polar surface[41] where every fourth cation is removed to expose an hexagonal array of Zn cations surrounding oxygen anions (see previous section).

Cheng and Kung[50] felt the CO adsorption mode would be stronger at surface anion vacancies (where three cations around a vacancy each

could have one coordinatively unsaturated bond pointing at the anion vacancy), or at steps (where the two Zn cations associated with the step have similar dangling bonds). At both types of site, the electron density available for interaction with the CO would be higher than on a stoichiometric $(10\bar{1}0)$ surface resulting in a stronger interaction that would lead to only CO desorption. CO interaction with the stoichiometric $(10\bar{1}0)$ surface was found by Cheng and Kung to be very weak (in contradiction with Esser et al[48]).

Bowker et al[25] found no detectable amounts of CO to be desorbed from a terminally reduced polycrystalline ZnO sample, but for CO dosed onto a less defected surface, coincident CO and CO_2 desorption occurred at temperatures the same as found after CO_2 dosage onto a reduced ZnO sample. This was also interpreted as indicating that CO adsorption was associated with surface anions and formed carboxyl-type surface species, which, dependent on the degree of non-stoichiometry of the ZnO, desorbed or decomposed to CO_2 and CO. The absence of this surface anion, as in the case of a reduced surface, resulted in no CO adsorption occurring.

Lavalley et al [72] have proposed a further site model corresponding to the edges formed by the intersection of the (0001) and $(10\bar{1}0)$ surfaces that exposed coordinatively unsaturated surface cations. These adsorption sites are similar to anion vacancies in that they expose two coordinatively unsaturated Zn cations in association with a lattice oxygen.

Contradictory results by Gay et al[39] have shown CO adsorption to be associated with well defined $(10\bar{1}0)$ structural terraces, rather than with any steps or point defect sites present, and the results have supported the hypothesis that adsorption involves a dominant

interaction of CO with coordinatively unsaturated Zn surface cations present in idealised face structures rather than with reconstructed or defected surface sites (as proposed above). Heinrich[73] proposed the adsorption sites on the Zn polar surfaces were associated with the presence of large numbers of steps that exposed edges of non-polar structure. Henrich felt the amount of CO adsorption on the polar surfaces could then be used as a measure of the step density on these faces.

McClellan et al[74] and Sayers et al[75] found that CO adsorbed onto the $(10\bar{1}0)$ and (0001) crystal surfaces formed a nearly linear Zn-C-O complex. On the polar face this complex was oriented approximately normal to the surface, while on the non-polar face it was oriented at approximately 30° from the surface normal. The (0001) face was found to be roughly as efficient as the non-polar face in adsorbing CO; the fractional coverage of the (0001) to $(10\bar{1}0)$ face was found to be approximately 0.7 at equivalent temperature and pressure.

(2.4.3) Carbon Dioxide Adsorption on Zinc Oxide

CO_2 adsorbs rapidly onto ZnO at room temperature[65]. The formation of surface carbonate species[76,77], and possibly carboxylate species[76], have been identified by IR spectroscopy. Pretreatment of ZnO in oxygen at 723 K was found to have little effect on the adsorption behaviour of CO_2[66] and it has been inferred that CO_2 adsorption is independent of the degree of non-stoichiometry of the ZnO surface. Other results, however, have shown[78] evidence for the competitive adsorption of CO_2 and oxygen, indicating the sites to be associated with Zn^+ cations or Zn atoms and precluding the adsorption of the CO_2 onto lattice O^{2-} ions to form carbonate species. The similarity

between the temperature programmed desorption characteristics of CO_2 and CO[48] strongly suggested an interaction with surface oxygen vacancy sites.

The presence of small amounts of adsorbed hydroxyl species does not appear to inhibit CO_2 adsorption[65], but little adsorption and associated carbonate formation was found on a fully hydroxylated surface[43,79,80]. The exposure of a partially hydroxylated ZnO surface to CO_2 was found to result in the rapid formation of carbonate ions[43], adding weight to the involvement of surface oxygen species (either in the ZnO lattice or remaining on the surface after dehydroxylation) in the chemisorption process. The amount of adsorbed CO_2 was found to decrease linearly with increasing hydroxyl coverage[79,80] suggesting that CO_2 chemisorbed on only vacant sites that were free from OH groups and also discounting the possibility of CO_2 reacting with the hydroxyls to form surface bicarbonate species.

A comparison of the temperature programmed desorption behaviour of ZnO non-polar single crystal $(10\bar{1}0)$ and polycrystalline ZnO surfaces[69,81,82] showed the CO_2 adsorption properties on ZnO were basically determined by the properties of the non-polar surface only. CO_2 chemisorption equilibrium was readily established at room temperature on clean $(10\bar{1}0)$ surfaces forming a carbonate species with surface oxygens. Oxygen vacancy defect sites were found to act as specific sites for strong CO_2 chemisorption and it was suggested CO_2 adsorbed on these sites to form a $ZnCO_2^-$ surface complex. The same complex has been shown to be formed by the adsorption and reaction of CO with lattice oxygen[48] (see previous section).

However, contradictory results were obtained by the temperature

programmed studies of Bowker et al[25,83] where adsorption of CO_2 onto polycrystalline ZnO was proposed to be largely confined to defect sites present on the Zn (0001) polar surface. No CO_2 adsorption/desorption was obtained from single crystal $(10\bar{1}0)$ surfaces by these workers.

The single crystal temperature programmed studies of Cheng and Kung and co-workers[49,50,84,85] have shown a structural dependency to the adsorption of CO_2. On stepped and prism single crystal surfaces, two types of adsorption were identified; one requiring a surface Zn-O pair, and in the form of a surface carbonate (as suggested by Gopel et al[69,81,82]), while the other was proposed to be associated with the surface steps sites (i.e. defect sites) since it was found to be more predominant on stepped prism surfaces. The carbonate form was found to be displaced by the adsorption of background water, while the other adsorption form appeared to be enhanced by the presence of the water. This could not be adequately explained although it was thought to be due to possible charge transfer effects. Stronger adsorption was observed associated with the Zn polar (0001) crystal surfaces but Cheng et al were unable to conclude whether this was due to the strong dipole moment of the polar surface, to atomic reconstruction or to the presence of defect sites.

Well defined CO_2 adsorption sites on the ZnO surface have been found by Saussey et al[52], with three forms of adsorbed CO_2 identified by IR spectroscopy. It was proposed that CO_2 adsorption was associated with the two-fold coordinated Zn cations present on the step and edge positions of the ZnO crystals where the $(10\bar{1}0)$ and (0001) surfaces met. The Zn^{2+} ions in these positions would carry two unshared coordinate vacancies in combination with a reactive oxygen in

an adjacent lattice position. Although such cations could also be present associated with anion vacancy sites, Saussey et al felt that the experimental oxygen treatment used precluded the presence of such defects. In powdered ZnO the number of such edge and step sites could be extremely high. The different forms of adsorbed CO_2 were associated with the following successively formed species: a bidentate carbonate (with one oxygen bonded to a Zn^{2+} cation and the carbon to an adjacent lattice oxygen on the $(10\bar{1}0)$ surface), a linear species (with the oxygen bonded to the Zn^{2+} cation of the step edge), and a second type of bidentate carbonate species proposed to form on the $(10\bar{1}0)$ surface away from the edge or step adsorption sites associated with a Zn-O pair (similar to that proposed by other workers as described above).

(2.4.4) Water Adsorption on Zinc Oxide

IR spectroscopy has identified several types of adsorbed hydroxyls to be formed by water adsorption on ZnO surfaces[43,44]. It has been suggested that these can be attributed to hydroxyl oxygen atoms bound to different numbers of lattice metal atoms[86]. On an ideal surface the surface hydroxyl oxygen atoms could be expected to occupy the positions of oxygen atoms in the infinite oxide crystal lattice thus restoring the natural coordination of the oxide metal atoms. In this manner, for ZnO, singly, doubly and triply coordinated hydroxyls can be formed. On the Zn polar surface triple coordination would predominate, while both single and double coordination are possible on the prism surface[86]. On the O polar surface, triple coordination would also be expected to occur in association with lattice oxygen vacancy sites present.

Water readily adsorbs onto the surface of zinc oxide to form hydroxyl species and saturation water surface coverages of approximately 8.5 OH per nm^2 have been measured[87], close to a coverage of one hydroxyl per Zn surface cation present[38]. It has been noted that unusually high dehydroxylation temperatures are required to completely remove the adsorbed hydroxyl species[43,44] (up to 770 K for the Zn polar surface[85]- see below). Both water (and CO_2) adsorb onto the surface of ZnO during sample storage in the atmosphere, and have been noted to evolve from the heating of fresh samples[25,88]. The formation of a hydroxy-carbonate complex has been identified[88] with stoichiometry $Zn(OH)_6(CO_3)_2$ due to slow reaction of the adsorbed atmospheric water and CO_2.

Water is well known as a surface poison for a number of ZnO catalysed reactions, for example hydrogenation and isomerisation of ethylene and H_2-D_2 exchange reactions[40] and for alcohol decomposition[89]. The adsorption of Type I hydrogen is particularly sensitive to the presence of water on the catalyst surface[40] since they occupy the same surface sites[27] (also see previous section). The adsorption of CO_2 and CO have also been shown to similarly be retarded by the presence of water on the catalyst[79,80,90] (also see previous sections).

The $(10\bar{1}0)$ non-polar face (which consists of equal numbers of Zn and O ions with coplanar centres) hydrates with hydroxyl groups bonding to Zn ions and hydrogens to oxygen. This leads to a completion of the tetrahedral coordination for both surface Zn and oxygen ions. The coplanar lattice structure results in the adsorbed hydroxyl groups forming prominent "rows" separated from one another by narrow "channels"[44]. This arrangement, in combination with the

close interionic distances, has been suggested to allow the formation of hydrogen bonding between all the hydrogens in the surface hydroxyl groups, producing an essentially closed surface structure[43,44].

Adsorption sites on the Zn polar surface are associated with the Zn ions of the outermost layer[43,44]. Adsorption of hydroxyls onto this surface produces an array in which every Zn ion is four coordinate, threefold to lattice oxygens, with the remaining tetrahedral position occupied by the oxygen atom of the hydroxyl [43,86]. The adsorption of hydroxyls onto the reconstructed $(000\bar{1})$ surface has been proposed to occur by hydroxyls bonding onto Zn ions present in the trigonal oxygen sites of the reconstructed lattice[43]. On the Zn (0001) (and to a lesser extent the O polar) surface the adsorbed hydroxyls will be coplanar, each OH group being oriented normal to the surface plane[43,44]. On the (0001) surface each hydroxyl has 6 equidistant neighbours at 3.25 Å. A combination of this distance and of the coplanar hydroxyl structure precludes the formation of inter-hydroxyl hydrogen bonds[43,44].

It has been proposed[44] that the hydroxylated polar (0001) and $(000\bar{1})$ faces will be more active for water physisorption than the non-polar faces because they contain only isolated hydroxyl groups, whereas the hydroxylated non-polar faces present a closed structure (due to the high degree of hydroxyl hydrogen bonding) to any oncoming water molecules. Only weak adsorption forces will be present, therefore resulting in the non-polar faces being the least active for water physisorption.

Thermal desorption studies[27,85] on ZnO have further shown water to be readily adsorbed and strongly held on ZnO. The hydroxyl species

present on O polar, non-polar and stepped non-polar single crystal surfaces have been found to be less stable than those adsorbed on the Zn polar surfaces where desorption temperatures of nearly 770 K are required to remove adsorbed hydroxyls[85]. These strongly bound hydroxyls have been shown in a recently published paper to be associated with the Type I hydrogen sites[27] (see section 2.4.1). Lower temperature desorption peaks are obtained from the prism surface indicative of weaker surface interactions, with the lowest temperature states (approximately 400 K) possibly due to molecularly adsorbed water[85]. Both the non-polar and stepped non-polar surfaces have been shown to behave in a similar manner indicating that step sites are not required for hydroxyl adsorption[85]. Desorption of water gave only a single low temperature peak at about 400 K for both types of crystal face. However, contradictory conclusions have been drawn from a temperature programmed study by Morishige et al[91] where the most stable hydroxyls were attributed to adsorption on the prism, rather than the Zn polar, surface. It was felt that the formation of inter-hydroxyl hydrogen bonds on this surface (described above) would result in additional adsorption[44,91] stability compared to the polar surfaces, where such hydrogen bonding is absent, and lead to the high observed desorption temperatures.

(2.4.5) Methanol Decomposition on Zinc Oxide

Methanol adsorbs and decomposes on ZnO to produce CO, H_2 and CO_2. Formaldehyde can also be formed depending on the reaction conditions. The decomposition proceeds by a sequential pathway involving adsorbed methoxy ($CH_3O_{(a)}$) and formate ($CHOO_{(a)}$) intermediates [25-27,92,93]. Confirmation of the existence of the formate intermediate

has been made in a number of temperature programmed and infra-red spectroscopy studies[25-27,92-94].

Temperature programmed studies have shown hydrogen to be evolved in the temperature range 450 to 550 K in a process corresponding to the decomposition of the methoxy to formate species[93,95], while the simultaneous desorption of H_2, CO and CO_2 in the temperature range 580-635 K has been assigned to the reaction limited decomposition of the formate[25,27,92,93,95]. The main path for formation of CO has been shown to be via the decomposition of formate rather than methoxide[92]. The formation of formate requires the incorporation of a surface oxide ion thus resulting in the net reduction of the ZnO surface[94,95]. The subsequent desorption of CO_2 removes this oxygen from the surface; calculations have shown that approximately 8% of the surface lattice oxygen can be removed in this manner[94]. It has been suggested that the removal of lattice oxygen results in a formal reduction of Zn cations to Zn metal[95].

It has also been suggested the formation of CO_2 and D_2 may possibly be the result of reaction between methanol and an adsorbed formate ion according to[84]:

$$CD_3OD_{(g)} + DCOO_{(a)} \rightarrow D_2 + CO_2 + CD_3O_{(a)} \qquad [1]$$

$$CD_3O_{(a)} + O_{(s)} \rightarrow DCOO_{(a)} + D_{2(g)} \qquad [2]$$

Tarawah and Hansen[94] have found in the temperature range 453-513 K, methanol decomposed to H_2 and CH_2O, while at higher temperature (563-613 K) CH_2O, CO, CO_2, and H_2 were formed. Temperature programmed desorption studies of methanol decomposition on polycrystalline ZnO[25,83] have also resolved two similar desorption regimes. At low temperature (340 K) coincident desorption of methanol, CH_2O, CO, H_2,

CO_2 and H_2O was found, with the methanol and CH_2O desorption peaks ascribed to formation and decomposition of a surface methoxy species according to:

$$CH_3O_{(a)} + H_{(a)} \rightleftarrows CH_3OH_{(g)} \quad [3]$$

$$CH_3O_{(a)} + O_{(s)} \rightleftarrows H_2COO_{(a)} + H_{(a)} \quad [4]$$

$$H_2COO_{(a)} \rightleftarrows H_2CO_{(a)} + O_{(s)} \quad [5]$$

$$H_2CO_{(a)} \rightleftarrows H_2CO_{(g)} \quad [6]$$

The coincident CO, H_2, CO_2 and H_2O desorption peaks are proposed to result from decomposition of a formyl type surface species:

$$H_2CO_{(a)} \rightleftarrows HCO_{(a)} + H_{(a)} \quad [7]$$

$$HCO_{(a)} \rightleftarrows H_{(a)} + CO_{(a)} \quad [8]$$

$$H_{(a)} + H_{(a)} \rightleftarrows H_{2(g)} \quad [9]$$

A second desorption regime at high temperature results in the coincident desorption of CO, H_2 and H_2O at 580 K and CO_2 and H_2O at 550 K, due to the decomposition of a formate intermediate:

$$HCOO_{(a)} \rightarrow H_{(a)} + CO_{(a)} + O_{(s)} \quad [10]$$

$$HCOO_{(a)} \rightarrow H_{(a)} + CO_{2(a)} \rightarrow CO_{2(g)} \quad [11]$$

$$CO_{(a)} \rightarrow CO_{(a)} \quad [12]$$

$$CO_{2(a)} \rightarrow CO_{2(g)} \quad [13]$$

$$2H_{(a)} \rightarrow H_{2(g)} \quad [14]$$

$$2H_{(a)} + O_{(s)} \rightarrow H_2O_{(g)} \quad [15]$$

On the basis of temperature programmed desorption from single crystals, separate mechanisms have been proposed by Cheng et al[84,85] for methanol decomposition on the polar and non-polar ZnO surfaces. On the non-polar and stepped surfaces methanol decomposes in two pathways; either to form methane and adsorbed oxygen at 423 K or via oxidation of the methoxide to a formate-like species which decomposes at 653 K:

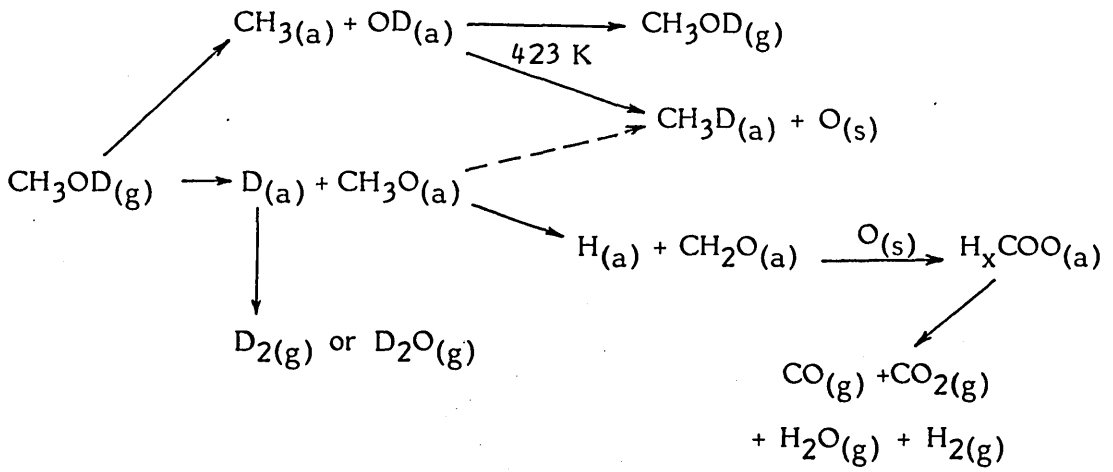

On the Zn polar surface two competitive decomposition pathways (dehydrogenation and oxidation), via a common formaldehyde intermediate, are proposed:

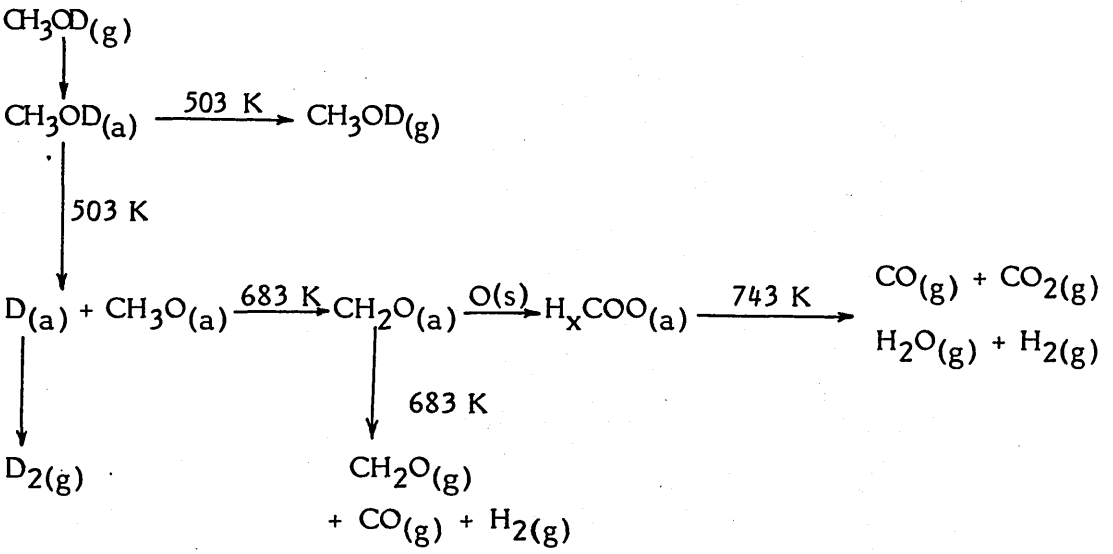

The formate species is labelled $H_xCOO_{(a)}$ to reflect the unknown stoichiometry of this species and to allow for a different hydrogen content at different coverages (for formic acid adsorption x=1, for methanol and formaldehyde adsorption x>1). The selectivity for the two routes was coverage dependent, with the dehydrogenation route favoured at higher coverages[85].

Two methanol decomposition channels have been resolved by Griffin et al[95] corresponding to the decomposition reactions of methoxy and

formate intermediates. The kinetic process for the conversion of surface methoxy into formate was evidenced by a hydrogen peak at 585 K, with simultaneous evolution of CH_2O (but not CO or CO_2). A mechanism was proposed, the first step being dissociative adsorption of methanol at Zn-O pair sites:

$$CH_3OH + Zn_{(s)} + O_{(s)} \rightarrow Zn_{(s)}\text{-}OCH_3 + HO_{(s)} \qquad [16]$$

Not all the methanol dissociatively adsorbs, as was shown by the formation of a low temperature desorption peak at 400 K due to co-ordinatively adsorbed methanol. Decomposition of the methoxy intermediate was proposed to occur before any recombinative CH_3OH desorption:

$$Zn_{(s)}\text{-}OCH_3 + Zn_{(s)} \rightarrow Zn_{(s)}\cdots OCH_2 + Zn_{(s)}H \qquad [17]$$

H_2 desorption observed immediately after this step inferred that the proton transfer was to a neighbouring Zn^{2+} cation, and not to an O^{2-} anion, since this would have resulted in water desorption:

$$Zn_{(s)}H + HO_{(s)} \rightarrow Zn_{(s)} + O_{(s)} + H_{2(g)} \qquad [18]$$

The adsorbed CH_2O intermediate produced by [17] is relatively short-lived, desorbing either as gas-phase CH_2O or reacting to form a stable adsorbed formaldehyde or formate by interaction with an O^{2-} anion. If such an anion is not present then desorption occurs:

$$Zn_{(s)}\cdots OCH_2 \rightarrow Zn_{(s)} + CH_2O_{(g)} \qquad [19]$$

but if such an anion is available, the intermediate is stabilised:

$$Zn_{(s)}\cdots OCH_2 + O_{(s)} \rightarrow Zn_{(s)}\text{-}OCH_2\text{-}O_{(s)} \qquad [20]$$

The subsequent desorption products (H_2, CO, CO_2) are observed at the same temperature (635 K) due to decomposition of the formate species. Conversion of adsorbed formaldehyde into a formate species readily occurs between 585 K and 635 K resulting in the formal reduction of the carbon atom oxidation state:

$Zn_{(s)}\text{-}OCH_2\text{-}O_{(s)} + Zn_{(s)} \rightarrow Zn_{(s)}OCHO_{(s)} + Zn_{(s)}H$ [21]

with hydride transfer again onto an adjacent Zn cation. It was suggested that removal of O^{2-} anions from the lattice was accompanied by the reduction of Zn cations to Zn metal.

A number of different proposals have been made as to which step of methanol decomposition is rate determining. These have included the decomposition of molecularly adsorbed methanol to methoxy and adsorbed hydrogen i.e O-H bond cleavage[96], cleavage of a C-H bond[94,95,25] and C-O bond cleavage during the decomposition of surface formate[85].

Several proposals have also been made as to the nature and location of the active sites on the ZnO surface. A certain degree of surface reduction has been found required for optimal decomposition activity, identified as a requirement for unsaturated O^{2-} surface anions to stabilise the formate and formaldehyde intermediates[95]. The active sites have been suggested to be situated at edge sites or as isolated patches of defected surface that exposed such ions[95]. Bowker et al[25,83] also felt that a defective surface (i.e. one that contained oxygen vacancy sites) was a requirement for good decomposition activity.

The decomposition reactivity has been found to depend markedly on the detailed atomic structure of the surface[84,85]. The polar (0001) surface was found to exhibit a completely different product distribution compared to the non-polar surfaces, with dehydrogenation the predominant reaction[84,85] (possibly resulting from the fact that this surface is more metal-like than the non-polar or stepped surfaces). The difference in the nature of decomposition on this surface has been attributed to the strong dipole moment present which enhanced

interaction between the surface and polar molecules (such as methanol)[84,85]. The decomposition activity order paralleled surface defect densities, further suggesting[84,85] the active sites are directly associated with anion vacancies or step defects, and also that step defects must behave like anion vacancies i.e. the local bonding environment of a step site is closer to that of an anion vacancy than a site on the terrace surface.

It has been proposed that the active sites for methanol decomposition and synthesis (i.e. the sites for formate formation) are confined to the polar surfaces only[25,83,94]. However, more recently it has been shown that the Zn polar surface does not appear to play an important role in methanol decomposition or synthesis[27] and the formate intermediate is associated mainly with the prism surfaces[26].

(2.4.6) Ethanol Decomposition on Zinc Oxide

The decomposition of ethanol on ZnO proceeds in two main reaction pathways[97]. Firstly, by dehydrogenation to acetaldehyde and hydrogen:

$C_2H_5OH \rightarrow H(CH_3)CO + H_2$ [1]

and secondly, by dehydration to ethylene and water:

$C_2H_5OH \rightarrow C_2H_4 + H_2O$ [2]

Oxidation can also occur (see below) to form surface acetate species ($CH_3COO_{(a)}$), analogous to formate formed from methoxy in methanol decomposition. The acetate decomposes to give products that include CO, CO_2, H_2 and water[97,98].

An investigation by Mokwa et al[97] of temperature programmed decomposition of ethanol on the non-polar surface found adsorption of ethanol produced the desorption peaks: ethanol (at 400 K),

acetaldehyde (400 K), molecular hydrogen (500 K), water (410 K), and ethylene (550 K). From the oxygen polar surface[97] a similar range of desorption products was observed but with desorption temperatures 20-40 K higher than from the non-polar surface. Adsorption of acetaldehyde on both surfaces produced only an acetaldehyde peak at 380-390 K, and confirmed the production of acetaldehyde from ethanol to be activated. Ethanol adsorption at 300 K onto a sintered ZnO sample[97] produced similar desorption products: ethanol (430 K), hydrogen and acetaldehyde (485 K). Methane and water were also evolved in this temperature range, while at above 600 K CO, water and CO_2 were detected. An increase in the measured surface conductivity at higher temperatures also pointed to a reaction of adsorbed acetaldehyde and surface oxygen to produce acetic acid and an oxygen vacancy:

$$H(CH_3)CO_{(a)} + O_{(s)} \rightarrow V_{(o)} + CH_3COOH_{(a)} \qquad [3]$$

Two routes were proposed for acetic acid decomposition to account for this compound not being detected in the desorption spectra:

$$CH_3COOH \rightarrow CH_2{=}CO + H_2O \qquad [4]$$

$$CH_3COOH \rightarrow CH_4 + CO_2 \qquad [5]$$

Although ketene (reaction [4]) was not observed directly, the detection of CO (mass 28) by mass spectrometer pointed to an occurrence of this species. The following overall reaction scheme was proposed for ethanol decomposition on sintered ZnO[97]:

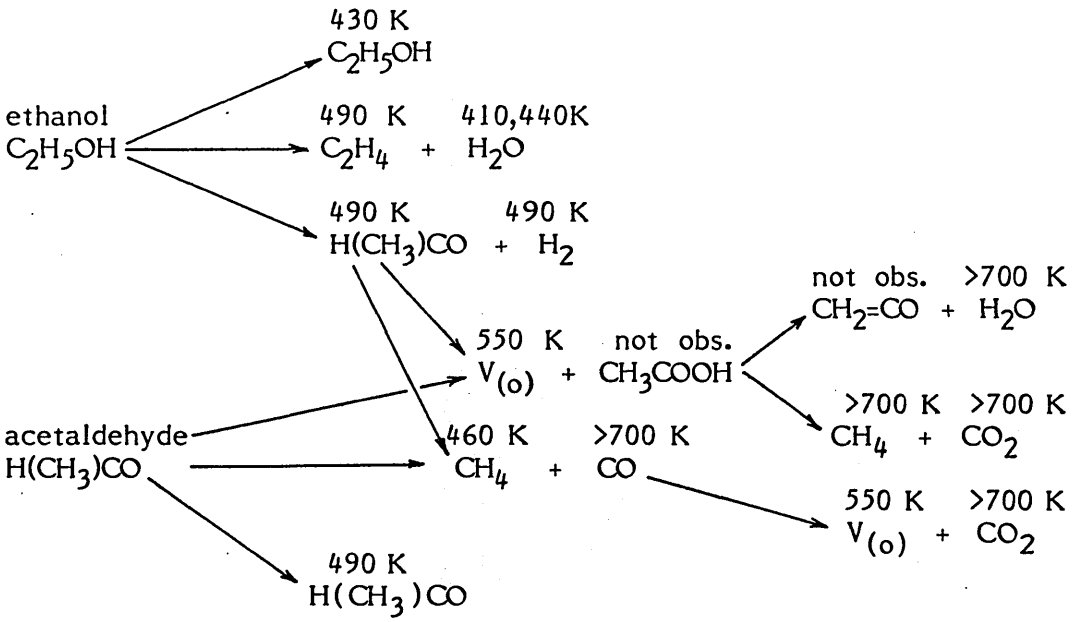

A study of the temperature programmed decomposition of ethanol on polycrystalline ZnO by Bowker et al[99] found the decomposition to be selective toward dehydration to ethylene (10:1 ethene to acetaldehyde ratio). Two temperature regimes of different reactivity were observed. The first, at 380-420 K, was characterised by desorption of the parent alcohol, while the second, at 510 K, corresponded to the formation of decomposition products. The initial step for ethanol adsorption was proposed to be formation of a surface ethoxide species:

$$C_2H_5OH_{(g)} + O_{(s)} \rightleftarrows C_2H_5O_{(a)} + OH_{(a)} \qquad [6]$$

Approximately 40% of the total amount of adsorbed ethanol was desorbed as the parent molecule at 360-410 K in a reverse of this reaction. The activation energy for the recombination process was suggested to be that for migration of hydrogen back to the surface alkoxide species. At 510 K the remaining adsorbed ethoxy species decomposed and desorbed as hydrogen, ethylene and C_2H_4O (most likely acetaldehyde although ethylene oxide was also felt a possibility). The temperature coincidence of the evolved ethylene, acetaldehyde and hydrogen peaks showed they were derived from a common intermediate, with β C-H bond

scission proposed to be the rate determining step (on the basis of the observed hydrogen evolution and the high ethylene selectivity). The dominance of β interaction over that of the α hydrogen (which would have produced acetaldehyde) further suggested that reaction was confined to the Zn (0001) face, in agreement with these workers earlier conclusions for methanol decomposition (see previous section). On the non-polar surface it was felt that α hydrogen interaction would have been an equally preferred route that would have resulted in the formation of acetaldehyde. The requirement for accessible O^- sites also suggested the active surface to be the highly defected (reduced) Zn polar face. At 510 K β hydrogen atom abstraction and hydrogen desorption was proposed to leave an unstable C_2H_4O species on the surface that had two possible decomposition channels; either C-O bond scission resulting in ethylene desorption, or Zn-O scission resulting in C_2H_4O desorption[99]:

$$CH_3CH_2O_{(a)} + O_{(s)} \rightarrow CH_2CH_2O_{(a)} + OH_{(a)} \qquad [7]$$

$$CH_2CH_2O_{(a)} \rightarrow CH_2CH_{2(g)} + O_{(s)} \qquad [8a]$$

$$CH_2CH_2O_{(a)} \rightarrow C_2H_4O_{(g)} \qquad [8b]$$

No water desorption was detected and it was proposed[99] that oxygen atoms remaining on the surface after reaction [8a] were redistributed by surface migration over the entire ZnO to result in surface reoxidisation. Bowker et al[98] also found acetaldehyde adsorption resulted in the formation of surface acetate species:

$$CH_3CHO_{(a)} + O_{(s)} \rightarrow CH_3CHOO_{(a)} \qquad [9]$$

$$CH_3CHOO_{(a)} \rightarrow CH_3COO_{(a)} + H_{(a)} \qquad [10]$$

Ethene desorption at 530 K also pointed toward the formation of ethoxide in a reverse of reaction [8b], followed by subsequent β hydrogen

abstraction.

Similar ethanol decomposition behaviour has been observed on other oxide catalyst surfaces. Ethoxide and acetate surface species have been detected after adsorption on both basic oxides, such as MgO[100-102], and acidic oxides, such as alumina[103]. Acetate formation has been shown to be an activated process since it does not occur below temperatures of approximately 425 K[100,101,103]. Kagel et al[100,103] have proposed the oxidation to acetate to occur by interaction of the ethoxide with surface oxygen (either lattice oxygen or adsorbed hydroxyl oxygen):

$$CH_3CH_2OH + O_{(s)} \rightarrow CH_3CH_2O_{(a)} + OH_{(a)} \qquad [11]$$

$$CH_3CH_2O_{(a)} + [O_{(s)} \text{ or } OH_{(a)}] \rightarrow CH_3COO_{(a)} + H_{2(g)} \qquad [12]$$

Mass-spectrometry has confirmed the presence of hydrogen[100,103].

MgO has been found to act as a dehydration catalyst at very low ethanol partial pressures[101,102] decomposing ethanol to either ethene[102] or to butadiene[101]. However, under relatively high ethanol partial pressure MgO becomes dehydrogenating and aldehyde is produced [101,102]. The presence of gas phase (or physisorbed) alcohol molecules, acting as Brønsted acids and reacting with adsorbed ethoxide was proposed by Parrott et al[102] to explain this dehydrogenation selectivity at high ethanol pressures:

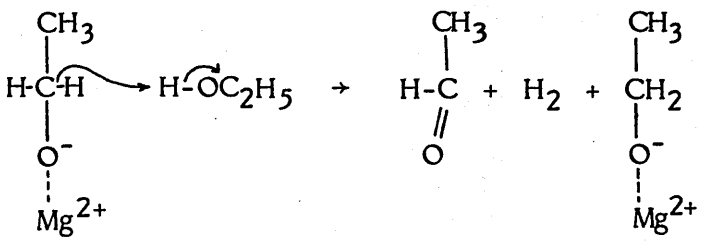

(2.4.7) Propanol Decomposition on Zinc Oxide

The decomposition of 2-propanol is used as a model reaction for studying the principles of catalyst selection[104]. On ZnO the decomposition has two main reaction pathways that are essentially free of side reaction[104]:

$$(CH_3)_2CH\text{-}OH \rightarrow (CH_3)_2C{=}O + H_2 \quad [1a]$$

$$(CH_3)_2CH\text{-}OH \rightarrow CH_3CH_2{=}CH_2 + H_2O \quad [1b]$$

i.e. dehydrogenation to acetone and hydrogen and dehydration to propene and water. ZnO is highly selective, under normal operating conditions to dehydrogenation, and has been chosen as a baseline standard dehydrogenation catalyst by Krylov[104]. The decomposition selectivity can, however, depend on the conditions of the alcohol adsorption or decomposition. Wheeler et al[105] adsorbed 2-propanol onto dehydroxylated ZnO at low temperature, and on thermal desorption, found the main decomposition product to be propene, with acetone only produced in a minor amount. The amount of water produced was less than the propene formed, while the quantity of hydrogen was in excess of the acetone. Carbon dioxide was also observed to form from the decomposition of an unidentified adsorbed complex. The high dehydration selectivity was proposed to be due to the ZnO surface behaving as a reactant rather than as a catalyst, and a consequence of the strong affinity shown by the ZnO surface for water (evidenced by high dehydration temperatures required to recover adsorbed water). In comparison, under the batch reactor conditions of a closed circulating reactor system at 363 K, Tamaru et al[106,107] found a more "typical" product distribution with acetone and hydrogen produced as the main decomposition products (90% selectivity), while only minor amounts of

propene and water were formed.

In the equivalent decomposition over ZnO, 1-propanol also undergoes dehydration to propene, while the dehydrogenation reaction forms propionaldehyde[108].

Using IR spectroscopy, Tamaru et al[106] identified 2-propanol to adsorb dissociatively at 363 K to form zinc alcoholate and a hydroxyl group on the surface of ZnO. Heating the alcoholate was found to produce hydrogen and to form the IR bands of an adsorbed enol species of the type:

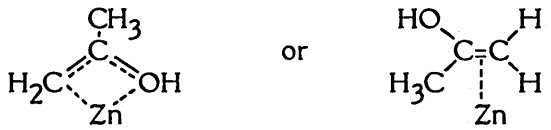

The enol structure was confirmed by acetone adsorption which was also found to produce the enol surface species[106] (see below). As desorption of 2-propanol derived acetone was found not to occur at 363 K in the absence of gas phase 2-propanol[107], it was proposed the reaction required the presence of 2-propanol to displace the surface enol. A certain amount of enol adsorbate also appeared to be converted into a non-volatile surface species that inhibited the reaction rate. This was suggested to be a polymerised species of acetone such as acetylacetone. Isotope labelling revealed that the hydrogen molecule was produced by the recombination between dissociatively adsorbed hydrogen and the α carbon of the alcoholate. The overall reaction scheme for 2-propanol decomposition was proposed to be[107]:

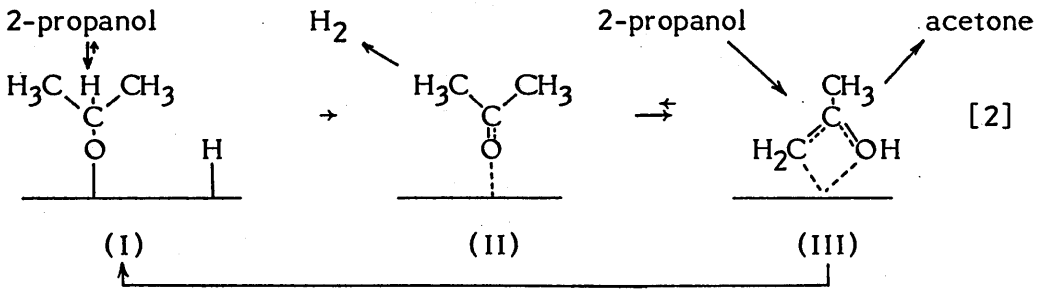

[2]

The dissociative adsorption of the 2-propanol, the desorption of the enol and the keto-enol configuration change (steps (II) to (III)), were all considered to be faster than the surface dehydrogenation of the alcoholate (steps (I) to (II)) i.e. the formation of the hydrogen molecule was rate determining.

Manazec has proposed[37] a mechanism for secondary alcohol dehydration over metal oxide catalysts, also through an intermediate enol species. In this mechanism the alcoholate is dehydrogenated by transfer of a hydride from the α carbon atom to a nearby metal ion or hydroxyl group to generate a bound ketone. The ketone is then deprotonated from the β carbon to give the enolate, which can then be reprotonated at the α carbon to liberate the olefin.

The enol surface species has also been identified by Miyata et al[109] as an intermediate in oxidation of 2-propanol over ZnO. Adsorbed isopropoxide species were observed to dehydrogenate to form acetone, and to oxidise to form surface acetate and formate species via the enolate complex at approximately 433 K. Similar acetate species have also been observed after 2-propanol adsorption on MgO[110]. The following reaction scheme was proposed:

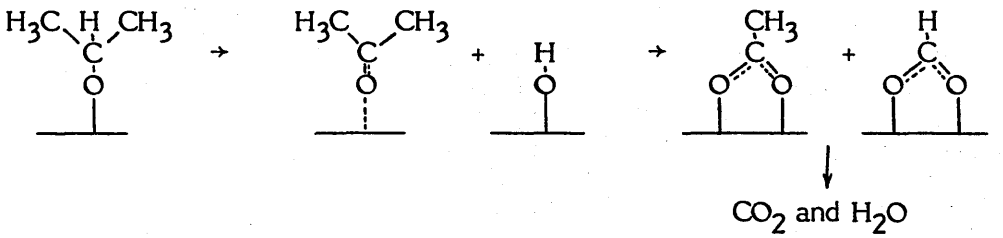

[3]

Acetate and carboxylate surface species have also been identified on a range of other metal oxide catalyst surfaces after 1-propanol and 2-propanol adsorption[103,111-113]. Carboxylate formation after 2-propanol adsorption on alumina[112] and ceria [113] has been

proposed[113] to occur by the reaction:

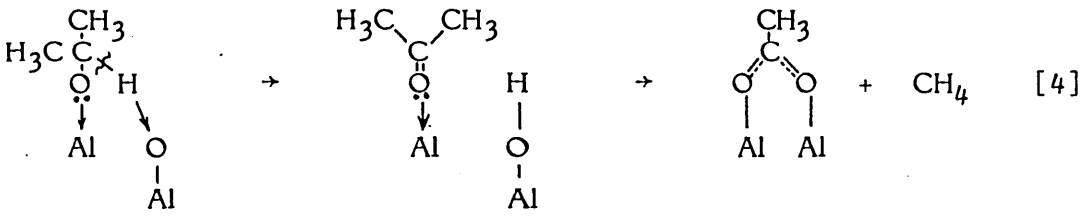

[4]

The formation of gaseous methane produced by this reaction was confirmed by mass spectrometry[112,113]. An acetone reaction intermediate was proposed (for adsorption on alumina) since the carboxylate was also observed after acetone adsorption by Deo et al[112]. An aldol condensation-type mechanism between a surface alkoxide and acetone has also been suggested as an alternative route for acetate formation on ceria that also gives i-butene as a reaction product[113].

Carboxylate formation after 1-propanol adsorption on alumina has been proposed to occur in an equivalent reaction to that given for 2-propanol[103, 111] above:

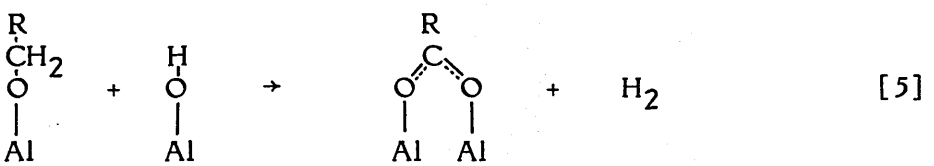

[5]

Gaseous hydrogen evolved by this reaction was detected during the course of the oxidation[103,111].

Temperature programmed desorption has shown 1-propanol and 2-propanol decomposition on ZnO to be structure sensitive[108,114,115]. A single crystal study of 2-propanol decomposition by Kung et al[114] found the Zn and O polar and prism surfaces to evolve five desorption and decomposition products: undecomposed 2-propanol, hydrogen, acetone, water and propene. Dehydrogenation was the dominant reaction, with the peak temperatures highest for the Zn polar surface and lowest

for the O polar surface. Acetone and propene always appeared at the same temperature suggesting that they were formed from a common surface intermediate. Hydrogen was evolved coincident with acetone on the Zn and O polar surfaces but at a lower temperature on the nonpolar surface. Water desorption peaks were found to be desorption, rather than reaction, limited. Although the low peak temperatures suggested the O polar surface should be the most active in 2-propanol decomposition, the high temperature for water desorption from this surface (598 K) indicated that under steady-state reactor conditions the surface would effectively become poisoned by adsorbed hydroxyls.

In a temperature programmed desorption study by Bowker et al[108] using a polycrystalline ZnO, 1-propanol was found to reversibly desorb at low temperature (300-500 K), with the decomposition products propionaldehyde, propene and hydrogen produced at higher temperature (approximately 540 K). The propionaldehyde peaked slightly before the other two products (by approximately 13 K). Similar results were obtained by the same workers for 2-propanol[115], where acetone also peaked slightly before propene and hydrogen. For both alcohols, the propene peak width was narrower than that of the dehydrogenation product, with the hydrogen peak width intermediate between the two. Although 2-propanol was found to decompose around 60 K lower in temperature than 1-propanol, it gave a similar decomposition product ratios. Bowker et al[108] proposed a general mechanism for C_{2+} alcohol decomposition on ZnO consistent with the temperature programmed desorption results:

Adsorption at 310 K:

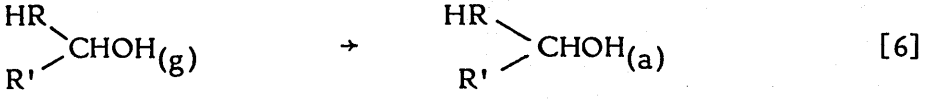

[6]

Reaction with the surface at 310 K:

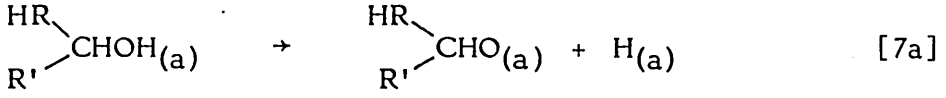

[7a]

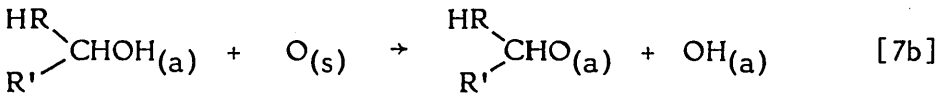

[7b]

[8a]

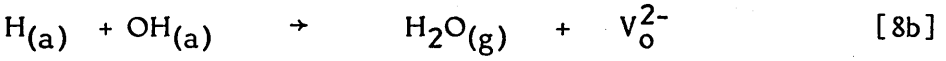

[8b]

Desorption (300-500 K):

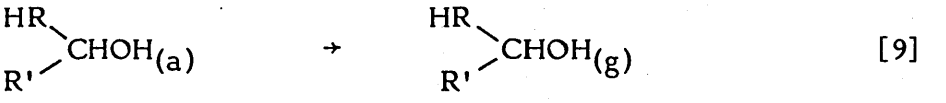

[9]

Decomposition at 500-550 K:

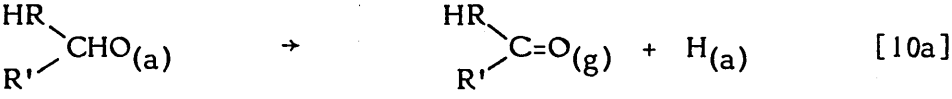

[10a]

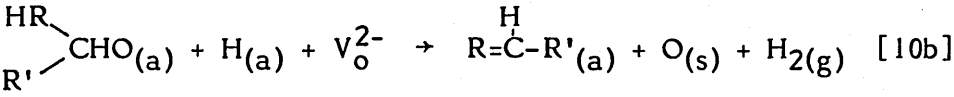

[10b]

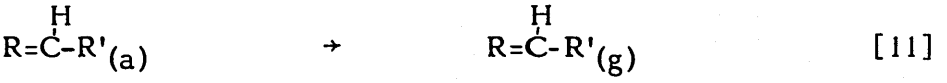

[11]

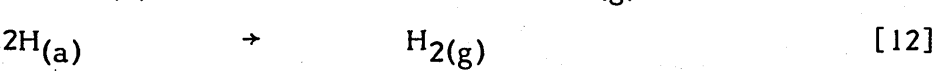

[12]

The initial adsorption step was thought to be activated since it was found to proceed slowly, followed by dissociation of the alcohol upon adsorption to form the corresponding surface alkoxide. Steps [7b] and [8b] were inferred from the reproducibility of the decomposition pattern without any prereduction treatment, while step [10b] was assumed in order to account for the fact that no water desorption was detected. Similarly, because no low temperature evolution of hydrogen was observed, it was thought steps [7a] and [8a] also occurred at the adsorption stage. Two types of alkoxide were postulated; one next to an anion vacancy V_o^{2-} and one at an unperturbed site. The former

resulting in the production of alkene through "healing" of the defect (steps [10b] and [11]), while the latter produced the aldehyde/ketone (step [10a]).

The dehydrogenation surface sites were proposed by Bowker et al[108,115] to be associated with the Zn (0001) polar surface, while the other reaction sites were thought to be located either on the O polar or non-polar surfaces. The α C-H bond scission yielding the dehydrogenation product (step [10a]) formed a highly mobile hydride species. Attack by this hydride species (from an adjacent cation site) on the alkoxide associated with the defects produced the alkene through an induced β hydrogen elimination/abstraction. The transition state for this reaction was visualised as[115]:

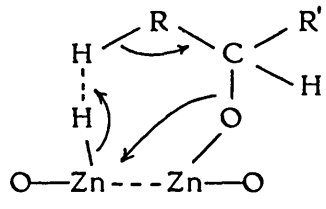

The two step mechanism of hydride production followed by β hydrogen abstraction was suggested[115] to explain the similarity in decompositional temperatures for the two different alkoxy species. The alkoxy associated with the anion vacancy was considered to be the more strongly bound and the hydride reaction caused C-O bond scission. The small difference in the decomposition temperatures of the two types of alkoxyls was proposed to be due to an additional small activation energy for the hydride induced β elimination/abstraction.

Since they are produced as decomposition products from 2-propanol, the adsorption behaviour of acetone and propene is also relevant. As noted previously, acetone adsorption on ZnO has been shown to result in the formation of IR bands corresponding to the presence

of adsorbed enol species[106] (the structural form of the enol has been given above). Temperature programmed desorption studies[114,115] have not, however, confirmed the formation of the enol, although the non-polar single crystal surface was noted by Kung et al[114] to produce a more stable form of acetone attributed as being possibly due to the enol. Isotopic hydrogen redistribution by adsorbed acetone has suggested Zn-O pair sites to be required for this dissociative adsorption[116]. Deo et al[112] found adsorption of acetone on alumina at 493 K to produce the same IR characteristics as 2-propanol derived carboxylate, and a mechanism was proposed with acetone as an intermediate in the formation of the carboxylate (see above). The detection of methane produced by the oxidation of acetone supported this mechanism. The adsorption of acetone at 423 K on ceria has also been found[113] to form the carboxylate species. Contrary to these findings, temperature programmed desorption has found no evidence for carboxylate formation after acetone adsorption on ZnO single crystal [114] and polycrystalline samples[115].

Propene is both weakly and strongly adsorbed on ZnO[117], although the weakly bound propene is rapidly desorbed at room temperature. The presence of propene was found by Dent et al[117] to block out the hydrogen chemisorption on Zn-O pair sites. Isotopic labelling supported the view that propene was adsorbed dissociatively as a π-allyl species. The adsorption of propene was proposed[117] to occur as:

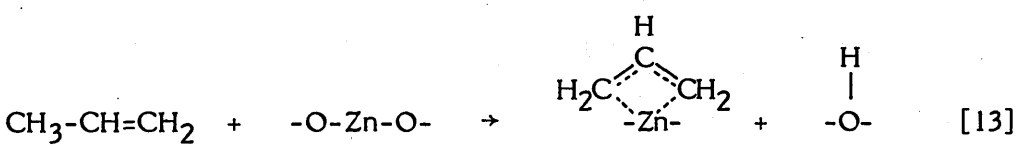

[13]

Davydov et al[118] found the thermal desorption of propene from an oxidised ZnO produced a high temperature peak (673 K) corresponding to the desorption of the products of complete oxidation (CO_2 and water) and an oxidised surface species in the form of a carbonate-carboxylate was proposed. Nakajima et al[119] has more recently confirmed the formation of carboxylates, such as acetate and formate, in the propene oxidation reaction. The precursor of the carboxylate species appeared to be formed by addition of two oxygen atoms to each adsorbed propene molecule and it was tentatively proposed[119] that the precursor had an olefinic as well as alcoholic character. Isotopic labelling suggested, in the reaction of the π-allyl species with adsorbed molecular oxygen, one adsorbed oxygen was incorporated into the π-allyl to form a surface complex, while simultaneously one surface lattice oxygen was transferred to the complex. The remaining adsorbed oxygen then reoxidised the surface. Propene appeared not to interact with lattice oxygen of ZnO in the absence of gaseous oxygen.

CHAPTER 3

TEMPERATURE PROGRAMMED DESORPTION

(3.1) Introduction

Temperature Programmed Desorption (TPD) provides information on how an adsorbate interacts, for example chemisorbs or decomposes, on the surface of a porous solid catalyst. The technique was first reviewed in detail by Cvetanović and Amenomiya[120,121] and more recently by Falconer and Schwarz[24]. TPD is an extension of the flash desorption techniques used to study adsorption onto metal filaments and single crystal surfaces under ultra-high vacuum conditions, applied to powdered porous catalyst surfaces in an inert gas flow, usually at atmospheric pressure.

In a typical TPD experiment a small amount of the catalyst is contained within a reactor and through which an inert carrier gas flows, for example helium, at atmospheric pressure. The reactor in turn is surrounded by a heating furnace. A gas is adsorbed onto the catalyst surface, typically by pulse injections of the adsorbate into the carrier gas stream above the reactor. After any extra adsorbate gas is flushed from the system, the catalyst is heated by the furnace at a steady linear rate. A detector downstream of the reactor measures changes in adsorbate concentration in the carrier gas as it desorbs from the catalyst surface as the temperature is increased. The desorption rate increases, eventually passes through a maximum, and falls back to the zero level as the catalyst surface becomes depleted in the adsorbate (figure 3.1). Further details of the TPD experimental method and equipment are presented in chapter 4.

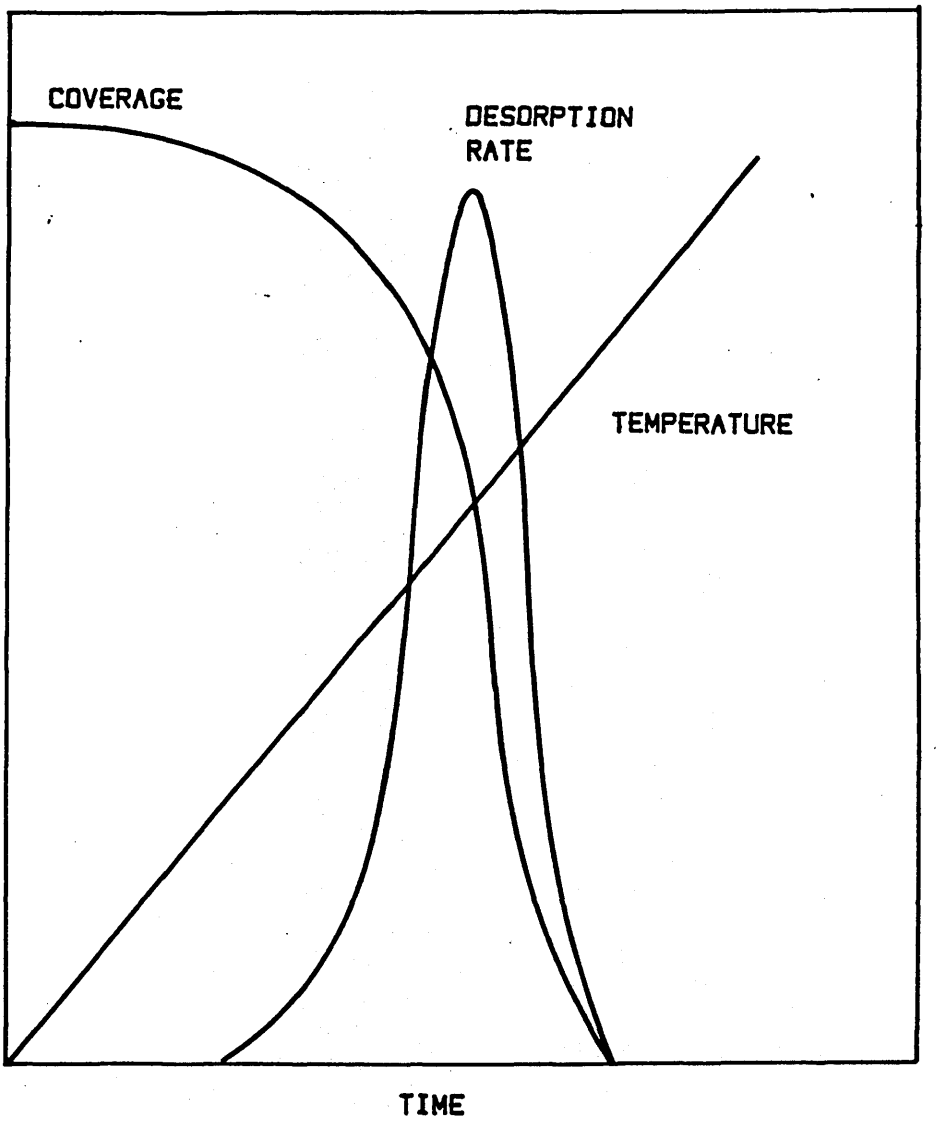

Figure 3.1: The time dependence of the surface coverage, desorption rate and temperature during temperature programmed desorption.

A record of the concentration of desorbed material in the carrier flow as a function of catalyst bed temperature is known as a TPD spectrum. In general, a spectrum will consist of one or more peaks. The shapes and positions of the peak maxima are related in a fundamental way to the desorption process and give information about the adsorption sites on the catalyst surface and the desorption kinetics related to these sites[120,121]. Provided mass transfer limitations (both intraparticular and within the catalyst bed) are not significant, the detector response is proportional to the rate of desorption (these aspects are considered more fully in section 3.2).

The following information can be obtained from analysis of a TPD spectrum[24]:

(i) specific activities are obtained directly for each product independent of surface area measurements. The number and activities of different adsorption sites can be determined since TPD can detect differences between the specific activities of different sites which steady state experiments on the same catalyst would not reveal.

(ii) the amount of an adsorbate desorbed is simply obtained by the area under the desorption curve.

(iii) the relative temperatures at which each of the desorption products leave the surface provide detailed information about reaction mechanisms.

(iv) reaction steps are separated in time by their relative rates.

(v) the surface coverages of reactants and the surface composition of adsorbed species at the time that the products are being formed are determined directly.

(vi) the order of reaction or desorption can be evaluated from analysis of curve shapes or from variation in initial coverages.

(vii) activation energies of reaction or desorption, from analysis of peak temperatures and curve shapes or from variations in the heating rates, can be calculated.

(viii) TPD can be used to make "fingerprint"-type characterisations, for example, to compare one catalyst against another.

Quantitative analysis of a TPD spectrum allows the kinetics of the desorption processes to be determined explicitly. However, such interpretations and analyses can be obscured by experimental considerations that can significantly distort the shapes of the spectra obtained. Recent studies with both real and model catalyst systems [122-128] have shown the desorption peak shape to be very strongly influenced by the effects of gas readsorption and diffusional mass transfer, as well as by the intrinsic desorption kinetics (see section 3.2). However, although these effects cannot be eliminated, they can be minimised by careful experimental design[122,123].

When the inert carrier gas is replaced by a reactive gas, or when two reactive gases are co-adsorbed, the technique is referred to as temperature programmed reaction (TPR). The desortion spectra obtained from TPR experiments can be extremely complex since they involve a combination of the desorption of reactants, reaction products and decomposition products from either the reactants or products or both. A TPR spectra gives information on rates of reaction as well as desorption activities. Falconer and Schwartz[24] think it unlikely that a complete theoretical description to explain TPR of single and multiple reactants will be developed in the same manner that the TPD of relatively simple unreacting adsorbate systems have been characterised. TPR

spectra can still provide direct information on surface reaction mechanisms and kinetics through analysis of the desorption spectra of both reaction products and unreacted reactants. For example, the temperatures of the peak maxima, the peak shapes and their multiplicity, all contain information about the mechanism and kinetics of the surface catalysed reaction.

(3.2) Theoretical Considerations

(3.2.1) Overall System Equations

The evaluation of kinetic parameters for adsorption and desorption from the results of a TPD experiment requires consideration of material balances for the surface and gas phase concentrations of the adsorbate. By assuming that interphase, intraparticle and catalyst bed concentration gradients (i.e. mass transfer or diffusional limitations) terms are negligible and that no adsorbate accumulation occurs within the catalyst bed, the master equations describing the system are as follows[24]. Mass balances on the catalyst surface coverage are given by:

$$\varepsilon u \frac{dC_g}{dz} = (1-\varepsilon).-V_m \frac{d\theta}{dt} \qquad [1]$$

and

$$\frac{-d\theta}{dt} = R_d - R_a \qquad [2]$$

where z= axial distance (m)

t= time (s)

C_g= gas phase adsorbate concentration ($mol.m^{-3}$)

θ= fractional coverage

u= interstitial fluid velocity ($m.s^{-1}$)

V_m= number of surface sites per unit volume ($mol.m^{-3}$)

ε= bed void fraction

R_d= adsorbate desorption rate (s^{-1})

R_a= adsorbate adsorption rate (s^{-1})

To a good approximation the bed void fraction, ε, can be taken as being 0.5[124] thus simplifying equation [1] to:

$$u \frac{dC_g}{dz} = -V_m \frac{d\Theta}{dt} \qquad [3]$$

Equations [2] and [3] describe the overall conservation of a single, non-reacting species inside the catalyst bed and form the basis for further analysis of the TPD spectrum.

(3.2.2) Adsorption

The amount of uptake of an adsorbate pulse injected into the carrier gas flow by the catalyst bed depends on several factors[124], such as the time dependent partial pressure distribution within the pulse, the contact time within the catalyst bed and the adsorption temperature. The first two factors are determined by the carrier gas flowrate, the amount of adsorbate injected by each pulse and the shape of the adsorbate pulse. Provided the amount of adsorbate injected per pulse remains constant, then the uptake should be determined by the carrier gas flowrate alone[24,124].

Ideally, the adsorbate injection pulse will be a square wave shape, but in the distance between the injection port and the catalyst bed, this shape will be distorted by interdiffusion of the adsorbate into the carrier gas. Over a wide range of carrier gas flowrates the adsorbate pulse can be approximated by a triangular wave of amplitude, I, and width, W[24,124]. Providing the concentration of adsorbate is

uniform throughout the catalyst bed (i.e. differential bed conditions exist), and there is no axial dependence on C_g, then the time dependence of the adsorbate concentration can be described by[24]:

$$\begin{aligned} C_g(t) &= 0 && t < 0 \\ &= \frac{2I\ ut}{W} && 0 < t < W/2u \\ &= \frac{2I\ (W-ut)}{W} && W/2u < t < W/u \\ &= 0 && t > W/u \end{aligned} \qquad [4]$$

The adsorption process can be described by equations [2] and [3]. If the catalyst temperature is low enough such that the desorption rate becomes negligible, equation [2] can be reduced to:

$$\frac{d\Theta}{dt} = R_a \qquad [5]$$

The simplest theoretical adsorption model is described by the Langmuir adsorption isotherm[24] which is based on the hypothesis that a fixed number of sites are present on the solid surface, and that the enthalpy of adsorption is independent of the fraction of unoccupied adsorption sites[24]. This can only be an approximation to the real situation. For a general Langmuir model of adsorption order p, equation [5] can be written[24]:

$$\frac{d\Theta}{dt} = k_a.C_g.(1-\Theta)^p \qquad [6]$$

where k_a= adsorption rate constant ($m^3.mol^{-1}.s^{-1}$)

p= reaction order of adsorption

Equation [6] has been written assuming that Θ represents an average coverage within the bed; Falconer and Schartz[24] question the likelihood of this, especially when strongly adsorbing reactants are being considered. In this situation preferential adsorption will occur on

the leading edge of the catalyst bed and result in a higher coverage on this edge with respect to the catalyst surface further down in the bed. The existence of spatial uniformity within the catalyst bed is not a parameter that can be easily verified experimentally[24]. However, theoretical calculations by Rieck and Bell[125] have shown for both first and second order desorption processes, any initial non-uniformity in adsorbate distribution is smoothed out as heating is commenced and before an appreciable amount of adsorbate is desorbed from the surface. Only slight differences in the peak temperatures result. To a good approximation then, spatial uniformity of θ can be assumed, allowing equation [6] to be written:

$$\int_0^{\theta} (1-\theta)^{-p}.d\theta = k_a \int_0^{\infty} C_g.dt \qquad [7]$$

From equation [3] the right hand side can be evaluated as:

$$RHS = v_a.\exp(-E_a/RT).(WI/2u) \qquad [8]$$

where the adsortion rate constant, k_a, has been expressed in Arrhenius form with E_a= adsorption activation energy ($J.mol^{-1}$)

v_a= adsorption pre-exponential factor (s^{-1})

For first order (p=1), non-dissociative Langmuir adsorption, the left hand side of equation [7] becomes:

$$LHS = 1/(\ln (1-\theta)) \qquad [9]$$

Similarly, for second order dissociative adsortion (p= 2) the left hand side can be evaluated as:

$$LHS = \theta/(1-\theta) \qquad [10]$$

The degree of "conversion" of coverage as the adsorbate injections are made can be measured experimentally as a function of the carrier gas flowrate for a fixed injection volume and constant catalyst temperature. The order of the adsorption reaction can be then

determined by fitting the data to equations [8], [9] and [10][24,124]. Once the adsorption kinetics have been determined in this manner, equation [8] can be further used to find the activation energy for the adsorption by conducting experiments at fixed carrier flowrate and adsorbate injection but varying the adsorption temperature[24]. Such in-situ determination of the adsorption kinetics can indicate the possible importance of readsorption effects that are liable to occur during subsequent temperature programmed desorption of the adsorbate[24].

(3.2.3) Desorption

In the analysis of the data obtained from the TPD, both mass balances given by equations [1] and [2] must be considered. By assuming that there are no axial concentration gradients within the catalyst bed (i.e. differential bed behaviour), the gas phase concentration $C_g(t)$ is, to a good approximation[24], uniform throughout the catalyst bed. By neglecting any diffusion in the pores of the catalyst, a mass balance over the catalyst surface gives:

$$\frac{-d\Theta}{dt} = k_d(\Theta)\ \Theta^n - k_a\ C_g\ (1-\Theta)^p \qquad [11]$$

i.e (net desorption rate) = (desorption) - (readsorption)

where $k_d(\Theta)$= desorption rate constant (may be coverage dependent)

n= reaction order for the desorption

Similarly a mass balance on the adsorbate concentration in the flowing carrier gas gives:

$$F\ C_g = V_c\ V_m\ k_d(\Theta)\ \Theta^n - V_c\ V_m\ k_a\ C_g\ (1-\Theta)^p \qquad [12]$$

where F= volumetric carrier gas flowrate ($m^3.s^{-1}$)

V_c= total solid volume in reactor (m^3)

V_m= mol of surface sites per solid volume ($mol.m^{-3}$)

For a linear heating schedule the temperature as a function of time is described by:

$$T = T_o + \beta\, t \qquad [13]$$

where T= temperature (K)

T_o= initial temperature (K)

β= linear heating rate ($K.s^{-1}$)

It then follows that:

$$dt = (1/\beta)\, dT \qquad [14]$$

Substitution for dt in equation [11] and equating with equation [12] gives the result:

$$C_g = \frac{-\beta\, V_c\, V_m}{F} \cdot \frac{d\theta}{dT} \qquad [15]$$

i.e the gas concentration is directly proportional to the desorption rate.

Rewriting equation [12]:

$$C_g = \frac{V_c\, V_m\, k_d(\theta)\, \theta^n}{F + V_c\, V_m\, k_a\, (1-\theta)^p} \qquad [16]$$

and further substituting for C_g gives the result:

$$\frac{-d\theta}{dT} = \frac{F}{\beta} \cdot \frac{k_d(\theta)\, \theta^n}{F + V_c\, V_m\, k_a\, (1-\theta)^p} \qquad [17]$$

Two important limiting cases of this equation are possible; firstly if readsorption does not occur, and secondly, if readsorption freely occurs[24,120,121]. The no readsorption limiting case corresponds to the situation where:

$$F >> V_c\, V_m\, (1-\theta)^p\, k_a \qquad [18]$$

i.e. the flow rate of the carrier gas is sufficiently high so that readsorption only occurs to a negligible extent. This simpliflies equation [17] to:

$$\frac{-d\Theta}{dT} = \frac{k_d(\Theta)\ \Theta^n}{\beta} \qquad [19]$$

In the second limiting situation where free readsorption occurs:

$$F << V_c\ V_m\ k_a\ (1-\Theta)^p \qquad [20]$$

i.e. readsorption of the sample occurs freely so that its rate is only limited by the availability of unoccupied adsorption sites $(1-\Theta)$. This allows equation [17] to be written:

$$\frac{-d\Theta}{dT} = \frac{F}{\beta} \cdot \frac{k_d(\Theta)\ \Theta^n}{V_c\ V_m\ k_a\ (1-\Theta)^p} \qquad [21]$$

The coverage dependent desorption rate constant can also be written in Arrhenius form[24]:

$$k_d(\Theta) = v_d(\Theta)\ \exp(-E_d(\Theta)/RT) \qquad [22]$$

where $v_d(\Theta)$ = desorption preexponential factor (s^{-1})

$E_d(\Theta)$ = activation energy for desorption $(J.mol^{-1})$

Both $v_d(\Theta)$ and $E_d(\Theta)$ may be coverage dependent. Rewriting equation [17] (no readsorption case) in Arrhenius form gives:

$$\frac{-d\Theta}{dT} = \frac{v_d(\Theta)}{\beta}\ .\exp(-E_d(\Theta)/RT).\Theta^n \qquad [23]$$

Similarly rewriting equation [19] (free readsorption case) in the same manner:

$$\frac{-d\Theta}{dT} = \frac{F}{V_c.V_m.\beta} \cdot \frac{v_d(\Theta)}{v_a} \cdot \exp(-\Delta H(\Theta)/RT) \cdot \frac{\Theta^n}{(1-\Theta)^p} \qquad [24]$$

where $\Delta H(\Theta) = E_d(\Theta) - E_a(\Theta)$, the heat of adsorption $(J.mol^{-1})$ i.e. the negative of the enthalpy change on adsorption.

Equations [23] and [24] express explicitly the temperature dependent gas concentration dependence in terms of the kinetic parameters, $E_d(\Theta)$ and $v_d(\Theta)$ and the mass action law for adsorption and desorption[24]. These require a knowledge of the order of adsorption, p, and the order of desorption, n. Generally n, the desorption order, is known from simple consideration of the molecularity of the desorption reaction[24], while p, the adsorption order, can be calculated experimentally using the method described in the previous section.

The equations can be solved for simple cases by making the assumption that the adsorption surface is homogeneous[120] so the kinetic parameters are not a function of coverage. The maximum concentration of the sample in the carrier gas stream will be attained at a temperature T_m when $dC_g/dT = 0$. By differentiating equation [16] and substituting for $d\Theta/dT$ from equation [17] gives the following expressions. For the no readsorption limiting case:

$$\ln \frac{T_m^2 \, n\Theta_m^{(n-1)}}{\beta} = \frac{E_d}{RT_m} + \ln \frac{E_d}{v_d R} \qquad [25]$$

and for the free readsorption limiting case:

$$\ln \frac{T_m^2 \, \Theta_m^{(n-1)}}{(1-\Theta_m)^{(n+1)}\beta} = \frac{\Delta H}{RT_m} + \ln \frac{V_c \, V_m \, \Delta H}{F \, q \, v' R} \qquad [26]$$

where v'= the effective preexponential= the ratio of the desorption to adsorption preexponential factors

q = (n + (p-n)Θ) which reduces to n if the adsorption and desorption steps are of the same order.

(3.3) Practical Considerations

The system equations presented in the previous section have been based on desorption from an ideal homogeneous surface, with limiting situations of no readsorption and free readsorption occurring during temperature programmed desorption. In TPD from a "real" catalyst surface, other factors can strongly influence the nature of the desorption spectra obtained and can lead to fundamental changes in the information content of the TPD spectrum[126]. A number of recent papers have modelled TPD systems in order to determine the relative effects of these various factors. For example, Gorte et al[122,123] have presented criteria for experimental design based on dimensional analyses of temperature programmed desorption in stirred tank and packed bed configurations.

With free readsorption, the effect is to "hold" the adsorbate in the bed for a longer time[124] so that peaks temperatures are raised and peak profiles are broadened. Calculations on real and model TPD systems[122-125,127] have shown readsorption cannot be eliminated and, for any reasonable set of experimental conditions, readsorption equilibrium usually exists. Variation of the carrier flow rate has been suggested as a method for determining the extent of readsorption [120,121,124,127], although Gorte[122] has noted that such a test would not in fact be informative.

The earlier work of Cventanović and Amenomiya[120,121] suggested readsorption effects could be minimised by the use of high carrier flowrates. However, Gorte et al[122,123] and Rieck et al[125] have more recently shown that if high flow rate conditions are used, then the desorption can become rate limited by mass transfer diffusion

within the catalyst particles. Gorte et al[123] notes that such experimental conditions should be avoided since they make data analysis complex, with the measured activation energy effectively being the sum of the true desorption energy, the particle diffusion coefficient and the inverse sticking coefficient. If, in addition, the activation energy is coverage dependent, then the presence of intraparticular concentration gradients can make the desorption spectrum too complex to analyse[123].

Lowering the carrier flowrate reduces mass transfer limitations but increases readsorption effects. Gorte[122] has noted that intermediate flow regimes, where both factors remain significant, should be avoided. By operating at low carrier flowrates, particle concentration gradients can be minimised so that free readsorption conditions exist[122]. Difficulties can arise in this situation if desorption does not occur evenly along the length of the catalyst bed due to changing concentration with position within the bed[123]. Rieck et al[125] have shown that although a non-uniform initial adsorbate distribution can shift the peak temperature, any initial non-uniformity is smoothed out as the temperature is raised and before appreciable desorption has occurred.

The model calculations of Rieck et al[125] have further shown that, in the absence of significant mass transfer effects, and assuming equilibrium adsorption, reasonably accurate estimates of the enthalpy of adsorption can be obtained. However, considerable inaccuracies occur in estimation of the preexponential factor for desorption when any significant readsorption effects are present.

Although other experimental considerations, such as detector lag times and axial mixing effects, can also cause distortion of

desorption peaks, the dimensional analyses of Gorte et al[122,123] have shown that these effects can be minimised by careful experimental design.

(3.4) Analysis Techniques

A number of techniques are available for extraction of kinetic parameters from desorption spectra[24]. The parameters most often determined in this respect are the order of desorption (or reaction), activation energy for desorption and the preexponential factor[24]. When applied to desorption, if the adsorption is not activated, the activation energy for desorption will also be equal to the heat of adsorption of the adsorbed molecule. This section will be restricted to detailing only those methods used for data analysis in this thesis.

(i) Redhead's Method

The Redhead equation[24,129] determines the energy of adsorption from the temperature of a single desorption peak. It makes the assumption that no readsorption takes place, and, in addition, a value for the preexponential factor, v_d, must be assumed. The equation is obtained by equating the $dC_g/dT = 0$ at the peak maximum in the same manner used in the derivation of equation [25] given previously and gives the expression:

$$(k_d)_m = v_d \exp(-E_d/RT_m) = \beta E_d / R T_m^2 \qquad [27]$$

Typically a preexponential of 10^{13} s^{-1} is assumed[25,129]. In section 3.3 it has been shown that readsorption effects cannot be eliminated for TPD from a powder catalyst and can result in a significant increase in the desorption peak temperature. Since the Redhead equation relies on an accurate measurement of the peak temperature, and assumes

that this value is undistorted by readsorption effects, at best, its accuracy is limited to providing an estimate of the heat of adsorption.

(ii) Heating Rate Variation Method

The heating rate variation technique[24,120,121] utilises the fact that with increasing heating rate, desorption peaks shift to higher temperatures and have larger amplitudes, but reach a maxima in a shorter time. By varying the experimental heating rate in this manner, two separate measures of the activation energy can be obtained. A plot of the ln (β/T_m^2) against $1/T_m$ will give a line of slope equal to $-E_d/R$ or $-\Delta H/R$, depending whether or not readsorption effects are significant (see equations [25] and [26] given previously).

A second plot of ln (peak amplitude) against $1/T_m$ provides an independent method for determining E_d or ΔH from the same experimental results. Again this plot will have slope $-E_d/R$ for the no readsorption limiting case, or $-\Delta H/R$ when free readsorption conditions exist.

This method has been shown to be very sensitive to minor experimental errors[130], particularly in the measurement of the peak temperature, and so it may be difficult to obtain reliable kinetic parameters. However, by using the two plots described above, an indication of the accuracy of the result obtained can be made[24].

(iii) Catalyst Mass Variation Method

This technique is only applicable for free readsorption situations[128]. The right hand term of equation [26], $V_c V_m$, expresses the number of surface sites and is proportional to the mass of catalyst used. The saturation coverage and the heat of adsorption will be essentially independent of catalyst mass[128], so for two separate experiments where only the catalyst weight has been changed, the ratio

of equation [26] applied to each weight will be:

$$\ln \frac{T_{m1}^2}{T_{m2}^2} = \frac{W_1}{W_2} + \frac{\Delta H}{R} \cdot (1/T_{m1} - 1/T_{m2}) \qquad [28]$$

For $\Delta H > 10$ kJ/mol and $T_m < 600$ K[128], the left hand side of the equation becomes neglible so allowing equation [28] to be simplified to:

$$\ln \frac{W_1}{W_2} = \frac{-\Delta H}{R} \cdot (1/T_{m1} - 1/T_{m2}) \qquad [29]$$

A plot of ln (catalyst weight) against $1/T_m$ has a slope of $-\Delta H/R$, and allows the heat of adsorption to be determined. Since this method relies on accurate measurement of the desorption peak temperature, it will also be sensitive to experimental error as described above for the heating rate variation method.

CHAPTER 4

EXPERIMENTAL

(4.1) Apparatus

(4.1.1) General Description of the Temperature Programmed Reactor System

The TPD experimental apparatus and associated experimental methods and computer operating software were developed specifically for this study. This involved design and construction of the reactor, heating furnace, valve connections and gas flow lines following apparatus designs presented in reviews by Falconer and Schwarz[24] and Cvetanović and Amenomiya[120,121]. A schematic flow diagram of the TPD experimental apparatus is given in figure 4.1, with details of the equipment components presented in table 4.1.

The system was operated at atmospheric pressure using helium as a carrier gas. A combination of high performance molecular sieve and oxygen traps were used to remove the main impurities from the helium. The gas flow was controlled by a constant pressure flow controller positioned after the sieve traps and measured on the vent side of the reactor (i.e. after passing through the reactor and catalyst bed) by rotameter. Calibration of the rotameter was made by bubble-flow meter.

All the gas flow lines until after the mass-spectrometer sampling inlet were constructed either of 1/4" stainless steel, 1/8" stainless steel or of 1/16" glass-lined stainless steel, with teflon tubing (1/8") used for the vent gas lines. Stainless steel tube connection fittings and valves were used throughout. To avoid any adsorbate or

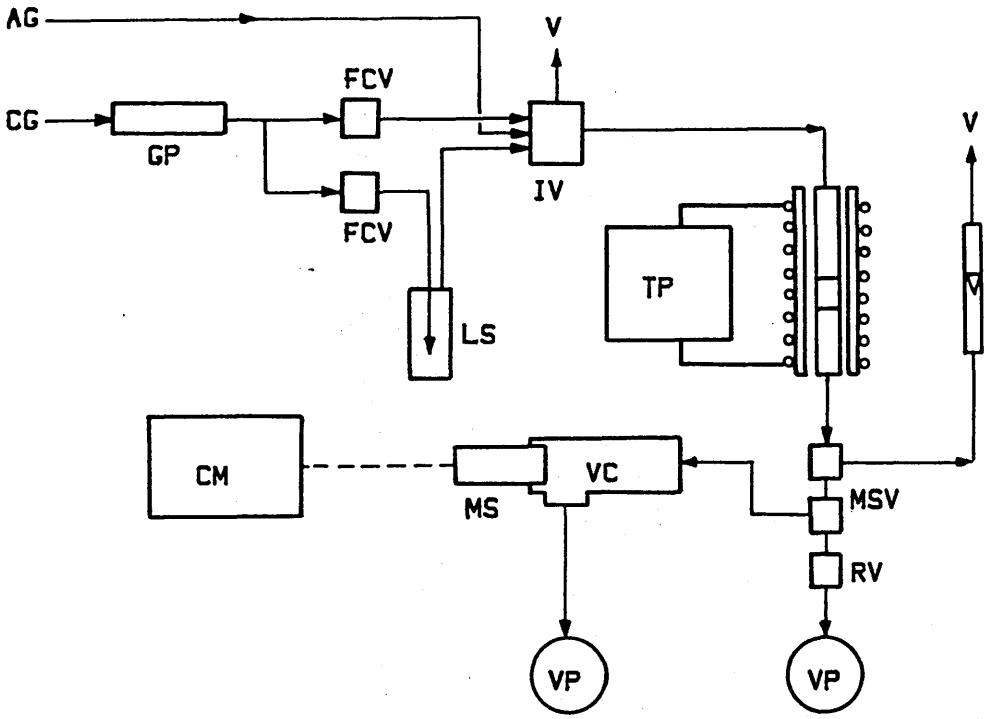

Figure 4.1: A schematic diagram of the temperature programmed desorption apparatus. The notation used is as follows: CG= carrier gas; AG= adsorbate gas; GP= gas purification; FCV= flow control valve; IV= injection valve; LS= liquid saturator; TP= temperature programmer; MSV= micro-sampling valves; RV= restrictor valve; VC= vacuum chamber; MS= quadrupole mass spectrometer; VP= vacuum pumping; CM= computer; V= vent.

desorption product condensation the lines both after the injection valve to the reactor and downstream of the reactor to the mass spectrometer sampling inlet were trace heated to approximately 335-345 K.

(4.1.2) Design of the Reactor and Heating Furnace

A cross-sectional diagram of the reactor and the heating furnace is given in figure 4.2. The reactor tube was constructed from 1/4" and 10mm OD quartz glass tubing with a quartz glass sintered frit welded in as a catalyst support. Measurement of the catalyst bed temperature was made by a 1/16" diameter stainless steel sheathed Type K thermocouple probe inserted vertically into the reactor. The output from the thermocouple passed through an electronic ice-junction and signal amplifier before being logged by computer. The reactor tube was positioned inside a 20mm diameter quartz glass tube around which nichrome heating wire was wound. The annular air space between the reactor tube and heating elements served two purposes. Firstly, it eliminated temperature fluctuations in the temperature heating ramp by providing a thermal buffer zone between the reactor and heating wires and secondly, it allowed low pressure air to be blown down to rapidly cool the reactor after each experiment. The reactor could be cooled from 800 K to 330 K in 2-3 minutes by this method. Into the annular space another Type K thermocouple probe was positioned for reactor temperature control and regulation of the linear heating ramp. The heating wires were insulated by approximately 25mm of kaowool high temperature insulation, in turn enclosed by 64mm diameter brass tube. The complete furnace and reactor arrangement were supported by a laboratory clamp and stand. Connections at the reactor inlet and outlet were stainless steel with teflon and graphite ferrules.

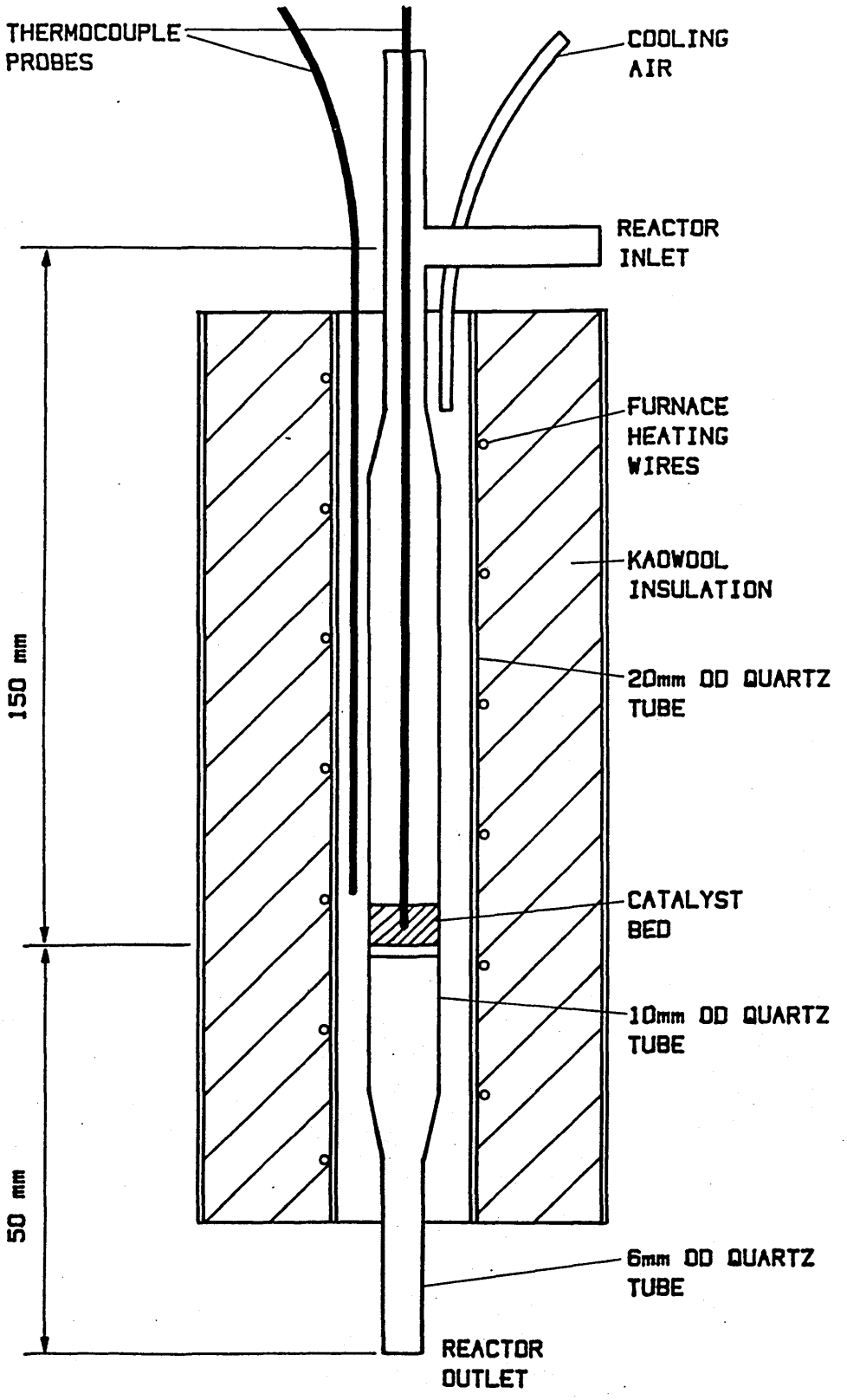

Figure 4.2: Cross sectional diagram of the reactor and heating furnace. (Not to scale)

(4.1.3) Adsorbate Injection Equipment

Injection of adsorbates into the carrier gas flow were made with an injection valve upstream of the reactor. Various volume injection loops could be fitted to to allow control over the amount of adsorbate injected and hence control of the adsorbate catalyst surface coverage. The valve was connected to an electric actuator that could either be operated manually or under computer control for multiple injection sequences. Adsorbates in gaseous form were injected by direct connection of the appropriate gas cylinder or aerosol can to the valve. Liquid adsorbates were contained in a saturator through which helium gas was passed which then flowed through the injection valve. Constant temperature control of the saturator temperature was achieved by placing the saturator in a cold water flask. The lines from the saturator to the valve and the valve itself were trace heated to approximately 335-345 K to avoid adsorbate condensation.

(4.1.4) Reactor Temperature Control

The reactor temperature and rate of linear heating were controlled by a PID controller constructed by the Departmental Electronics Workshop. A 0-10 v voltage ramp generator was connected to the controller unit to provide a linear ramp signal, with a programmable power supply wired to the reactor furnace. Temperature ramping was commenced by activation of the voltage generator ramp and achieved by the controller matching the thermocouple input voltage (from the thermocouple positioned in the annular space outside of the reactor) against the input from the ramp generator. As the ramp generator output increased linearly with time, the furnace temperature was also

increased at a linear rate as the power from the power supply progressively increased. Variation of the heating rate could be made by adjustment of either the rate of the generated voltage rate or of the temperature span of the ramp on the main controller. The controller could also be used to maintain a constant reactor temperature by resetting the voltage generator and adjustment of the temperature set point.

(4.1.5) Desorption Product Sampling and Detection

A kathrometer (thermal conductivity detector) and sampling valves for the mass spectrometer detector were positioned downstream of the reactor and furnace for detection of the desorption products in the carrier gas stream. The principal advantage of the mass spectrometer was that it could discriminate between simultaneously desorbing masses whereas the kathrometer detected only the overall desorption product envelope. Operation of the kathrometer was also severely limited due to its low sensitivity. As a result no significant use was made of the kathrometer in this study and it will not be discussed further.

Two micro-sampling valves controlled the helium flow into the mass-spectrometer detector chamber. The first valve was connected to a low volume roughing vacuum chamber and the second with the main vacuum chamber. A quadrupole mass spectrometer with a Faraday-cup detector was used, and enabled high helium partial pressures to be used within the chamber resulting in high detection sensitivities. The total helium flow to the mass-spectrometer however remained low and did not cause a discernable decrease in the total helium carrier flowrate. The mass spectrometer head was connected to a remote control unit in turn interfaced with an Apple IIe computer.

Table 4.1: The main experimental items used in the TPD apparatus.

apparatus item	model/grade	specifications
O_2/H_2O trap	Messer Greisheim Oxisorb cartridge	< 0.1ppm O_2, < 0.5ppm H_2O
gas flow controller	Porter Instruments Model 1000 VCD	A-110 flow element, max flow 110ml/min
1/4", 1/8" tubing	SS-304	seamless tubing
1/16" glass-lined tubing	SGE Eng (UK) Ltd	
adsorbate injection valve	Valco 2-position GC sample valve	variable loop volumes, elec--tric actuator
reactor tube	constructed in department	quartz glass with quartz sintered catalyst support
reactor heating reactor	" " "	quartz glass wound with nichrome wire, kaowool insulated
type K thermocouple probes	TC Ltd	1/16" SS sheathed probes
ice junction thermo-couple compensators	Electroplan Ltd	electronic compen--sation units
PID ramp controller	constructed in department	variable temperature start and span
programmable power supply	Philips PE 1644	40V, 10A max output
voltage ramp generator	Wenking Model VSG 72	0-10v ramp generator
kathrometer	Servomex Model DK 458	2.6µl internal volume
kathrometer control unit	Servomex Ltd.	0-8v bridge
mass-spectrometer sample flow control valves	SGE BMCV Micro-Control valves	PTFE seals
diffusion pump	Edwards Diffstak	
mass spectrometer	VG Ltd Masstorr MX	Faraday cup detector
computer	Apple IIe	
A/D interface	U-Microcomputers	12 bit, 8 channel
D/A interface	Applab	0-6.5v output

(4.2) Experimental Methods

(4.2.1) Temperature Programmed Desorption Experimental Method

(4.2.1.1) Adsorbate Injection

After catalyst pretreatment (described in chapter 5) adsorbate dosage would be carried out at the required adsorption temperature set by the furnace temperature controller. Dosing of the catalyst could be accomplished in two ways:

(i) by use of the injection valve either with manual operation of the valve actuator or by computer control for multiple injections. Variation in the injection loop volume (approximately 25µl to 1ml) controlled the quantity injected. The same effect could also be achieved by changing the concentration of the injected gas.

(ii) appropriate reconnection of the valve inlet tubing allowed the valve to be used in a switching rather than a pulse injection mode enabling the carrier gas to be changed from pure helium to an alternative gas mixture, for example, the gas flow from the saturator. The alternative gas flow could be maintained for as long as the valve remained in the 'inject' position thus subjecting the catalyst to a steady flow of adsorbate over its surface for an indefinite time length.

After adsorbate dosage the catalyst would be left for a minimum of 2-3 minutes to allow the background gas concentrations to return to their baseline levels before temperature programming was commenced.

(4.2.1.2) Experimental Technique

After dosage of the catalyst and before commencement of the temperature programming, the helium partial pressure in the mass-spectrometer was set by adjustment of the helium flow with the micro-valves. A constant helium partial pressure (and hence constant flow to the mass spectrometer) of 8×10^{-8} mbar was used for virtually all the TPD experiments carried out. Because of the proximity of the hydrogen peak at mass 2 to the large helium signal at mass 4, experiments requiring an accurate record of hydrogen desorption used a reduced partial pressure of 1.4×10^{-8} mbar and data was obtained without computer scanning i.e. a direct reading of the mass 2 signal was made.

Temperature programmed heating of the catalyst bed was begun by activating the linear ramp generator. While the majority of experiments used a ramping rate of 39 ± 1 K/min, rates as high as 108 K/min and as low as 7.9 K/min were achieved by the controller. Figure 4.3 illustrates the excellent linear characteristics of the heating ramp as measured by the change in temperature within the catalyst bed.

Computer control of the mass-spectrometer and logging of the desorption data would also commence at this point (see section 4.2.2). Table 4.2 details the atomic masses used to identify the various desorption products. Further information on the cracking patterns of some of these compounds is given in Appendix 1.

The maximum experimental temperature generally used was 800 K. Once this temperature had been reached the ramp generator was switched off which turned off the power to the reactor furnace and the low pressure air flow turned on to cool the catalyst temperature to the

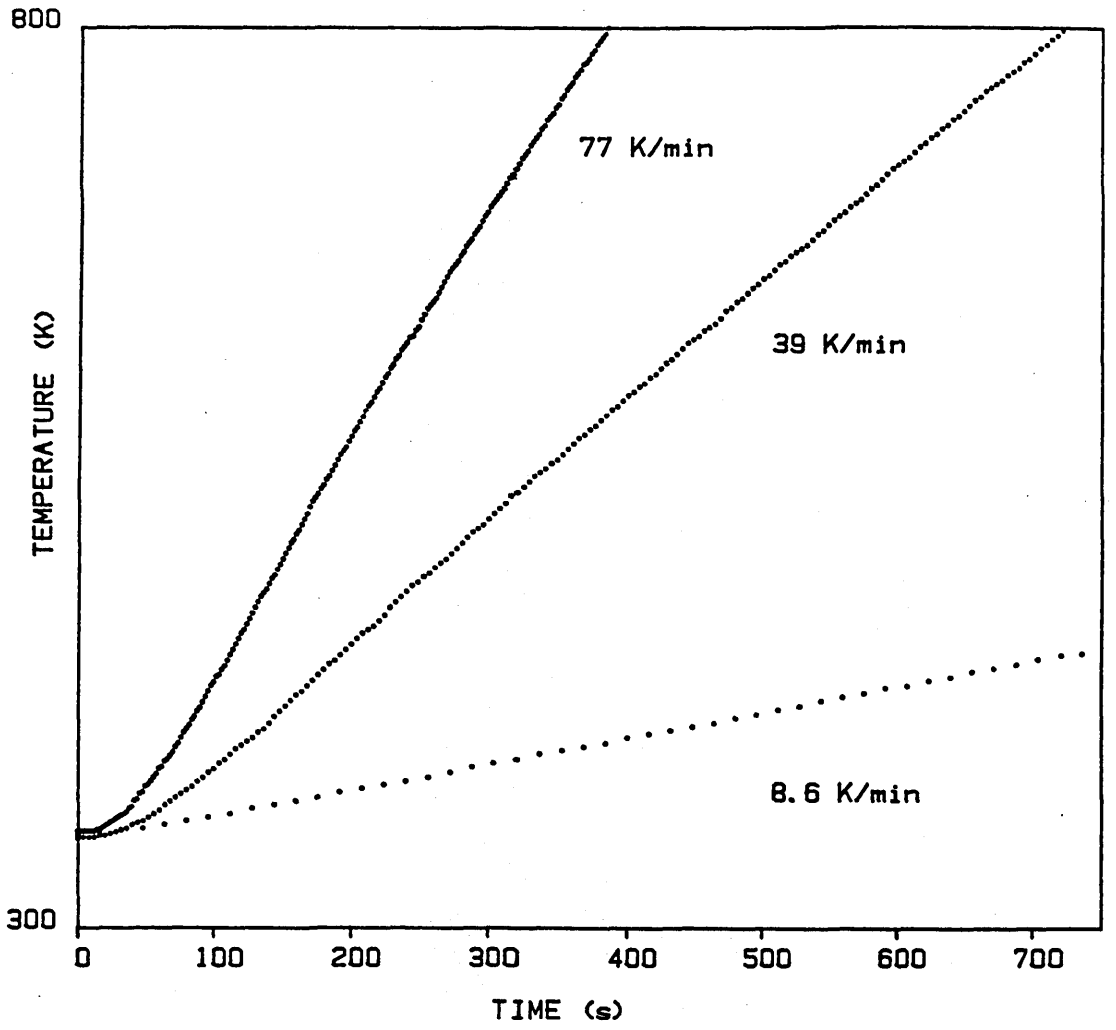

Figure 4.3: Characteristics of the experimental linear heating rate as measured by the catalyst bed temperature.

adsorption temperature again. The experimental data would be saved to disk at this stage.

A summary of the typical experimental parameters used is given in table 4.3.

Table 4.2: The characteristic atomic masses used for mass spectrometer desorption product detection.

desorption product	characteristic mass(es) (amu)
hydrogen	2
water	18
carbon monoxide	28
carbon dioxide	44,28
methane	15,16
propene	41,39
acetone	43,58
2-propanol	45,43
1-propanol	31,29
propionaldehyde	29(a)

(a)= after reference (108)

Table 4.3: Typical Experimental Operating Parameters

parameter	value
helium carrier flowrate	58±2 ml/min
linear heating rate	39±1 K/min
catalyst sample weight	450-500 mg
adsorption temperature	315-345 K typically
maximum experimental temperature	800 K
injection loop volume	25 µl - 1 ml

(4.2.2) Computer Software for the Control of the Mass Spectrometer and for Data Acquisition

All the computer programs for the control of the mass spectrometer and for the acquisition of experimental data were written specifically for this study. Assembly language programming was used extensively because of the precise timing restraints for mass spectrometer control and data logging.

(4.2.2.1) Control of the Mass Spectrometer Peak Scanning

For the complex desorption spectrum exhibited by adsorbates, such as 1- and 2-propanol, the ability to simultaneously monitor several desorption masses is essential. To accomplish this computer software was written that enabled up to 5 peaks to be scanned by the mass spectrometer each experiment.

Normal operation of the mass spectrometer control unit to scan a mass range used an internally generated voltage ramp to alter the mass

number continuously with time. Modifications were made to the unit to allow the input of a computer generated voltage ramp. Precise control could then be made of the masses scanned by generation of only the required portion of the ramp that defined each mass. A calibration of the voltage against atomic mass number showed an excellent linear relationship that allowed the required D/A output voltage from the computer for a given mass to be accurately determined. These voltages were generated using an 'Applab' D/A interface that allowed mass scanning in the range 0 to 65 amu.

The maximum rate at which different masses could be scanned was determined by the time constant on the preamplifier in the mass spectrometer control unit. A time constant setting of 200mS was selected as a compromise between good signal magnitude and low noise level and the maximum scanning rate was set at one mass per second so that sufficient time was left for the mass spectrometer signal to settle from a voltage 'jump' before 'scanning' through a mass peak. For a given mass the initial voltage used was slightly below that of the true peak value and the peak maximum determined by making 15 stepwise increments in the voltage (one every 30mS) so that the mass spectrometer output signal 'passed' through the peak as shown in figure 4.4. To reduce the signal noise, at each voltage step continuous readings of the mass-spectrometer signal were made with the final eight readings averaged at the end of the 30mS period. This result was then compared to the previous highest signal value to determine if the peak maximum had been reached and the maximum updated accordingly. After the 15 steps thermocouple and kathrometer channel readings were made, all three results were stored in computer memory and plotted on the computer screen both graphically and numerically to provide a visual

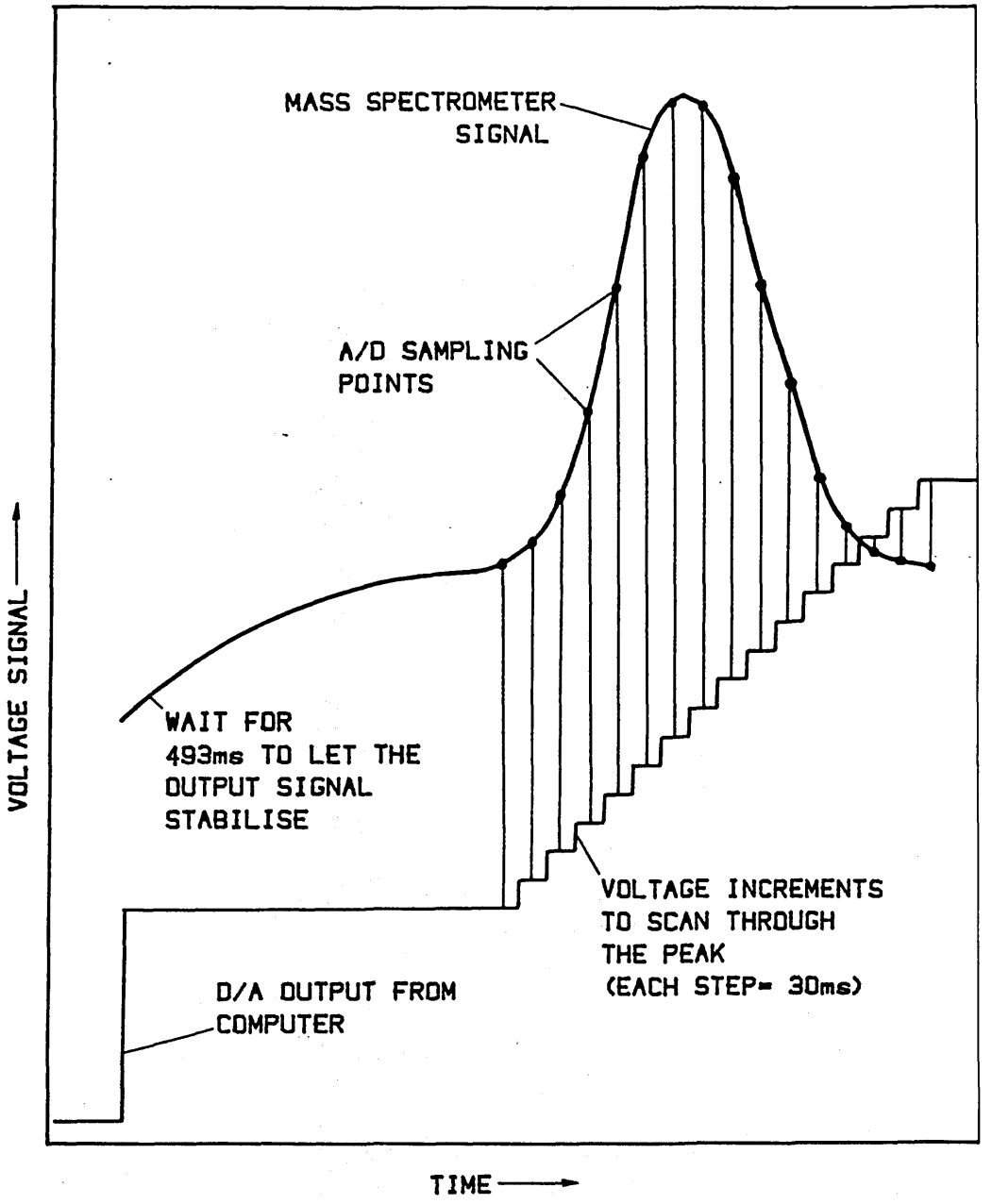

Figure 4.4: Plot of the D/A output from the computer and the mass spectrometer ion signal against time during computer control of the mass spectrometer peak scanning.

record of the progress of the experiment. After the set masses were scanned a selected number of one second delay periods could be implemented if a lower data acquisition rate was required. Since each mass peak value had an associated thermocouple reading the accuracy of the results was independent of the rate of data acquisition. A flow diagram of the main steps of control/data acquisition program is given in figure 4.5. The program was written in assembly language using Applesoft Basic to select and define the D/A voltages. At the end of an experiment the data could be saved to disk as a block of binary along with pertinent experimental details such as the experiment number, date, catalyst type and weight and the masses scanned.

(4.2.2.2) Data Analysis

The binary data for a given experiment was recalled from disk and an analysis of the results for each of the scanned masses carried out. The results for each mass were loaded into the Applesoft array variable space and analysis of the desorption spectrum carried out by plotting on the graphics screen the mass spectrometer signal against either sampling time or catalyst temperature. The raw data thermocouple readings were converted to temperature values by a two step process, the first step converting the amplified A/D signal to a mvolt value (by a linear regression equation) and the second, converting this mvolt value to an actual temperature using a machine code routine that 'looked' up a data table within the computer memory (this method being more accurate than making use of a second linear calibration equation). A further correction was then applied to this temperature to account for the reactor temperature and heating rate dependent time lag between the thermocouple reading and the mass spectrometer signal

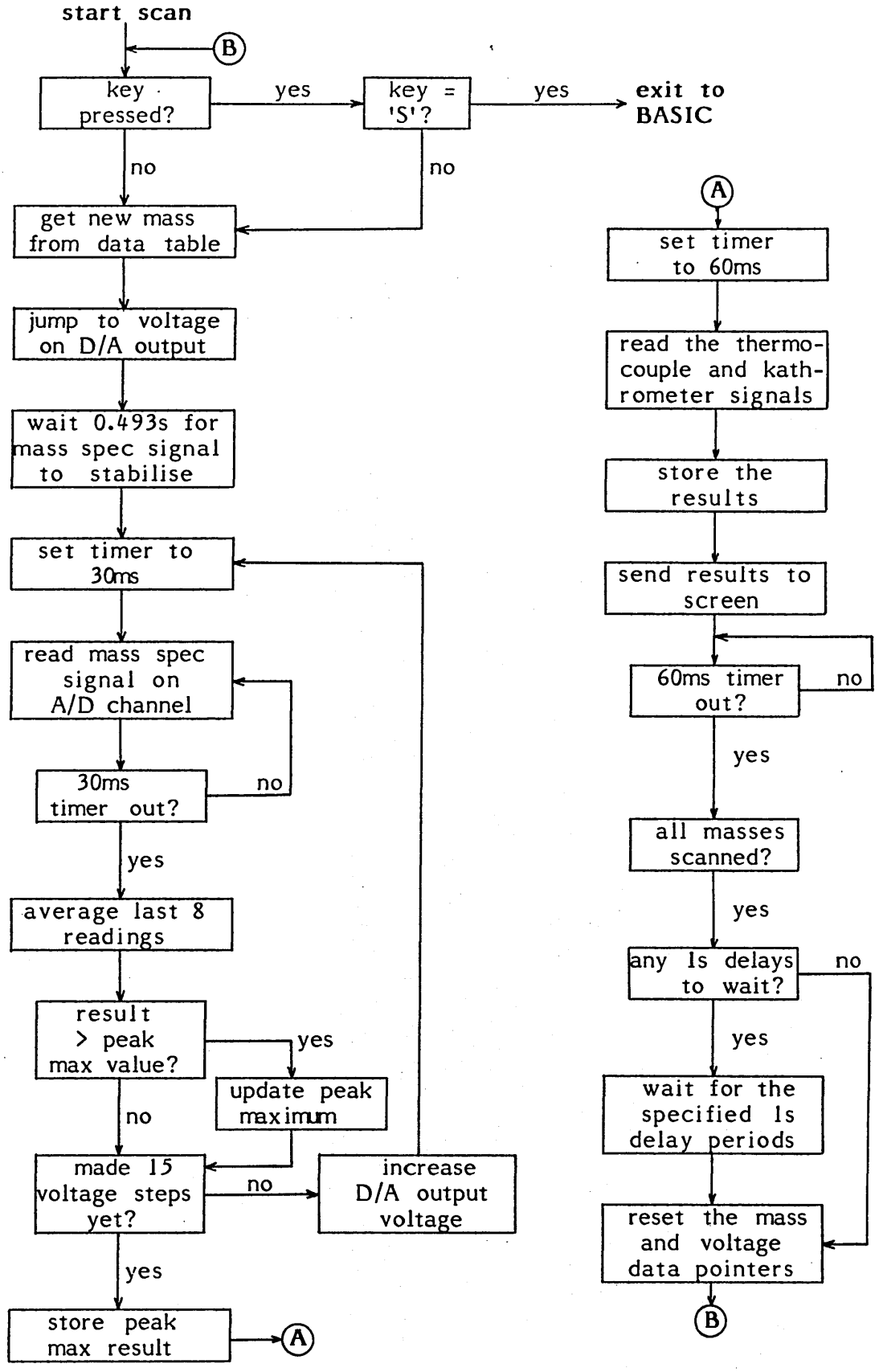

Figure 4.5: Flow diagram of the main steps of the mass spectrometer control and data acquisition program.

(2 K at low temperature decreasing to 1 K at high temperature for a carrier flowrate of 58 ml/min). Both the mass spectrometer signal data and temperature readings could be filtered to reduce signal noise levels. A 7-point least squares filtering algorithm[131-133] was written in assembly language to accomplish this. Once plotted on the computer screen the individual data point values (mass spectrometer signal and temperature) could then be read by use of a keyboard controlled cursor.

Peak areas were determined using Simpsons Rule[134] with either with a horizontal or sloping linear baseline, allowing surface coverages to be calculated by multiplication by the appropriate calibration factor. Corrections to the peak areas for cracking fraction overlap were made according to the method outlined in Appendix 3. The deconvoluted data for each mass could be stored on disk by using the space in each data file provided by the unused kathrometer channel.

(4.2.3) Mass Spectrometer Calibration

The mass spectrometer was calibrated by the injection of a known amount of adsorbate into the helium carrier stream, and after passing the flow through an empty reactor, measuring the response of the mass spectrometer. The method and rate of calibration peak scanning were identical those used for collection of experimental data during a TPD experiment (i.e. peak scanning at a rate of one reading per second), as were the conditions of helium flowrate and mass spectrometer partial pressure. Calibration factors expressed in terms of peak area per quantity of injected adsorbate are summarised in table 4.4. Peak area units were 2.44×10^{-3} volt.sec, with overall accuracy of the given calibration factors estimated to be in the order of $\pm 20\%$.

Liquids were calibrated by the injection of an adsorbate saturated helium flow. The amount of adsorbate injected was calculated from vapour pressure data of the adsorbate liquid at the saturator temperature i.e. saturation of the helium gas flow was assumed. Condensation of the adsorbate in the valve was minimised by maintaining the saturator at below the ambient room temperature and by the trace heating of the valve, injection loop and flow lines leading from the injection valve. The water calibration factor was also determined separately by measurement of the steady-state uptake of water from a saturated helium flow. Cross-checks of the reproducibility of the calibration factors for gaseous adsorbates (e.g. CO_2 and propene) could be made by injecting different composition of adsorbate/ helium gas mixtures.

Table 4.4: Mass spectrometer calibration factors.

adsorbate	calibration factor [(a)]
water	16
CO_2	30
2-propanol	36
acetone	22
propene	42
1-propanol	23
propionaldehyde	22 (est.)
hydrogen	26,11[(b)]

(a)= units: 10^{12} molecules/ (2.44×10^{-3} volt.sec), helium partial pressure of 8×10^{-8} mbar
(b)= helium partial pressure of 1.4×10^{-8} mbar

(4.3) Materials

(4.3.1) Zinc Oxide Catalysts

Three types of zinc oxide catalyst were used in this study:- AnalaR grade ZnO supplied by BDH Chemicals Ltd, Poole, England (referred to as ZnO), an older sample of AnalaR grade ZnO from the same manufacturer and supplied by ICI New Science Group (referred to as ICI low surface area ZnO) and a high surface area ZnO supplied by ICI Agricultural Division (referred to as ICI high surface area ZnO). Both AnalaR grade catalysts were prepared by ignition of Zn metal in oxygen, while the high surface area ZnO was prepared by precipitation from zinc nitrate solution followed by calcination. The behaviour of the ICI low surface area ZnO as an adsorption and decomposition catalyst had already been part of an extensive TPD study by the ICI New Science Group[25,83,98,99,108,115]. Other studies have also reported on the behaviour of a similar high surface area ZnO[83,135,136].

The manufacturers purity specifications for both AnalaR catalysts were the same as given in table 4.5. The specifications for the ICI high surface area ZnO are detailed in table 4.6 using information supplied from ICI Ltd.

Puriss grade K_2CO_3 supplied by Fluka was used as the promoter for the ZnO catalysts.

(4.3.2) Adsorbates

Gaseous adsorbates were either supplied in high pressure cylinder (hydrogen and CO_2), low pressure lecture size gas bottle (propene) or in aerosol-type cans (hydrogen and CO_2). Both the high pressure gas cylinders were of BOC CP grade purity and the lecture bottle of

Table 4.5: Manufacturers purity specifications for AnalaR grade ZnO.

specification	level (%)
minimum assay after ignition	99.6
acid-insoluble matter	0.01
loss at 600°C	0.5
carbonate (CO_3)	0.25
chloride (Cl)	0.001
nitrogen compounds (N)	0.0005
sulphur compounds (SO_4)	0.01
arsenic (As)	0.0001
cadmium (Cd)	0.002
calcium (Ca)	0.001
copper (Cu)	0.0002
iron (Fe)	0.0003
lead (Pb)	0.005
manganese (Mn)	0.0005
nickel (Ni)	0.0005
sodium (Na)	0.001
reducing substances (O)	0.0016

Table 4.6: Elemental analysis for the high surface area ZnO. (Source: ICI Ltd.)

specification	level (%)
zinc oxide (ZnO)	96.5
sulphur (S)	<0.02
chlorine (Cl)	<0.02
sodium (Na_2O)	0.12
% loss at 900°C	3.5

research grade purity. The aerosol can adsorbates were made up as mixtures in helium or nitrogen.

Distilled and deionised water was used directly in the liquid saturator without any further purification or treatment. The 1-propanol, 2-propanol and acetone were supplied by Fluka Chemicals and were of puriss grade specification. No further purification was also carried out before use of these chemicals. The manufacturers specifications for the water levels were 0.1% and 0.2% for the alcohols and acetone respectively; however, an increase in the amount of water desorbed with the alcohols in particular showed that although water levels remained low, there was an increase in the water content with time after the opening of the storage bottles. Attempts at drying of the alcohols with molecular sieves proved unsuccessful.

CHAPTER 5

CATALYST PREPARATION AND CHARACTERISATION

(5.1) Catalyst Preparation

(5.1.1) Particulate Size Distribution

Studies have shown that intraparticular mass transfer effects can cause significant distortion of a catalysts desorption behaviour[123-125]. A reliable test for the presence of mass transfer limitations is to determine if there is any particle size dependence to the TPD spectra[124].

To determine any particle size dependency in the TPD spectra, the ZnO catalysts were sieved into discrete particle size ranges. The same method of preparation used for all three catalyst types:- the as-received fine ZnO powder was pressed into a friable disc using a 13mm diameter die-press. Pressures in the range 2000 to 5000kg were used for the two AnalaR grade catalyst samples, with the TPD behaviours of these catalysts found to be independent of pelletising pressure employed. A lower pressure (approximately 500kg) was used for the ICI high surface area ZnO as the desorption behaviour of this catalyst was found to be dependent on the pelletising pressure. However, since this catalyst was not involved in the major part of the experimental programme, this dependency was not investigated further. For all catalysts, the pressed discs were then crushed and sieved into discrete particle several size fractions ranging from 150 to 1250μm in diameter.

(5.1.2) Method of Alkali Promotion

The impreganation method used for the potassium promotion of the ZnO followed that outlined by Smith and Anderson[14] and by earlier work on higher alcohol synthesis[12]. Only the particulate ZnO was used for promotion and not the as-recieved powder. Alkali promotion was achieved by the addition of the required amount of K_2CO_3 in solution with distilled and deionised water. A minimum volume of solution was added so as to form a wet slurry. The catalyst was then air dried to remove excess moisture, with final drying and decomposition of the carbonate taking place during the catalyst pretreatment stage (see section 5.1.3).

The effective potassium loadings for the three alkali promoted catalysts made are given in table 5.1. The 0.085 wt% and 0.20 wt% K loadings were confirmed by atomic emission measurements made on used samples of these catalysts.

Table 5.1: The effective potassium loadings for the promoted zinc oxide catalysts.

K_2CO_3 added (wt%)	effective K loading (wt%)
0.075	0.042
0.15	0.085
0.35	0.20

(5.1.3) Catalyst Pretreatment

(5.1.3.1) Unpromoted Zinc Oxide

An in-situ pretreatment was carried out to desorb and decompose any surface impurities on the fresh catalyst samples. The weighed catalyst sample would be heated to 800 K under normal TPD experimental conditions (i.e. of helium flowrate, heating rate, etc) and then cooled to the required adsorption temperature for subsequent experimentation. The main desorption products observed from all three unpromoted catalysts during pretreatment were water and CO_2 plus smaller amounts of CO and traces of O_2. The desorption spectra obtained from the heating of fresh AnalaR catalyst samples are shown by figures 5.1 and 5.2. Figure 5.2 for the ICI low surface area ZnO sample was similar to that previously found by Bowker et al[25] for the same catalyst. The coincident water and CO_2 peaks in each spectrum indicated the reaction limited decomposition of a common surface intermediate. Nagao et al[88] have shown that atmospheric water and CO_2 combine to form a hydroxy-carbonate species on the surface of ZnO during storage which decomposes to water and CO_2 on heating. The coincident water and CO_2 peaks were then assigned to the decomposition of such an intermediate, with the larger peaks from ICI low surface area ZnO sample being a consequence of its greater age. The differences in the water desorption profiles between catalysts is considered in chapters 6 and 8 and so will not be discussed at this point. Subsequent heating of a sample after the initial treatment did not evolve any further carbonate derived CO_2 or water peaks, although a small high temperature water peak was generally found due to the adsorption of background water onto the ZnO surface.

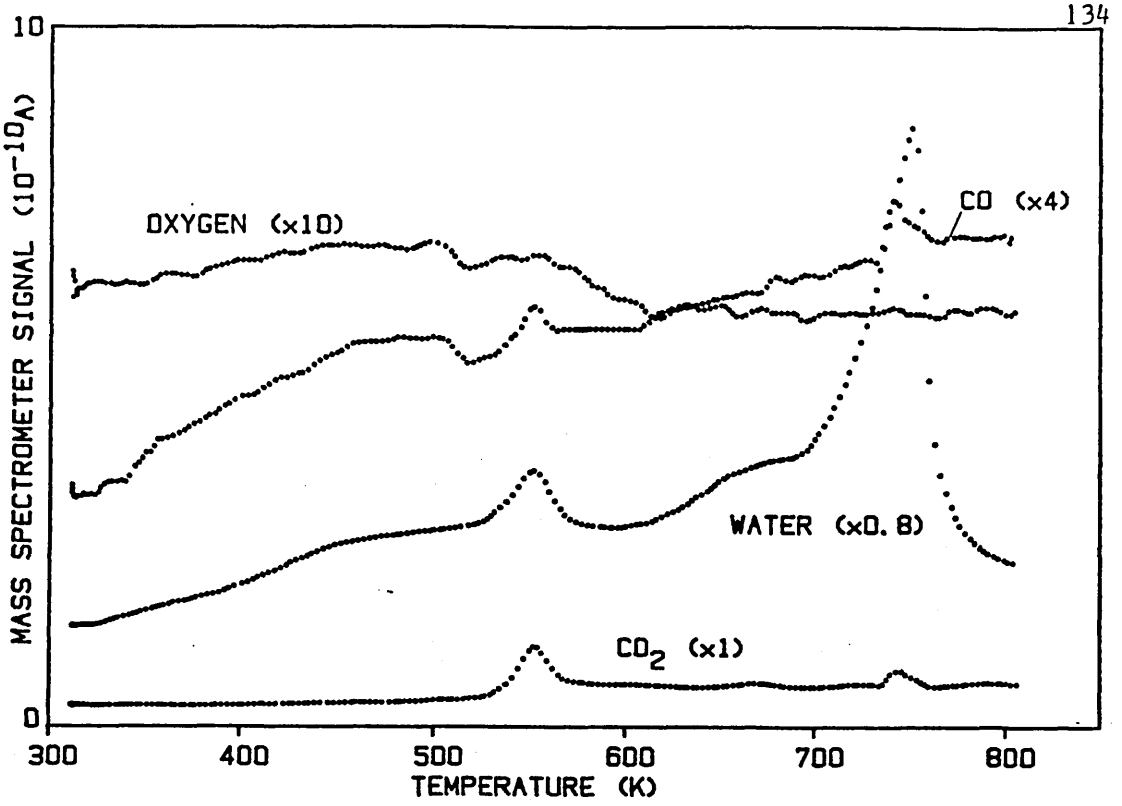

Figure 5.1: The desorption spectrum obtained from the pretreatment of a fresh zinc oxide sample.

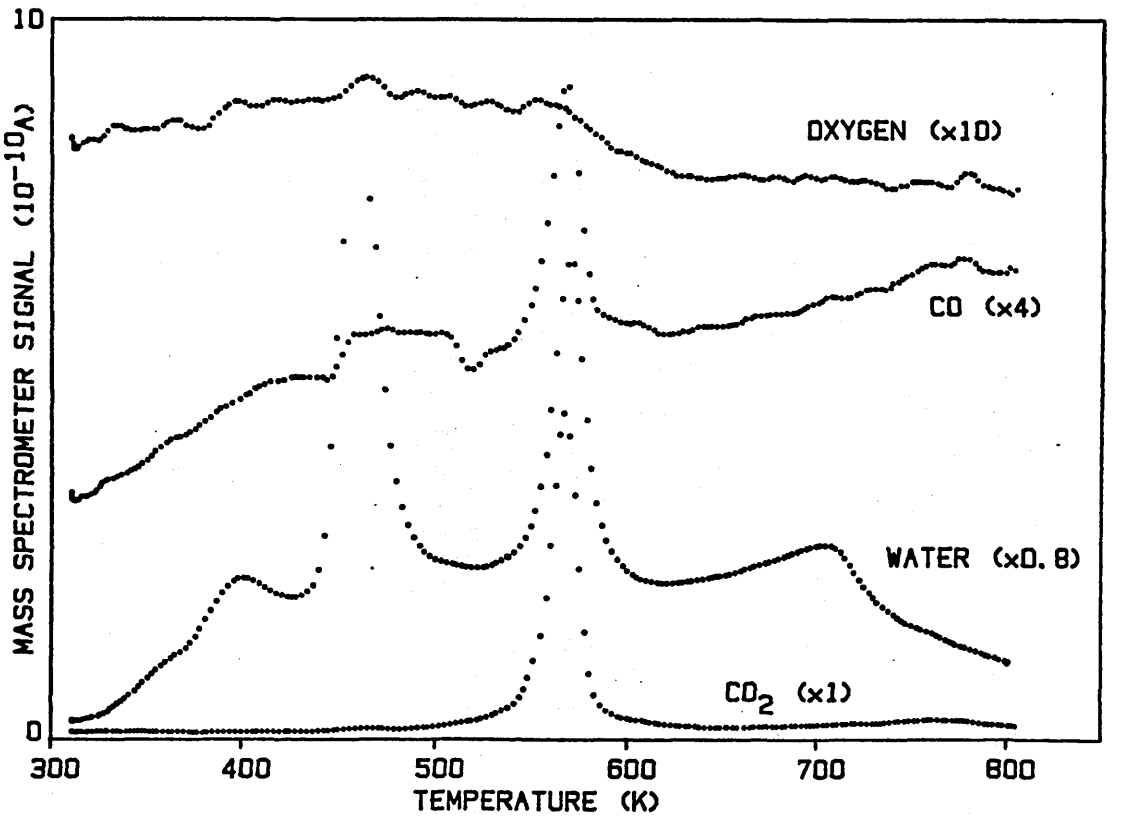

Figure 5.2: The desorption spectrum obtained from the pretreatment of a fresh ICI low surface area zinc oxide sample.

(5.1.3.2) Potassium Promoted Zinc Oxide

The pretreatment of the potassium promoted ZnO followed an indentical procedure to that used for the unpromoted catalyst. For these catalysts the pretreatment desorption spectra were dominated by a large CO_2 peak at approximately 553-573 K due to K_2CO_3 decomposition. A typical pretreatment desorption spectrum for the 0.20 wt% K promoted catalyst is shown in figure 5.3. There did not appear to be any significant loss of potassium (39 amu) during the carbonate decomposition process, which was confirmed by atomic emission measurements on pretreated catalyst samples. XPS measurements showed the potassium underwent redistribution over the catalyst surface during the pretreatment stage (see Appendix 4). Subsequent heating of a promoted catalyst after this pretreatment did not evolve any further CO_2.

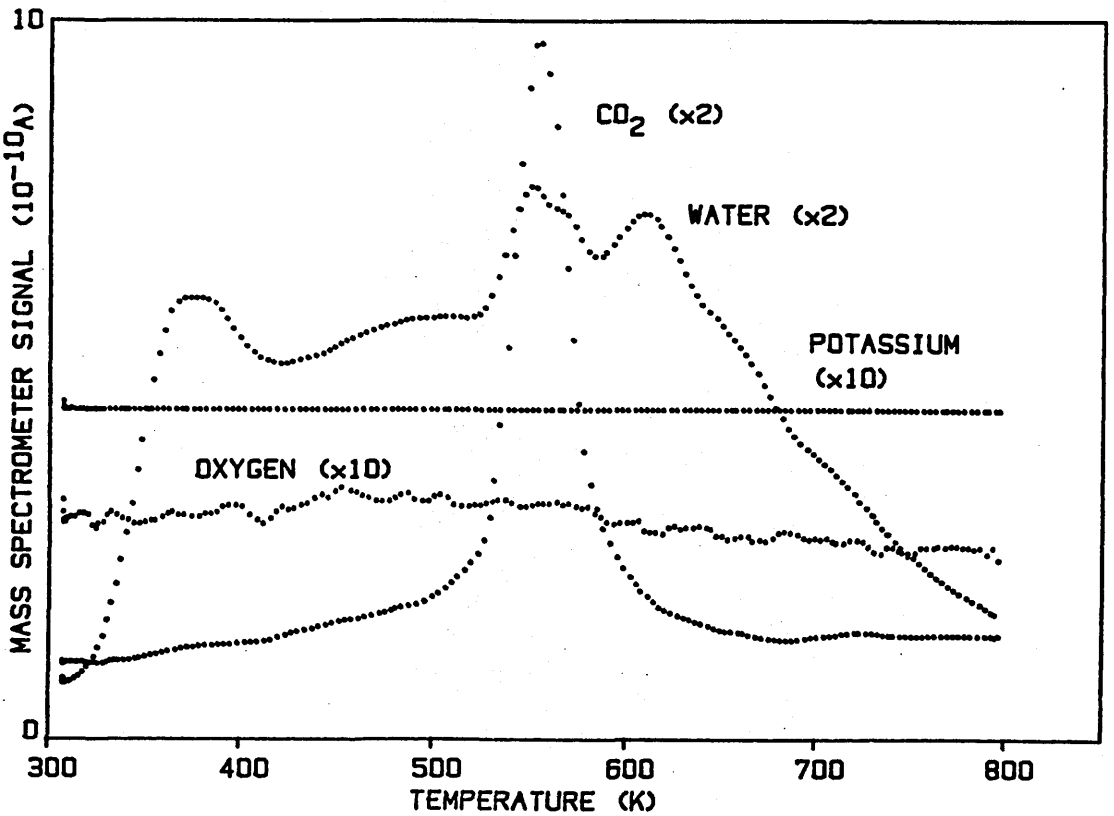

Figure 5.3: The desorption spectrum obtained from the pretreatment of a fresh 0.20 wt% K promoted zinc oxide sample.

(5.2) Catalyst Characterisation

(5.2.1) Surface Area Measurement

Catalyst surface areas were determined by a continuous flow method[137] and calculated according to the BET Equation[138] (see Appendix 2). The reactor and furnace were replaced with a glass U-tube containing the catalyst sample and the helium carrier gas by a 9.74% N_2 in He gas mixture. The equilibrium quantity of N_2 physisorbed onto the sample was measured when the tube was immersed in a flask of liquid N_2 by monitoring of the 28 amu mass spectrometer signal. Table 5.2 summarises the results obtained for the surface areas of a series of fresh and used catalyst samples. The area determined for ICI low surface area ZnO was in good agreement with that reported by Bowker et al[25]. Both the ZnO and ICI low surface area ZnO surface areas were found to be stable even after repeated experimental use. In addition, the loss of surface area after alkali promotion was not significant to within the accuracy of the measurements made. In contrast however, the surface area of the high surface area catalyst appeared sensitive to experimental usage and its surface area decreased significantly due to sintering effects. This made estimation of reliable surface coverages for this catalyst difficult.

(5.2.2) Transmission Electron Microscopy

The catalysts were analysed by TEM in order to characterise the crystal morphology of the catalysts studied. Both the AnalaR ZnO and ICI low surface area ZnO were found to have a well defined structure, with "typical" crystallite dimensions for the former estimated to be in the order of 250 nm across the polar surfaces by 300 nm along the

Table 5.2: Catalyst specific surface areas.

catalyst description	specific surface area ($m^2/g, \pm 0.2$)
fresh ZnO	4.6
used ZnO	4.2
fresh 0.20 wt% K promoted ZnO	4.3
fresh ICI low surface area ZnO	3.3
fresh ICI high surface area ZnO	43 ± 2
used ICI high surface area ZnO	~20

prism edges. The ICI low surface area ZnO crystals appeared to be of similar dimensions that were consistent with those previously reported by Bowker et al[25]. However, as would be expected with a "real" crystalline solid, a significant fraction of the crystals observed under the microscope were more irregular, ranging from near spherical to long needle crystallite shapes.

The presence of this significant amount of irregular crystallite shapes made estimation of the relative fraction of the crystal surfaces difficult. For an ideal ZnO crystal shape, figure 5.4 shows the fraction of total polar surfaces, for the $4.6\text{-}4.2 \pm 0.2$ m^2/g specific surface areas measured, to be in the region of 30-40% of the surface area. This is similar to the 20% estimate of the fraction of total polar surface for ICI low surface area ZnO made by Bowker et al[25], with the slightly higher figure being in line with higher ZnO surface area (4.6 m^2/g compared to 3 m^2/g).

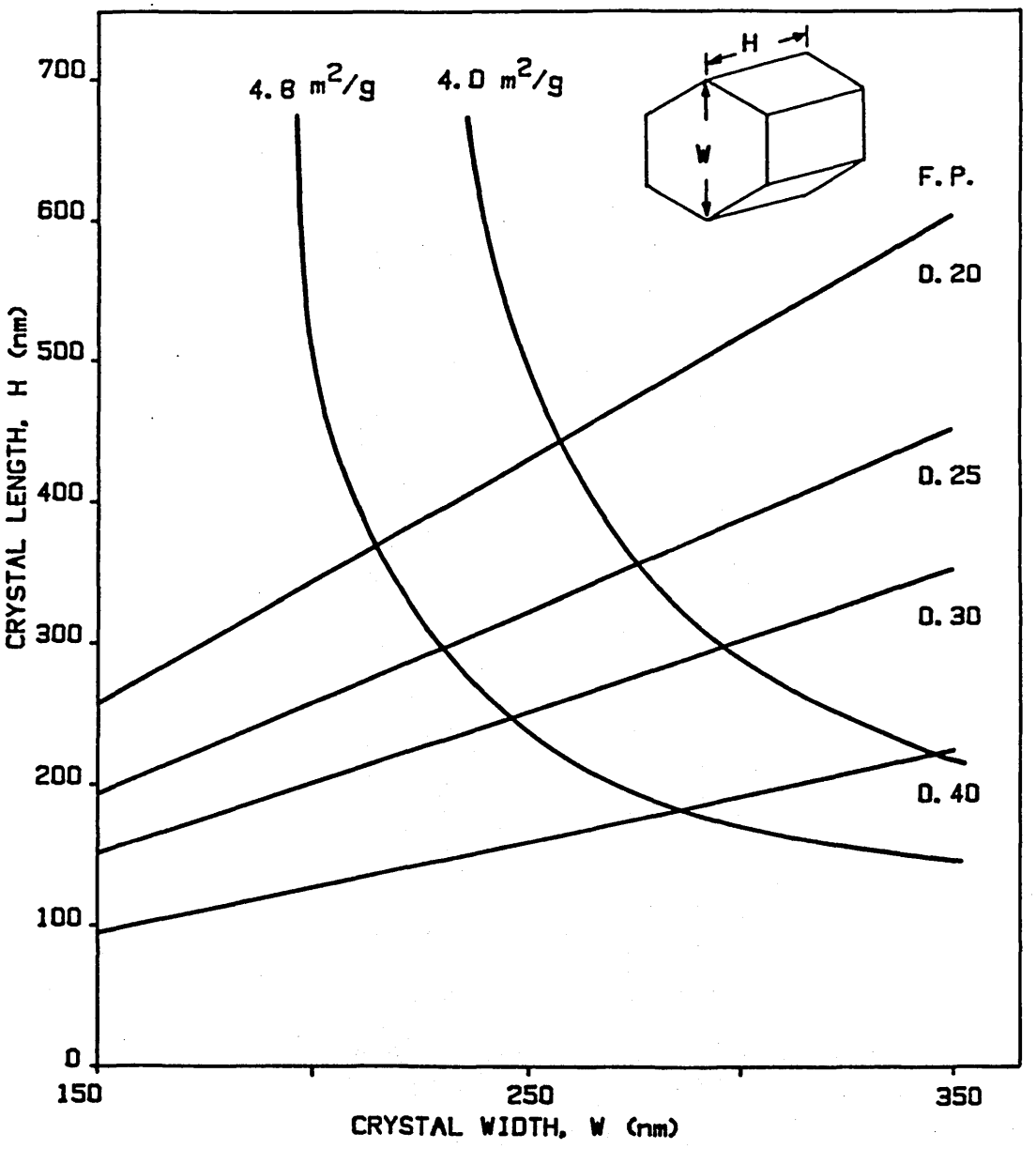

Figure 5.4: Plot of the relationship between the specific surface area and the fraction of polar surface area for an ideal zinc oxide crystal as a function of crystal dimensions. (F.P.= fraction polar surface)

The ICI high surface area catalyst crystal dimensions were observed to be much smaller than the AnalaR samples, consistent with the higher specific surface area. Bowker et et[98] has previously reported a similar high surface area ZnO as having crystallite dimensions in the order of 15 nm across, with an aspect ratio of one and estimated the fraction of polar surfaces to be in the order of 33% for this catalyst.

CHAPTER 6

ADSORPTION STUDIES ON ZINC OXIDE

(6.1) Adsorption on Unpromoted Zinc Oxide

(6.1.1) Water Adsorption on Zinc Oxide

(6.1.1.1) Thermal Desorption Spectrum

The desorption spectrum obtained after a saturation dose of water onto ZnO at 340 K is given in figure 6.1. The several peaks observable in the spectrum are designated α, β, γ, δ and ε with peak temperatures as given in table 6.1. Although molecularly adsorbed forms of water are possible, the desorption spectrum obtained is most likely derived from adsorbed hydroxyl species since Atherton et al[43] has shown only adsorbed hydroxyl species to be present on ZnO at 320 K. Monitoring of the mass 2 and mass 32 signals during the desorption of water after saturation coverage did not detect any desorption of either hydrogen or oxygen inferring that the hydroxyl condensation reactions leading to water desorption did not result in significant amounts of either residual hydrogen or oxygen being left on the catalyst surface.

Saturation of the catalyst by pulse injection of water resulted in desorption that corresponded to an effective surface coverage of $4.9\pm0.4\times10^{14}$ H_2O molecules/cm^2 in good agreement with the measurements of Morimoto et al[87]. The same coverage was also obtained after water was adsorbed from a continuous water/helium flow over the catalyst. Since the effective contact times of the water vapour with the catalyst bed of the two methods (injection and steady-state flow)

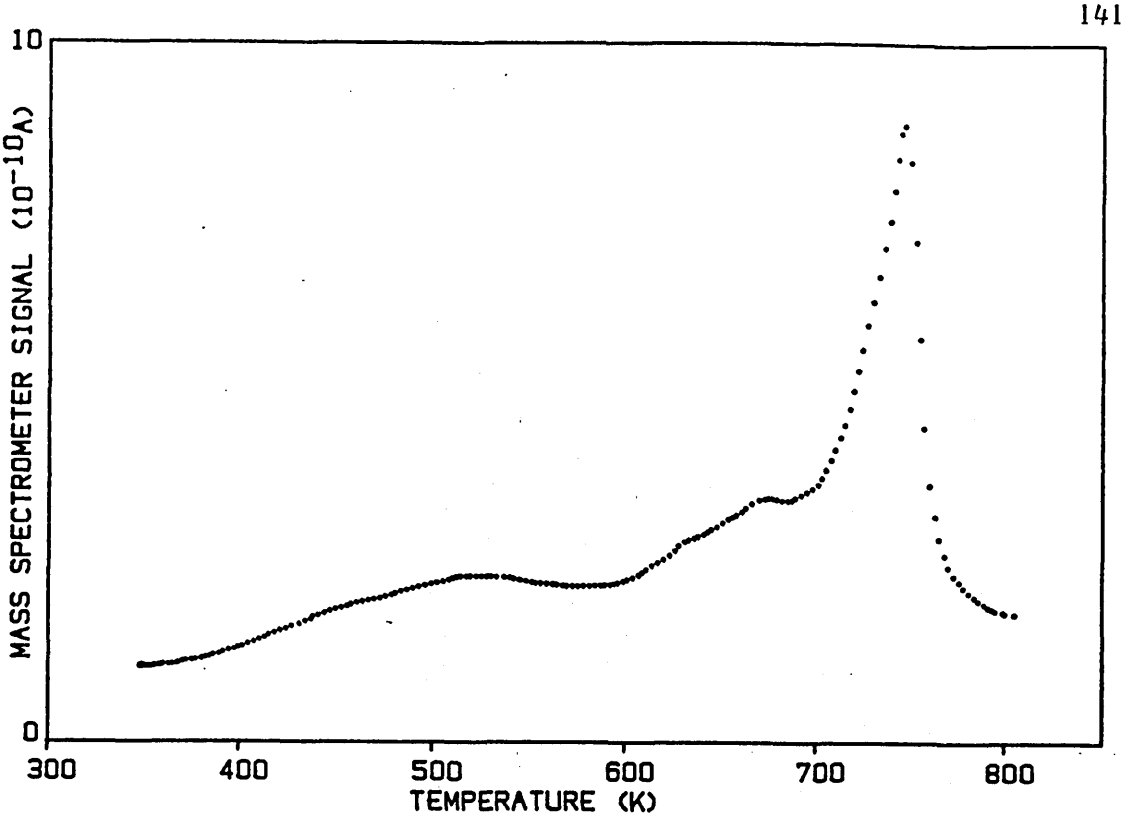

Figure 6.1: The water desorption spectrum after adsorption at 340 K to saturation coverage on zinc oxide.

differed by nearly two orders of magnitude, the observed similarity in the respective saturation coverages showed the adsorption of water onto ZnO to be very rapid i.e little or no activation energy barrier existed at 340 K. Further evidence to support this conclusion was provided by experiments where water was dosed at elevated temperatures (up to 530 K). No change in the form of the water desorption TPD spectra was found (other than the removal of the desorption states below or at the adsorption temperature) inferring the absence of any activated hydroxyl adsorption sites.

No significant changes in the desorption peak profiles were observed with experimental use of a catalyst sample except for a slight decrease in the coverage in the α state after a large number of experiments (>15). This showed the catalyst structure to be stable to repeated water adsorption and heating cycles as was also

Table 6.1: The water desorption peaks after adsorption at 340 K to saturation coverage on zinc oxide.

peak designation	peak temperature (K)
α	743±2
β	668±5
γ	627±5
δ	521±10
ε	383±10

indicated by the stability of its specific surface area (see Chapter 5).

(6.1.1.2) Coverage Dependence

Experiments were conducted where the dose of water was varied from approximately 8% of saturation to full saturation coverage. The changes in the resultant desorption spectra are summarised in figure 6.2. At the lowest coverage the desorption spectrum consisted of a rise in the baseline signal beginning at approximately 655 K which did not form into a peak. Adsorption of D_2O confirmed this rise to be due to desorption from surface adsorbed species rather than diffusion of water from the catalyst bulk. As the water dose was increased, the α adsorption sites (i.e. those with the highest peak temperature) were selectively populated with the temperature of the α peak increasing from 708±2 K at low coverage to 743±2 K at full population. Full saturation of these sites (as determined by the point at which lower temperature peaks began to populate) corresponded to a surface

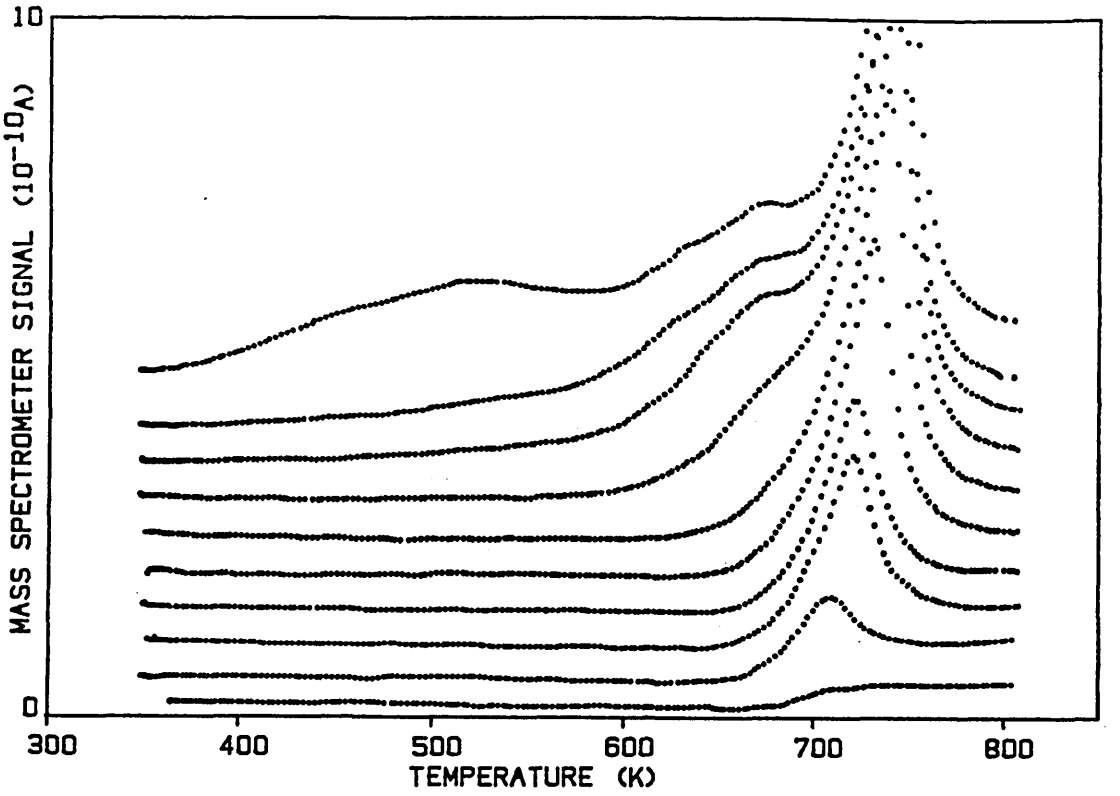

Figure 6.2: The coverage dependence of the water thermal desorption spectrum after adsorption at 340 K on zinc oxide.

coverage of $1.5\pm0.2 \times 10^{14}$ H_2O/cm^2. After this point as the dose was increased further, lower temperature adsorption states were populated as shown by the development of peaks at 668 ± 5, 627 ± 5 and 521 ± 10 K plus a poorly resolved shoulder at 383 ± 10 K. A further peak at approximately 365 K could also be populated but was not observed at the 340 K adsorption temperature used. Compared to the high temperature peak, these new desorption peaks were broad, ill-defined and distorted by overlapping. For the β peak, this is illustrated in figure 6.3 where the α desorption peak has been subtracted from the saturation water spectrum. The broadness of these lower temperature peaks showed a wider spread of desorption energies existed for their corresponding surface sites compared to the sharp peak produced from the α sites i.e. the sites were energetically less well defined.

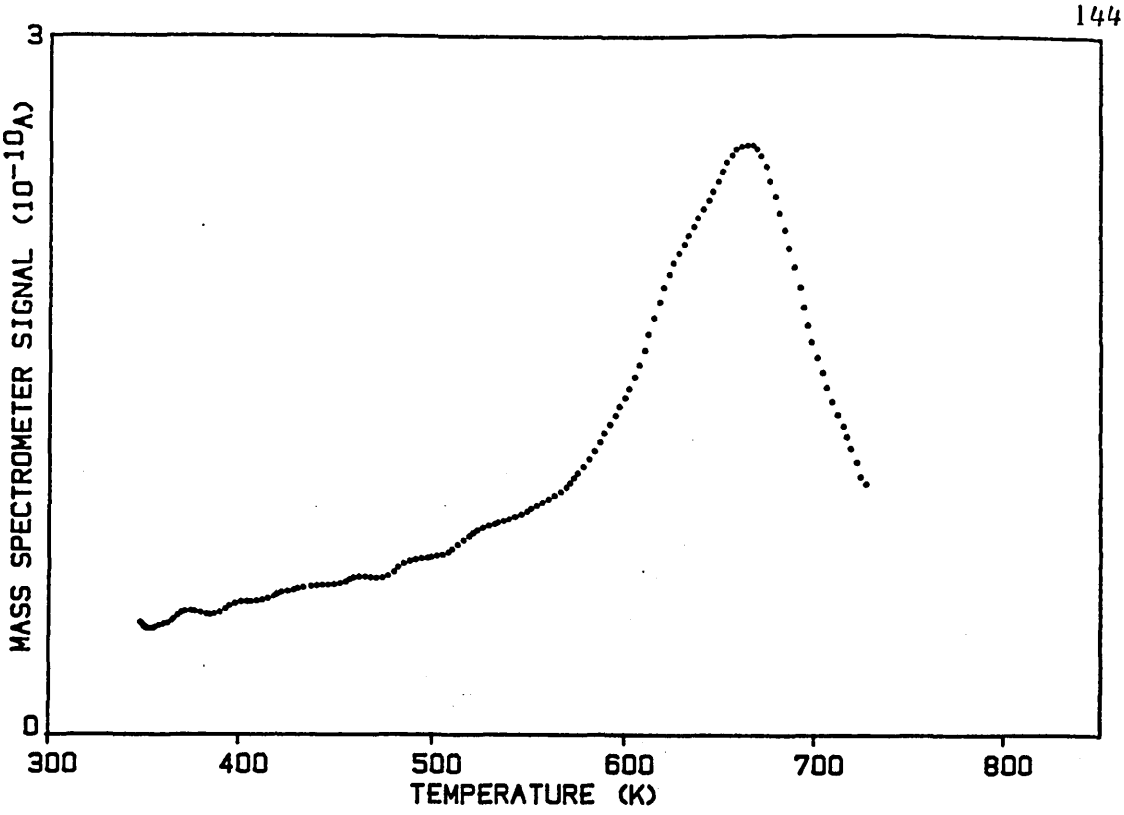

Figure 6.3: The saturation coverage water desorption spectrum with the α desorption peak subtracted.

(6.1.1.3) Determination of the Heats of Adsorption

(6.1.1.3.1) Extent of Readsorption Within the Catalyst Bed

Before the energetics of the hydroxyl desorptions could be quantified, the extent of readsorption that occurred within the catalyst bed during a TPD experiment had to be determined. Readsorption effects produce large distortions in TPD peaks by broadening and raising the peak temperatures and, unless accounted for in the TPD results analysis, large inaccuracies in the determined desorption energetics can be introduced[122,124,125,127] (see chapter 3). The extent of readsorption can be qualitatively determined by the dependence of the desorption peak temperature on carrier gas flowrate[120]. Experiments were conducted where the helium carrier flowrate was varied in the

range 26 to 164 ml/min with the other experimental conditions otherwise standard. The log-linear plot of flowrate against peak temperature for the α state (figure 6.4) was linear and indicated[120] that conditions of free readsorption existed within the catalyst bed over the complete range of experimental flowrates tested. Similar temperature shifts were also observed for the other water desorption states in the same flowrate range.

The results established that quantitative analysis of the water desorption spectra measured the heat of adsorption rather than the activation energy of desorption, with the difference being the activation energy of adsorption[24].

(6.1.1.3.2) Intraparticular Mass Transfer Effects

A reliable test for intraparticular mass transfer gradients can be made through varying the catalyst particle size[124]. Catalyst particle sizes ranging from 215 to 925 μm were investigated. Table 6.2 shows the α water desorption peak temperature to be independent of the catalyst particle size. Therefore, to within experimental error limits, intraparticular mass transfer effects were not significant.

Table 6.2: The influence of catalyst particle size on the α water desorption peak temperature

mean catalyst particle size (μm)	peak temperature[a] (K, ±2)
925	474
925	472
510	473
510	473
215	473
215	471

(a)=peak temperature corrected for sample mass (see section 6.1.1.3.4)

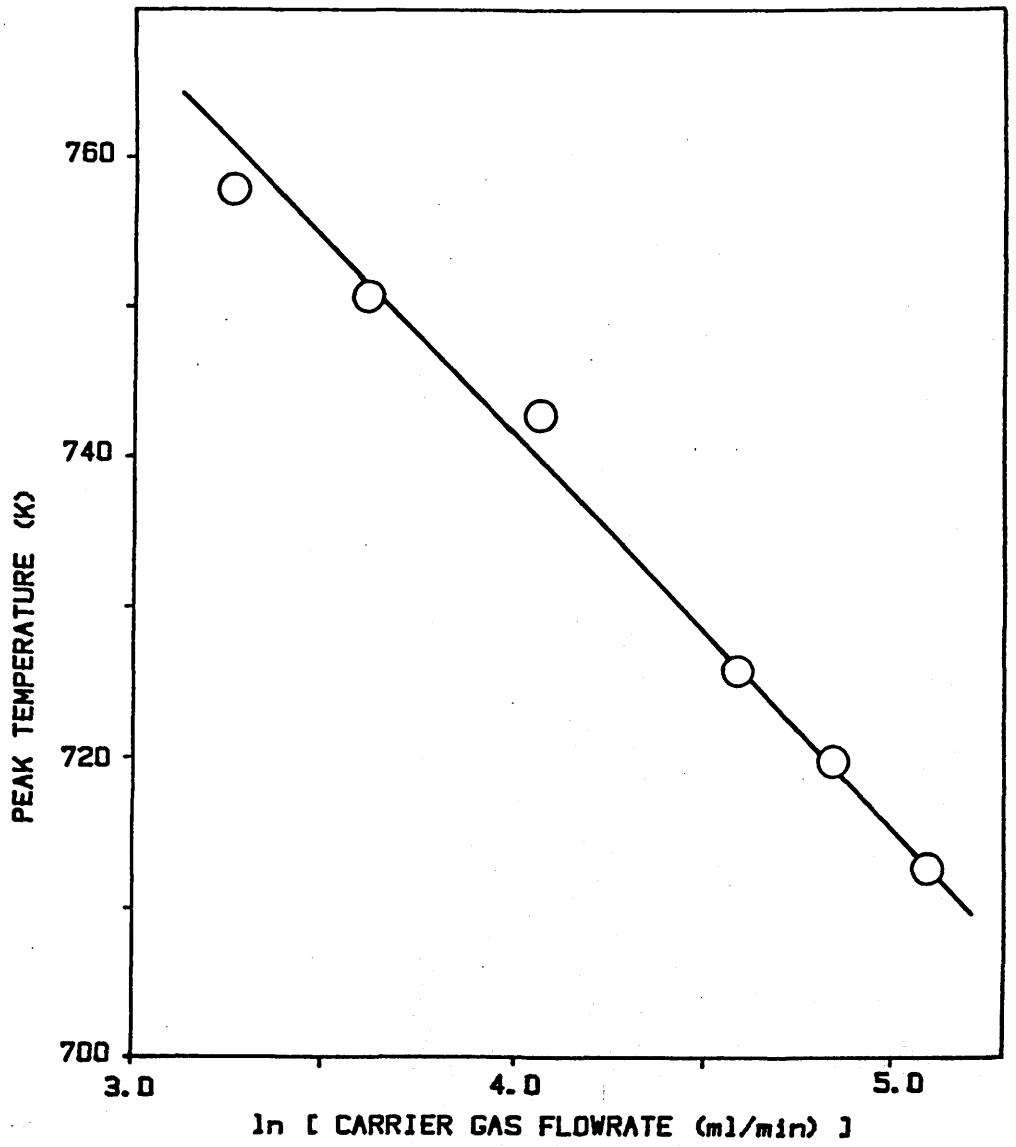

Figure 6.4: Plot of the extent of readsorption within the catalyst bed as shown by variation in the α water desorption peak temperature from zinc oxide with helium carrier gas flowrate.

(6.1.1.3.3) Heat of Adsorption by Heating-Rate Variation Method

The previous sections showed the water desorption spectrum to be readsorption limited, but not to be distorted by mass transfer effects. These results established the validity of using the variation in peak temperature with heating rate to measure the heat of adsorption, according to the method described in section 3.4[24]. However, since this method of analysis is sensitive to error in the measurement of the desorption peak temperature[130], meaningful results were only able to be obtained for the sharp α desorption state where the peak position could be accurately measured. The peaks of the lower temperature desorption states could not be determined with sufficient accuracy. From the plot of β/T_m^2 against $1/T_m$ (figure 6.5) for the α peak, a value for the heat of adsorption of 151±10 kJ/mol was obtained.

(6.1.1.3.4) Heat of Adsorption by Catalyst Mass Variation Method

As described above, the water desorption spectrum was readsorption, but not diffusion, limited. In an analogous manner to the method described above, the variation in the peak temperature with catalyst sample mass was able to be used to determine the heat of adsorption according to the method described in section 3.4[128]. Again this analysis could only be applied to the α desorption peak since the position of the lower temperature states could not be determined with sufficient accuracy. For the α state a plot of the dependence of peak temperature on catalyst weight (figure 6.6) yielded a heat of adsorption value of 166±10 kJ/mol, in good agreement with the result obtained by the heating rate variation method.

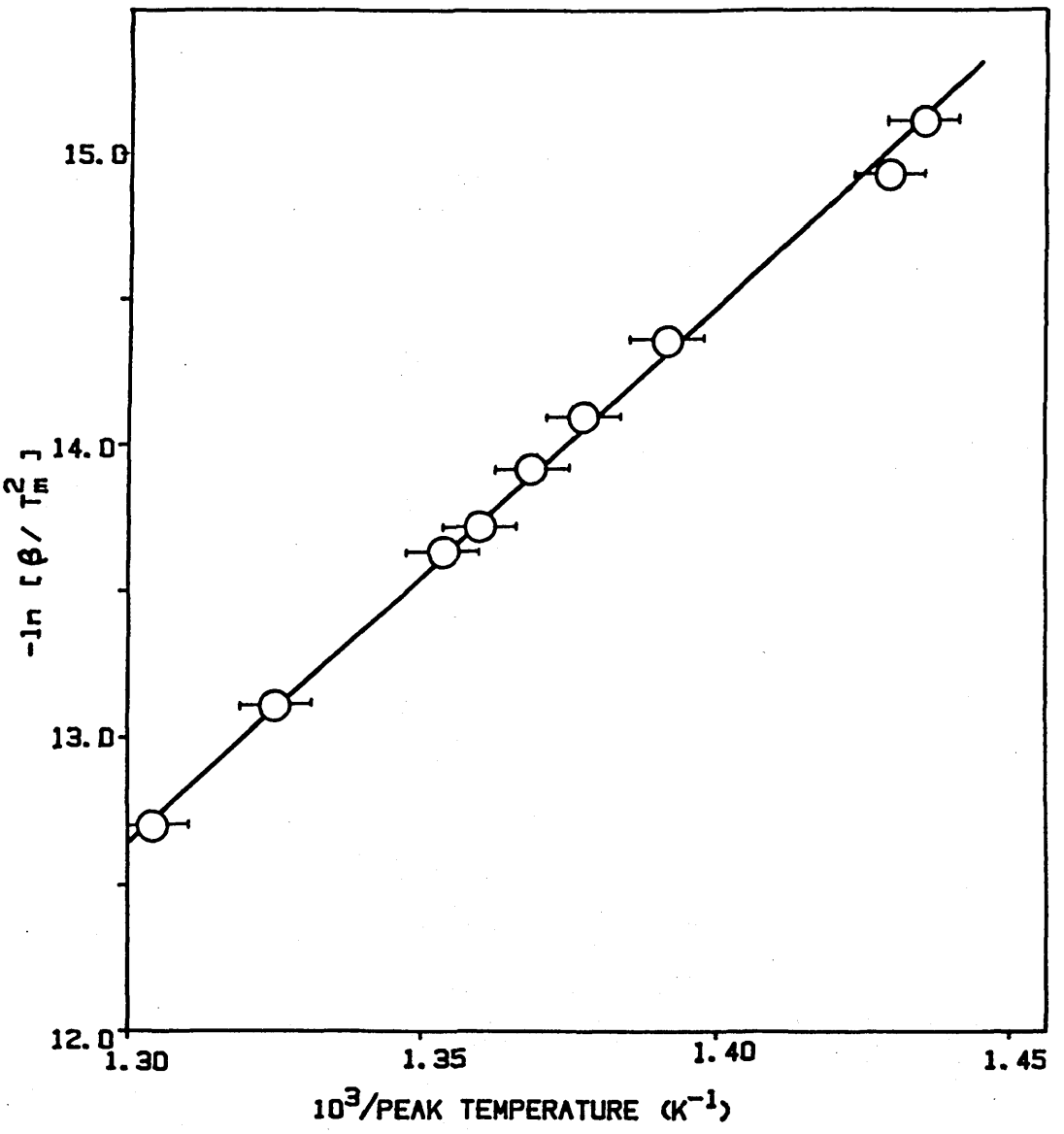

Figure 6.5: Characteristic plot of ln (β/T_m^2) against $1/T_m$ for α water desorption from zinc oxide.

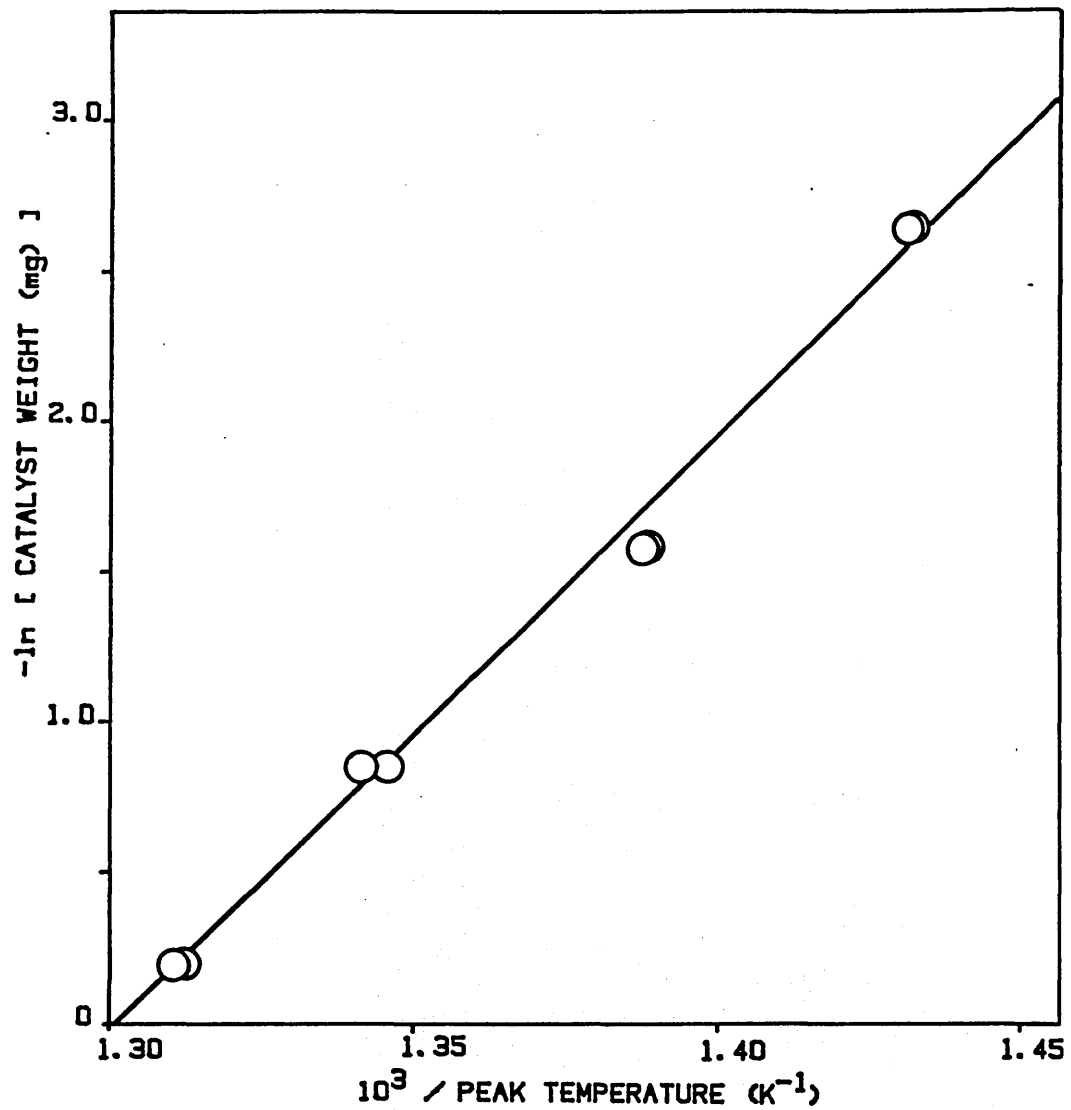

Figure 6.6: Characteristic plot of ln (catalyst mass) against $1/T_m$ for α water desorption from zinc oxide.

(6.1.1.3.5) Heats of Adsorption by Redheads Method

Estimates of the heats of adsorption for the lower temperature desorption states were made by the Redhead Equation[24,129] with a 'pseudo' preexponential value calculated from the experimentally determined heat of adsorption for the α peak i.e. the preexponential was effectively scaled to take into account readsorption effects. The preexponential factor calculated in this manner was found to be 5×10^9 s^{-1}. The heats of adsorption for the water desorption peaks determined by this method are given in table 6.3; because of the assumptions involved in application of the Redhead Equation (see section 3.4), these results should only be interpreted as order of magnitude estimations of the true values.

Table 6.3: Estimates of the heats of adsorption for water desorption from zinc oxide using Redheads Method.

desorption peak	heat of adsorption[a] (kJ/mol)
α	161
β	144
γ	135
δ	111
ε	81

(a)= determined using a preexponential of 5×10^9 s^{-1}

(6.1.2) Carbon Dioxide Adsorption on Zinc Oxide

(6.1.2.1) Thermal Desorption Spectrum

The desorption spectrum obtained after a saturation dose of CO_2 at 325 K is given in figure 6.7. The several peaks in the spectrum were designated α, β, γ, δ and ε respectively. Their corresponding temperatures are given in table 6.4, along with estimates of the heats of adsorption calculated using the Redhead Equation[24,129] (these are based on a preexponential factor of 10^{13} s^{-1}[25] that assumes no readsorption; although not quantified, as for water desorption, the CO_2 peaks were also indicated to be readsorption limited, so the values for the heats of adsorption will be overestimates of the true heats). The poorly defined state at approximately 720 K shown in figure 6.7 was only observed from some ZnO samples, while the α peak was also not found on all ZnO samples tested. This effect appeared to be possibly related to the quantity of background water adsorbed on the catalyst surface. Monitoring of the mass 28 signal during the desorption of CO_2 showed only the CO contribution from the CO_2 mass spectrometer cracking pattern to be present i.e. no CO itself appeared to be desorbed. A small amount of water also evolved due to adsorption of background water present in the CO_2 and helium carrier gases.

The saturated surface coverage corresponded to approximately 400×10^{12} molecules/cm^2, although the coverage associated with the ε peak was found to be sensitive to the adsorption temperature used and on the time period between adsorption and heating, as shown in figure 6.8. A further time dependent effect was observed, also shown in figure 6.8; if a catalyst saturated with CO_2 was left for a longer time period, a positive shift in the α and β peak temperatures

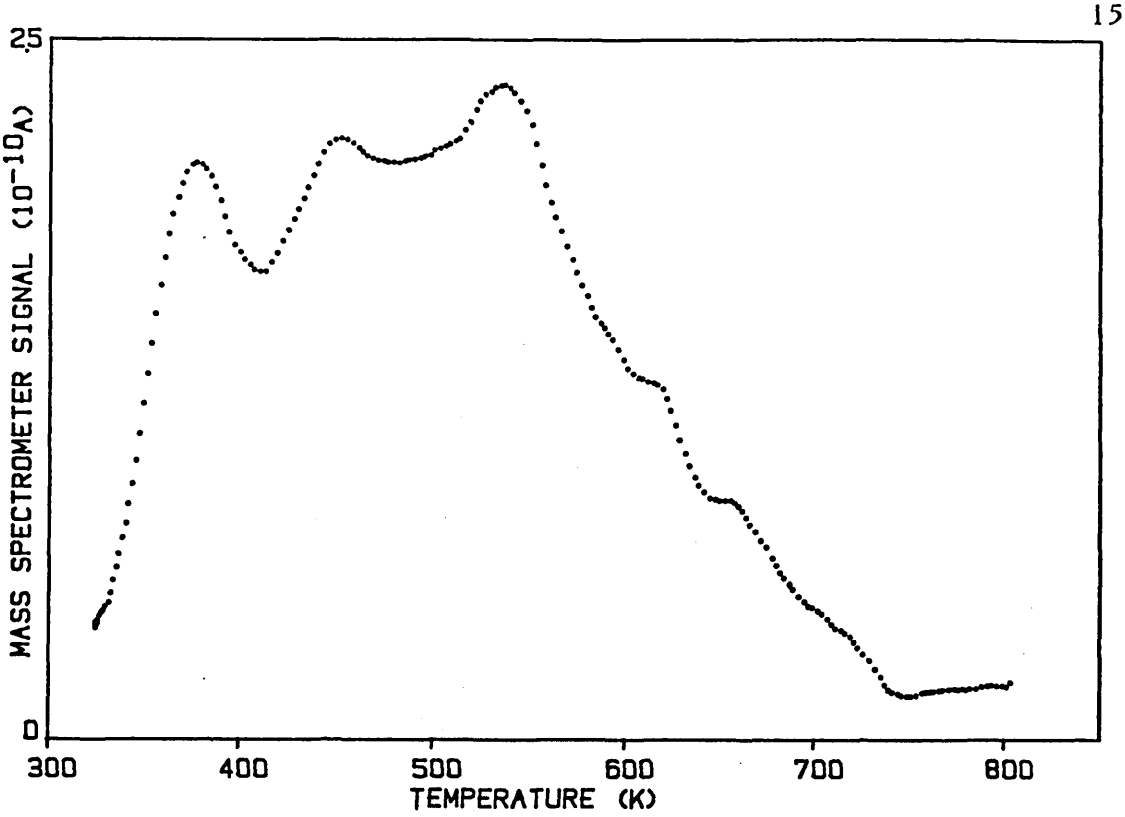

Figure 6.7: The carbon dioxide desorption spectrum after adsorption at 325 K to saturation coverage on zinc oxide.

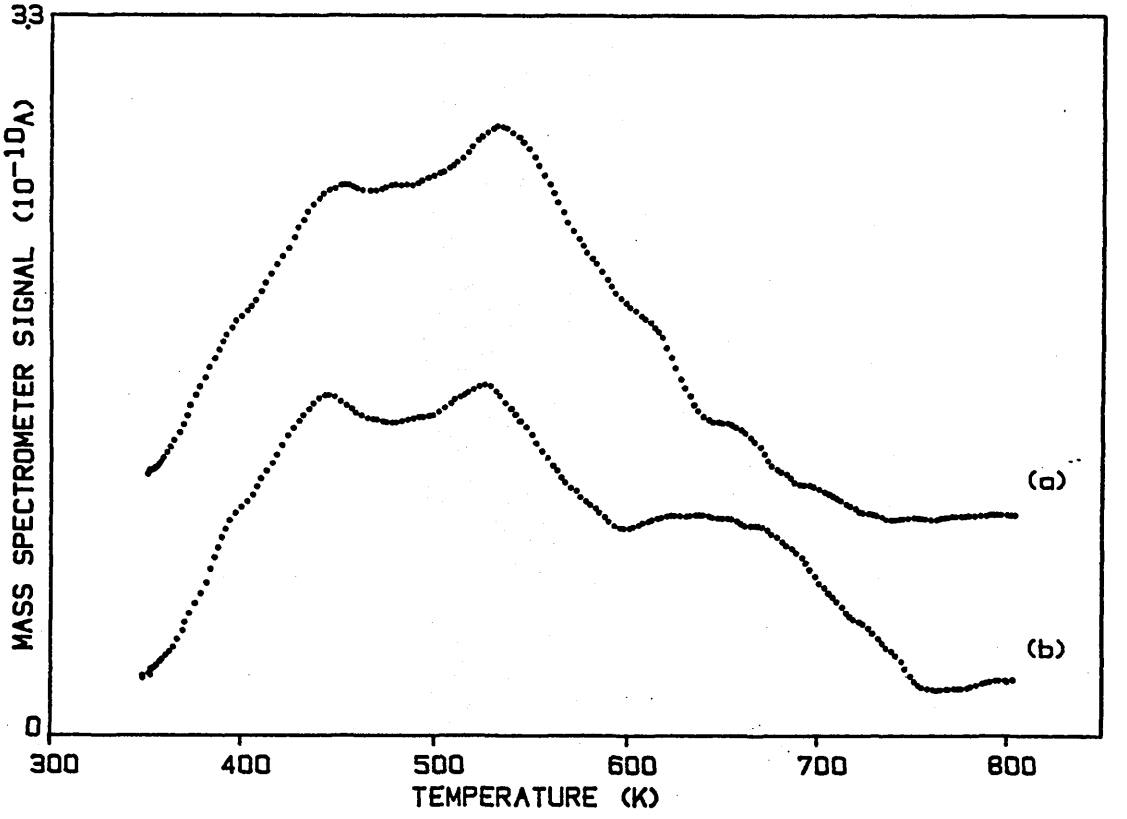

Figure 6.8: Time dependence of the CO_2 desorption spectrum after adsorption at 325 K to saturation coverage on zinc oxide. Time between adsorption and heating: (a)= 3 minutes; (b)= 30 minutes.

Table 6.4: The carbon dioxide desorption peaks and heats of adsorption after adsorption at 340 K to saturation coverage on zinc oxide.

peak designation	desorption temperature (K, ±5)	adsorption[(a)] energy (kJ/mol)
α	655	182
β	617	171
γ	535	147
δ	451	124
ε	375	102

(a)= based on a preexponential= $1x10^{13}$ s^{-1}

occurred accompanied by an apparent increase in the coverage associated with each peak.

Adsorption of CO_2 at an elevated temperature (approximately 530 K) did not reveal the formation of any additional adsorption states, with the only effect being to remove the low temperature peaks from the desorption spectrum.

(6.1.2.2) Coverage Dependence

The changes in the desorption spectra as surface coverage was varied from 10% of saturation to full surface saturation are summarised in figure 6.9. The particular catalyst sample used in this series of experiments was found not to form a distinct α peak as described above. At the lowest dose adsorption was confined to the most stable β sites. Saturation of the β sites occurred at a coverage of

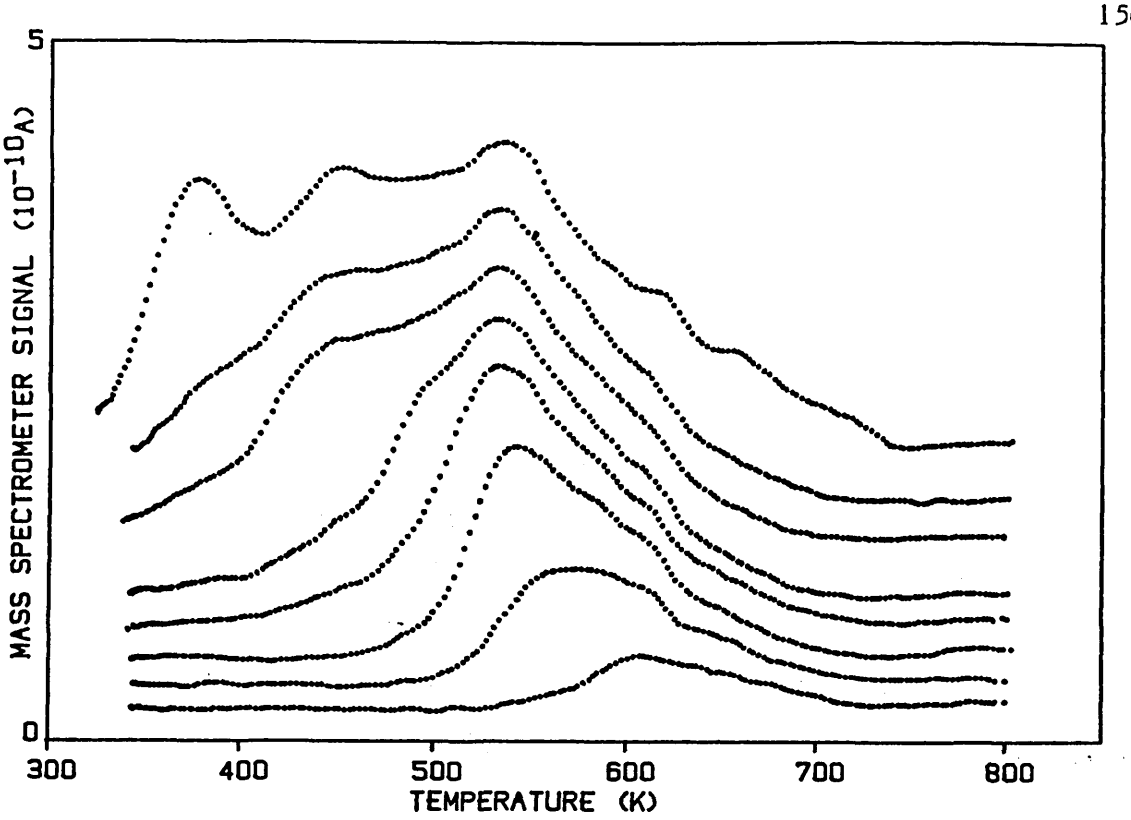

Figure 6.9: The coverage dependence of the carbon dioxide desorption spectrum after adsorption at 340 K on zinc oxide.

approximately 10% of the full saturation coverage. As the dose was increased the remaining surface sites were progressively populated in reverse order to their desorption temperature, analogous to the coverage dependent behaviour for water adsorption (section 6.1.1). No breakthrough of CO_2 was detected during adsorption until surface saturation was attained indicating a rapid adsorption with a low activation energy barrier. No coverage dependence was observed with any of the CO_2 peak temperatures.

(6.1.3) Propene Adsorption on Zinc Oxide

(6.1.3.1) Thermal Desorption Spectrum

After propene adsorption at 330 K to saturation coverage the desorption spectrum of figure 6.10 was obtained. Propene desorbed in a single peak at 403 K with an estimated heat of adsorption of 110

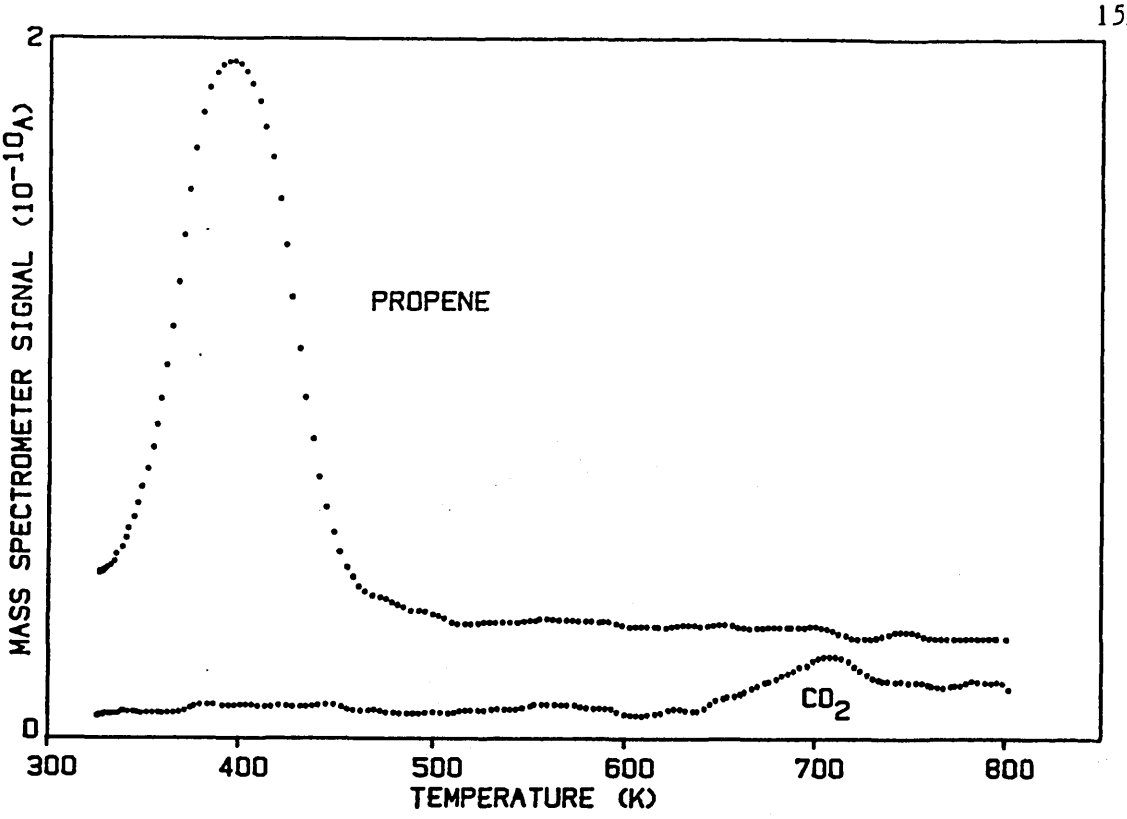

Figure 6.10: The propene desorption spectrum after adsorption at 330 K to saturation coverage on zinc oxide.

kJ/mol (by Redheads method[24,129] again based on a preeexponential factor of 10^{13} s^{-1} [25]). Although no other significant desorption or decomposition products were observed, the detection of small quantities of mass 15 (indicative of the CH_3 fragment) and water (propene to water molecular ratio of approximately 10:1) coincident with the propene, indicated the possibility of a minor side reaction accompanied by a surface reduction. The presence of a further high temperature water peak at 716 K (coverage $40x10^{12}$ H_2O/cm^2) suggested the presence of water impurities in the injected propene. The almost complete absence of a high temperature CO_2 desorption peak showed that surface oxidation did not take place as reported by Davydov et al[118] (see chapter 7). The saturated propene coverage of $90x10^{12}$ molecules/cm^2 was in reasonable agreement with the figure of $60x10^{12}$ species/cm^2 reported by Davydov et al[118].

(6.1.3.2) Propene and Water Coadsorption

The effect of propene coadsorption with water was investigated by the sequential adsorption of propene and water. Various predosed hydroxyl surface coverages were used ranging from approximately 10-15% of hydroxyl surface saturation to full surface saturation. Adsorption of water to a low hydroxyl coverage such that only adsorbed hydroxyls into the α state (see section 6.1.1) did not effect the propene desorption spectrum, which indicated no site competition i.e. adsorption sites were independent. Predosing to a higher hydroxyl coverage such that adsorption into the β and γ adsorption sites also occurred reduced the amount of propene desorbed, while preadsorption of water to full saturation coverage before propene adsorption resulted in only a small amount of propene desorption (approximately 5×10^{12} molecules $/cm^2$).

(6.1.3.3) Propene and Oxygen Coadsorption

Sequential injections of propene and oxygen were made at 330 K to test for any evidence of oxidation, for example, as reported by Davydov et al[118] and Nakajima et al[119]. The resulting propene desorption spectra were found to be the same as after adsorption of propene-only indicating that the presence of adsorbed oxygen did not result in any propene oxidation to form the carbonate/carboxylate complex (as would be shown by CO_2 evolution at high temperature- see chapter 7). Extended oxidation treatment of the catalyst (2 hours at 458 K followed by 2 hours at 623 K in 10% O_2/He gas flow) followed by propene adsorption at 323 K also failed to show any evidence of oxidation, as did coadsorption of oxygen and propene at high temperature (443 K).

(6.1.4) Hydrogen Adsorption on Zinc Oxide

(6.1.4.1) Thermal Desorption Spectrum

Unlike water and CO_2 (sections 6.1.1 and 6.1.2), hydrogen did not easily adsorb onto the surface of ZnO indicative of the effective sticking coefficient for dissociative hydrogen adsorption being low. Since the hydrogen adsorption sites on ZnO are known to be easily poisoned by adsorbed hydroxyls[27,40], the presence of any water impurity in either the hydrogen or in the carrier flow would have resulted in hydroxyl adsorption, and, therefore, contributed to the effective depletion of sites available for hydrogen adsorption. The rate of adsorption was so low that experiments, where pulse injections of pure hydrogen were made into the carrier flow, could not detect any subsequent hydrogen desorption during catalyst heating. However, by use of the valve as a flow switching device it was possible to pass a pure hydrogen flow over the catalyst surface for several minutes, and thereby increase the contact time of the hydrogen with the ZnO surface so that a detectable quantity of desorption was found during TPD.

The steady-state adsorption of hydrogen in this manner over a 10 minute period at a temperature of 340 K resulted in the formation of a single hydrogen desorption peak at 400 ± 8 K (figure 6.11), with an effective coverage of approximately 20×10^{12} H_2/cm^2. Based on a pre-exponential factor of 10^{13} s^{-1} [25], the heat of adsorption of this peak was estimated to be 109 kJ/mol by Redheads method[24,129]. No other hydrogen desorption peaks were detected. Monitoring of the water signal showed that some water desorption from the α sites (see section 6.1.1) also occurred at 723 K with an effective hydroxyl coverage corresponding to approximately 15% population of the α sites.

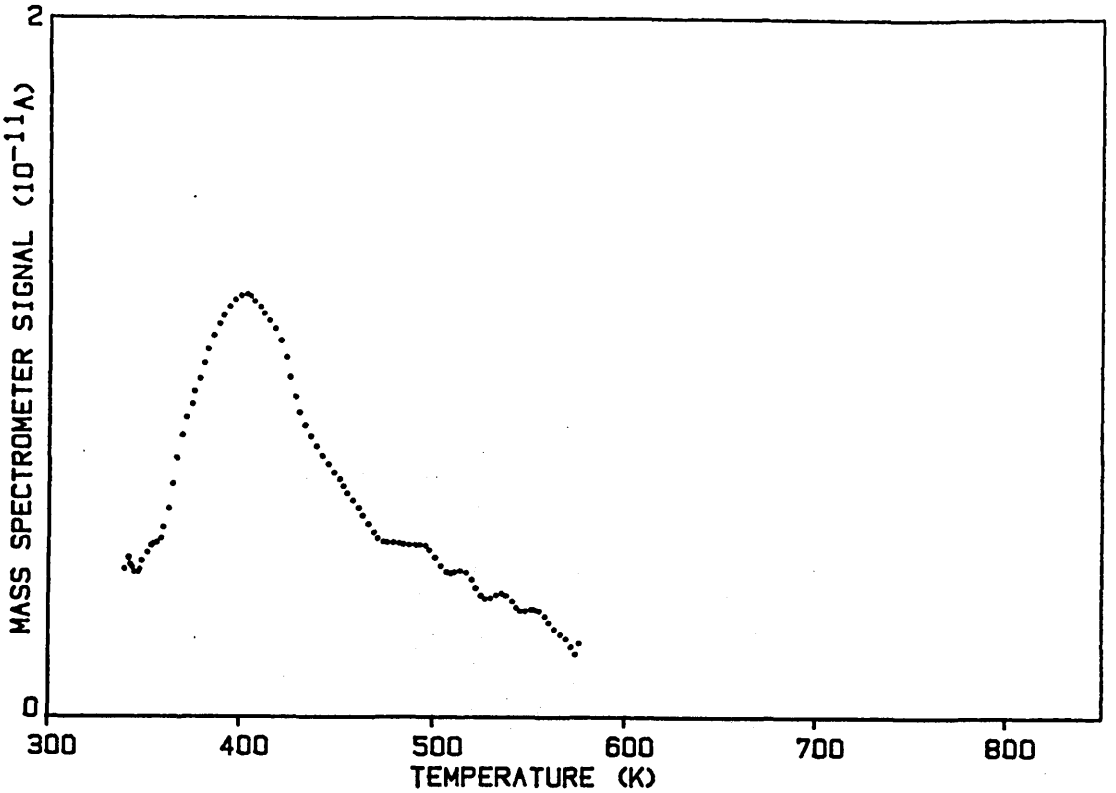

Figure 6.11: The hydrogen desorption spectrum after adsorption at 340 K on zinc oxide.

A blank experiment showed that this was not significantly greater than the small amount of water desorption due to the water impurity present in the helium carrier gas. Adsorption of hydrogen in the same manner but over a 225 minute period resulted in a reduced amount of hydrogen at 397 K and a significantly larger amount of water desorption such that saturation of the α sites was achieved.

Because of the difficulty in achieving hydrogen adsorption, no investigation was made of the coverage dependence of the hydrogen desorption spectrum.

(6.1.4.2) Effect of an Increased Adsorption Temperature

Increasing the adsorption temperature to 375 K resulted in the formation of a desorption peak at the slightly higher temperature of 433 K. However, there was no change in the quantity of either the hydrogen associated with this peak, or in the amount of high tempera-

ture water desorption. A further increase in the hydrogen adsorption temperature to 520 K gave no hydrogen desorption and only the water desorption peak was formed. The quantity of water desorbed was, however, significantly greater than after a low temperature hydrogen dose (by a factor of approximately 2.5) suggesting that at elevated temperature, hydrogen adsorbed and reacted with the ZnO surface to form strongly bound hydroxyl species with lattice oxygen that desorbed as water at high temperature, in a manner previously noted by Marshneva et al[139] i.e. surface reduction occurred. After this reduction treatment, no change was observed either in the desorption spectrum for hydrogen after low temperature adsorption, or in the TPD behaviour of both water and CO_2.

(6.2) Adsorption on Potassium Promoted Zinc Oxide

(6.2.1) Water Adsorption on Promoted Zinc Oxide

(6.2.1.1) Thermal Desorption Spectrum

The presence of the potassium promoters at all three loadings investigated was found to have a significant effect on the water desorption spectra. The desorption spectra obtained from the three promoted catalysts (0.042 wt%, 0.085 wt% and 0.20 wt% K loading respectively) after a saturation dose of water at 340 K are shown in figure 6.12.

In the high temperature region, α hydroxyl desorption in the 750 K peak was selectively reduced as potassium loading increased. At the 0.042 wt% K loading, where there appeared to be still a significant number of α sites remaining, the α peak was reduced in temperature to

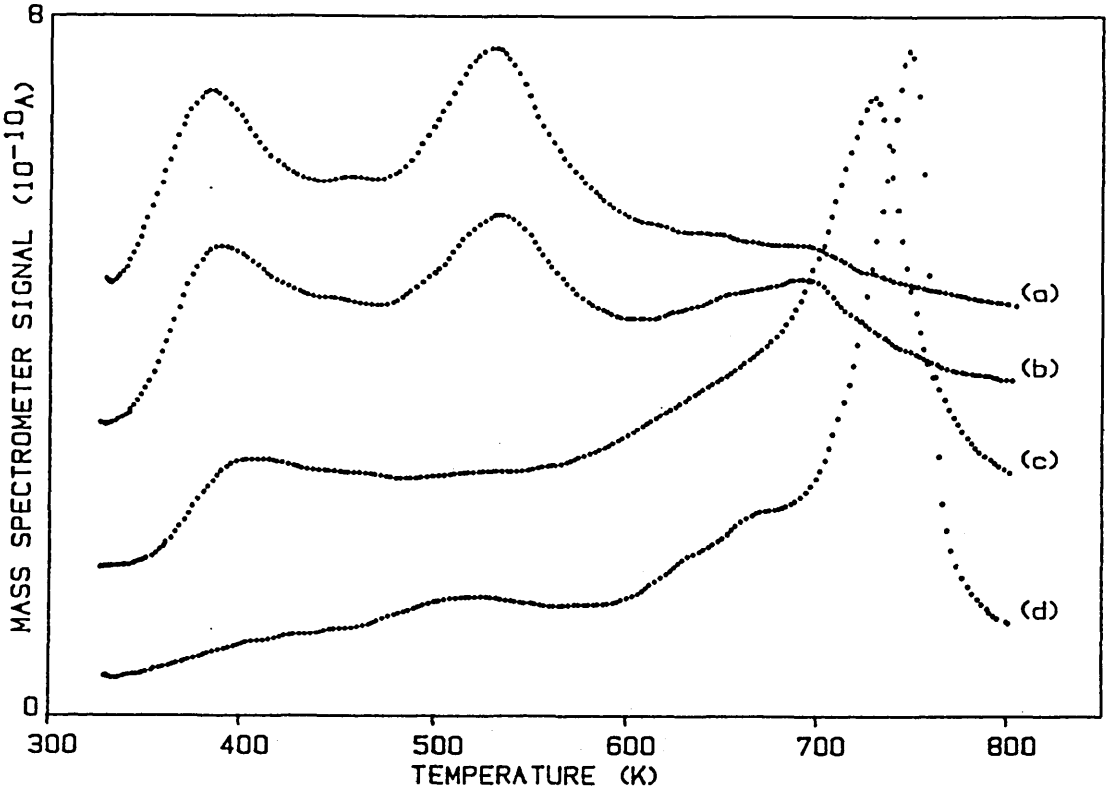

Figure 6.12: The effect of potassium loading on the water desorption spectrum after adsorption at 340 K on promoted zinc oxide.
(a)= 0.20 wt% K; (b)= 0.085 wt% K; (c)= 0.042 wt% K; (d)= unpromoted.

725 K indicative of a destabilising effect caused by the presence of the alkali. For the higher 0.085 wt% K loading the α peak was completely absent from the spectrum, and as the loading was increased further to 0.20 wt% K, the β peak normally underlying the α desorption peak was also diminished in size.

In the low temperature region the potassium promotion caused an increase in the amount of water desorption with peaks formed at 388 K and 533-541 K. The low desorption temperature of the first peak indicated that it was probably due to molecularly rather than dissociatively adsorbed water, particularly since adsorption of atmospheric water into this state appeared to continue during storage of pretreated catalysts as shown by a significant increase in the size of the peak at 388 K. This result also indicated that saturation of this

state was not achieved in the TPD experiments. The coverage associated with both peaks increased with potassium loading with the largest peaks produced for the 0.20 wt% K loading.

The total amount of water desorbed, after a fixed exposure at 340 K (by injection of water/He) was found to reduce with increasing potassium loading as shown in figure 6.13. This appeared to be a consequence of the reduction associated with the α and underlying β hydroxyl desorption peaks, with this decrease not being matched by an increased amount of desorption in the lower temperature region.

(6.2.1.2) Coverage Dependence

The coverage dependence for the water desorption spectra from the 0.085 wt% and 0.20 wt% K promoted catalysts are shown by figures 6.14 to 6.15. Coverages were varied from approximately 10% of saturation up to full surface saturation. Both catalysts were found to behave in a manner that was analogous to the behaviour shown by unpromoted ZnO i.e at low coverage only the most stable surface sites were populated. As described above, the effect of potassium promotion was to remove the α sites from both desorption spectra. As the potassium level was further increased to 0.20 wt% K, a reduction was also apparent in the β peak. The β peak temperature for both catalysts appeared to decrease with increasing water coverage, indicative of a decrease in the heat of adsorption.

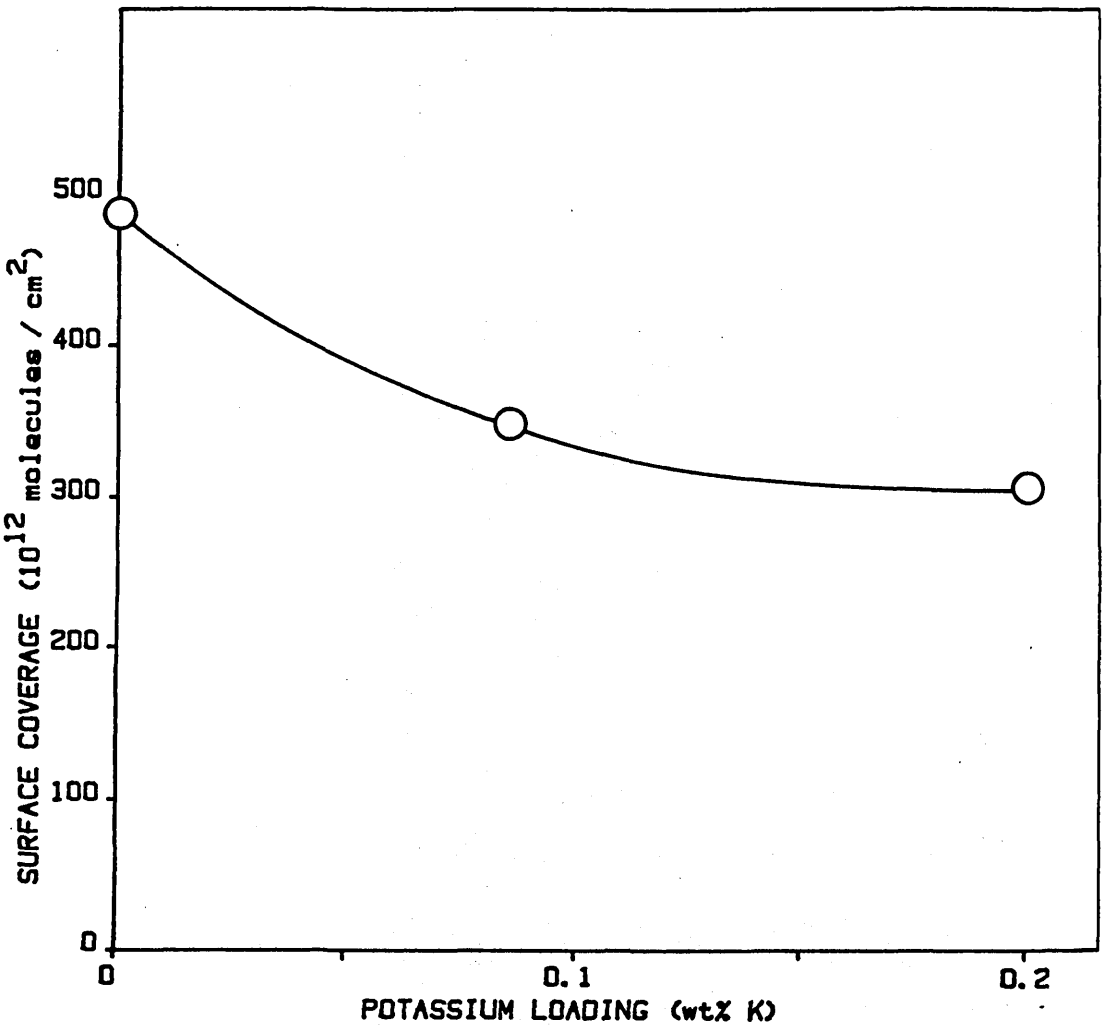

Figure 6.13: Plot of the effect of potassium loading on the saturation water surface coverage after adsorption at 340 K on promoted zinc oxide.

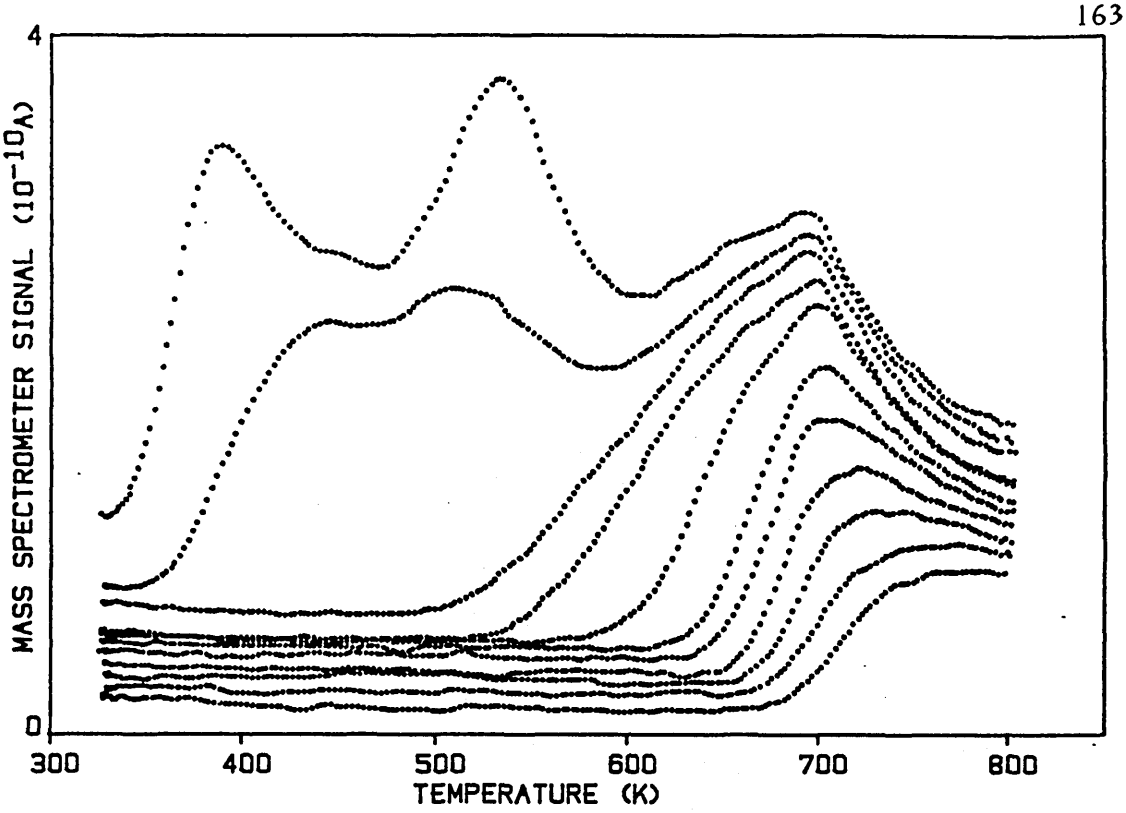

Figure 6.14: The coverage dependence of the water desorption spectrum after adsorption at 340 K on 0.085 wt% potassium promoted zinc oxide.

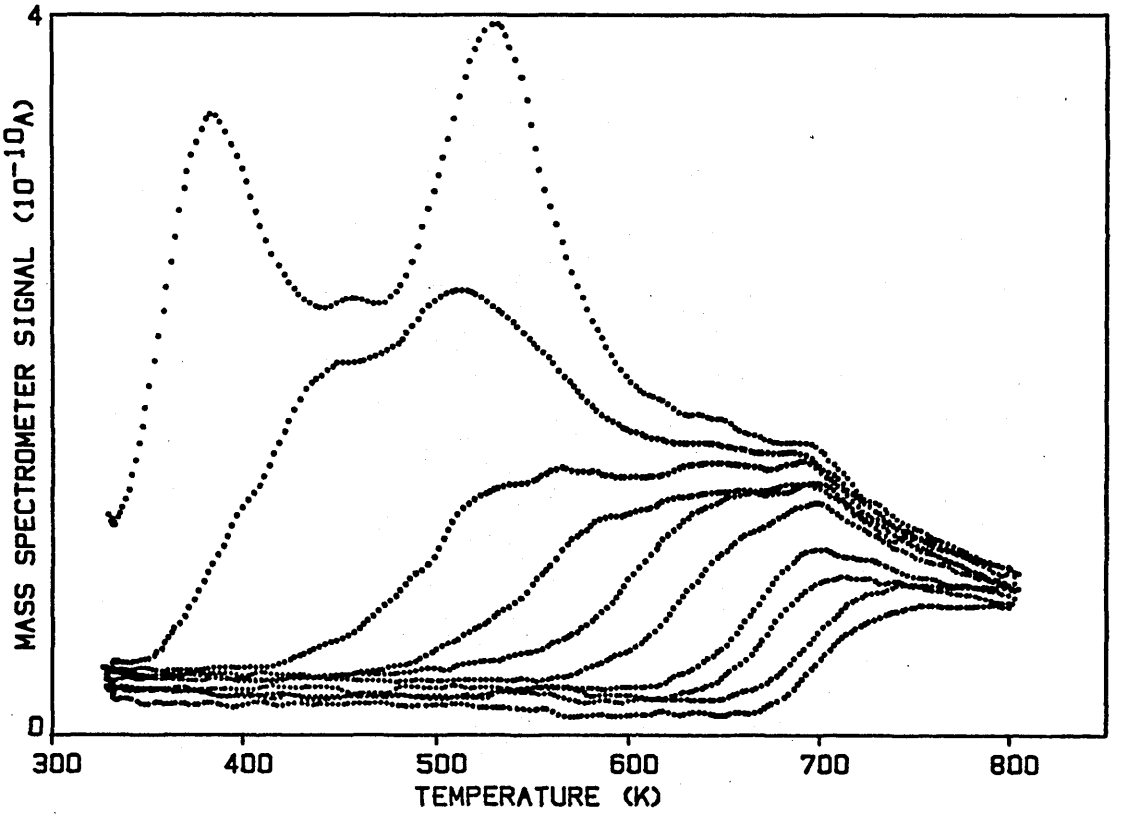

Figure 6.15: The coverage dependence of the water desorption spectrum after adsorption at 340 K on 0.20 wt% potassium promoted zinc oxide.

(6.2.2) Carbon Dioxide Adsorption on Promoted Zinc Oxide

(6.2.2.1) Thermal Desorption Spectrum

The influence of potassium loading on the CO_2 thermal desorption spectrum is shown in figure 6.16. The potassium promotion was found to cause two main effects:- increased desorption at high temperature, and decreased desorption in the low temperature region. The coverages associated with all three low temperature peaks (γ, δ and ε) were progressively reduced as alkali loading was increased. At the 0.042 wt% K loading the larger reductions were in the γ and ε states, with a smaller decrease in the δ peak. The overall coverage in the low temperature region was in the order of 300×10^{12} molecules/cm^2, although an accurate determination was not possible due to desorption contributions from the higher temperature states and a rising baseline (see below). Total coverage at this loading was approximately 500×10^{12} molecules/cm^2. Increasing the potassium levels to 0.085 wt% and 0.20 wt% further reduced the coverage in the γ and ε peaks but the main change occurred with the δ peak which, at the higher loading, was no longer present in the desorption spectrum. At 0.20 wt% K the coverage associated with the low temperature peaks had reduced to 160×10^{12} molecules/cm^2, with the total coverage being 300×10^{12} CO_2/cm^2. At this loading the ε peak temperature had increased to 415 K, and the γ peak decreased to 520 K. Although the β peak was still apparent at the 0.042 wt% K promoter level, it was removed from the spectra of the two higher potassium loadings. The α state was enhanced by the alkali promotion although the peak temperature decreased to 644 K at the 0.20 wt% loading.

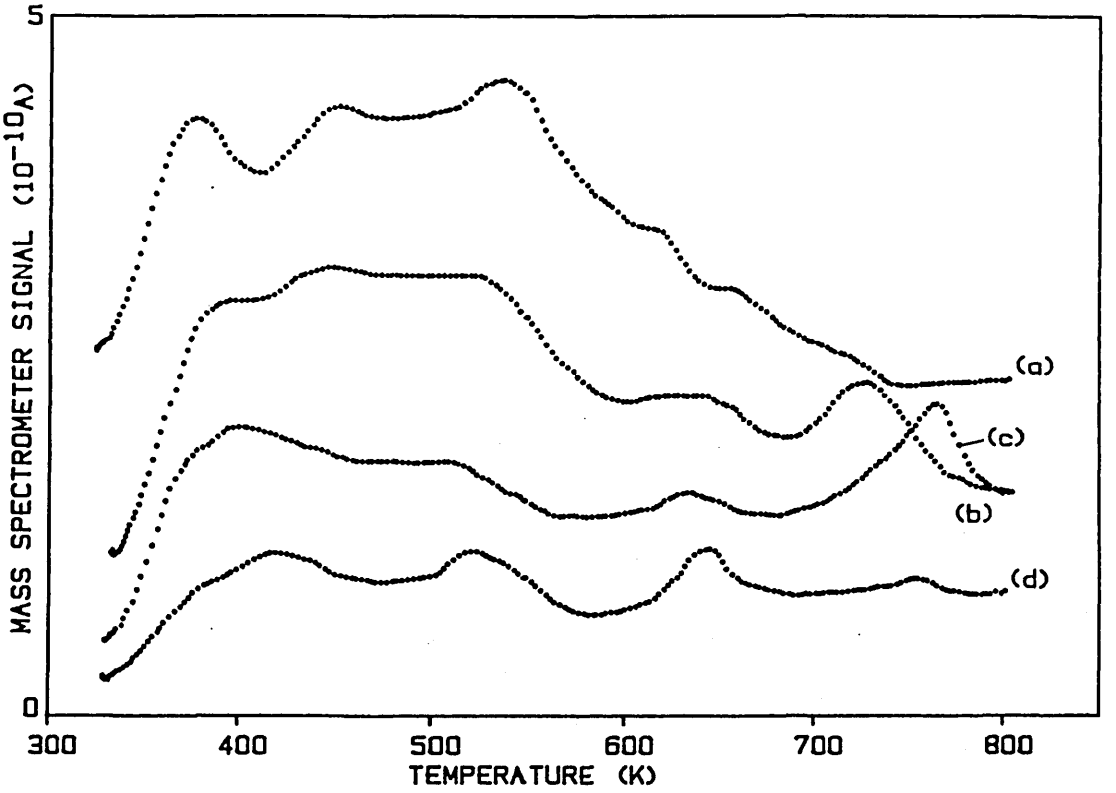

Figure 6.16: The effect of potassium loading on the carbon dioxide desorption spectrum after adsorption at 340 K on promoted zinc oxide. (a)=unpromoted; (b)=0.042 wt% K; (c)=0.085 wt% K; (d)=0.20 wt% K.

The poorly resolved state at 720 K on the unpromoted ZnO became very prominant on the 0.042 wt% and 0.085 wt% K catalysts, with an approximate coverage of 22×10^{12} molecules/cm^2. Its peak temperature, initially at 726 K on the 0.042 wt% K catalyst, increased to 763 K for the 0.085 wt% loading. Increasing the alkali loading to 0.20 wt% K resulted in a significant reduction in this peak and a slight reduction in peak temperature to 755 K. At all potassium loadings the CO_2 baseline signal was found to increase at higher temperature which indicated that more stable adsorption states may have remained on the catalyst surface at the experimental maximum of 800 K. On unpromoted ZnO a similar rise was not found with the baseline remaining level.

(6.2.2.2) Coverage Dependence

The coverage dependence of the CO_2 desorption spectra obtained from the promoted catalysts are shown in figures 6.17 to 6.19. Although the peaks of the desorption spectra obtained were significantly different to those obtained for the unpromoted ZnO, similar trends were observed in the coverage dependent behaviour. In common with the unpromoted ZnO, the highest temperature sites were populated first, with population of the lower temperature peaks only occurring at high coverage.

(6.3) Carbon Dioxide and Hydrogen Coadsorption on Unpromoted and Promoted Zinc Oxide

(6.3.1) Unpromoted Zinc Oxide

The coadsorption of CO_2 and hydrogen on ZnO has been reported by Bowker et al[25] to lead to the formation of an adsorbed formate species, which decomposes on heating to evolve CO_2, CO and hydrogen [25-27]. Experiments were carried out where CO_2 and hydrogen were sequentially adsorbed onto unpromoted and potassium promoted zinc oxide at temperatures ranging from 325 K to 475 K to determine if the presence of the potassium promoter affected the formation of formate.

After low temperature (325 K) sequential adsorption of CO_2, followed by hydrogen onto unpromoted ZnO, the resulting CO_2 desorption peak profile was found to be the same as previously obtained after CO_2-only adsorption (section 6.1.2). No hydrogen desorption was observed. Increasing the adsorption temperature to 427 K and 475 K resulted in the formation of a progressively larger CO_2 desorption peak at 602 K, at a similar temperature to CO_2 evolution previously

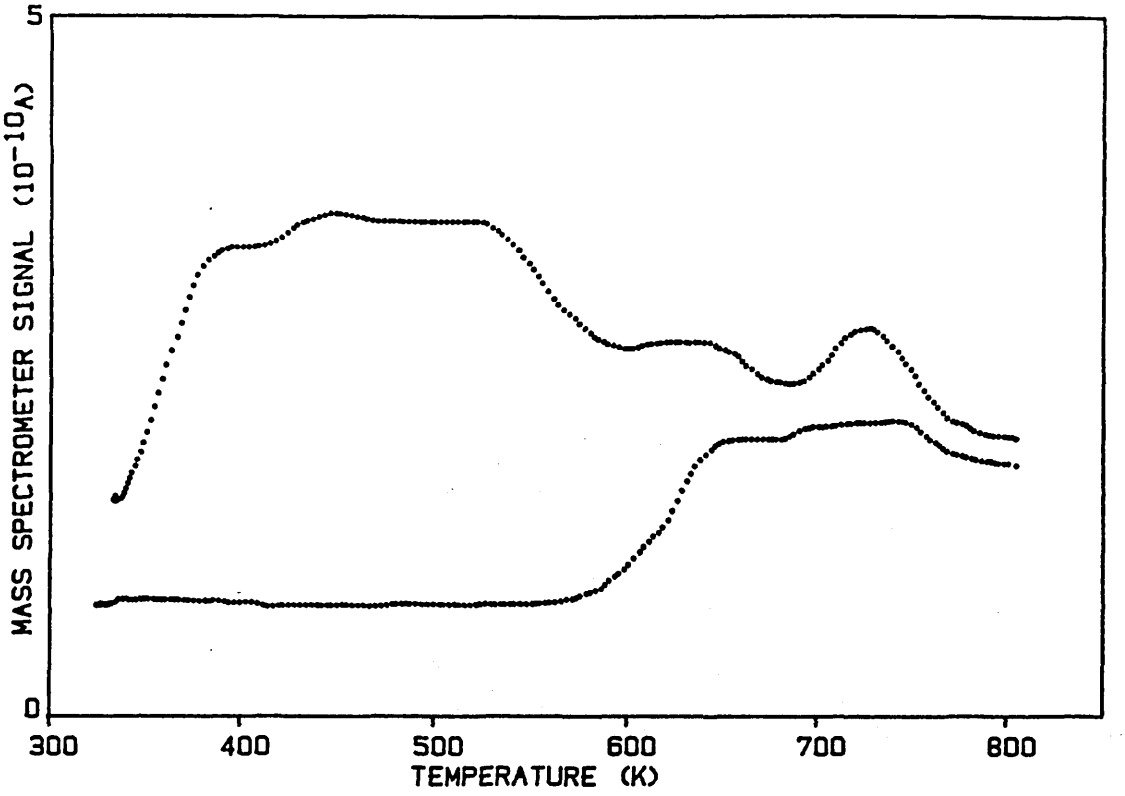

Figure 6.17: The coverage dependence of the carbon dioxide desorption spectrum after adsorption at 340 K on 0.042 wt% potassium promoted zinc oxide.

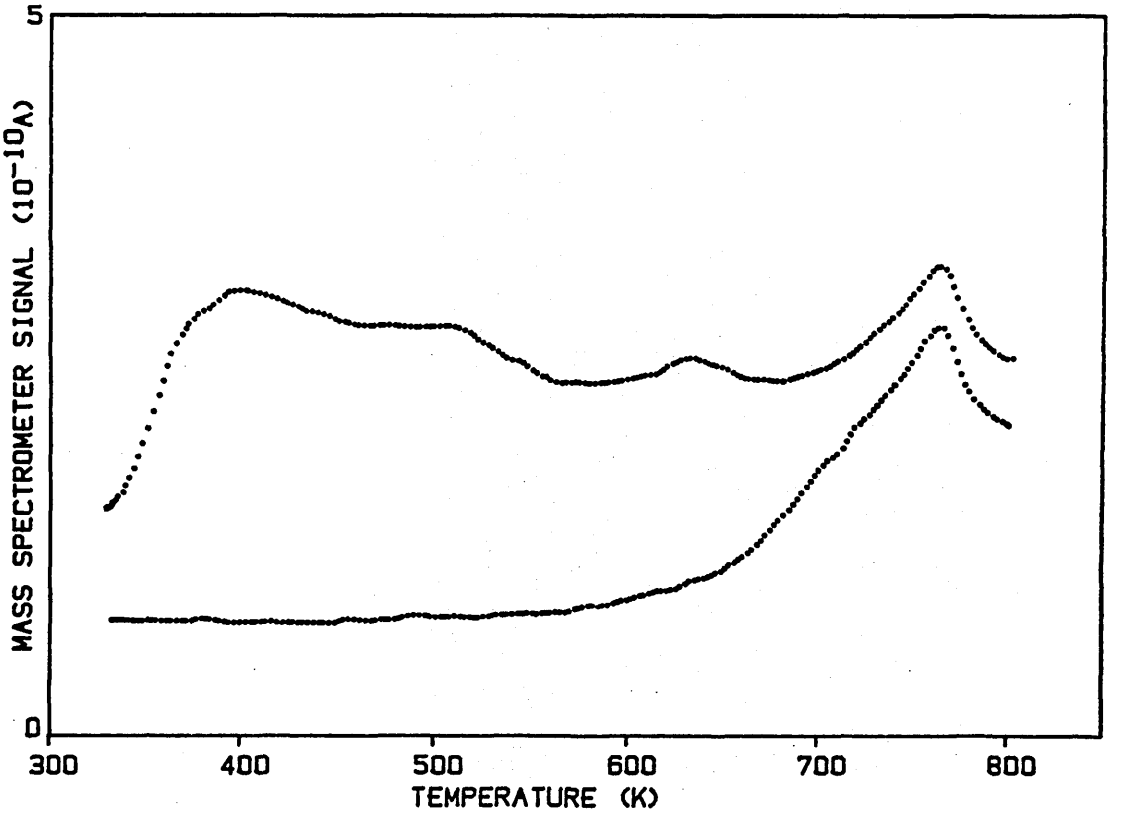

Figure 6.18: The coverage dependence of the carbon dioxide desorption spectrum after adsorption at 340 K on 0.085 wt% potassium promoted zinc oxide.

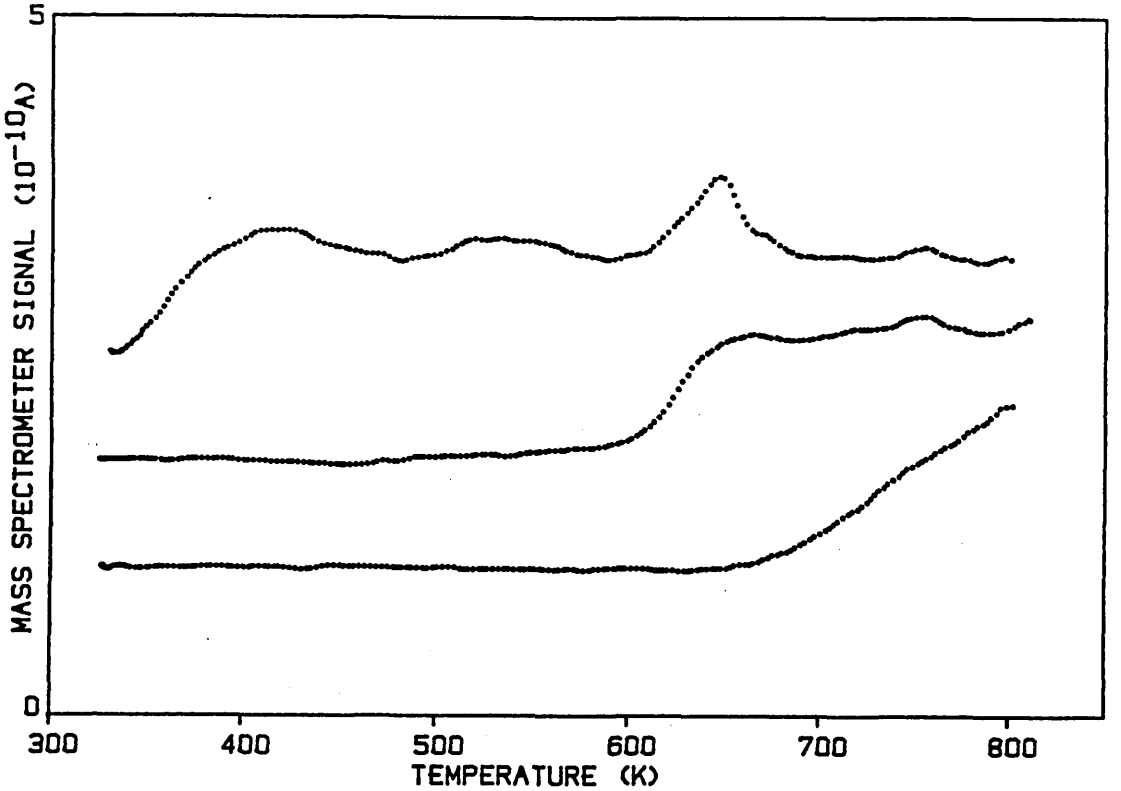

Figure 6.19: The coverage dependence of the carbon dioxide thermal desorption spectrum after adsorption at 340 K on 0.20 wt% potassium promoted zinc oxide.

attributed to formate decomposition on ZnO[25,27]. This peak would therefore also appear to be due to decomposition of a formate surface species. Hydrogen was also evolved coincident with this CO_2 peak, along with a small quantity of water. No CO desorption (not accountable in the CO_2 cracking pattern) was detected at this temperature.

A strong temperature dependence to the formate synthesis reaction was indicated by the variation in the coverage of the 602 K CO_2 and hydrogen peaks (see figure 6.20). The coverages, given in table 6.5, showed the CO_2:hydrogen to be approximately 3:1, compared to the 2:1 ratio predicted by the formate stoichiometry ($HCOO_{(a)}$). The presence of a small quantity of water after adsorption at 475 K, coincident with CO_2, and a further coverage of approximately 55×10^{12} H_2O/cm^2 associated with desorption at high temperature, indicated the

Table 6.5: Surface coverages associated with formate decomposition at 602 K after CO_2 and hydrogen coadsorption on zinc oxide.

coadsorption temperature (K)	surface coverage (10^{12} molecules/cm^2)		
	CO_2	hydrogen	water
325	0	0	0
430	37	11	0
475	63	21	2

possibility of hydrogen desorbing as water after recombination with adsorbed hydroxyls present on the surface due to impurities injected with the adsorbate gases. This temperature dependence in formate synthesis was consistent with previous observations reported by Bowker et al[25]. The maximum formate coverage of $63x10^{12}$ cm^{-2} was greater than the $30x10^{12}$ found by Bowker et al after coadsorption on ICI low surface area ZnO.

(6.3.2) Promoted Zinc Oxide

Corresponding CO_2 and hydrogen coadsorption experiments were carried out on potassium promoted ZnO (0.085 wt% K loading) to investigate the effect of potassium promotion on formate synthesis. The adsorptions were carried out at temperatures of 326 K, 423 K and 475 K. The CO_2 desorption profiles obtained, shown in figure 6.21, indicated no evidence of formate decomposition, since the profiles were the same as previously obtained after CO_2-only adsorption on the same 0.085 wt% K promoted catalyst (section 6.2.2).

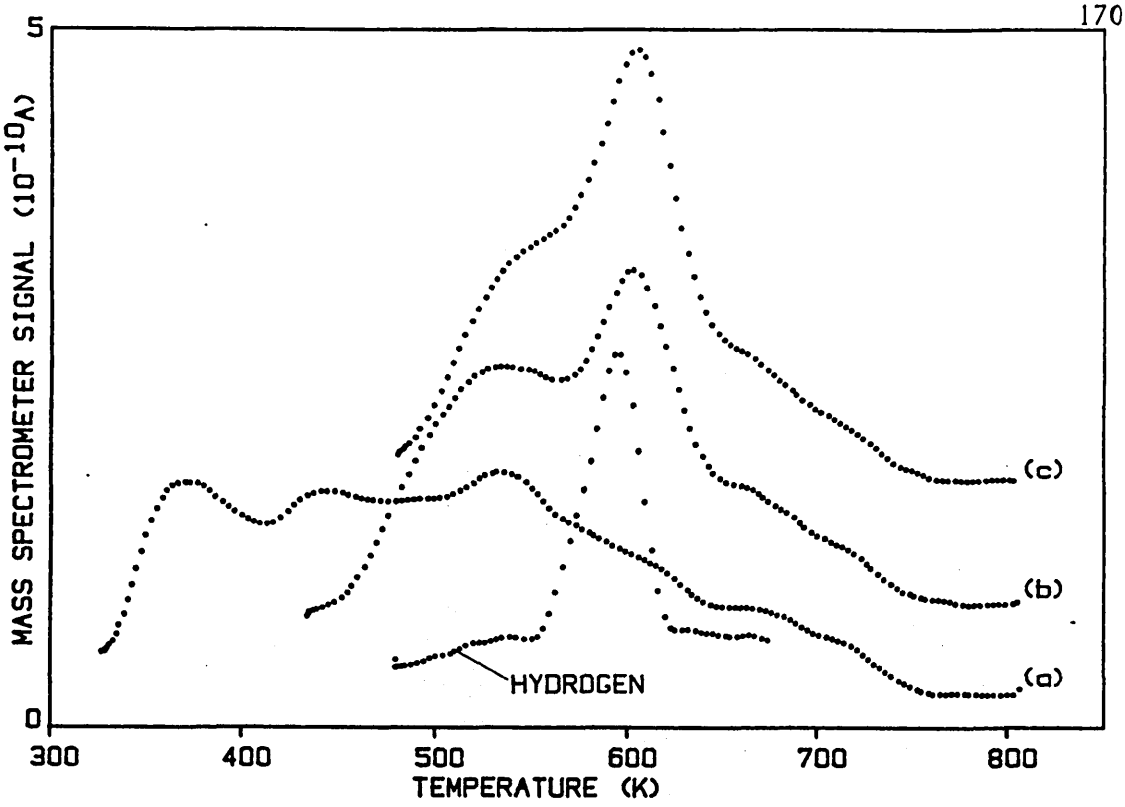

Figure 6.20: The carbon dioxide and hydrogen desorption spectra obtained after carbon dioxide and hydrogen coadsorption on zinc oxide at various temperatures. (a)= 325 K; (b)= 430 K; (c)= 475 K.

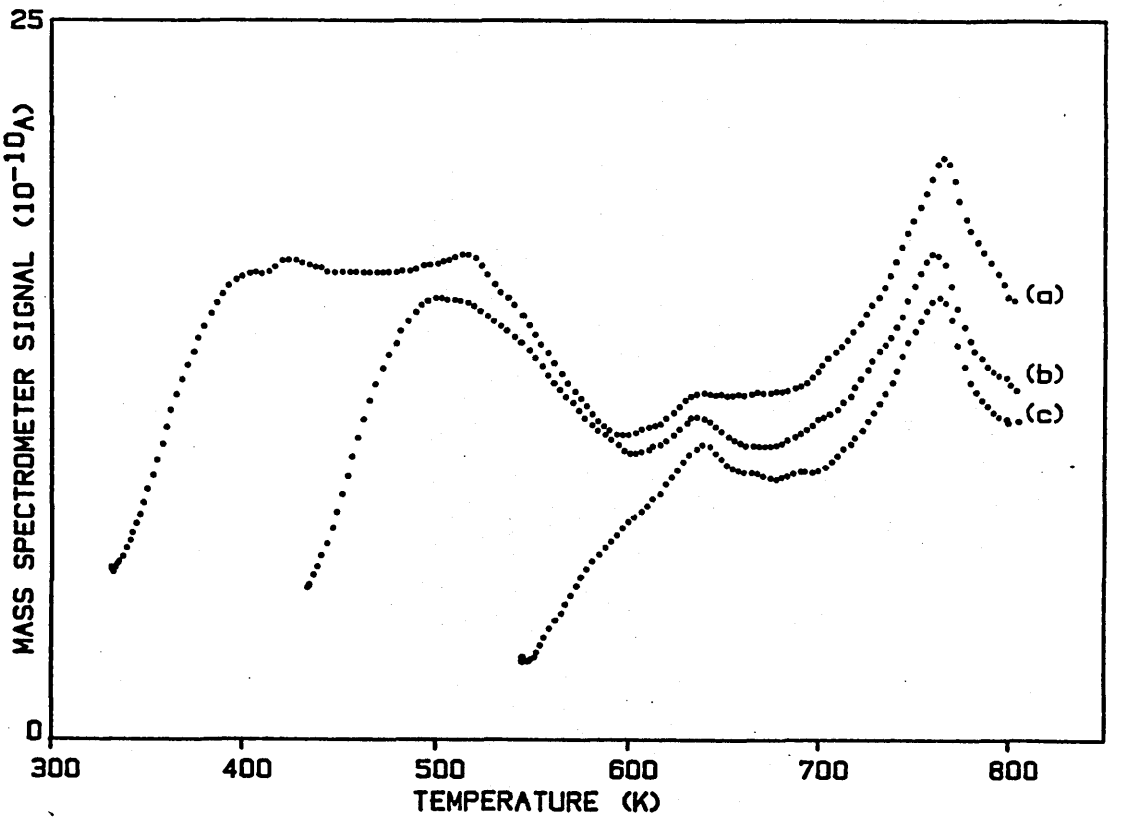

Figure 6.21: The carbon dioxide desorption spectra obtained after carbon dioxide and hydrogen coadsorption on 0.085 wt% K promoted zinc oxide at various temperatures. (a)= 325 K; (b)= 430 K; (c)= 475 K.

(6.4) Discussion of Results

(6.4.1) Unpromoted Zinc Oxide

The presence of several peaks in the water desorption showed that there were a number of adsorption sites, with different heats of adsorption, present on the ZnO surface. This result was consistent with the results reported by previous IR spectroscopic studies[27, 85,91] that have identified several different forms of adsorbed hydroxyls, and with proposed adsorption models that predict greater than one possible form of hydroxyl surface coordination on ZnO[86]. Of particular interest in the desorption spectrum was the thermally stable α peak at 743 K. A recent TPD study by Roberts and Griffin [27] has reported the formation of a similar high temperature water desorption peak from ZnO, and assigned this to hydroxyl adsorption on Type I hydrogen adsorption sites associated with the polar surfaces [40,41] (this is discussed further below). A similar water desorption peak at 753-803 K has also been observed by Ahkter et al[85] from the Zn polar single crystal surface. Using IR spectroscopy, Atherton et al[43] have also placed the most stable adsorbed hydroxyls on the Zn polar surface, while the adsorption model of Tsyganenko et al[86] predicts a triple coordination of the hydroxyl oxygen to Zn polar surface cations that results in a stronger bonding mode than is associated with the non-polar surface (see figure 6.22 and below).

The coverage dependence of the water spectrum established that saturation of the α sites occurred at an effective coverage of $1.5 \pm 0.2 \times 10^{14}$ water molecules/cm^2. If a 10.5 Å^2 hydroxyl cross-sectional area is assumed[91], this corresponds to a surface coverage equivalent to 16% of the total available catalyst surface area. This is in good

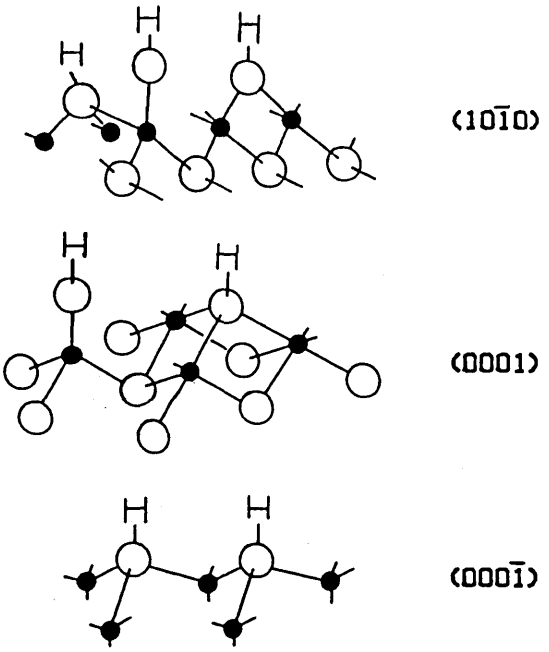

Figure 6.22: Hydroxyl bonding modes on the surface of zinc oxide. From reference (139).

agreement with the fraction of Zn polar surface estimated at 15-20% (see section 5.2.2). Accordingly, the α hydroxyls sites are assigned to be located on the Zn (0001) polar crystal surface. The propene desorption results also support this assignment since an independence was found between the α hydroxyl adsorption sites and the surface sites for propene adsorption on the non-polar surface (see below).

The heat of adsorption of 155±10 kJ/mol determined for the α peak was in good agreement with Roberts and Griffin[27]. The similarity of this value to estimates of the energy required for reduction of the ZnO lattice[140] further shows the hydroxyl oxygen to gain a stability approaching that of lattice oxygen. This is consistent with the bonding model of Tsyganenko et al[86] which predicts tetrahedral coordination of the hydroxyl oxygen to the Zn polar surface atoms so to be positioned in the space between surface Zn atoms and to form an

effective extension of the bulk structure (figure 6.22). The slight increase in the peak temperature as the α sites were populated indicates an increase in adsorption energy, possibly associated with a stabilisation of the Zn polar surface structure as it became more completely covered by hydroxyls. It also showed that repulsive interactions between adsorbed hydroxyls were not significant.

The remaining hydroxyl adsorption sites, corresponding to the observed β, γ, δ and ε desorption peaks, are associated with the remaining crystal surfaces i.e. the non-polar and O polar surfaces since the total coverage in these peaks ($3.4\pm0.6\times10^{12}$ H_2O/cm^2) was too high for them to also be located on the Zn polar surface. However, adsorption onto the O-polar face would have been limited due to the strong steric hindrance effects of the outward layer of surface oxygen atoms shielding the sub-surface Zn atoms, and to the repulsive effects of the surface oxygen and hydroxyl dipole moments[141]. Hydroxyl adsorption on this plane is likely to be confined to defect sites only, such as those produced by surface oxygen vacancies formed to maintain surface charge neutrality. Since defects produced in this manner will occupy 25% of the O polar surface (or the order of 5% of the total catalyst surface area), as a first approximation it can be assumed that the remaining hydroxyls are adsorbed on the non-polar surface, with negligible contribution to the desorption spectrum from the O polar surface.

On this surface, each adsorbing water molecule will produce the equivalent of two surface hydroxyl species (due to the coplanar structure of the Zn-O pairs[43,44]), so the resulting coverage of $6.8\pm1.2\times10^{12}$ hydroxyls/cm^2 will occupy 74±13% of the total available

catalyst surface area. This result is in good agreement with the 60-70% fraction of actual available non-polar surface and shows that full saturation of non-polar surface was reached.

The desorption spectrum did not resolve the apparent contribution from any hydroxyls adsorbed on defect sites on the O polar surface. However, if limited adsorption did occur associated with these sites, then it is likely that the strength of adsorption would be similar to that of hydroxyls on the Zn polar surface (as suggested by the results of Atherton et al[43]), so the resulting desorption peak may have been 'lost' in the larger α peak.

The presence of the three broad peaks, assigned to desorption from the non-polar surface, is consistent with the Tsyganenko model where more than one hydroxyl bonding mode (and hence adsorption strength) is predicted to form on this surface (figure 6.22). In addition, the broader nature of these desorption peaks correlated with the occurrence of more extensive interhydroxyl hydrogen bonding, as predicted by Morishige et al[91] and Atherton et al[43]. These interactions could be expected to increase the range of desorption energies, hence increasing the desorption peak width.

Roberts and Griffin[27] have recently assigned the α peak to be due to hydroxyl adsorption on Type I hydrogen sites, while the Type I sites have earlier been associated with ion vacancies formed by polar surface reconstruction[40,41,46]. Such a site competition effect between adsorbed hydroxyls and Type I hydrogen was evidenced in the present results by the lack of fast hydrogen adsorption, characteristic of the Type I mode[40]. However, the high hydroxyl coverage obtained for the α peak demonstrates clearly that adsorption is not

limited to surface defect sites only, but that it involves the extensive bonding of hydroxyls onto the cation layer of the Zn polar surface until an overall one-to-one relationship is achieved at saturation. Since it has been reported that adsorption of water on perfect single crystal ZnO surfaces, in the absence of vacancy defects, gives only nondissociative molecular adsorption[142], the possibility is raised of the vacancy defects acting as specific sites for water dissociation, and from which, surface migration of hydroxyls onto neighbouring cations takes place.

The CO_2 desorption spectra also demonstrate the existence of well defined sites for CO_2 adsorption on the surface of ZnO. The results show these sites to be independent of the α hydroxyl adsorption sites on the Zn polar surface since the CO_2 desorption spectrum was not affected (with the possible exception of the α CO_2 peak) by the presence of adsorbed α hydroxyls. Therefore the main CO_2 adsorption sites are assigned to the non-polar $(10\bar{1}0)$ surface of the ZnO. This assignment is consistent with the results of other CO_2 adsorption and TPD studies in the literature:- Runge and Gopel[82] in a comparison of the properties of $(10\bar{1}0)$ single crystal and polycrystalline ZnO surfaces concluded the properties of CO_2 adsorption are determined by the non-polar surface, while another TPD study by Cheng and Kung[50] also obtained similar CO_2 peaks from the non-polar surface. Saussey et al[52] identified the involvement of $Zn^{2+}O^{2-}$ ion pairs by IR spectroscopy and, using the same technique, Atherton et al[43] found the CO_2 IR spectroscopic bands to be unperturbed by the presence of stable hydroxyl species (i.e. those on the polar adsorption sites); both these results are consistent with adsorption onto the non-polar sur-

face. The CO_2 desorption spectra obtained in the present study are similar to those reported by Runge et al, with the β, γ and δ peaks of the present study identifiable in the spectrum from Runge's polycrystalline ZnO (although because the spectrum of Runge et al was obtained during continuous CO_2 flow, the γ peak was more prominent). The peaks temperatures also correspond to the CO_2 desorption peaks observed by Cheng and Kung[50] from non-polar ZnO crystal surfaces. These workers also identified a further high temperature peak from the Zn polar surface that appears to correspond with the α peak observed. The α sites found in the present study could then correspond to a limited adsorption on the Zn polar surface; this will be discussed further in section 6.4.2.

The CO_2 saturation coverage of 400×10^{12} molecules/cm^2, equivalent to 18.5×10^{18} molecules/gram of catalyst, which when compared to the approximate $17\text{-}20 \times 10^{18}$ available non-polar ion pair sites/gram (assuming 60-70% fraction non-polar) shows, to a first approximation (and including the limited quantity of α sites), that sufficient pair sites are available, within the experimental error limits, for the non-polar surface to adsorb the detected quantity of CO_2 with full saturation of the $(10\bar{1}0)$ surface being achieved. Although it has been suggested by Saussey et al[52] that the CO_2 adsorption sites might be associated with edges, steps and vacancies that exposed more reactive Zn ions, this coverage is too high for the adsorption sites to be limited to defect features and implies, as with water adsorption, that CO_2 adsorption is associated with the extensive nondefective surface structure.

The form of the adsorbed CO_2 is not apparent directly from the desorption results themselves. The adsorption dependence on the non-polar surface implies a dependence on Zn-O pair sites for CO_2 adsorp-

tion. Carbonates have been identified by IR measurements on adsorbed CO_2[52] and imply the involvement of lattice oxygen as proposed in the bonding models of Gopel et al[82]. Runge and Gopel found the peak height ratios of the β and γ peaks to be strongly dependent on the surface oxygen vacancy concentration and proposed the β peak to be due to strong adsorption of CO_2 molecules on surface vacancy sites to form "$ZnCO_2^-$" surface complexes, and the γ state to be due to "CO_3^{2-}" complex formation. In the present study, saturation of the β peak occurred at a coverage of approximately 10% of saturation, equivalent to 8% of the $(10\bar{1}0)$ surface area. This figure is in good agreement with the 10% non-polar surface defect concentration determined by Runge and Gopel[82].

It is interesting to note that Cheng and Kung[50] also observed effects on the CO_2 spectra that were related to the time between the last high temperature heating and CO_2 exposure, in a manner similar to that found for ZnO in the present study. Cheng and Kung suggested this to be due to the presence of background water on the ZnO surface, although this seems unlikely, since the effect was observed to occur at relatively low hydroxyl coverages. The results found that this effect appeared not to be dependent on the time between when the CO_2 was adsorbed on the surface and the catalyst heated, but on the time period only, independent of at what stage the CO_2 adsorption occurred. It would then seem that it may be related to a time dependent change of the actual ZnO surface rather than a stabilisation of the adsorbed CO_2 itself.

The results of water and propene coadsorption also clearly establish an independence between the propene adsorption sites, and the α

water sites located on the Zn polar surface. On this basis it appears that propene is adsorbed only on the non-polar surface of ZnO. This assignment is consistent with the work of Dent et al[117] that showed Zn-O ion pair sites to be required for the dissociative adsorption of propene to form the π-allyl species and associated surface hydroxyl. The saturation coverage of 90×10^{12} molecules/cm^2 corresponded to approximately 25% saturation of the ion pair sites available on the non-polar surface, although since some desorption of propene occurred at the 340 K adsorption temperatures, a higher population closer to surface saturation may have been obtained if a lower adsorption temperature was used. The figure of 25% saturation is, however, in good agreement with the 30% coverage reported by Dent et al[117]. These workers concluded that the sites for π-allyl formation may be associated with crystal edges or edge type surface defects.

The lack of evidence for any significant oxidation of the adsorbed propene intermediate is contrary to the findings of Davydov et al[118]. However, since Nakajima et al[119] have shown that adsorbed propene does not appear to interact with the lattice oxygen of ZnO in the absence of gaseous oxygen, this result may have been due to an absence of gaseous oxygen in the helium carrier gas.

The slow adsorption process observed for hydrogen on ZnO is consistent with adsorption into the Type II sites designated by various workers[40,41,46,57]. The Type I hydrogen adsorption sites, characterised by rapid hydrogen adsorption[40], were absent from the hydrogen desorption spectra, suggesting the small coverage of surface hydroxyls, due to background water adsorption onto the ZnO surface, was sufficient to poison the Type I sites for hydrogen adsorption (as

noted above). The observed hydrogen desorption from the Type II sites must then be due to adsorption on the non-polar surface, consistent with the models of Fubini et al[57] and Ghiotti et al[64] that have placed the Type II sites on this surface.

(6.4.2) Potassium Promoted Zinc Oxide

Single crystal studies have shown potassium ions to be more strongly held on the polar surfaces of ZnO than the non-polar[143]. In particular, the ions are very strongly bound to the O polar surface where impurity stabilisation effects lead to a one third monolayer coverage required for charge stabilisation[144] (see also Appendix 4 and chapter 8). On the basis of these results from single crystal surfaces, the potassium promoter might be expected to be preferentially, and more strongly, adsorbed on the polar surfaces of the polycrystalline ZnO studied.

If the density of available ion sites on the Zn polar surface is assumed to be 1.1×10^{15} ions/cm^2[80], and the effective density of the corresponding adsorption sites on the O polar face is one third this figure (since only a 1/3 monolayer is required for charge stabilisation on this surface[144]), then approximately $(10\text{-}14) \times 10^{18}$ polar adsorption sites would have been present per gram of ZnO (assuming the fraction of polar surface is 30-40%). Saturation of these sites will require the addition of 0.12-0.16 wt% K_2CO_3, if it is assumed that all the potassium is located on the polar sites. The actual water desorption spectra obtained from the 0.15 wt% K_2CO_3 loading (0.085 wt% K) catalyst has shown the α water peak from the Zn polar surface to be selectively removed from the desorption spectra in a manner consistent with the alkali distribution weighted toward the polar surfaces as

assumed by this calculation.

As a corollary to this calculation, assuming an ion density of 1.4×10^{15} ions/cm^2 on the non-polar surface, and that saturation by potassium of the polar sites (O and Zn) is attained, then the highest loading of 0.35 wt% K_2CO_3 (0.20 wt% K) will give only approximately 50% saturation of the non-polar surface sites i.e 30-35% of the total catalyst surface area will still consist of unpromoted surface sites located on the non-polar surface.

Therefore, the experimental results present a consistent picture of the distribution of the potassium promoter, showing that at low potassium loadings (0.042 wt% and 0.085 wt% K) the alkali is concentrated toward the polar surfaces. The presence of potassium ions on the O polar face will result in impurity stabilisation[144] and a reduction in the number of oxygen vacancies. Since the Zn^{2+} ions exposed at these oxygen vacancies are probably the sites for hydroxyl adsorption, the addition of potassium will decrease the availability of sites for water adsorption. On the Zn polar surface, the presence of OK^- groups will also effectively prevent the dissociative adsorption of water. Overall, the addition of potassium appears to deactivate the polar surfaces by the blockage or removal of adsorption sites. As the alkali loading increases a larger proportion of non-polar surface sites are occupied by K^+ or OK^- species. The effect of potassium on this surface, however, is not as clearly resolved. The higher alkali loading of 0.20 wt% potassium, as well as demonstrating a complete absence of α sites, also appears to show some loss of β sites associated with the non-polar surface, consistent with a blockage effect where adsorbed potassium reduces the available hydroxyl

adsorption sites. It is not possible to clearly associate the larger amount of low temperature water desorption solely with desorption from the non-polar surface; indeed, the single crystal results of Akhter et al[85] show a water desorption peak at 503 K produced from the Zn polar surface similar to the 533-541 K peak of the present study. The results of Akhter et al suggest that the 533-541 K peak could be evolved from the Zn polar surface. This raises the possibility of a form of water adsorption, either molecular or dissociative, where bonding occurs onto OK^- species located on the Zn polar surface. Similarly, the 388 K peak could also be due to adsorption, possibly molecular, on potassium ions located on the non-polar surface. A molecular type of adsorption, in particular, could be surface independent, so the 388 K peak could contain contributions from all ZnO crystal surfaces present.

On unpromoted ZnO, CO_2 appeared to adsorb mainly on the non-polar surface, with only a small coverage possibly associated with the Zn polar surface. Adsorption of CO_2 on the lowest alkali loaded catalyst (0.042 wt% K) gave a desorption spectrum that was not dissimilar to that obtained from the unpromoted catalyst (with the exception of the additional peaks evolved at higher temperature discussed below). The reduction in surface coverage associated with the non-polar surface sites (approximately 25% lower than from unpromoted ZnO) suggests that only a relatively small amount of alkali is present on this surface at this loading. This is consistent with the alkali distribution weighted toward the polar surfaces, and in line with results for water adsorption on the promoted catalysts. As the alkali loading is increased, CO_2 adsorption on the non-polar sites can be seen to progressively reduce, indicative of the higher alkali coverage resulting in

CO_2 adsorption site blockage. At the highest 0.20 wt% K loading the reduction in CO_2 coverage on the non-polar sites is consistent with the calculated 50% loss of surface Zn-O pair sites due to adsorbed potassium.

Both the β and γ desorption peaks were suppressed by the alkali promotion. The β sites on the unpromoted ZnO have been previously associated with surface anion vacancy defects on the unpromoted ZnO. The potassium would be expected to adsorb on these more reactive defects sites first, as found on single crystal surfaces[143,144].

The α state was enhanced by the alkali promotion. This peak is assigned to adsorption on the Zn polar surface by comparison to the single crystal TPD results of Cheng and Kung[50]. It is interesting that Cheng and Kung note the presence of potassium contaminants on the surface of their single crystal surfaces as not affecting the desorption spectra. However, the prominence of the CO_2 peak from the Zn polar surface suggests their results are, in fact, influenced by the alkali, as is also indicated in the water desorption spectrum from the same surface (noted previously).

The surface formate has been previously reported as an intermediate in the synthesis of methanol on ZnO[25]. Although the results showed the formate to be produced on unpromoted ZnO through coadsorption of CO_2 and hydrogen, on potassium promoted ZnO no evidence for the synthesis of the formate was found. This suggests that it is unlikely for the formate to be an important intermediate in the synthesis of higher alcohols with potassium promoted ZnO since the alkali clearly suppressed its formation.

CHAPTER 7

PROPANOL DECOMPOSITION ON ZINC OXIDE

(7.1) 2-Propanol

(7.1.1) Thermal Desorption and Decomposition Spectrum

A typical desorption spectrum obtained after a saturation dose of 2-propanol (2-PrOH) onto unpromoted ZnO catalyst is shown in figure 7.1. The main desorption and decomposition products, their peak temperatures and surface coverages are summarised in table 7.1. The main desorption products (2-propanol, acetone, propene and CO_2) can be classified according to the surface reactions they represent:

(i) reversible desorption (2-propanol),

(ii) dehydrogenation (acetone),

(iii) dehydration (propene) and

(iv) oxidative decomposition (CO_2).

In addition to these major products, minor amounts of a number of other hydrocarbons were also detected (possibly propane, ethane and ethene) although precise identification and quantification of these products could not be carried out because of the small quantities involved and the considerable overlap of their mass spectrometer cracking fractions. However, compared to the main decomposition routes they represented minor reaction pathways only.

The spectrum in figure 7.1 differed significantly to that obtained after 2-PrOH adsorption on both the other ZnO catalysts used in this study (ICI low and high surface area ZnO) in that additional propene, water and CO_2 desorption peaks were observed. These differences are discussed further in chapters 8 and 10.

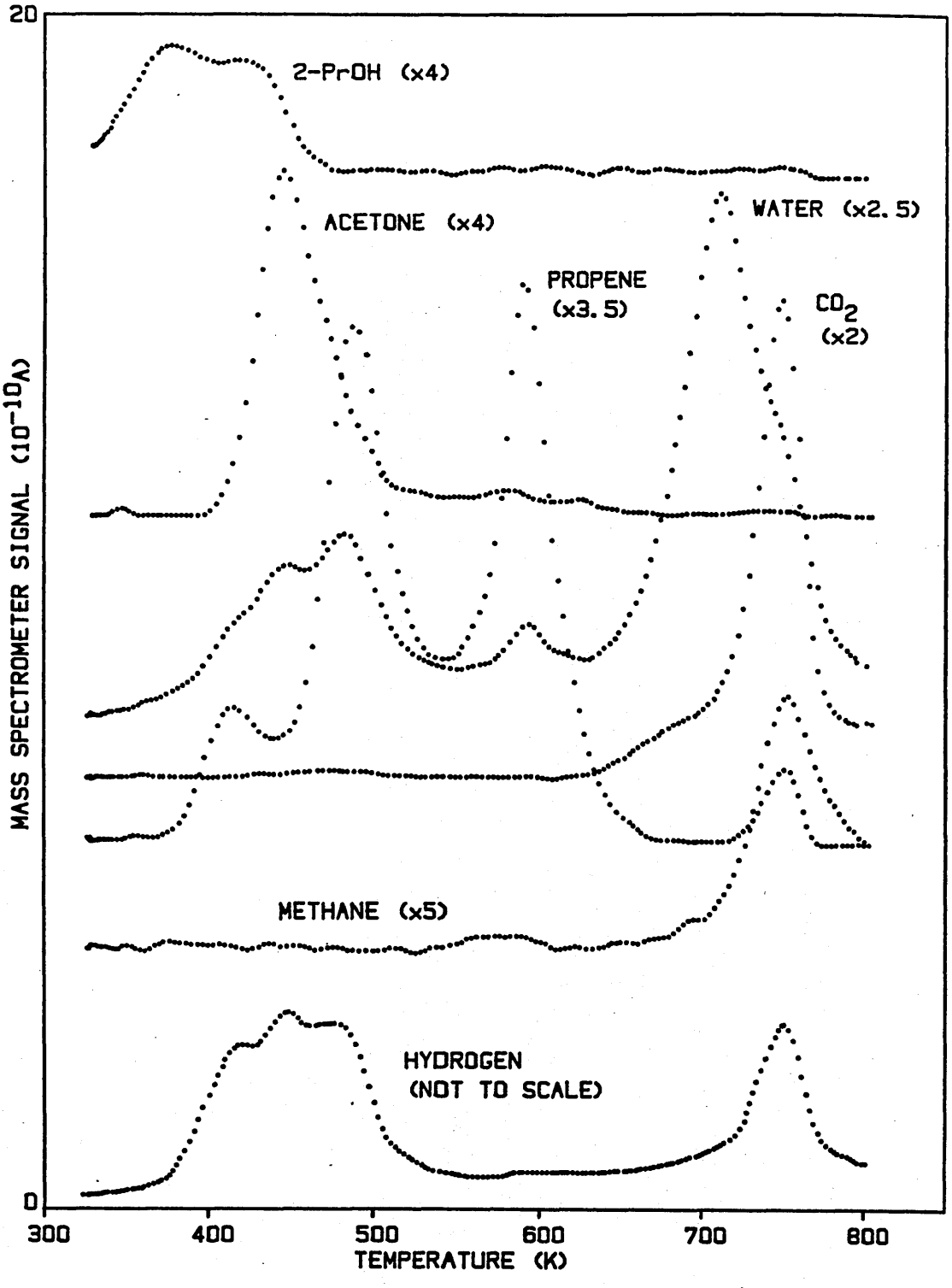

Figure 7.1: The desorption spectrum after adsorption of 2-propanol at 330 K to saturation coverage on zinc oxide. The acetone and propene peaks have been corrected for cracking fraction overlap with 2-propanol. No correction has been made for differences in the mass spectrometer sensitivities.

Table 7.1. The desorption products, peak temperatures and surface coverages following 2-propanol adsorption to saturation coverage at 320 K on zinc oxide.

desorption product		peak temperature (K, ±2)	surface coverage (10^{12}molec/cm^2)
2-propanol	β	376	21
	α	421	20
acetone		441	37
propene	γ	412	27
	β	487	160
	α	589	150
CO_2		750	150
water		412,446,480	55
		592	5
		711,748	125
hydrogen		419	7
		447	150
		478	11
		750	55
methane		757	-

Two overlapping but distinct 2-PrOH desorption peaks (designated α and β) were observed with peak temperatures at 421 and 376 K. The amount of reversible desorption relative to the quantity of decomposition products formed was less than 10% of the total desorption products.

A complex desorption pattern was found for propene with three separate peaks being formed, designated α, β and γ at 589 K , 487 K and 412 K respectively. Water was found to desorb in varying amounts with each of the three propene peaks. Estimates, for the two main peaks, of the ratios of propene to coincidently desorbed water gave

values of 1:20 for α propene and 1:4 for β propene respectively. The major part of the water formed (approximately 60%) by these dehydration reactions was desorbed at higher temperatures at approximately 711 K due to readsorption within the catalyst bed, since any water evolved with the propene was below the normal water desorption temperature (see section 6.1.1). Hydrogen also appeared to be desorbed at temperatures similar to the β and γ propene peaks (419 K and 478 K), and also appeared just detectable with the α propene. Estimates of the propene to hydrogen molecular ratios were >100:1 for α propene, 15:1 for β propene and 4:1 for γ propene. Like the ratios given for water, these values should only be treated as being very approximate, particularly for γ propene where the hydrogen was evolved at a temperature close to the peak produced after hydrogen adsorption and may have been due to hydride recombination reactions unrelated to the dehydration process.

At similar temperatures to that of propene formation, small quantities of hydrocarbon mass fragments not accountable in the propene cracking fraction were also found to desorb. These were identified as possibly propane plus traces of ethene and methane. More propane than ethene appeared to be desorbed with the α than the β peak, while methane was only detected with the α peak. No hydrocarbons desorbed with the γ state. No peaks at 30 amu were found showing that ethane was not formed. Trace quantities of 54 amu (possibly butadiene) were also detected with the β peak, plus similar amounts of 56 amu (possibly isobutene) with the α and β peaks.

Acetone desorbed in a single peak at 441 K although, in addition, there appeared to be a small amount of acetone evolved coincident with the α propene at 589 K. Hydrogen was found to desorb coincident with

acetone at 447 K. The estimated amount of hydrogen at this temperature was significantly greater than acetone evolved by a factor of approximately 4. A small amount of water was formed at a similar temperature to acetone. Although the quantity of water was variable (for example compare figures 7.4 and 7.17), the acetone to water molecular ratio was in the order of 4:1. Small quantities of possibly ethene and propane were also evolved coincident with the acetone/hydrogen peaks.

The formation of CO_2, methane, hydrogen, and other products at high temperature (approximately 750 K) was indicative of an oxidative decomposition surface reaction. In addition to the main desorption peaks of the CO_2, H_2 and CH_4 evolution at 750-757 K, also observed were minor quantities of water, 27 and 26 amu (possibly ethene) plus small amounts of 43, 41 and 39 amu (possibly acetone and propene). Since all these products were evolved at the same temperature it showed that they were derived from the reaction limited decomposition of a common surface intermediate. The number of detected desorption products reflected a relatively complex stoichiometry for the oxidation product precursor on the catalyst surface.

Mokwa et al[97] also observed the formation of CO_2 at high temperature after ethanol adsorption on sintered ZnO and proposed the formation of a surface acetate, while previous studies of oxidation processes on a variety of oxide catalysts have also identified the formation of carboxylate type complexes[103,111-113] after alcohol adsorption. Thus the evolution of CO_2 and related products would appear to be due to the decomposition of an adsorbed carboxylate type species. Table 7.1 shows the total amount of propene formed to be in

excess of the total water indicating that an overall net consumption of hydroxyl oxygens may have taken place in formation of the carboxylate. The spectra were found to be reproducible over a number of experiments without any intermediate reduction treatment of the catalyst, although long term use (>15 alcohol desorption experiments) did result in a gradual reduction of the α propene and CO_2 desorption peaks. This long term stability of the catalyst indicated the net surface reduction rate to be low, providing further evidence to there being a direct involvement of hydroxyl oxygen in the oxidation process. These points are discussed further in section 7.4.

The total surface saturation coverage excluding the water was determined to be approximately 570×10^{12} molecules/cm^2 compared to the figure of 220×10^{12} molecules/cm^2 obtained by Bowker et al[115]. This discrepancy arises from the contributions of the additional propene and CO_2 desorption peaks that corresponded to an additional coverage of 330×10^{12} molecules/cm^2. These points are considered further in chapter 8.

(7.1.2) Coverage Dependence

The selectivity of the alcohol decomposition was found to be strongly dependent on the initial 2-PrOH dose; for 2-PrOH coverages in the range 6% to 50% of surface saturation only propene, water, hydrogen and CO_2 desorption peaks were observed. Acetone evolution did not occur until the initial 2-PrOH coverage exceeded 50% of full saturation, with reversible 2-PrOH desorption peaks only appearing as the coverage exceeded 63% of full surface saturation.

The coverage dependence of propene formation is shown in figure 7.2. The three propene states were populated in reverse order to

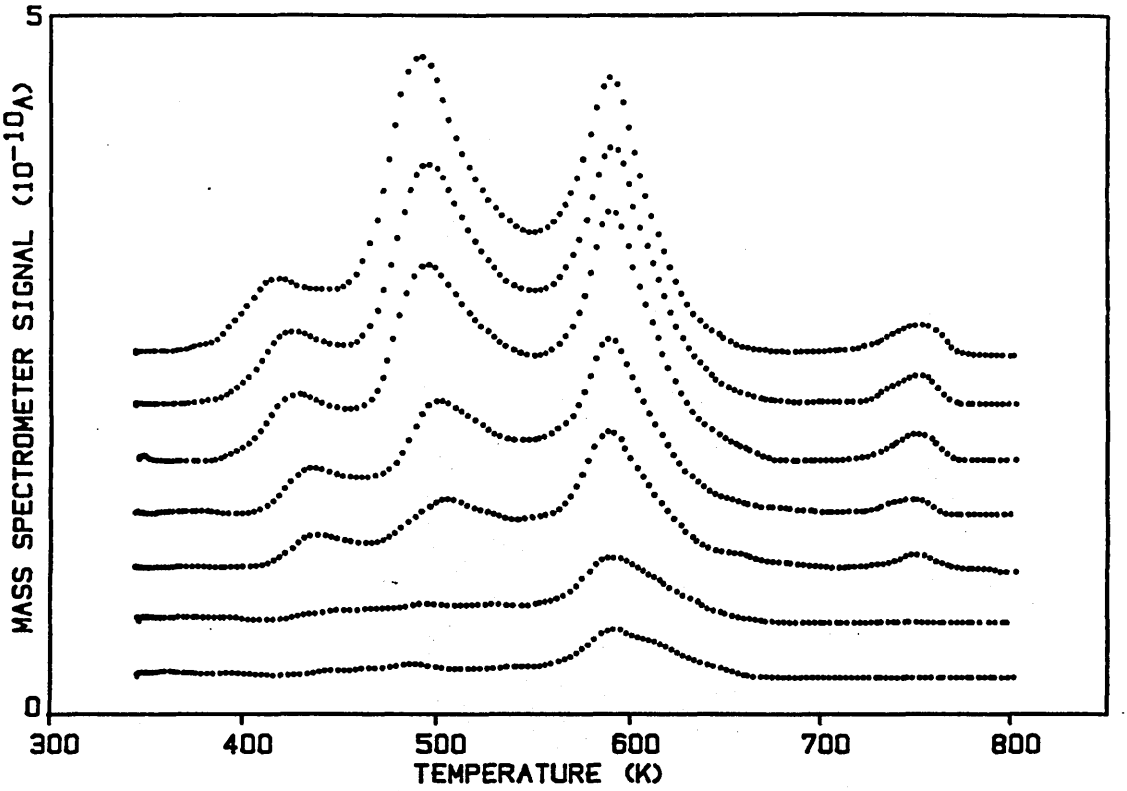

Figure 7.2: The coverage dependence of the propene desorption spectrum as a function of 2-propanol dose on zinc oxide.

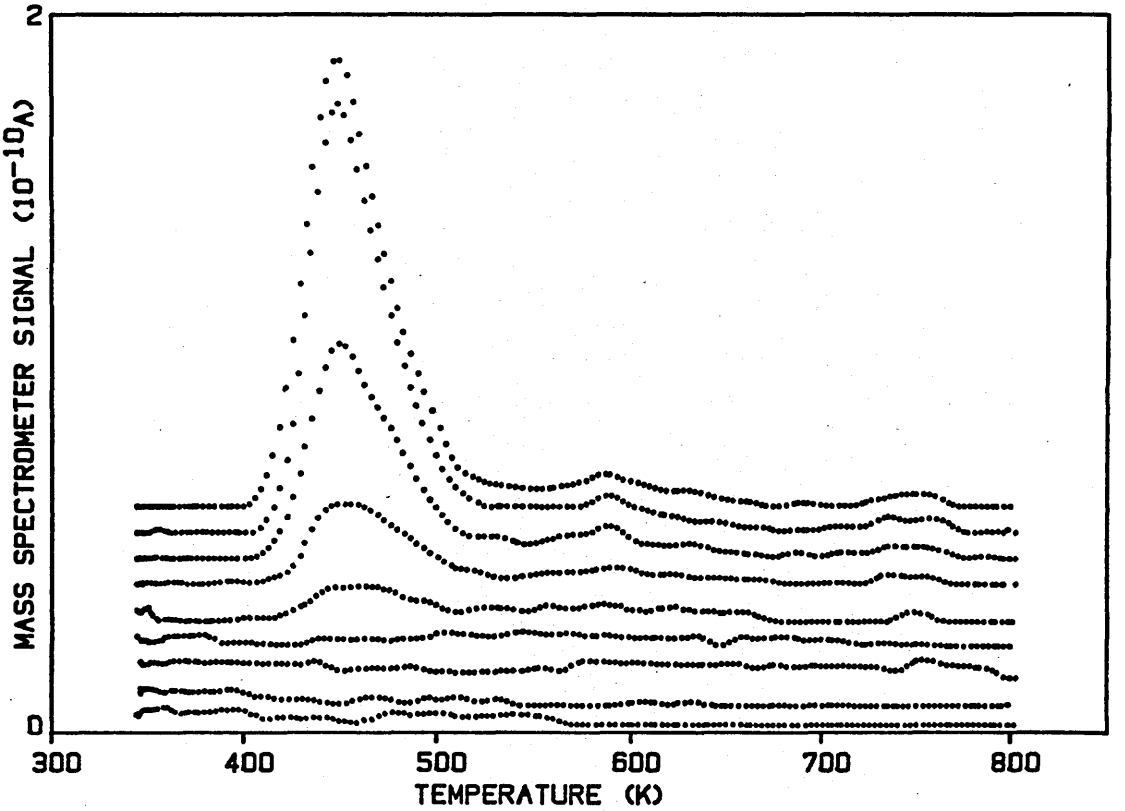

Figure 7.3: The coverage dependence of the acetone desorption spectrum as a function of 2-propanol dose on zinc oxide.

their desorption temperatures, with only the α peak present for coverages below approximately 10% of saturation.

Acetone was observed to desorb as a single main peak for 2-PrOH doses greater than 50% of saturation (figure 7.3), with a decrease in the acetone peak temperature from 459 K at 50% saturation to 446 K at full saturation occurring. A further minor acetone peak at approximately the same temperature as the α propene was also apparent. Associated with the main acetone peak was a coincident hydrogen desorption peak, with additional hydrogen peaks at temperatures slightly above (478 K) and below (419 K) this main peak. Although acetone desorption did not occur at low surface coverages, hydrogen desorption in these three peaks was in fact observed. This point is discussed further below.

At low 2-PrOH dose (<10-15% of saturation) water desorbed only at high temperature forming two overlapping peaks; one coincident with CO_2 at 753 K and the other at approximately 713 K. Figure 7.5 shows that this high temperature water desorption increased with 2-PrOH dose, with further water desorption occurring coincident with the α propene and in smaller peaks associated with the β and γ propene and acetone states. The temperature of the small high temperature shoulder at 753 K state remained independent of 2-PrOH coverage while that of the main high temperature peak decreased from an initial 719 K at low 2-PrOH coverage to 700 K at full saturation.

The oxidative decomposition reaction as evidenced by CO_2 desorption also occurred from the lowest 2-PrOH dose used, the amount of CO_2 progressively increasing until surface saturation (figure 7.5). At low coverage two CO_2 peaks could be resolved; a sharp peak at 752 K superimposed over an underlying broader peak at approximately 698-708K

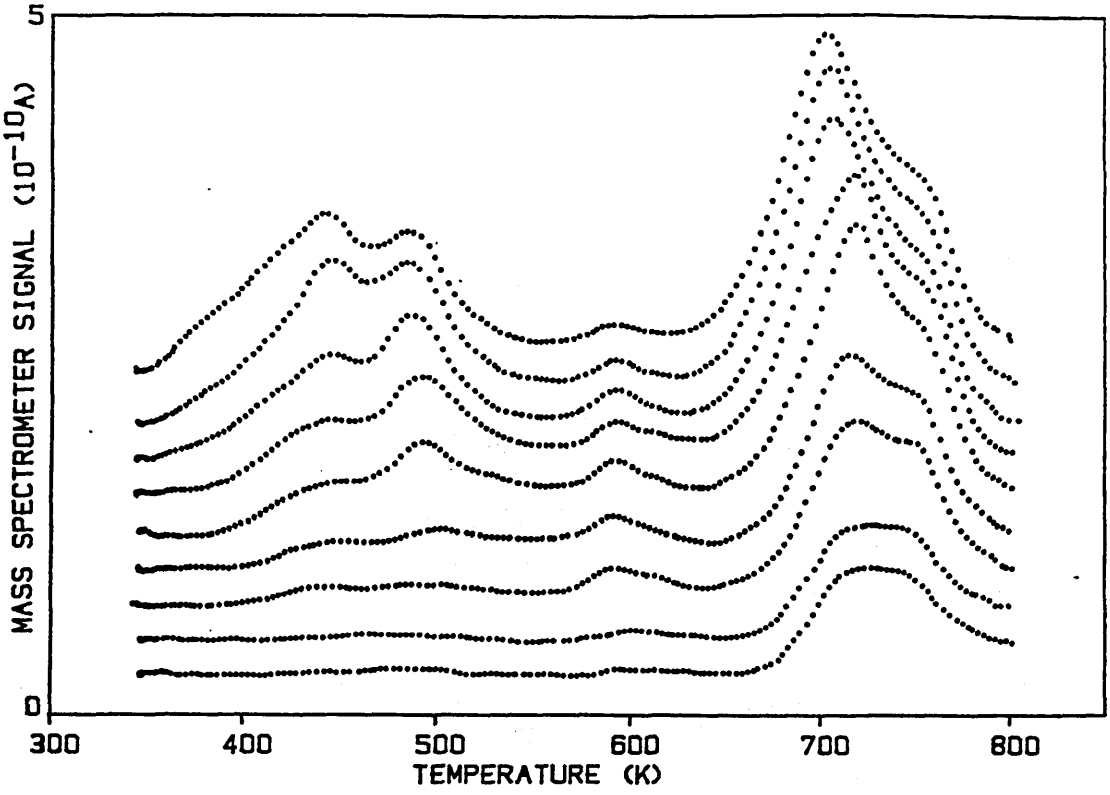

Figure 7.4: The coverage dependence of the water desorption spectrum as a function of 2-propanol dose on zinc oxide.

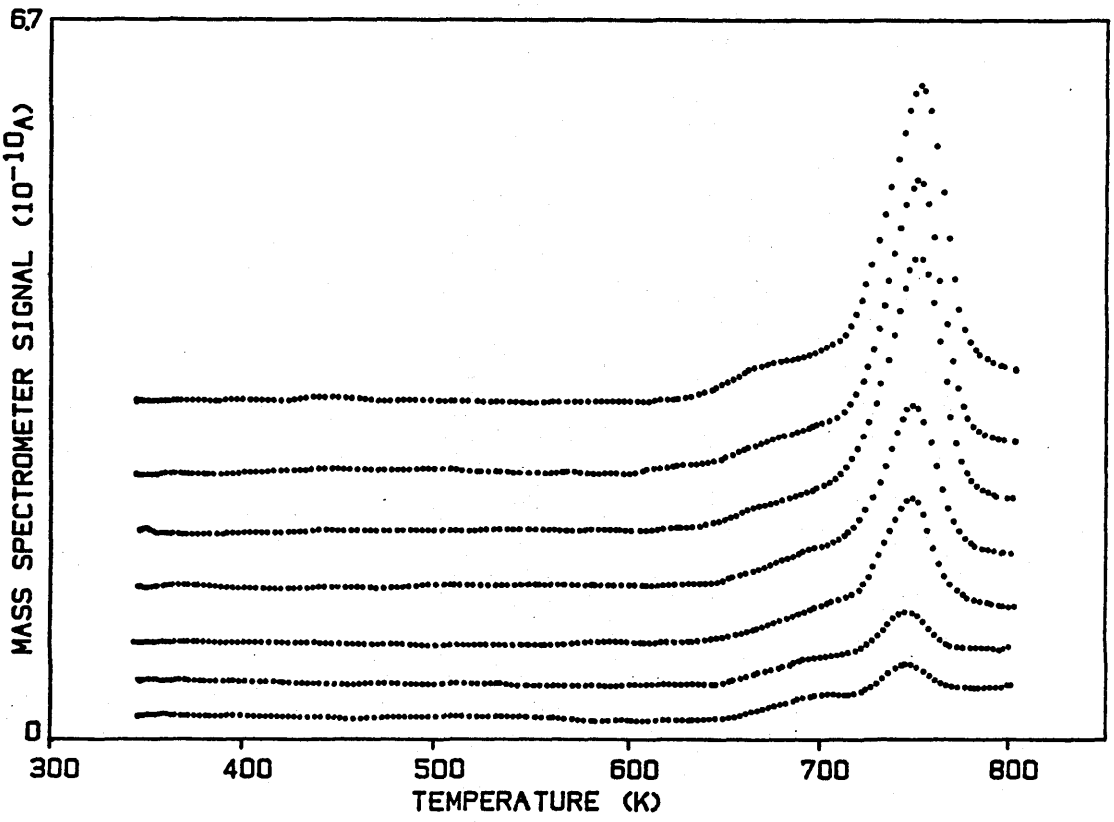

Figure 7.5: The coverage dependence of the carbon dioxide desorption spectrum as a function of 2-propanol dose on zinc oxide.

Saturation of the underlying state appeared to be reached at low coverage while desorption from the sharp peak continued increasing until surface saturation was reached. No change in the CO_2 peak temperature with coverage was found.

For doses above 63% of surface saturation, population of the two reversible 2-PrOH states occurred in reverse order to their desorption temperature (figure 7.6). The peak temperatures of both states remained invariant with coverage.

Hydrogen desorption was observed at all 2-PrOH doses as shown in figure 7.7. In the high temperature region, a peak at 751 K was evolved coincident with CO_2 formed from carboxylate decomposition. In the low temperature region, population of the three peaks appeared to occur simultaneously. In particular, the peak at 446 K was present at low coverage before acetone evolution was observed. However, the results for low coverage acetone adsorption on the same catalyst (section 7.3) would suggest that any acetone formed after low coverage 2-PrOH adsorption would be dehydrated to propene on vacant dehydration sites. Comparison of figures 7.1 and 7.4 shows the water peak associated with acetone formation after a saturation 2-PrOH dose also to be present at low 2-PrOH coverage, further suggesting that acetone may have been formed but readsorbed on dehydration sites.

Figure 7.8 summarises the dependence of the product surface coverages as a function of the initial 2-PrOH dose. Dominant on the graph is the large amount of propene produced relative to the other desorption products. In section 7.1 it was noted that hydroxyl oxygen appeared to be consumed in the surface oxidation process to leave an apparent excess of propene; clearly according to the figure this trend was followed at all surface coverages.

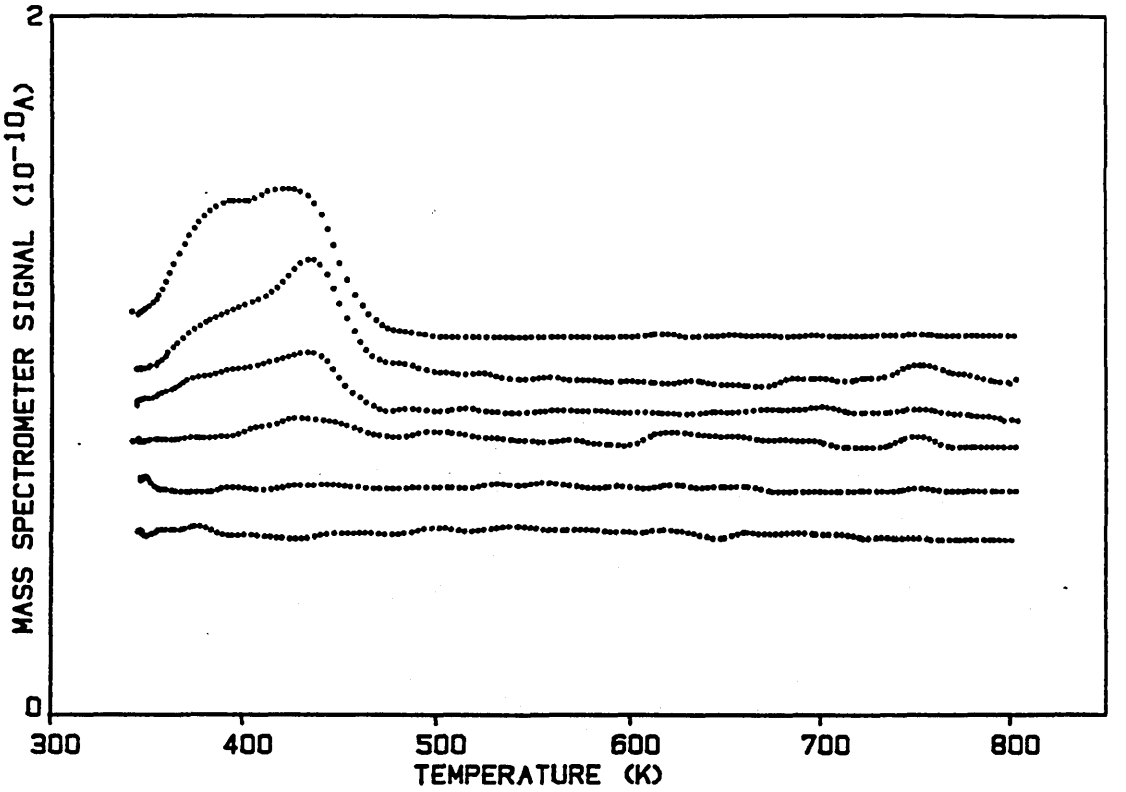

Figure 7.6: The coverage dependence of the 2-propanol desorption spectrum as a function of 2-propanol dose on zinc oxide.

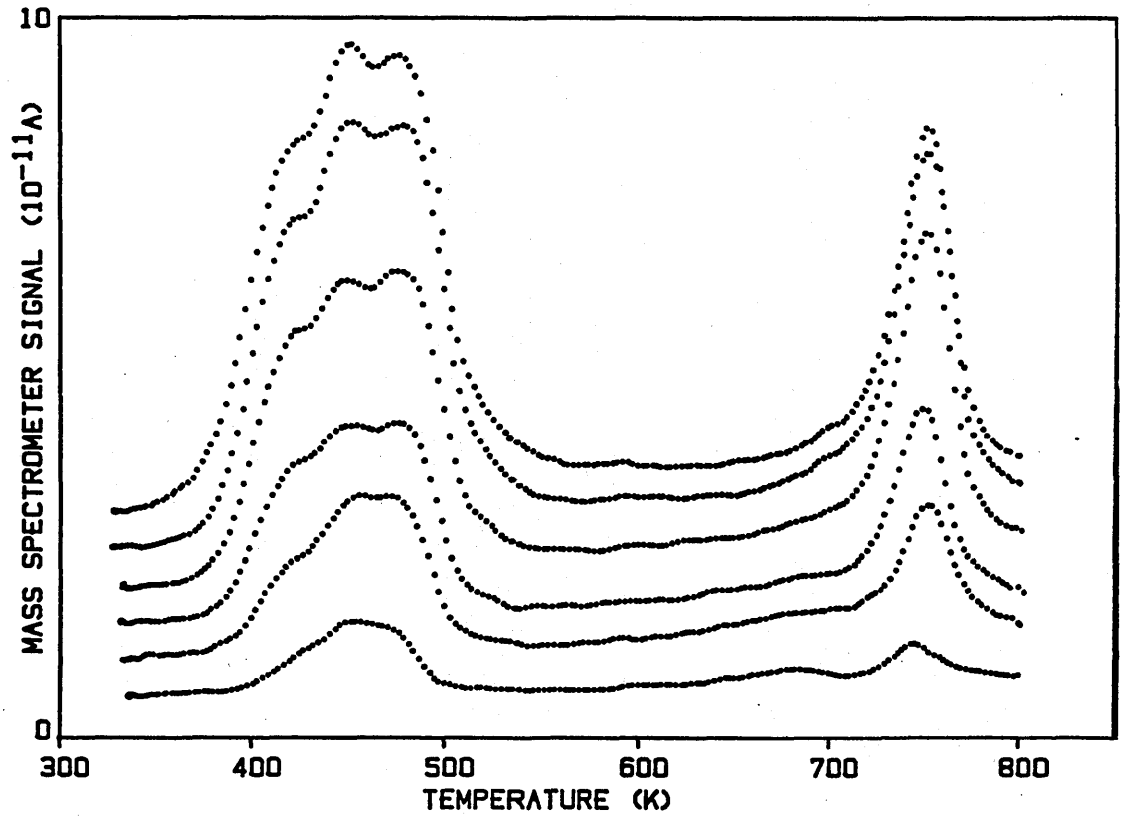

Figure 7.7: The coverage dependence of the hydrogen desorption spectrum as a function of 2-propanol dose on zinc oxide.

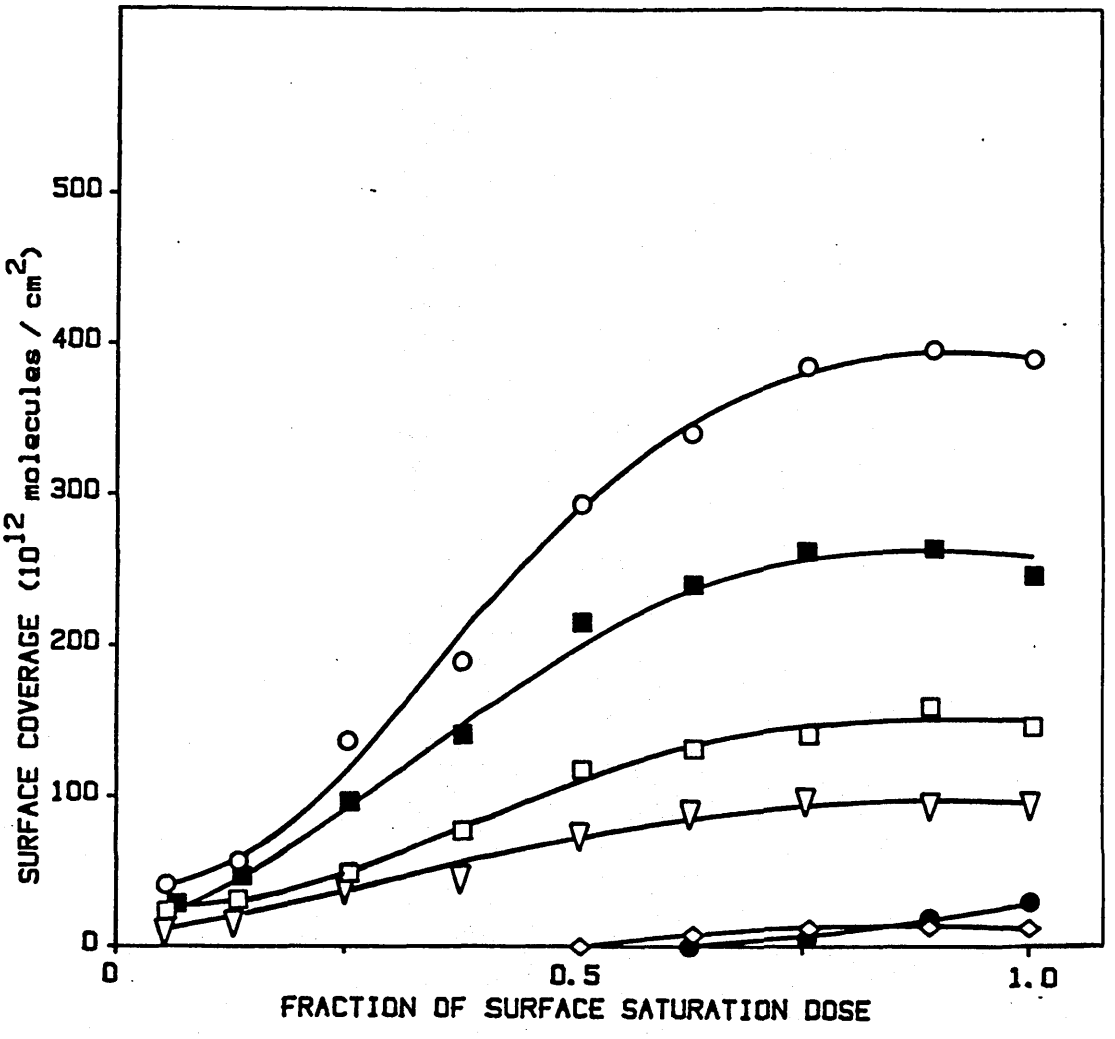

Figure 7.8: Plot of the desorption product surface coverages as a function of 2-propanol surface saturation dose at 340 K on zinc oxide. ○ total coverage (excluding water); ■ propene; □ water; ▽ CO_2; ● 2-PrOH; ◇ acetone.

(7.1.3) 2-propanol and Water Coadsorption

Water was used as a probe molecule in "selective poisoning" experiments[145]. 2-PrOH and water coadsorption experiments were conducted to investigate site competition effects between adsorbed hydroxyls and the alcohol derived surface species and the results used to determine the crystal face dependence of the surface reactions. Water proved to be a useful coadsorbant since its adsorption characteristics were found to be well defined on ZnO (see section 6.1.1). One ml volumes of water were progressively added to approximately 25-30 ml of 2-PrOH in the liquid saturator and a saturation dose of the diluted alcohol made. Although a maximum dilution of 40% water was used, no further changes to the TPD spectra were found for a dilution factor greater than 15%.

The changes in the water desorption spectra with increased alcohol dilution are shown in figure 7.9, where a comparison to the desorption spectrum after the adsorption of water-only is also made. As dilution was increased the profile of the high temperature desorption peak can be seen to approach that of the peak obtained after water-only adsorption on the same catalyst, with the presence of coadsorbed water significantly increasing the quantity of water desorbed at approximately 713 K. This confirmed the high temperature water peak found after alcohol adsorption to be due to hydroxyl recombination rather than to be a decomposition product of an alcohol derived surface complex. In the low temperature region the amount of water produced did not alter as significantly, although increases can be seen in the water peak produced at a temperature similar to acetone and in the desorption at approximately 373 K.

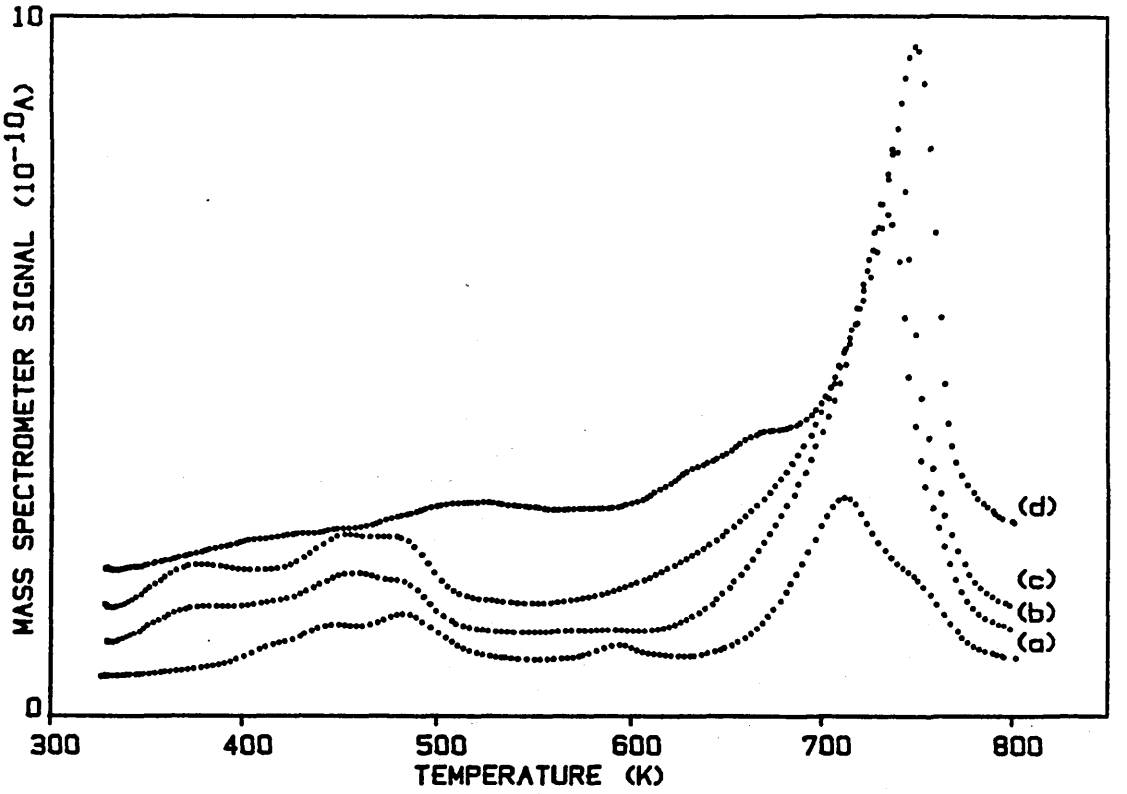

Figure 7.9: The water desorption spectrum after 2-propanol and water coadsorption on zinc oxide. (a)= no added water; (b)= 5% dilution; (c)= 10% dilution; (d)= water only adsorbed.

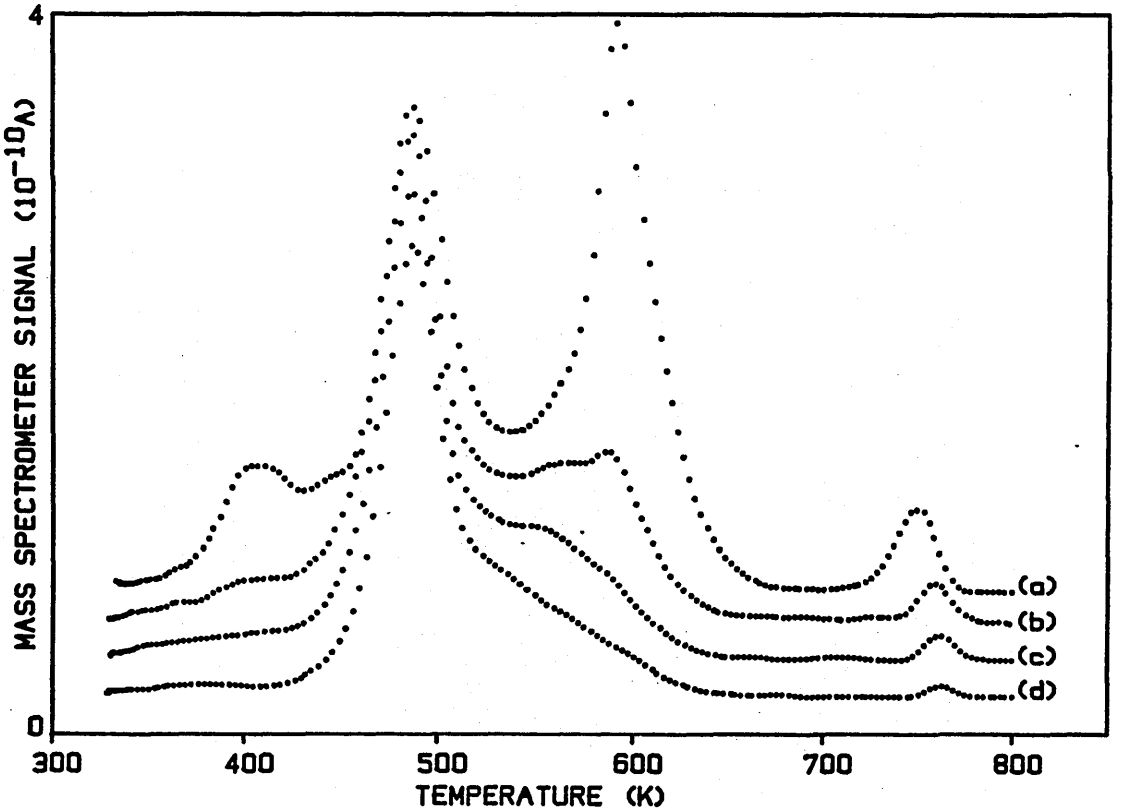

Figure 7.10: The propene desorption spectrum after 2-propanol and water coadsorption on zinc oxide. (a)= no added water; (b)= 5% dilution ; (c)= 10% dilution; (d)= 15% dilution.

The presence of coadsorbed water was found to significantly alter the selectivity of the 2-PrOH decomposition reactions. The α and γ propene peaks were progressively reduced as the alcohol dilution was increased, while the β propene peak remained unaffected at all dilution factors as shown in figure 7.10. Both the 2-PrOH and acetone desorption peak profiles and their corresponding surface coverages remained essentially unaffected by the addition of the dilutant water (figures 7.11 and 7.12) although the acetone peak temperature did increase to 458 K indicative of a stabilisation effect. The quantity of CO_2 desorbed was significantly reduced with increasing alcohol dilution as shown in figure 7.13, although, even at the highest dilution complete suppression of CO_2 desorption did not occur (49×10^{12} molecules/cm^2 desorbed). The presence of the water was found to suppress hydrogen desorption in the 419 K and 478 K peaks, but to only slightly reduce desorption in the main 447 K peak. The temperature of this peak also increased similar to the increase shown by the acetone desorption peak. The estimated quantity of hydrogen evolved (115×10^{12} molecules/cm^2) remained in excess of the acetone formed.

(7.1.4) Effect of a Lower Maximum Heating Temperature

A previous TPD study of 2-PrOH decomposition on ZnO by Bowker et al[115] had used a maximum temperature of only 600 K. On the basis of the results presented in section 7.1.1, this temperature was too low to desorb the strongly adsorbed hydroxyl and carboxylate species and may have been contributory in producing the different 2-propanol desorption spectrum obtained by these workers. To investigate this aspect and to complement the results of the water/2-PrOH coadsorption, further experiments were conducted based on a lower maximum

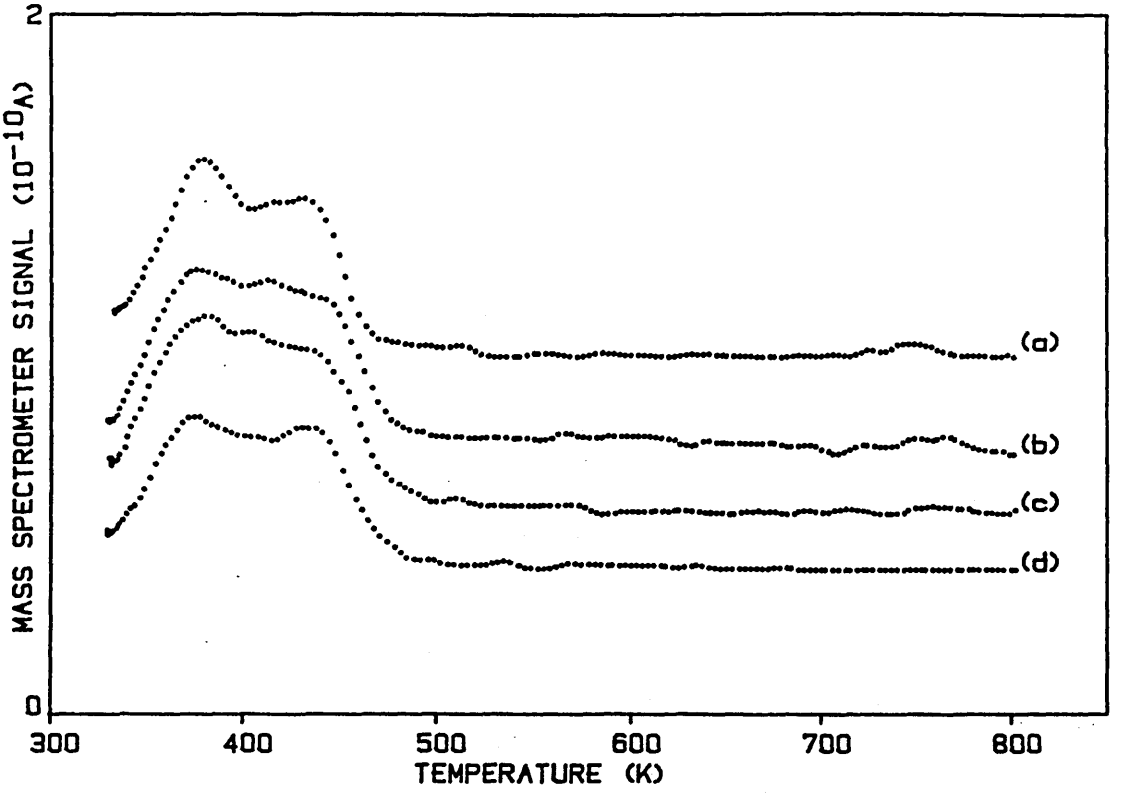

Figure 7.11: The 2-propanol desorption spectrum after 2-propanol and water coadsorption on zinc oxide. (a)= no added water; (b)= 5% dilution ; (c)= 10% dilution; (d)= 15% dilution.

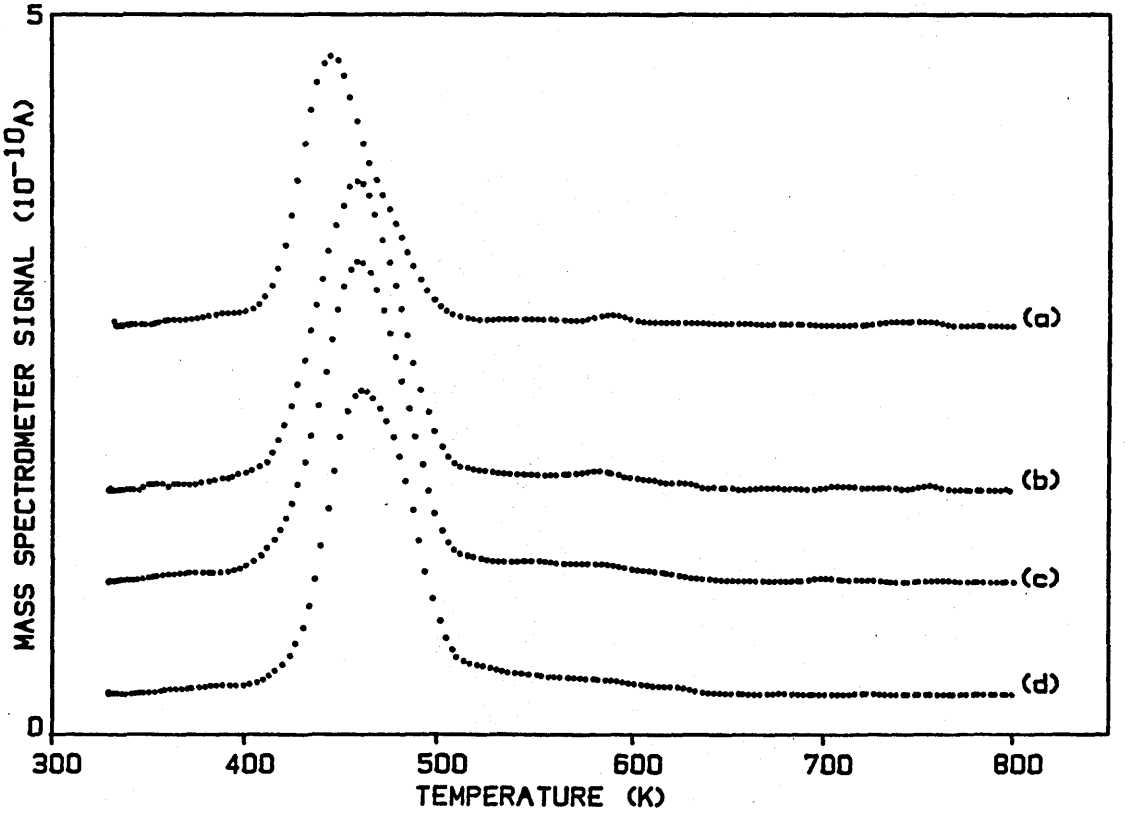

Figure 7.12: The acetone desorption spectrum after 2-propanol and water coadsorption on zinc oxide. (a)= no added water; (b)= 5% dilution; (c)= 10% dilution; (d)= 15% dilution .

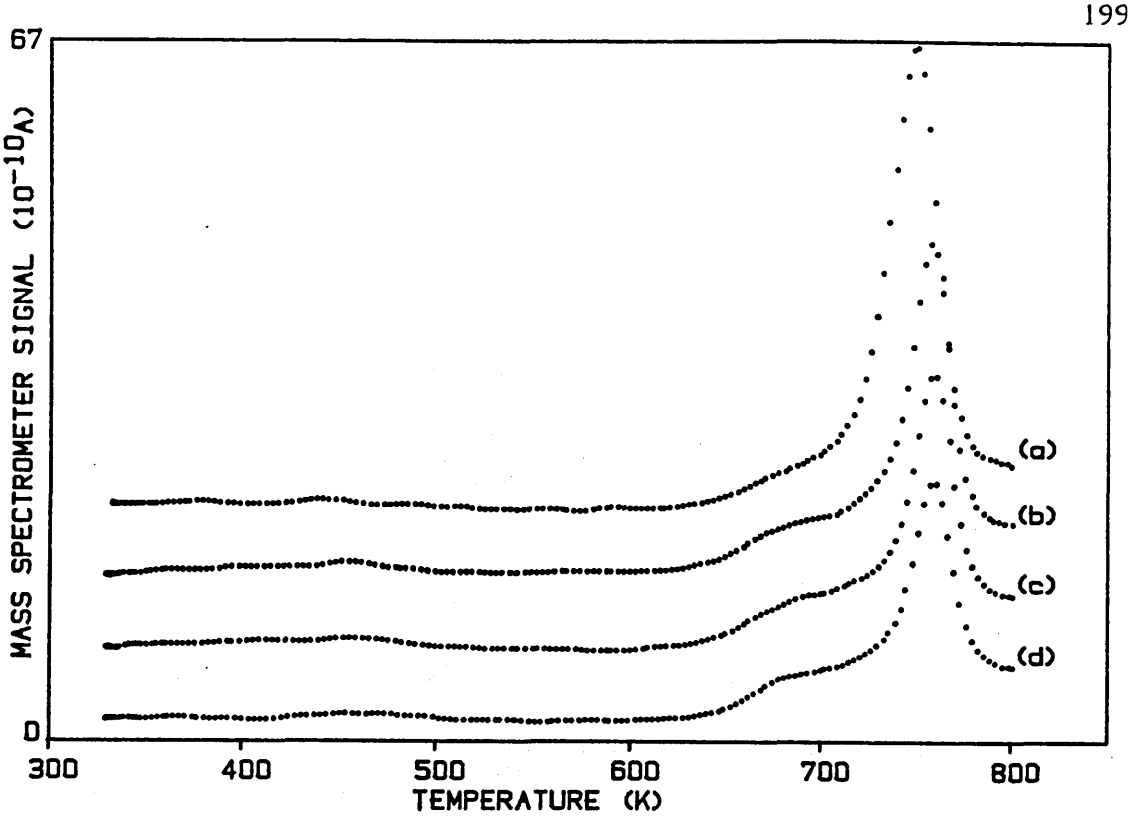

Figure 7.13: The carbon dioxide desorption spectrum after 2-propanol and water coadsorption on zinc oxide. (a)= no added water; (b)= 5% dilution; (c)= 10% dilution; (d)= 15% dilution.

temperature (approximately 673 K compared to the normal experimental maximum of 800 K) so that the high temperature alcohol decomposition product surface precursors were not desorbed from the catalyst surface. The catalyst was then cooled and with these species still present on the surface, a further 2-PrOH adsorption dose made. Several consecutive experiments were conducted so the cumulative effect of the build-up in coverage of the high temperature surface species could be studied.

The presence of the undesorbed stable high temperature species was found to significantly modify the 2-PrOH decomposition reaction. Figures 7.14 to 7.17 show the changes in the corresponding desorption peak profiles.

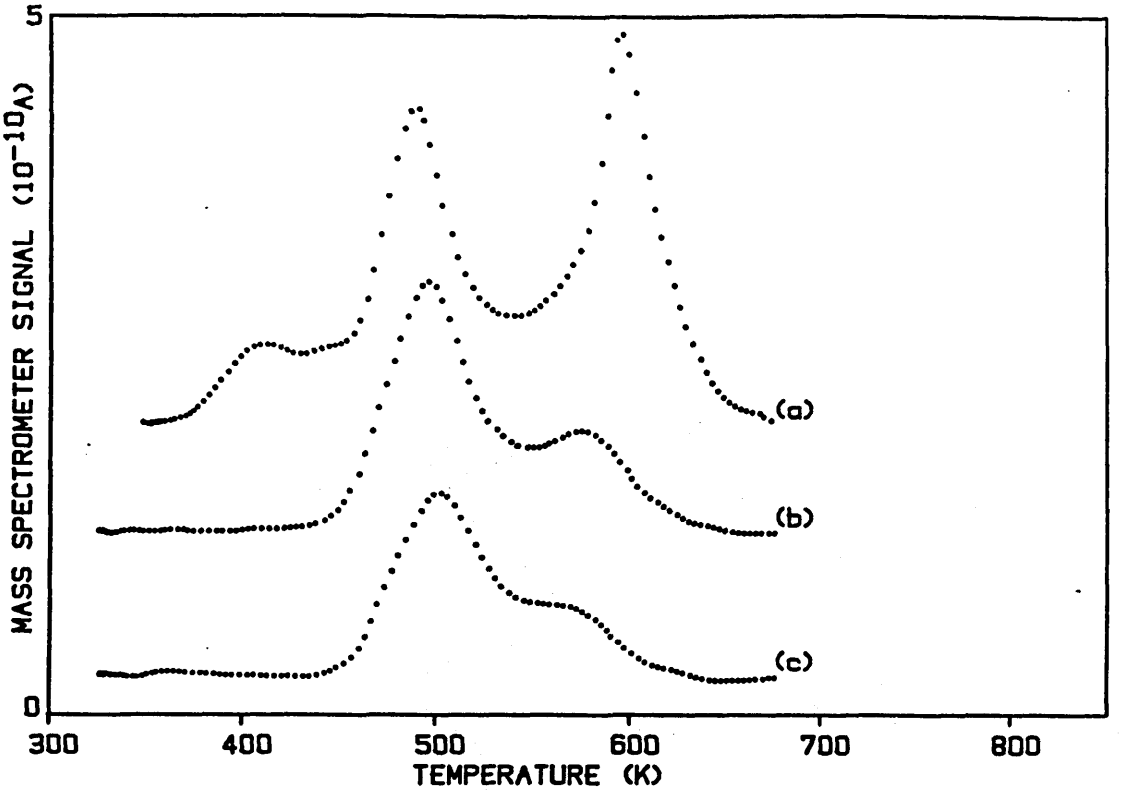

Figure 7.14: The effect of a low maximum temperature on the propene desorption spectrum after consecutive 2-propanol adsorption/desorption cycles on zinc oxide. (a)→(c)= order of experiments.

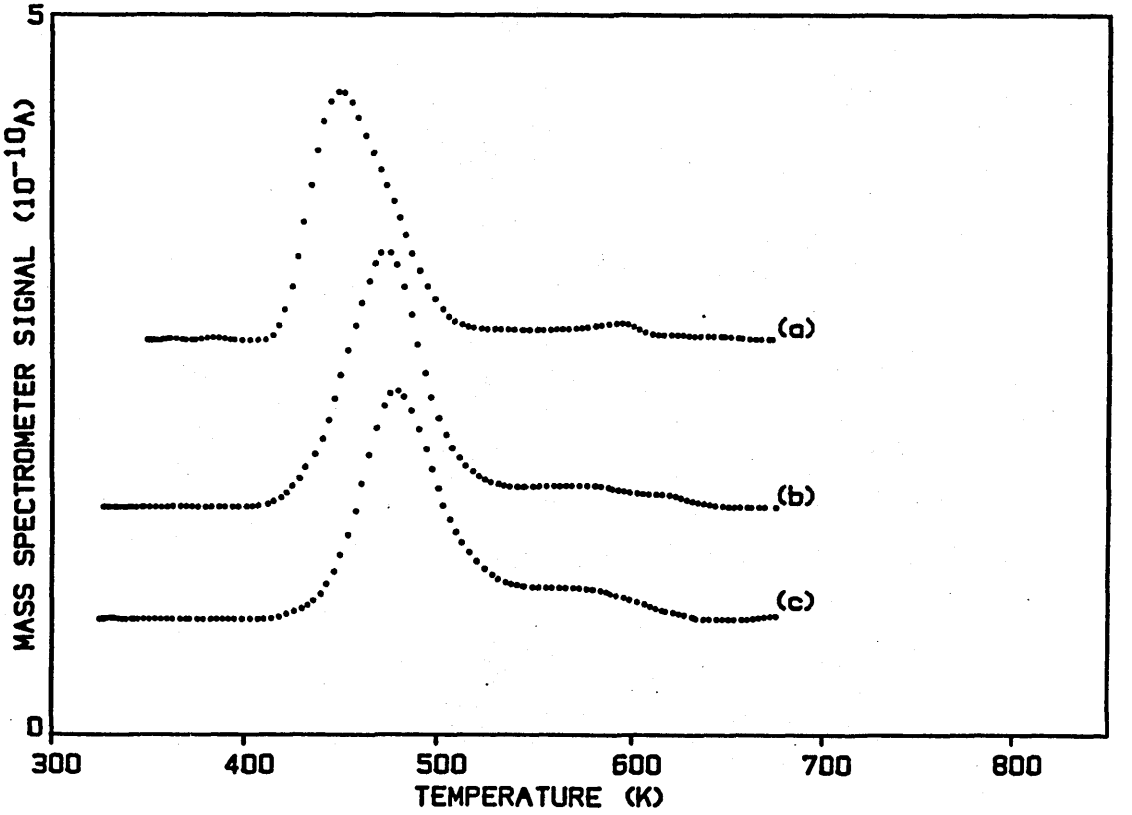

Figure 7.15: The effect of a low maximum temperature on the acetone desorption spectrum after consecutive 2-propanol adsorption/desorption cycles on zinc oxide. (a)→(c)= order of experiments.

Desorption in both α and γ propene desorption peaks was significantly reduced with each successive experiment (figure 7.14), while a smaller but still significant reduction in desorption from the β propene state also occurred. The similarity of the reduction in the α and γ peaks to the result obtained after water and 2-PrOH coadsorption (see previous section) suggested that the decrease in these peaks was also due to the presence of the higher hydroxyl coverage. The reduction in the β peak (not found for the coadsorption experiments) may be related to the additional presence of the higher carboxylate coverage.

The quantity of acetone desorbed remained unaffected over the same three experiments. Figure 7.15 shows that while no distortion in the desorption peak profile was found, an increase in the acetone peak temperature from 446 to 476 K occurred.

The coverage of reversibly adsorbed 2-PrOH increased by approximately 70% over the same three experiments. Accompanying this increase was a distortion of the 2-PrOH desorption peak profiles (figure 7.16), with the desorption associated with the α peak being slightly reduced and that with the β peak increased. The temperature of the α 2-PrOH peak increased from 435 to 463 K, while the β state decreased from 392 to 371 K.

The low temperature water desorption peak profiles also underwent significant change (figure 7.17). A peak developed coincident with the α 2-PrOH state plus a further broad peak coincident with the acetone and propene states. The total quantity of water desorbed in the low temperature region (up to 630 K) decreased by approximately 40% over the three experiments.

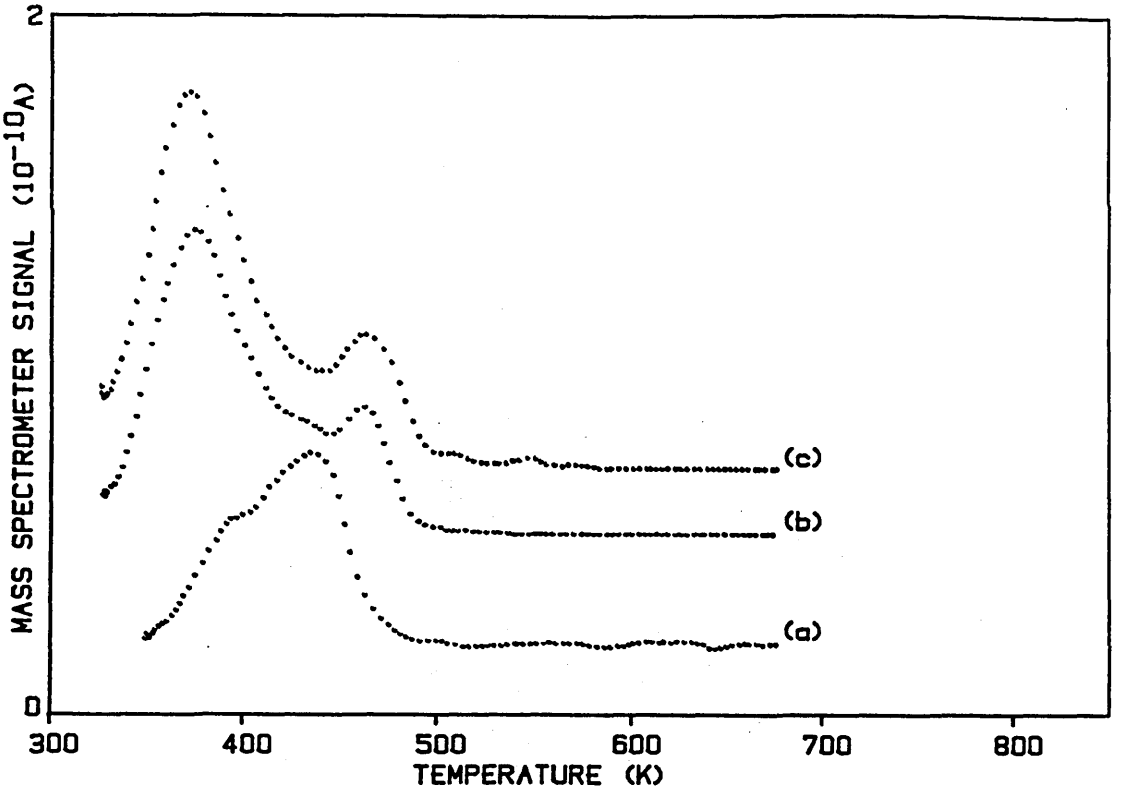

Figure 7.16: The effect of a low maximum temperature on the 2-propanol desorption spectrum after consecutive 2-propanol adsorption/desorption cycles on zinc oxide. (a)→(c)= order of experiments.

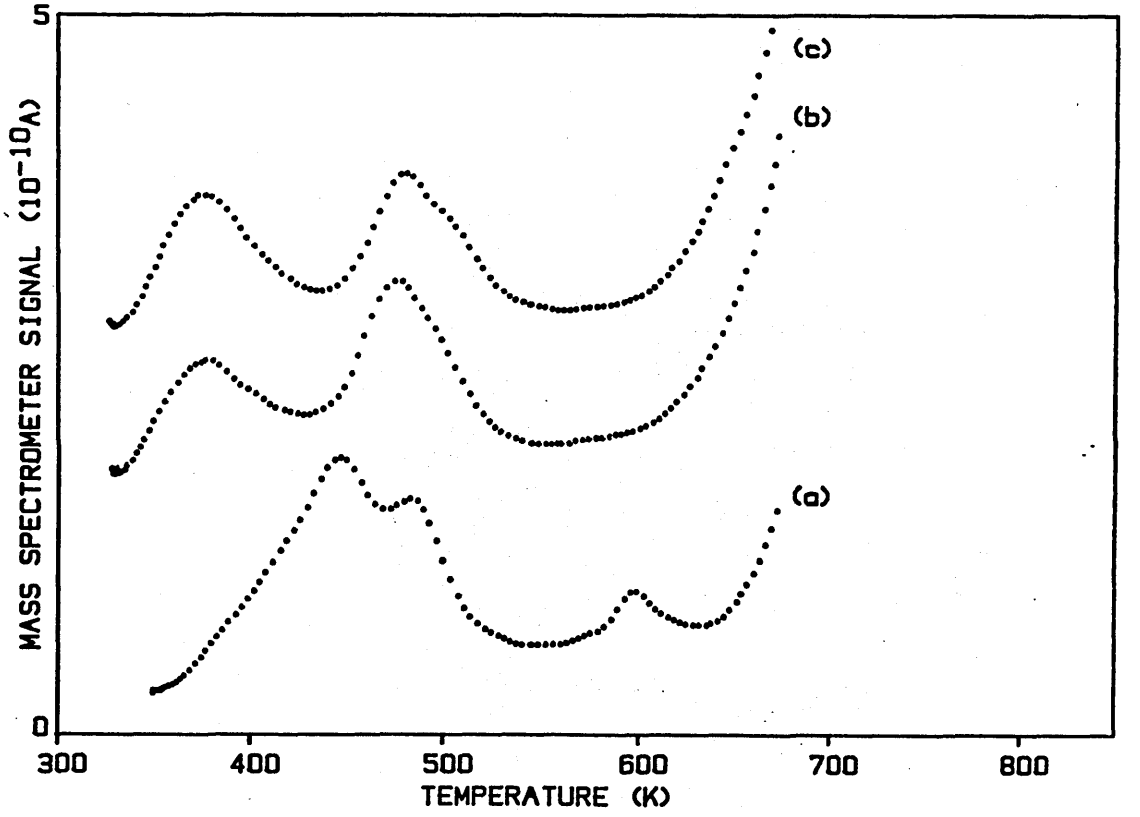

Figure 7.17: The effect of a low maximum temperature on the water desorption spectrum after consecutive 2-propanol adsorption/desorption cycles on zinc oxide. (a)→(c)= order of experiments.

(7.1.5) Effect of an Increased Adsorption Temperature

The adsorption temperature dependence of 2-PrOH decomposition was investigated by experiments where alcohol was adsorbed onto the catalyst at high temperature (approximately 658 K) and either temperature programmed from this temperature (to 800 K), or cooled to 330-340 K and a further dose of 2-PrOH made, before temperature programming in the normal manner.

After 2-PrOH adsorption at 658 K and subsequent heating to 800 K, only water and CO_2 (plus also hydrogen and methane) were observed as the major desorption products. Figure 7.18 shows the desorption peak profiles to be similar to that obtained after low temperature 2-PrOH adsorption, although the water peak was slightly broader. A small amount of mass 41 (propene) desorbed between 704 and 745 K but no acetone or 2-PrOH were observed (since the alcohol adsorption was made at a temperature above their normal desorption temperatures). The appearance of the minor propene peak appeared to be associated with the oxidative decomposition reaction similar to the small mass amount of propene normally observed coincident with the CO_2 peak after low temperature 2-PrOH adsorption. The high temperature adsorption resulted in an increase of roughly 50% in the amount of CO_2 desorbed compared to the CO_2 obtained after low temperature 2-PrOH adsorption. This was indicative of a temperature dependence to the oxidation reaction consistent with an activated reaction process. A decrease in the amount of high temperature water desorbed was found compared to that obtained after a low temperature adsorption (in spite of the increased peak width) possibly associated with increased hydroxyl consumption in carboxylate formation.

The desorption spectrum obtained after a high temperature 2-PrOH adsorption at 658 K, followed by cooling to 336 K and a further 2-PrOH dose is shown in figure 7.19. The combination of high and low temperature adsorption resulted in a significantly larger amount of CO_2 compared to that evolved after a normal low temperature adsorption, similar to the amount obtained after the high temperature only adsorption. This indicated that the oxidation occurred during the high temperature adsorption stage, with no apparent further oxidation associated with the low temperature alcohol dose. The quantity of propene desorbed was significantly reduced with only the single β desorption peak at 505 K formed, consistent with the effect of a higher surface hydroxyl coverage as described in sections 7.1.3 and 7.1.4. The quantity of water desorbed after the high and low adsorption sequence was found to be greater than after a low temperature 2-PrOH adsorption by approximately $40x10^{12}$ molecules/cm^2. A further minor propene peak evolved at 709 K would again appear to be related to the oxidative decomposition reaction (although the peak temperature was slightly lower than normally observed).

Both acetone and 2-PrOH surface coverages were relatively unaffected by the presence of the increased coverage of water/carboxylate surface species resulting from the initial high temperature dose. Although the acetone did not undergo any significant distortion in peak profile, its peak temperature increased by 37 K from 443 to 480 K in a similar manner to that observed after the low maximum temperature experiments.

In the low temperature region, water desorption occurred in a peak at 493 K and a smaller shoulder at 391 K. The overall quantity of low temperature water desorption was reduced.

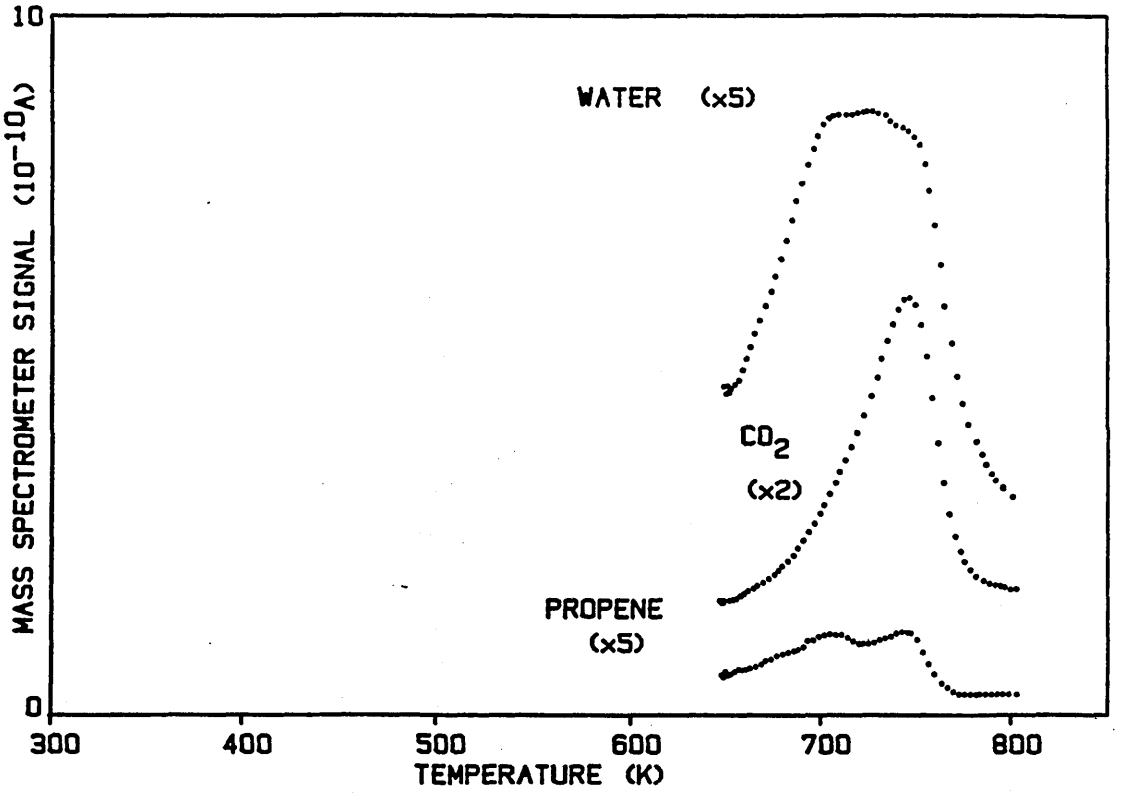

Figure 7.18: The desorption spectrum after adsorption of 2-propanol at 660 K on zinc oxide.

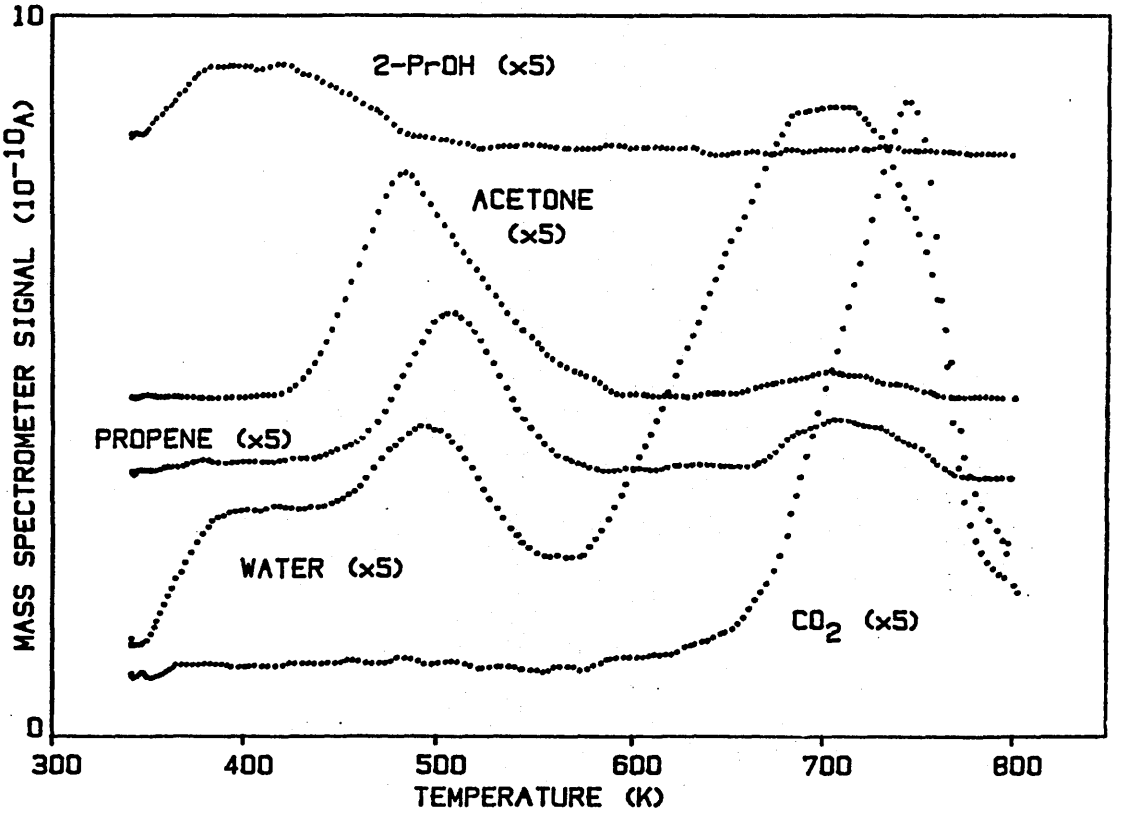

Figure 7.19: The desorption spectrum after adsorption of 2-propanol at 660 K and 340 K on zinc oxide.

A low temperature only 2-PrOH adsorption following the experiments described above was found to give a desorption spectrum similar to figure 7.1, with the exception of a decrease in the temperature of the high temperature water peak to 688 K.

(7.1.6) Effect of an Increased Catalyst Sample Mass

The effect of variation in the mass of catalyst sample on the desorption temperature is a method used for determination of the heat of adsorption[128], relying on readsorption effects to cause a shift in the peak temperature as the catalyst mass is changed. For a kinetically limited desorption product, readsorption effects are not significant since the desorption process corresponds to an essentially irreversible reaction step. A shift in peak temperature should not then be observed as the catalyst mass is changed. This analysis method was applied to investigate 2-PrOH decomposition as a qualitative means of determining which desorption products were readsorption, rather than kinetically, limited.

2-PrOH was adsorbed onto several catalyst samples with weights ranging from 0.166 g to 0.989 g, with figure 7.20 summarising the shifts in desorption peak temperatures that occurred with change in catalyst mass. The peak temperatures for all three propene states and for the acetone peak can be seen to be invariant with changing catalyst mass, which indicated the evolution of these products to be under kinetic control. The high temperature water desorption peak, however, showed a strong dependence on catalyst mass (as was found after water-only adsorption- see section 6.1.1) confirming its evolution to be dominated by readsorption. Since the CO_2 peak was formed at a similar temperature to that of the water, if it were also readsorption

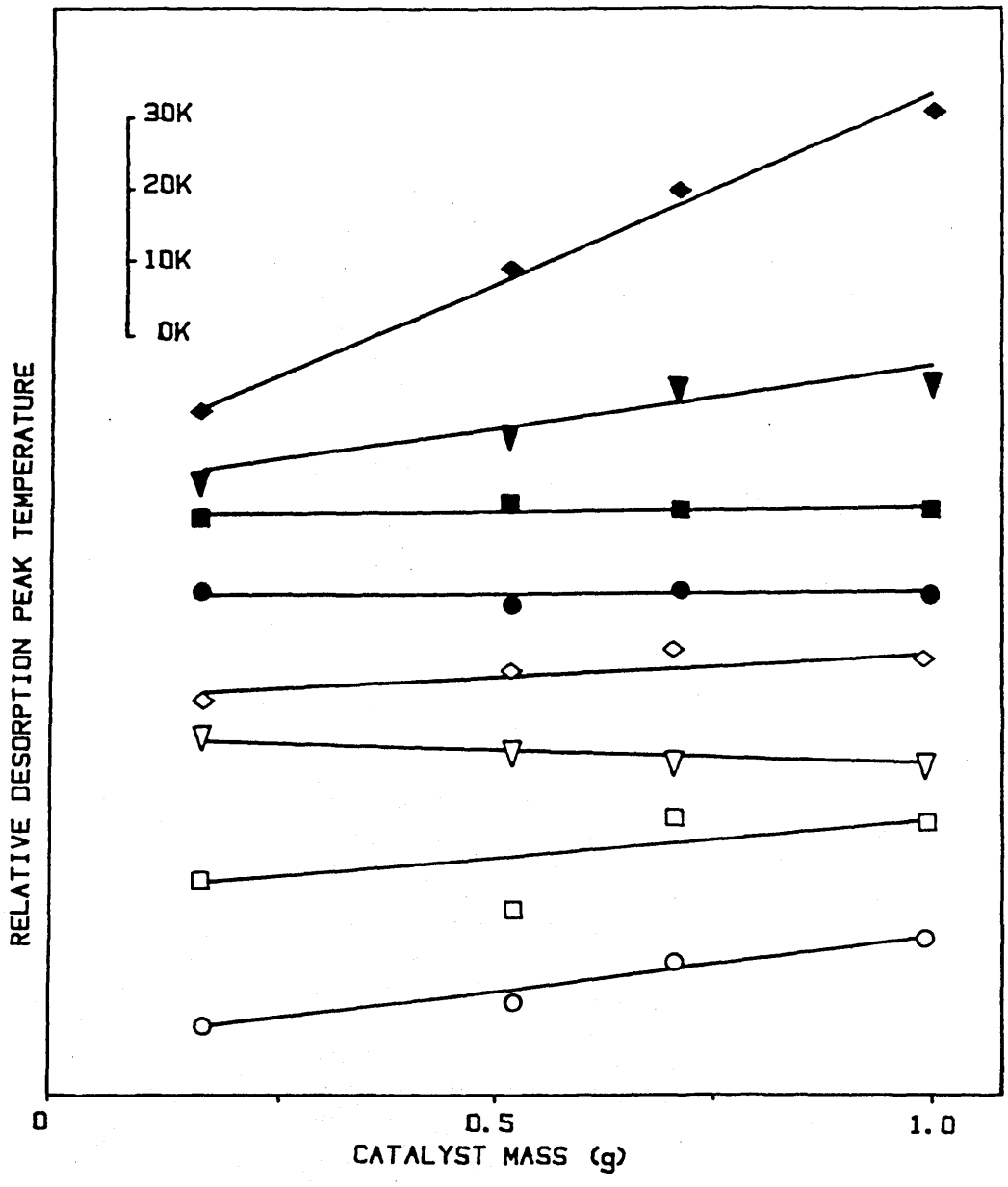

Figure 7.20: Plot of the effect of catalyst mass on the 2-propanol desorption product peak temperatures from zinc oxide.
◆ = α water; ▼ = CO_2; ■ = α propene; ● = β propene;
◇ = γ propene; ▽ = acetone; □ = α 2-PrOH; ○ = β 2-PrOH

dominated, then it also would have exhibited a similar magnitude temperature change. However, since the CO_2 peak showed only a small temperature shift with catalyst mass, it was shown to be essentially kinetically limited (although the slight shift observed would indicate some minor readsorption effects occurred, possibly due to limited formation of adsorbed carbonate species[27]). Both 2-PrOH peaks exhibited small positive shifts in peak temperature with catalyst mass due to readsorption effects (the smaller shifts were consistent with their lower peak temperatures since the shift is proportional to the heat of adsorption).

(7.2) 1-Propanol

(7.2.1) Thermal Desorption and Decomposition Spectrum

A typical desorption spectrum obtained after a saturation dose of 1-propanol (1-PrOH) at 340 K onto unpromoted ZnO is shown in figure 7.21. The main desorption products were 1-PrOH, propionaldehyde, propene, CO_2, hydrogen and water, plus a further unidentified mass 29 desorption peak at 640 K. Ethene (identified by 28, 27 and 26 amu) was also detected at high temperature in the region of 740 to 750 K. The desorption spectrum was dominated by reversible adsorption of the alcohol and by the oxidative decomposition surface reaction producing CO_2. Only a very small quantity of propionaldehyde desorption was detected, while the extent of dehydration to propene was also limited in comparison to 2-PrOH. No methane desorption was detected.

The peak temperatures and surface coverages are summarised in table 7.2. The total surface coverage, excluding the water desorbed, was estimated to be 686×10^{12} molecules/cm^2. Although this was

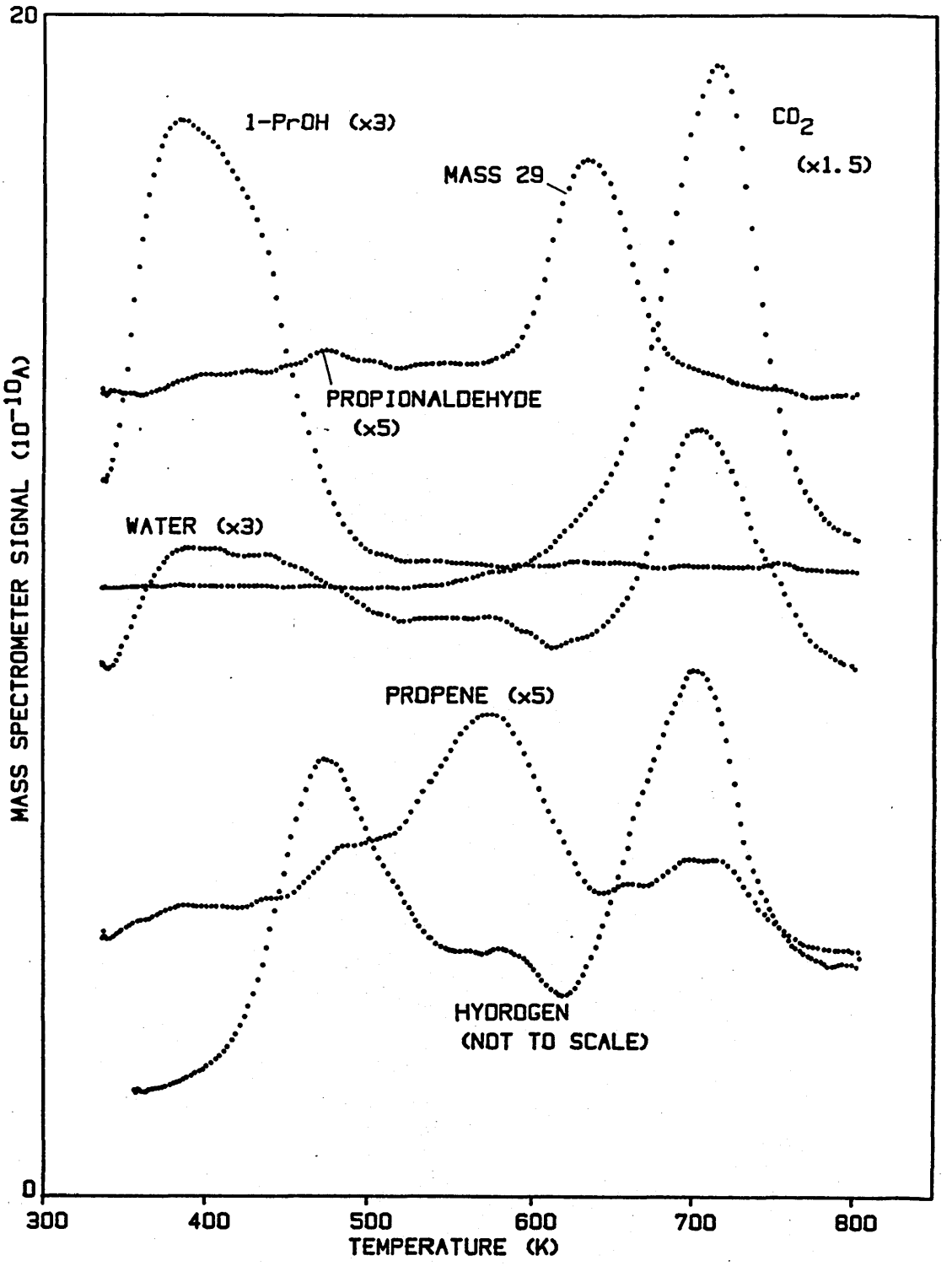

Figure 7.21: The desorption spectrum after adsorption of 1-propanol at 340 K to saturation coverage on zinc oxide. The propionaldehyde and propene peaks have been corrected for cracking fraction overlap with 1-propanol. No correction has been made for differences in the mass spectrometer sensitivities.

Table 7.2: The desorption products, peak temperatures and saturation surface coverages following 1-propanol adsorption at 340 K on zinc oxide.

desorption product	peak temperature (K, ±2)	surface coverage (10^{12}molec/cm^2)
1-propanol	(381),405,(427)	162
propionaldehyde	475	4
propene	481	16
	573	79
CO_2	713	425
water	386,407,438	50
	576	~10
	703,743	56
hydrogen	473	350
	588	45
	713	490
mass 29	640	-
ethene	716	-

significantly higher than the corresponding 2-PrOH saturation coverage, a closer correspondence between the two alcohol coverages was obtained if the contribution of reversibly adsorbed alcohol was also excluded to give coverages of 524×10^{12} and 529×10^{12} molecules/cm^2 for 1-PrOH and 2-PrOH respectively.

Reversible 1-PrOH desorption occurred in three closely overlapping states that produced a single large and broad desorption peak at approximately 405 K, along with poorly defined minor peaks at 381 K and 427 K. The reversible adsorption represented approximately 24% of the total desorption products.

Propene formed in two main peaks at 573 K and 481 K, with a further mass 41 peak (possibly propene) at 706 K associated with the carboxylate decomposition (described below). Minor quantities of mass 41 desorption also occurred at 662 K and 694 K. The broad 573 K peak (compared to propene formed after 2-PrOH adsorption- see figure 7.1) suggested that it was possibly made up of more than one desorption state. Approximately 80% of the total propene formed was desorbed in this peak. Hydrogen and water were also desorbed at temperatures similar to the 573 K propene. The estimated molecular ratios of propene to hydrogen and propene to water were 2:1 and 10:1 respectively. A larger relative amount of water appeared to be desorbed with the 481 K propene peak, with propene to water ratio estimated to be in the order of unity.

In common with the behaviour of 2-PrOH, only approximately half the total quantity of water was desorbed in the low temperature region (mainly 400-440 K), with the majority of the water desorbed at higher temperatures. The temperature of the high temperature water peak at 703 K was significantly lower than observed for the corresponding 2-PrOH derived water peak, although the water/1-PrOH coadsorption experiments (section 7.2.3) established it was still derived from adsorbed hydroxyls i.e. readsorption limited.

A barely detectable quantity of propionaldehyde was observed at 475 K, 34 K higher than the acetone formed from 2-PrOH dehydrogenation. Although only limited dehydrogenation appeared to occur, a large amount of hydrogen was still desorbed at 473 K. Two further hydrogen desorption peaks were formed; at 713 K associated with carboxylate decomposition (see below), and in a small peak at 588 K as described above. The additional mass 29 peak at 640 K would not

appear to have been due to propionaldehyde desorption; identification of this peak is considered in the discussion section.

As described in section 7.1, the formation of CO_2 and hydrogen at high temperature (713 K) was indicative of an oxidative decomposition surface reaction that involved the formation of a surface carboxylate species. The 1-PrOH carboxylate decomposition temperature was approximately 40 K lower than found for both 2-PrOH and acetone, indicative of a slightly lower stability surface intermediate. The quantity of CO_2 evolved after 1-PrOH adsorption was significantly greater than that produced from either 2-PrOH or acetone (section 7.3), accounting for approximately 55% of the observed desorption products. Also produced on carboxylate decomposition was a quantity of mass 41 (possibly propene) similar to that found with 2-PrOH and acetone derived carboxylate decomposition. Quantities of mass 28, along with 27 and 26 amu (indicative of ethene formation) were also detected in a similar temperature range as the CO_2 peak. However, the poor signal response of the mass spectrometer Faraday-cup detector for mass 28 made it impossible to quantify the amount of ethene desorbed. No methane desorption was detected in the temperature range of the carboxylate decomposition.

(7.2.2) Coverage Dependence

A series of experiments were conducted where the initial 1-PrOH dose was varied from 20% of saturation to full saturation surface coverage. The desorption spectra from experiments at three of these coverages (20%, 50% and 80% of saturation) are given in figures 7.22 to 7.24. The results showed the selectivity of 1-PrOH decomposition

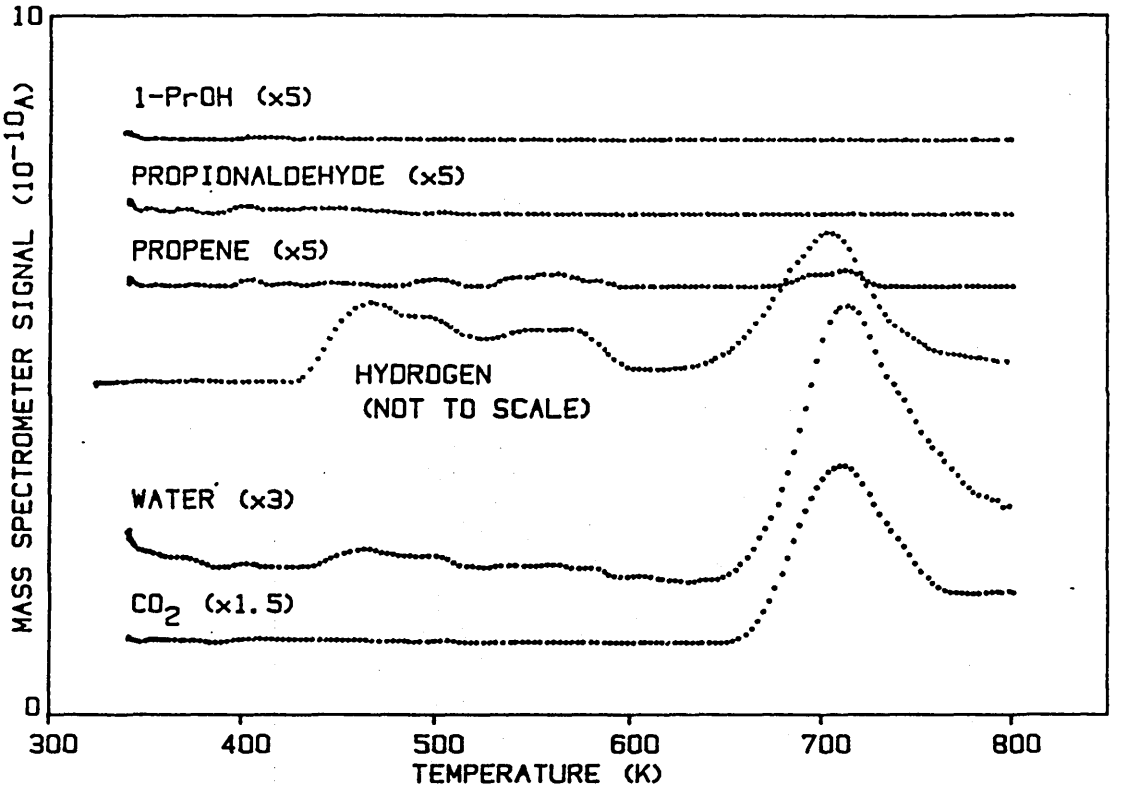

Figure 7.22: The desorption spectrum after 1-propanol adsorption to 20% coverage at 340 K on zinc oxide.

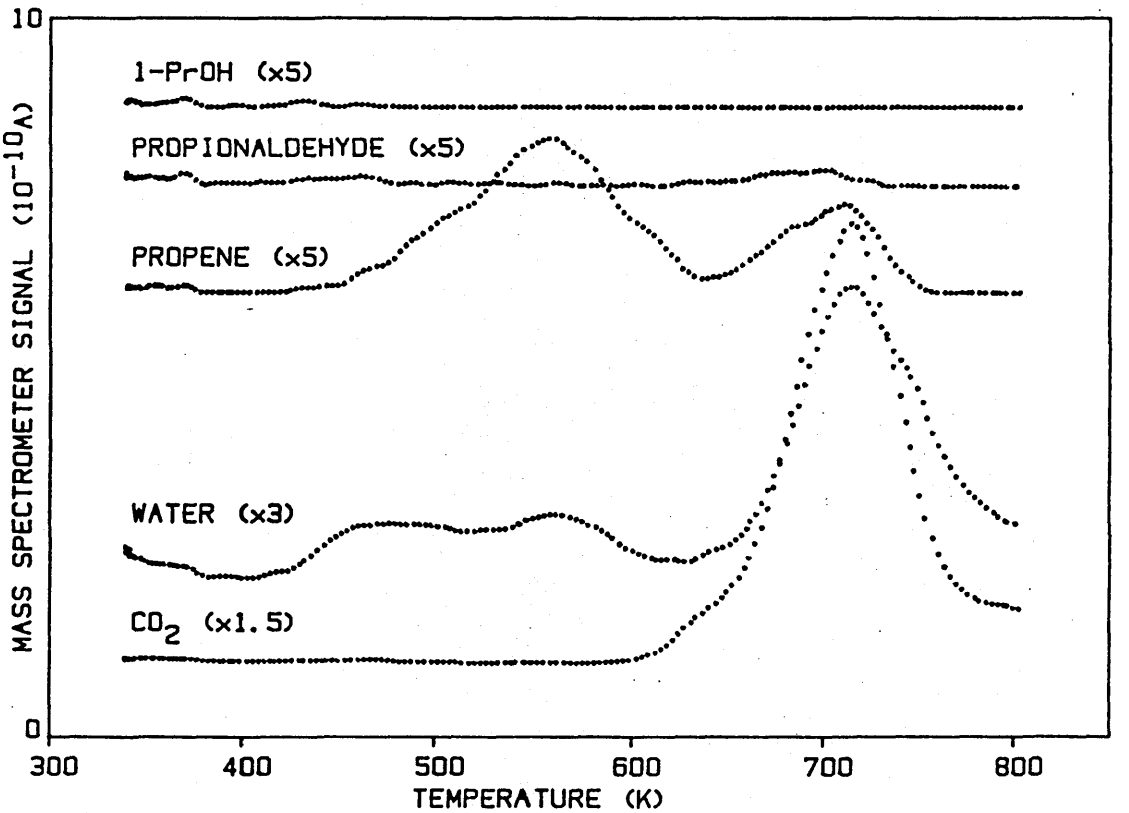

Figure 7.23: The desorption spectrum after 1-propanol adsorption to 50% coverage on zinc oxide

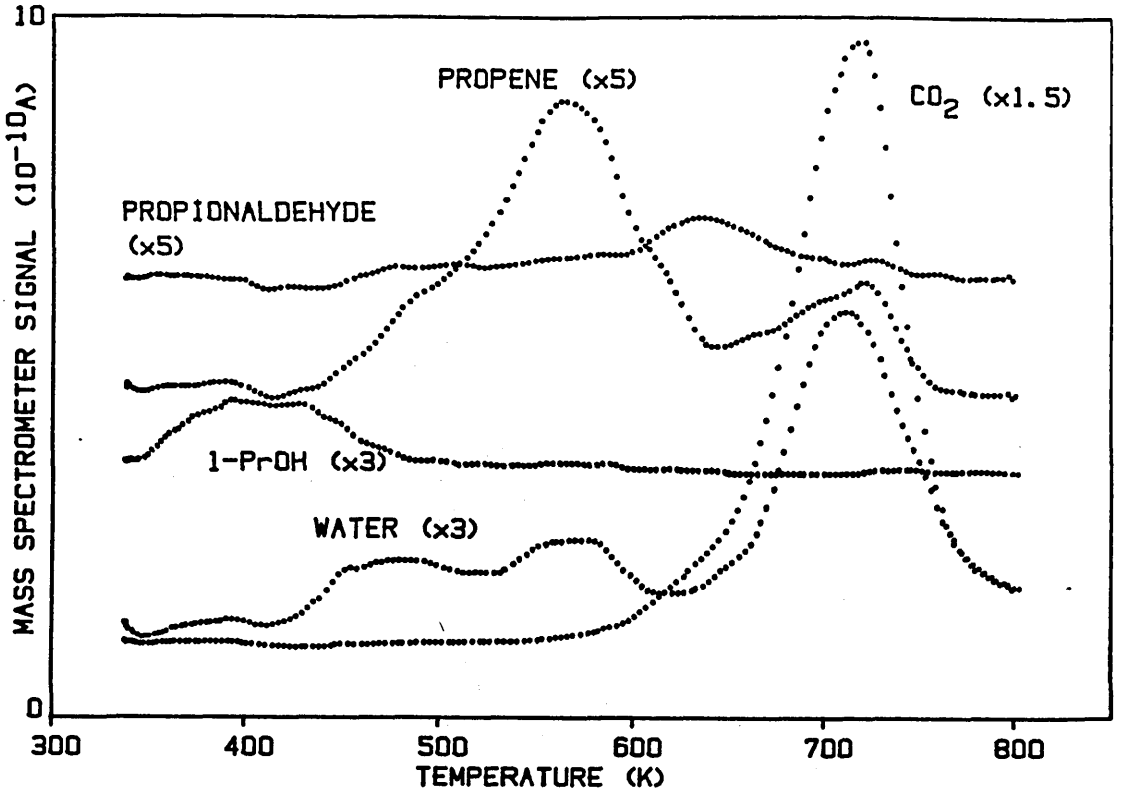

Figure 7.24: The desorption spectrum after 1-propanol adsorption to 80% coverage on zinc oxide

to be dependent on the initial surface coverage; figure 7.25 summarising the changes in coverage of the main desorption products with 1-PrOH dose shows clearly the high selectivity of the decomposition toward carboxylate formation and reversible desorption of the parent alcohol.

At low coverage (figure 7.22) the main desorption products were CO_2, water and hydrogen, showing oxidation to the carboxylate/acetate species to be the dominant reaction. This result should be compared to the behaviour of 2-PrOH where at low coverage dehydration was also a significant decomposition pathway (section 7.1). For 1-PrOH, only a trace of propene at 705 K was detected associated with the carboxylate decomposition reaction. In spite of this low selectivity for dehydration, water was still present in a relatively large amount indicating that either this water was produced on carboxylate formation or was

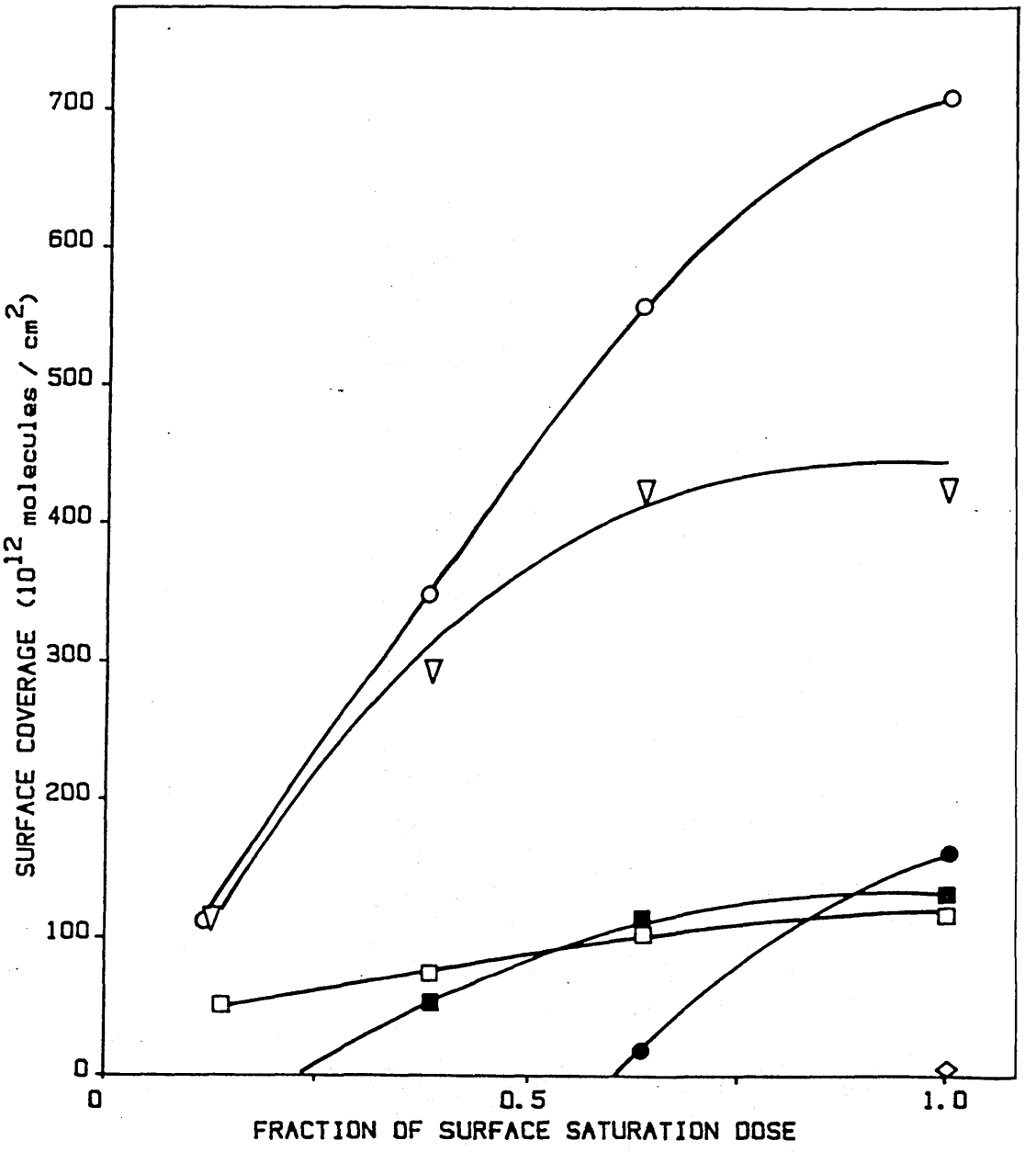

Figure 7.25: Plot of the desorption product surface coverages as a function of 1-propanol surface saturation dose at 340 K on zinc oxide. ○ total coverage (excluding water); ■ propene; □ water; ▽ CO_2; ● 1-PrOH; ◇ propionaldehyde.

present as an impurity in the injected alcohol. As the quantity of water desorbed did not increase at the same rate as CO_2 evolution with increasing 1-PrOH dose, the latter explanation would appear to have been the more likely. Hydrogen desorption was also detectable at lower temperatures similar to that found after a saturation 1-PrOH dose (467 K and 558 K). As the coverage was further increased the high oxidation selectivity was maintained, although dehydration products were also detectable in significant quantity. Figure 7.23 at 50% coverage shows the presence of a further propene peak at 557 K in addition to the propene derived from carboxylate decomposition. No significant quantity of propionaldehyde was detected for this dose.

Alcohol or propionaldehyde desorption was not observed until the surface coverage reached 70-80% of saturation as shown in figure 7.24. At this dose an additional minor propene peak at 484 K was also apparent.

(7.2.3) 1-Propanol and Water Coadsorption

Water and 1-PrOH were coadsorbed using the same method as previously described for 2-PrOH i.e. by addition of distilled water to the alcohol in the liquid saturator, with a maximum dilution factor of approximately 15% water in the alcohol used. The presence of coadsorbed water was found to reduce the quantities of propene, CO_2 and mass 29 produced but not to effect either the amount of reversibly adsorbed alcohol or to change its desorption peak profile.

As the amount of coadsorbed water was increased the quantity of water produced at high temperature rose, while the amount of desorption in the low temperature region increased in the region of 480 K (figure 7.26). This effect was similar to that previously noted for

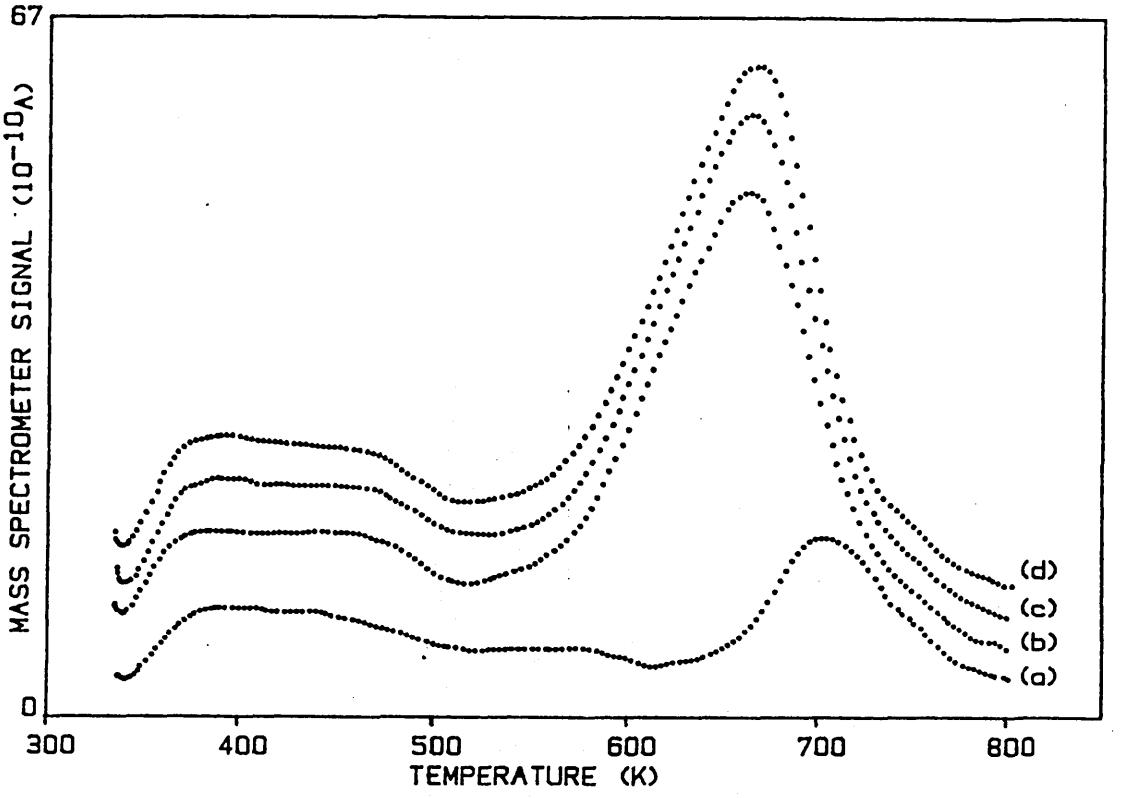

Figure 7.26: The water desorption spectrum after 1-propanol and water coadsorption on zinc oxide. (a)= no added water; (b)= 5% dilution; (c)= 10% dilution; (d)= 15% dilution.

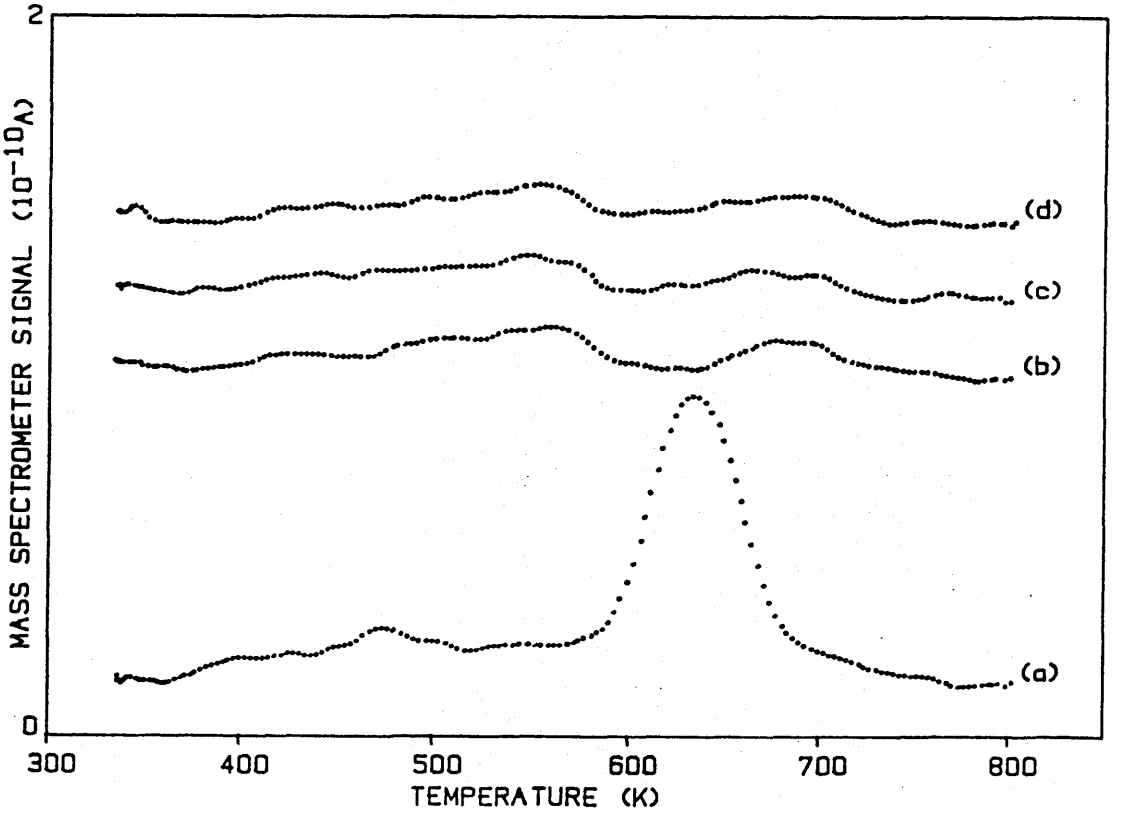

Figure 7.27: The mass 29 desorption spectrum after 1-propanol and water coadsorption on zinc oxide. (a)= no added water; (b)= 5% dilution; (c)= 10% dilution; (d)= 15% dilution.

2-PrOH and water coadsorption (section 7.1.3), although for 1-PrOH the high temperature water desorption peak temperature was at a lower temperature and was found to decrease from 703 K to 663 K as the alcohol dilution was increased. (For 2-PrOH the peak temperature was found to increase with alcohol dilution- see figure 7.9).

Figure 7.27 shows the presence of coadsorbed water almost entirely suppressed the formation of the mass 29 desorption at high temperature, which also shifted to a higher temperature (approximately 673 K). The reduction in this peak, not matched by a reduction in the carboxylate derived CO_2, suggested its formation may have been in fact independent to the oxidative decomposition process. A small amount of mass 29 desorption also appeared at approximately 550 K although it was not possible to determine if this was propionaldehyde. The 475 K propionaldehyde state appeared to be suppressed by the water coadsorption.

Similarly, propene desorption was suppressed by the coadsorbed water (figure 7.28). The mass 41 (possibly propene) associated with carboxylate decomposition was not suppressed to the same extent since even the highest dilution failed to totally suppress carboxylate formation (see below).

The presence of coadsorbed water was found only to reduce the amount of CO_2 desorbed by approximately 20% compared to the quantity obtained after undiluted 1-PrOH adsorption (giving a coverage of 324×10^{12} molecules/cm^2). This was accompanied by an 8 K decrease in the CO_2 peak temperature to 705 K and a decrease in the desorption peak width (figure 7.29).

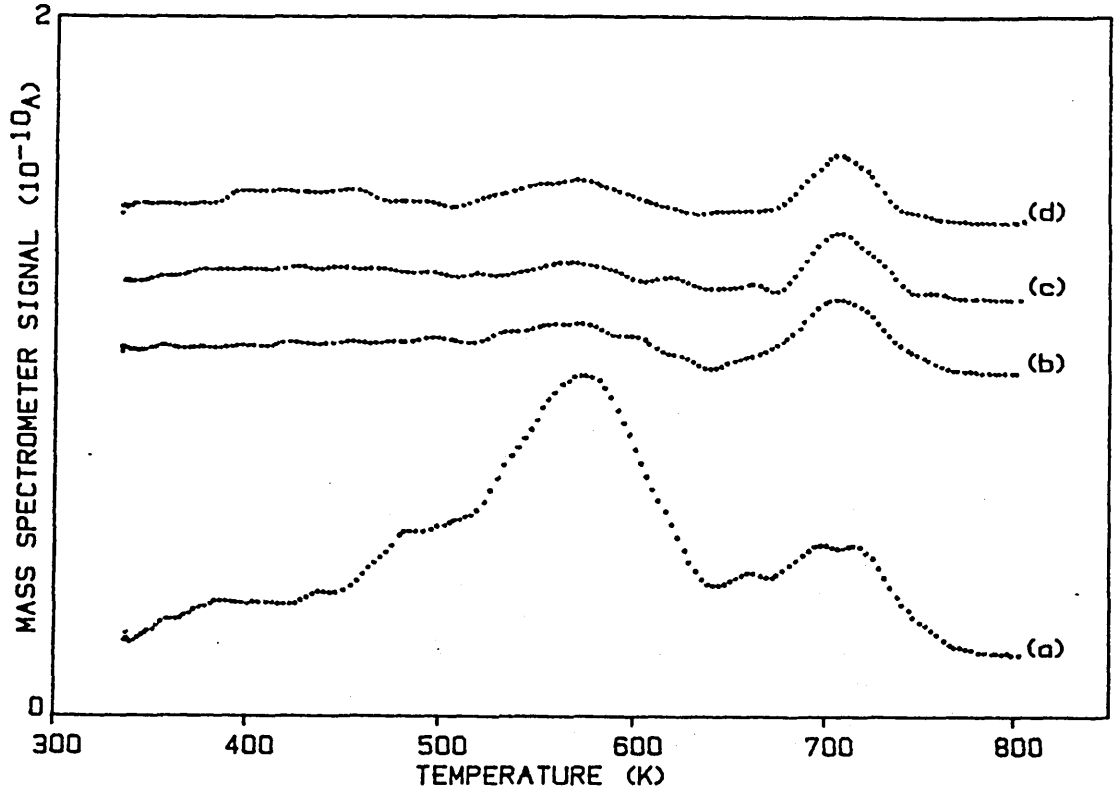

Figure 7.28: The propene desorption spectrum after 1-propanol and water coadsorption on zinc oxide. (a)= no added water; (b)= 5% dilution, (c)= 10% dilution, (d)= 15% dilution

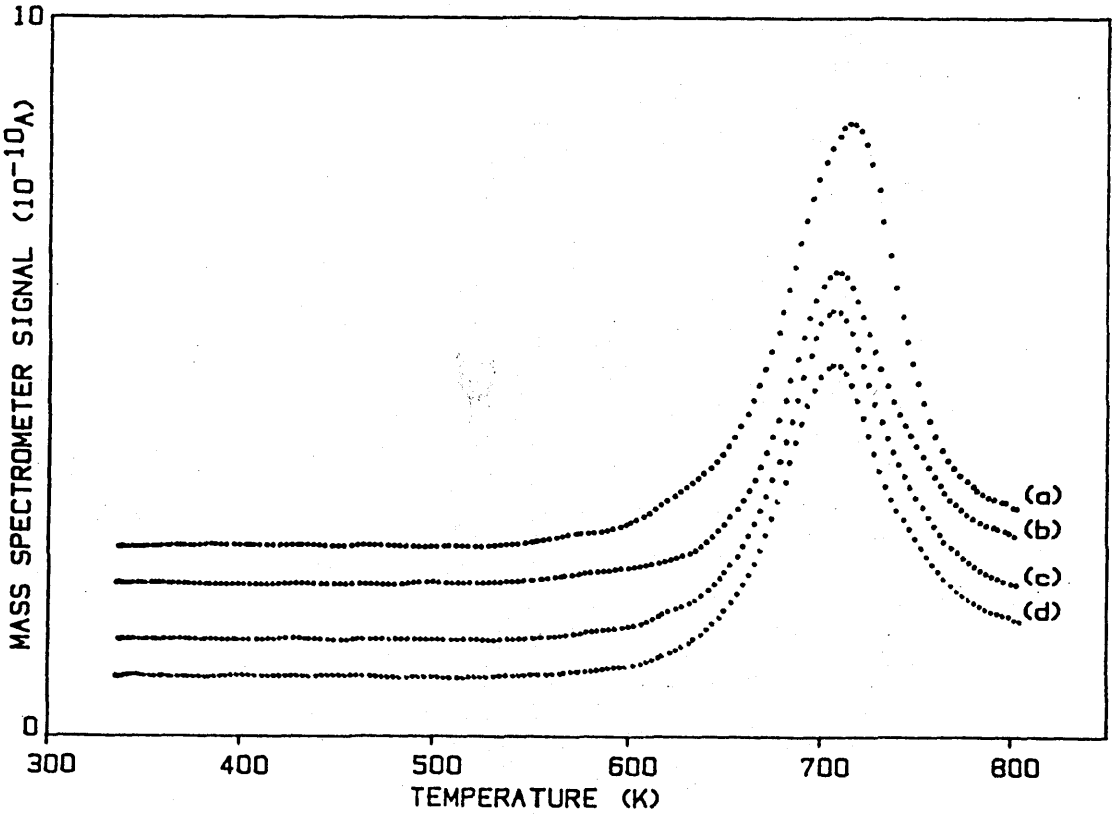

Figure 7.29: The carbon dioxide desorption spectrum after 1-propanol and water coadsorption on zinc oxide. (a)= no added water; (b)= 5% dilution; (c)= 10% dilution; (d)= 15% dilution.

(7.2.4) Effect of an Increased Catalyst Sample Mass

Following a similar method to that used for 2-PrOH (section 7.1.6), 1-PrOH was adsorbed onto ZnO samples of different mass and the resulting variations in the desorption product peak temperatures used to determine which desorption peaks were dominated by readsorption effects. Catalyst sample masses in the range 0.142 g to 0.913 g were tested, with the resulting peak temperatures of the main desorption and decomposition products summarised in figure 7.30.

As for 2-PrOH, the high temperature water desorption peak was shown to be readsorption limited since a large positive shift in peak temperature occurred with catalyst mass. The reversible 1-PrOH peak at low temperature showed a smaller shift as would be expected from such a reversibly adsorbed state, although the accuracy of detecting such changes in this temperature region was limited (since the temperature shift is proportional to the heat of adsorption). Both the mass 29 and propene peaks showed a slight negative shift in temperature with increasing catalyst weight. The reason for this effect was not clear, although the result did, however, indicate that formation of these products appeared to be under kinetic, rather than readsorption, control. The CO_2 peak showed a slight increase in temperature with catalyst weight (as also found for 2-PrOH). The magnitude of the shift would, however, again indicate that readsorption was not significant i.e. the CO_2 evolution was under kinetic control. Any shift associated with the propionaldehyde peak temperature could not be determined since the very low amount of propionaldehyde formation meant that the peak for this product could not be accurately established.

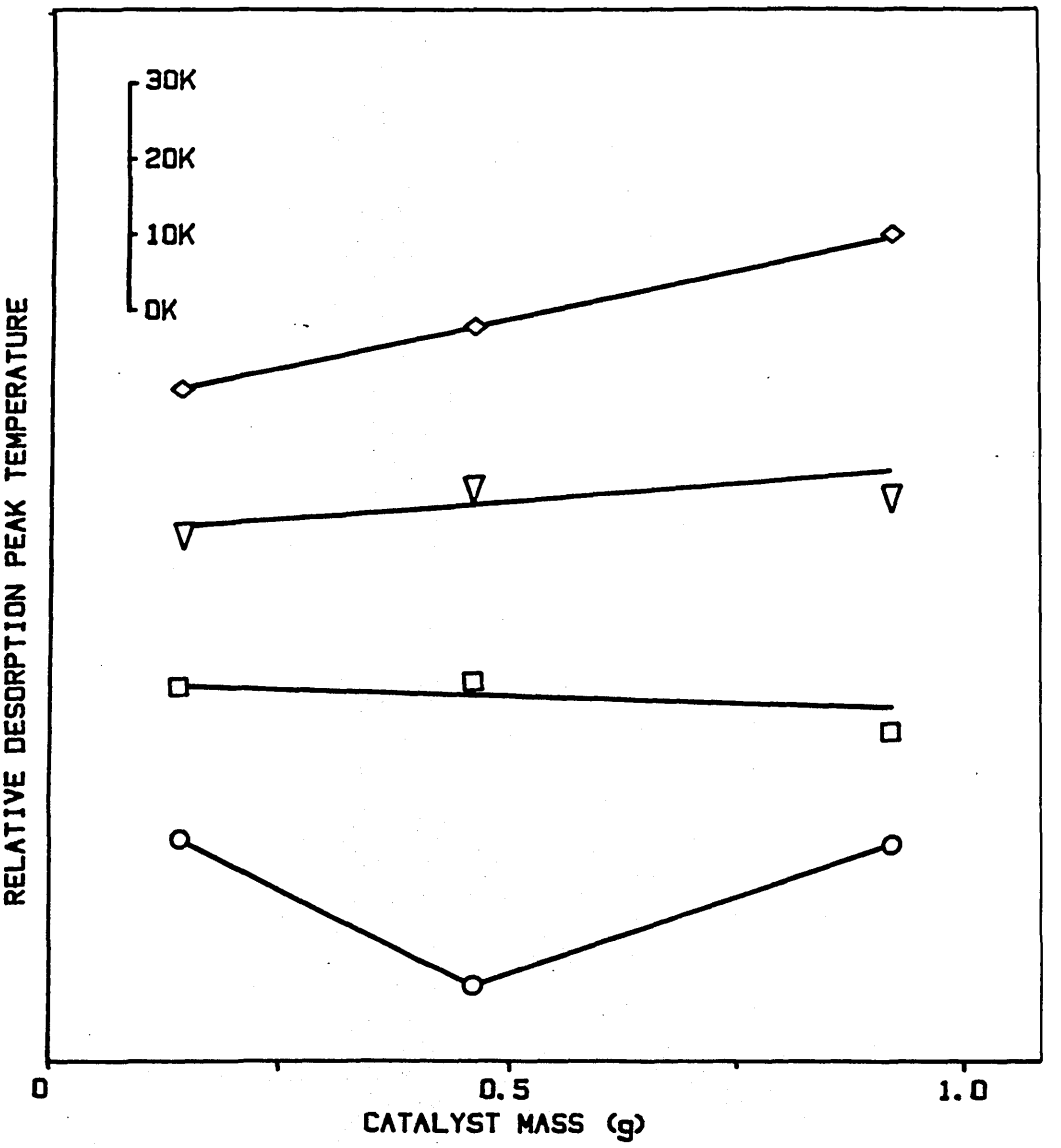

Figure 7.30: Plot of the effect of catalyst mass on the 1-propanol desorption product peak temperatures from zinc oxide.
○ = 1-PrOH; □ = propene; ▽ = CO_2; ◇ = water

(7.3) Acetone

(7.3.1) Thermal Desorption and Decomposition Spectrum

A typical desorption spectrum obtained after adsorption of acetone to saturation coverage at 340 K is shown in figure 7.31 with the corresponding main product surface coverages and peak temperatures detailed in table 7.3. The main desorption products obtained were acetone, propene, CO_2, hydrogen, methane and water.

Acetone desorbed in a single broad peak at approximately 428±7 K, with a further minor desorption peak at higher temperature (approximately 553 K) indicated in the trailing edge of the main peak. The main peak was 10-20 K lower than the acetone peak observed after 2-PrOH adsorption on the same catalyst (section 7.1), the larger error limits being a reflection of variability in the position of this peak between different experiments under the same conditions. The surface coverage was similar to that obtained for acetone after 2-PrOH adsorption.

Propene was evolved in two overlapping desorption peaks at temperatures of 473 K and 555 K, that appeared to correspond to the α and β propene peaks formed from 2-PrOH. Compared to the 2-PrOH derived propene, these peaks were 15 K and 35 K lower in temperature respectively. The total propene surface coverage as given in table 7.3 was lower than for propene evolved after 2-PrOH adsorption. Water was evolved with the propene (approximate ratio of 6:1), while hydrogen was also produced in a broad and rather unstructured peak in the same temperature region. Further water desorption occurred at high temperature, while the total quantity of water was in excess of the propene formed indicating the possible presence of water impurities in the injected acetone.

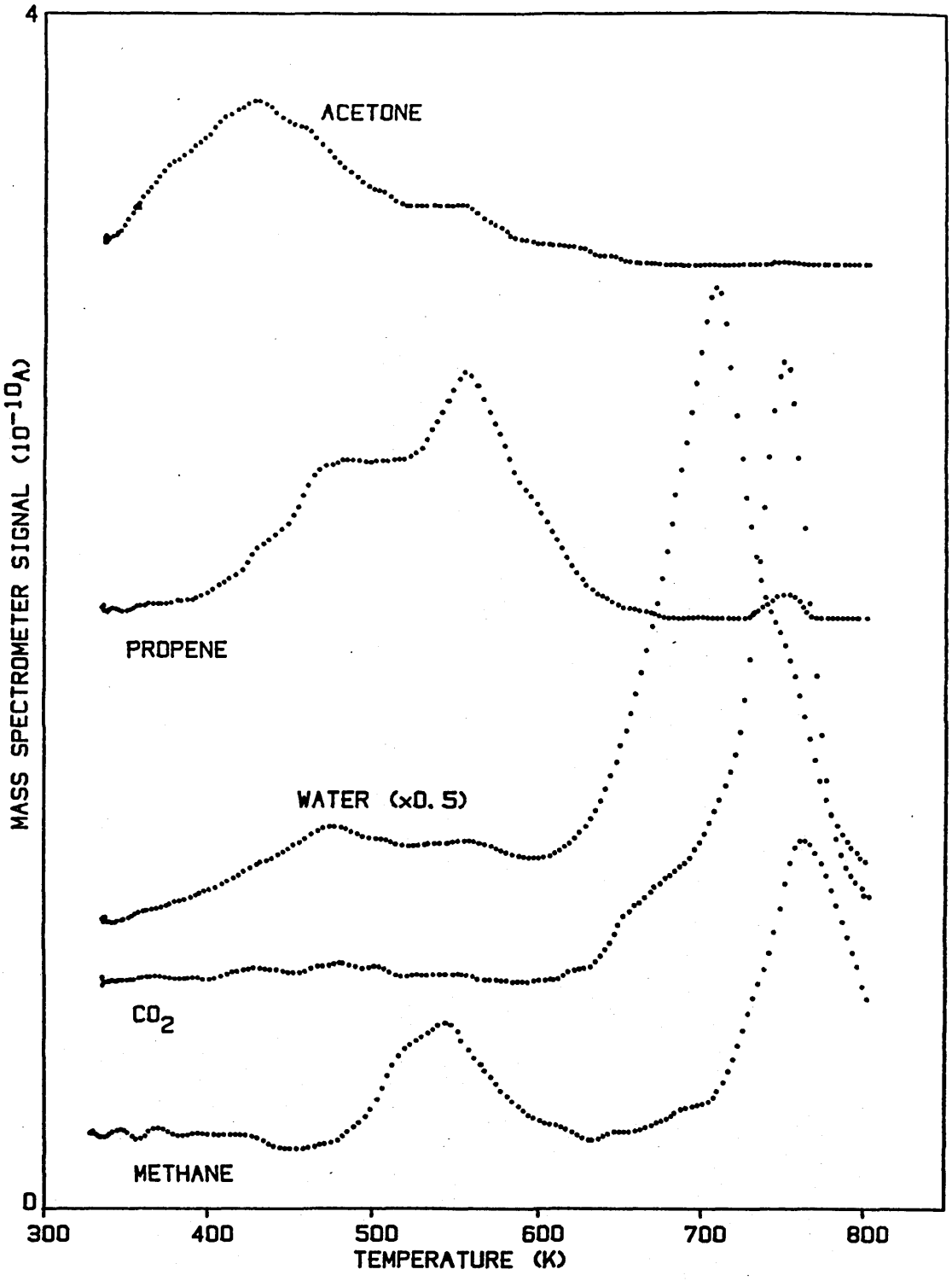

Figure 7.31: The desorption spectrum after acetone adsorption to saturation coverage at 340 K on zinc oxide.

Table 7.3: The desorption products, peak temperatures and saturation surface coverages following acetone adsorption at 340 K on zinc oxide.

desorption product	peak temperature (K, ±2)	surface coverage (10^{12} molec/cm^2)
acetone	428±7	41
propene	483	65
	555	100
CO_2	751	250
water	475	40
	554	~5
	709	250
hydrogen	742	158
methane	573,751	-

Water, hydrogen, methane and CO_2 were evolved at high temperature, indicative of the decomposition of a surface carboxylate. The decomposition temperature and composition of the desorption products were similar to those observed after 2-PrOH adsorption.

A further methane peak was formed at lower temperature at 573 K in a manner not previously observed with 2-PrOH.

(7.3.2) Coverage Dependence

In common with the behaviour of both 1-PrOH and 2-PrOH, the decomposition selectivity of acetone was found to be coverage dependent. Adsorption of acetone to a low initial surface coverage (approximately 40% of full surface saturation) gave the desorption spectrum of figure 7.32. As for 2-PrOH at low coverage, the decomposition was

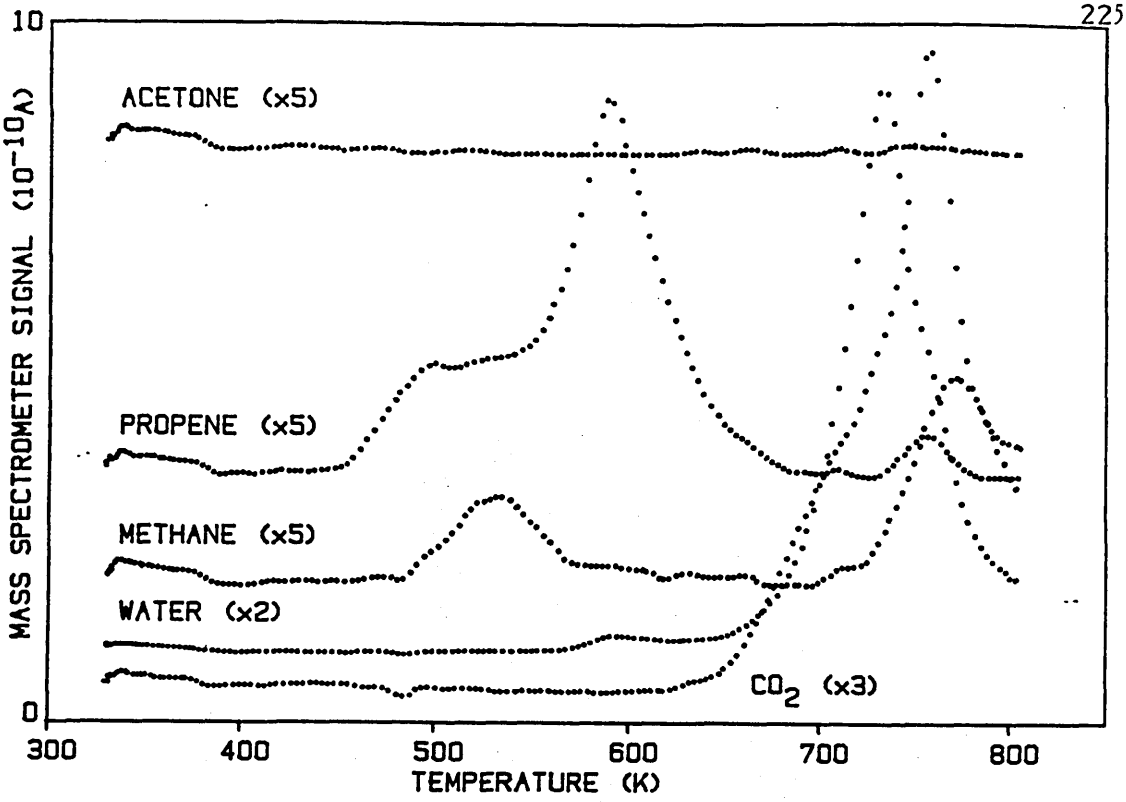

Figure 7.32: The desorption spectrum after acetone adsorption to low coverage at 340 K on zinc oxide.

selective toward dehydration and oxidation, with only propene, CO_2, methane and water produced. No acetone evolution was detected. Both propene peak temperatures were approximately 25 K and 35 K higher respectively than those obtained after saturation coverage (see table 7.3) and were close to the peak temperatures obtained for the α and β propene states after 2-PrOH adsorption. The CO_2 and water desorbed at temperatures similar to that obtained after a saturation acetone dose (756 K and 731 K respectively). A small amount of methane desorbed at approximately 531 K, with a further larger peak at 765 K associated with carboxylate decomposition.

(7.3.3) Low Maximum Heating Temperature

Two consecutive experiments were conducted where, after acetone adsorption at 340 K, the catalyst was heated to a lower maximum

temperature (633 K) so the carboxylate and hydroxyl surface species were not desorbed. The subsequent adsorption of acetone with these surface species present was found to give a desorption spectrum where neither the temperature nor the surface coverage of the main acetone desorption peak was changed compared to a spectrum obtained from a 'clean' surface. However, α propene desorption was suppressed consistent with the results obtained for 2-PrOH (section 7.1.4), while the β propene peak was also absent.

Following these two experiments, a further low temperature acetone adsorption, followed by heating to the full 800 K, resulted in evolution of acetone and CO_2 desorption peaks with surface coverages similar to those obtained after a normal low temperature adsorption of acetone on the 'clean' catalyst surface. A slightly greater water coverage was obtained, while no propene desorption was observed. The peak temperatures for acetone, CO_2, and in particular, for water, were lower than normal (393 K, 744 K and 678 K respectively). Similar effects have also been noted for the water desorption peak temperature after the equivalent experiments conducted with 2-PrOH.

(7.4) Discussion of Results

(7.4.1) Introduction

This chapter has presented, in some detail, results concerned with the decomposition behaviour of 2-PrOH and 1-PrOH on ZnO. Two important aspects require further consideration. Firstly, it is important to establish as far as possible the relationship between the TPD spectra and the catalyst structure, and secondly, to determine the significance of the TPD results in terms of a decomposition mechanism.

The ZnO catalyst used in this study possessed a well defined crystal structure that exposed both polar and non-polar surfaces. The observed TPD spectra from the decomposition of 1-PrOH and 2-PrOH would be expected to contain contributions from these various surfaces in a similar manner to that shown for water desorption (chapter 6). Inconsistancies between published schemes for alcohol decomposition on ZnO also make it also worthwhile to discuss the results in terms of a decomposition mechanism.

(7.4.2) 2-Propanol

(7.4.2.1) Crystal Face Dependence of the Decomposition Products

Assignments for the crystal face dependence of the 2-PrOH decomposition products have been made by consideration of the surface coverages, the interaction observed between coadsorbed 2-PrOH and water, and the effects of potassium promotion and chlorine treatment of ZnO on the TPD spectra (these results are presented in chapters 8 and 9).

2-PrOH and water coadsorption was found to give a larger high temperature water desorption peak which confirms this peak in the 2-PrOH decomposition spectrum to be due to desorption limited surface hydroxyl recombination from the α and β hydroxyl sites (and not to be related to a surface decomposition reaction). Furthermore, these experiments showed the α and γ propene states to be selectively displaced by adsorbed α hydroxyl species, while β propene, acetone and 2-PrOH peaks remained unaffected.

The interactions indicate clearly α propene to be produced from the same sites as the α hydroxyls i.e the Zn polar (0001) surface.

Consistent with this assignment, the saturation surface coverage of α propene was in good agreement with the coverage of α hydroxyls produced after water adsorption, and with the estimated number of exposed Zn cations on the Zn polar surface (see chapter 6). Less water was produced with α propene than β or γ propene, also consistent with the stronger water readsorption effects associated with this surface. Further evidence in confirmation of this assignment was given by the effects of potassium promotion and of chlorine treatment, which both caused a suppression of α propene formation. Described fully in chapter 8, chlorine will be shown to be a selective poison for the polar surfaces of ZnO.

The β propene peak is attributed to the non-polar $(10\bar{1}0)$ surface, since it remained unaffected by the presence of hydroxyls on the Zn polar surface during 2-PrOH and water coadsorption, suggesting a site independence to both the hydroxyls and to the α propene. Confirmation of the assignment was also given by the effect of chlorine treatment which was found not to effect β propene formation.

The assignment of the γ propene state is more uncertain. Although suppressed in a similar way to the α state by an increased hydroxyl coverage, it seems unlikely that two such different propene states could exist on the one surface. A comparison of the propene desorption spectrum to the temperatures obtained by Lui et al[114] for propene desorption from the (0001), $(50\bar{5}1)$ and $(000\bar{1})$ single crystal surfaces after 2-PrOH adsorption is given in figure 7.33. Although appearing to confirm the above assignments for α and β propene and to suggest that the γ state may have been produced on the $(000\bar{1})$ face, this comparison must be treated with caution. In the single crystal

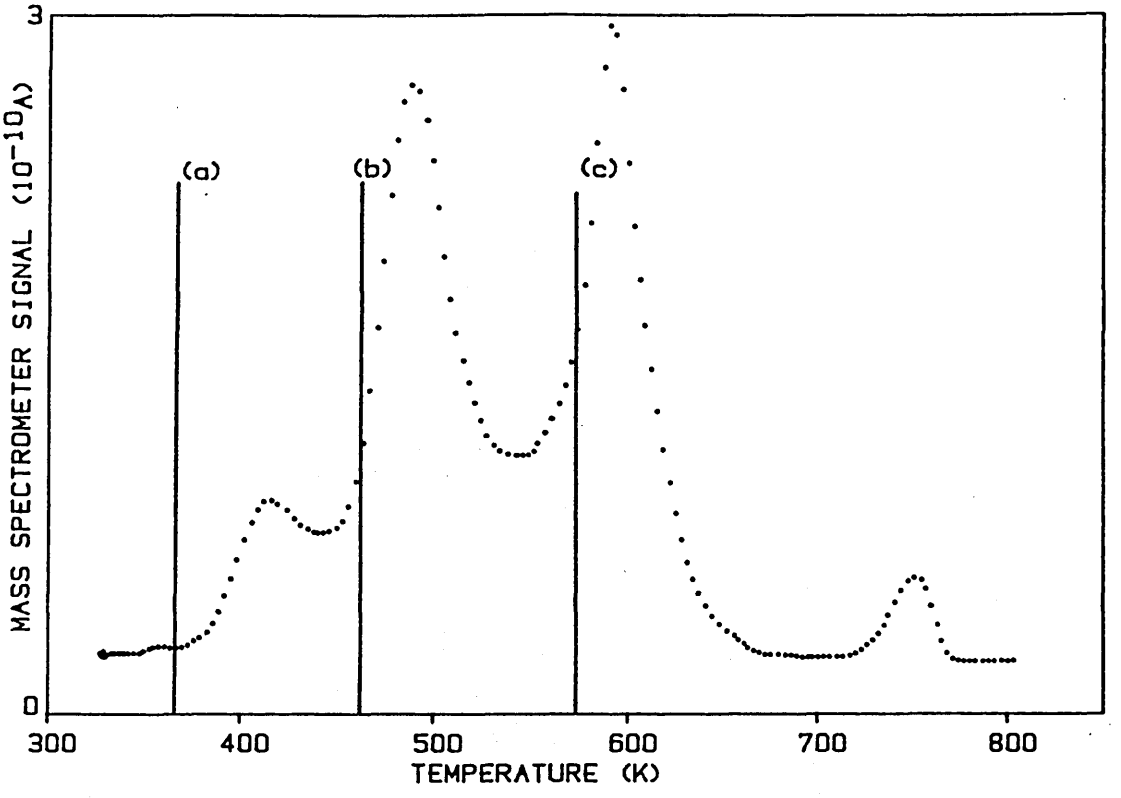

Figure 7.33: A comparison of the propene desorption spectrum after 2-propanol adsorption on zinc oxide to the propene peak temperatures found by Lui et al[114] on single crystal zinc oxide surfaces. (a)= $000\bar{1}$; (b)= $10\bar{1}0$; (c)= 0001

study[114] acetone was observed to desorb at the same temperature as propene for all three surfaces whereas in the present study only a trace of acetone was observed with the α propene. Nevertheless, since a small amount of acetone produced with γ propene would be impossible to detect, the single crystal work tended to support the view that the γ propene was produced at a defect site on the O polar surface.

The acetone and 2-PrOH peaks are both attributed to the non-polar ($10\bar{1}0$) surface, since these peaks also remained unaffected by the presence of the increased hydroxyl coverage on the Zn polar surface. The acetone peak, obtained after acetone adsorption, also exhibited behaviour that was characteristic of adsorption on the same surface; such an assignment for the acetone surface precursor is consistent with Nagai et al[116] who have shown acetone adsorption to require Zn-

O pair surface sites (as found on the non-polar surface). On the Zn polar surface such Zn-O ion pair sites can only form in association with surface defects (such as steps or Zn vacancies) that expose the subsurface lattice oxygen. The detection of the small amount of acetone at a similar temperature with α propene is then consistent with acetone being formed at defect sites on this face.

Carboxylate formation, although also significantly reduced by an increased hydroxyl presence, could not be entirely suppressed, making the crystal plane dependence of the oxidation surface sites less obvious. The reduction in the observed CO_2 evolution (approximately 50%) when 2-PrOH was coadsorbed with water is consistent with a possible association with the Zn polar surface. However, this may equally well be due to the effect of hydroxyl adsorption onto the β sites of the non-polar surface. In addition, the coverages are too high for both carboxylate and α propene precursors to be present on this single surface. Assuming a 65% fraction of non-polar surface and taking the density of Zn-O pairs on this surface to be 1.4×10^{15} cm^{-2} (115), then the carboxylate would occupy only approximately 33% of the available cation sites if it is formed solely on the non-polar surface. Similarly, β propene, acetone and 2-PrOH would occupy a further 35%, 8% and 9% of the surface respectively, to make a total of 85% of the cation sites occupied. This shows sufficient surface area to be available for carboxylate formation, as well as for the other product precursors, to be adsorbed to this surface. Accordingly, the carboxylate formation sites are assigned to be associated with the non-polar surface.

The next section, discussing the mechanism of 2-PrOH decomposit-

ion, will further demonstrate the oxidation mechanism of carboxylate formation to be closely associated with the dehydrogenation mechanism in a manner that requires the two products to be formed on the same sites. Although the similarity in coverage of β propene and carboxylate might also suggest a further possible reaction link, as chlorine treatment was found to suppress carboxylate but not β propene formation, the similar coverages must just be coincidental.

Evidence in the literature for this assignment for the carboxylate sites is given by several investigations of methanol decomposition on ZnO. Formation of the carboxylate can be considered analogous to the formate obtained in methanol decomposition/synthesis on ZnO. Although the work of Bowker et al[25] assigned the formate to the Zn polar surface, Edwards and Schrader[26] and Roberts and Griffin[27] have more recently shown that oxidation of methoxy to formate occurs in significant amount only on the non-polar surface (or Type II H_2 adsorption sites, see section 6.3.1), consistent with the assignment made for the carboxylate in the present study.

(7.4.2.2) Decomposition Mechanism on Zinc Oxide

Several mechanisms have been proposed for 2-PrOH decomposition on ZnO. Tamaru et al[106,107] and Manazec[37] have both proposed schemes that involve the reaction of a surface enolate species, while the mechanism of Bowker et al[108,115] is based on the sequential reaction of an adsorbed alkoxy species.

Bowker et al propose the initial reaction step to be the non-dissociative adsorption of the alcohol molecule through interaction of the lone pair electrons of the alcoholic oxygen with the ZnO surface:

$$(CH_3)_2CHOH_{(g)} \rightarrow (CH_3)_2CHOH_{(a)} \qquad [1]$$

The adsorbed alcohol then undergoes dissociation to form the surface alkoxy species according to:

$(CH_3)_2CHOH_{(a)} + O_{(s)} \rightarrow (CH_3)_2CHO_{(a)} + OH_{(a)}$ [2]

$(CH_3)_2CHOH_{(a)} + OH_{(a)} \rightarrow (CH_3)_2CHO_{(a)} + H_2O_{(g)} + V_o$ [3]

Bowker et al inferred step [3] from the lack of water desorption detected during temperature programming and by the reproducibility of their desorption spectrum. The water loss was inferred from this experimental reproducibility, although the dosing method used could not confirm this. This mechanism, producing a surface anion vacancy, V_o, applies to the fraction of the surface which subsequently produces propene. The acetone formation proceeds through a mechanism that does not evolve water from the surface, but produces hydrogen by recombination of dissociated hydrogen atoms:

$(CH_3)_2CHOH_{(a)} \rightarrow (CH_3)_2CHO_{(a)} + H_{(a)}$ [4]

$2H_{(a)} \rightarrow H_{2(g)}$ [5]

Steps [1]-[4] produce a surface populated by adsorbed alcohol and alkoxy species. Low temperature alcohol desorption occurs through recombination in the reverse of [4] or by the desorption of intact alcohol molecules in the reverse of [1]. The surface is then left covered with two types of adsorbed alkoxy species, depending whether they are produced by step [3] or by step [4]. Acetone is produced by the rate limited dehydrogenation at the α carbon atom of the alkoxys associated with the unperturbed sites (i.e produced by [4]) leaving a reactive hydride on the surface:

$(CH_3)_2CHO_{(a)} \rightarrow (CH_3)_2CO_{(g)} + H_{(a)}$ [6]

By surface diffusion the hydrides then attack the remaining alkoxy groups at the β hydrogen position to yield propene and hydrogen into

the gas phase:

$$(CH_3)_2CHO_{(a)} + V_o \rightarrow C_3H_{6(g)} + H_{(a)} + O_{(s)} \quad [7]$$

$$2H_{(a)} \rightarrow H_{2(g)} \quad [8]$$

The similarity between acetone and propene desorption temperatures, and the order of their desorption in the TPD results of Bowker et al was consistent with this two step mechanism.

Using IR spectroscopy, Tamaru et al[106,107] identified the formation of alkoxy species after adsorption of 2-PrOH on ZnO at room temperature. When the adsorbed alkoxy was heated to 363 K, IR bands corresponding to adsorbed enol species were also identified, with simultaneous hydrogen liberation into the gas phase. Isotopic labelling clearly showed the hydrogen to be produced by recombination of dissociatively adsorbed hydrogen and the α hydrogen of the alkoxy. Desorption of acetone was also found but only when 2-PrOH was present in the gas phase, suggesting that the adsorbed enol species, formed by decomposition of the alkoxy, were replaced by gaseous 2-PrOH to form acetone. On the basis of these observations, Tamaru et al[106,107] propose the following mechanism for 2-PrOH decomposition on ZnO:

$$(CH_3)_2CHOH_{(g)} \rightarrow (CH_3)_2CHO_{(a)} + H_{(a)} \quad [9]$$

$$(CH_3)_2CHO_{(a)} \rightarrow H_3C(CH_3)C(O_{(a)}) \rightleftarrows H_2C=C(CH_3)OH_{(a)} \quad [10]$$

$$H_2C=C(CH_3)OH_{(a)} + (CH_3)_2CHOH_{(g)} \rightarrow CH_3CHO_{(g)} + (CH_3)_2CHO_{(a)} + H_{(a)} \quad [11]$$

As propene was only obtained as a minor decomposition product (10% selectivity), its formation has not been included in this reaction scheme. The buildup of an inactive surface species during the course of reaction was found to cause a decrease in activity. Although not identified this was suggested to be a polymerised species of acetone,

such as acetylacetone.

A similar interaction of gas phase alcohol molecules with adsorbed surface species is also proposed by Parrott et al[102] as a mechanism for acetaldehyde formation after ethanol adsorption on MgO. However, in this scheme, it is the adsorbed ethoxy, rather than the enol, that reacts with the gas molecules to form the dehydrogenation product (see section 2.4.6 for further details).

Parrott et al also propose the dehydration of ethanol to ethylene to occur by β hydrogen elimination from the adsorbed ethoxy species. Manazec[37] has, however, postulated a mechanism for secondary alcohol dehydration over basic metal oxide catalysts, such as ZnO, where an adsorbed enol is the intermediate species. In the Manazec mechanism, the alkoxy, formed by dissociative adsorption of 2-PrOH, is dehydrogenated by a transfer of a hydride from the α carbon to a nearby cation or hydroxyl group to generate a bound ketone:

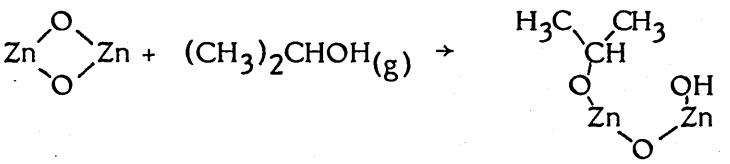

[12]

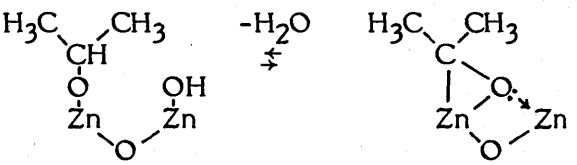

[13]

The resulting bound ketone is deprotonated from the β carbon to give the enolate species, which is reprotonated at the α carbon to liberate propene:

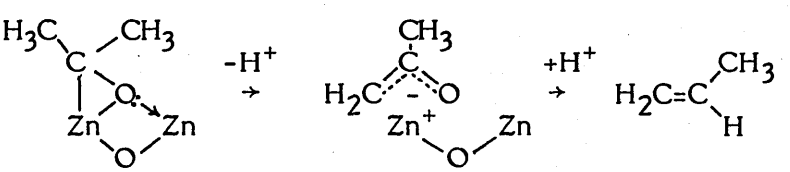

[14]

The formation of alkoxy species after adsorption of alcohols on the surface of metal oxide catalysts is well documented in the literature[100,103,109,110], including 2-PrOH adsorption on ZnO, for example, as found by Tamaru et al[106,107] (described above). It seems clear, then, formation of alkoxy species occurred as the initial step in the dissociative adsorption of 2-PrOH on ZnO in the present study. However, the weak surface coordination of the lone pair electrons of the alcoholic oxygen, such as proposed by Bowker et al[108,115], forming the molecularly adsorbed alcohol, is likely to have been the first step of the adsorption process:

$$(CH_3)_2CHOH_{(g)} \rightarrow (CH_3)_2CHOH_{(a)} \qquad [15]$$

The 376 K and 421 K temperatures found for the reversible desorption peaks are similar to those reported for methanol[25,95] and ethanol [97,99] desorption from ZnO surfaces suggesting a similar mode (and strength) of surface interaction that is consistent with a common molecularly adsorbed form as given in [15]. Recombination of alkoxy and adsorbed hydrogen (the reverse of [16] below) leading to 2-PrOH desorption, however, is also a possibility that cannot be ruled out, especially for the higher temperature α 2-PrOH peak.

Alkoxy formation is proposed as follows:

$$(CH_3)_2CHOH_{(a)} + O_{(s)} \rightarrow (CH_3)_2CHO_{(a)} + OH_{(a)} \qquad [16]$$

The simultaneous desorption of water (accompanied by formation of an anion vacancy) as suggested by Bowker et al[108,115] (given in reaction [3] above) was not specifically investigated. However, it seems unlikely to occur since the results from this study found water to be evolved during TPD (Bowker et al did not). Although less water than propene was in fact evolved, hydroxyl consumption as a result of carboxylate formation can account for the deficit (see below).

Repetition of 2-PrOH adsorption on the ICI low surface area ZnO (the same as used by Bowker et al[108,115], see chapter 8) found an excess of water compared to propene to be evolved in subsequent thermal desorption, suggesting the apparent absence of water desorption reported by these workers may have simply been due to a lack of equipment sensitivity.

An important test for the formation of the enolate species (as found by Tamaru et al[106,107]) was to compare the temperatures of acetone formation in the desorption spectra after both acetone and 2-PrOH adsorption. The temperature of the acetone desorption peak after acetone adsorption was 10-20 K lower than for acetone formed after alcohol adsorption showing the 2-PrOH derived acetone peak to be reaction limited. In addition, the desorption of hydrogen coincident with acetone, and the constant acetone peak temperature with varying catalyst sample mass, were both indicative of its formation being due to the kinetically limited, rather than the desorption limited, evolution of a surface species. However, the presence of a common intermediate reaction structure, that may have been the enol, in the decomposition pathways of both acetone and of 2-PrOH was suggested by the similarities in their respective desorption spectra. This is discussed further below.

Acetone is proposed to be formed by the reaction limited decomposition of the isopropoxy species through abstraction of the α hydrogen, as in the mechanism of Bowker et al[115]:

$$(CH_3)_2CHO_{(a)} \rightarrow (CH_3)_2CO_{(a)} + H_{(a)} \qquad [17]$$

$$(CH_3)_2CO_{(a)} \rightarrow (CH_3)_2CO_{(g)} \qquad [18]$$

$$2H_{(a)} \rightarrow H_{2(g)} \qquad [19]$$

Reaction [17] was the limiting step since hydrogen appeared coincident with acetone. The possibility that the small amount of hydrogen which appeared just before acetone arose from recombination of hydrides produced by reaction [16] cannot be ruled out. The source of the third hydrogen peak at 478 K, at a similar temperature to β propene, is discussed below. The short lived intermediate species formed by reaction [17] is possibly of the enol-type structure, although without a direct method of identification of the structure of the adsorbed intermediates (for example, through the use of IR spectroscopy), this can only be a speculative conclusion. The involvement of the enol structure was further suggested by the similar decomposition behaviour of acetone and 2-PrOH.

The formation of water at the same temperature as acetone suggests that limited side reaction of the adsorbed hydrogen also occurs with surface hydroxyl species. An increase in water desorption coincident with acetone after 2-PrOH and water coadsorption suggests that the hydroxyls in [20] below may be derived from the water impurity present in the injected alcohol.

$$H_{(a)} + OH_{(a)} \rightarrow H_2O_{(g)} \qquad [20]$$

The quantity of hydrogen liberated with acetone was too large to be accounted for simply by the dehydrogenation reaction only. This showed that an additional surface reaction, that also evolved hydrogen, must have also occurred at this temperature. IR studies in the literature have identified the formation of surface carboxylate bands in the temperature region of 440-470 K after alcohol adsorption on metal oxides[97,103,111-113], and in particular, after 2-PrOH adsorption on ZnO[109]. This is close to the temperature at which the hydrogen and acetone were evolved in the present study. The evolution

of hydrogen in carboxylate formation has been reported by Kagel et al[103] for 1-PrOH on alumina, although Kagel[112] has also found methane to be evolved from 2-PrOH in an equivalent oxidation process (this is considered further below).

It seems likely then that formation of carboxylate occurred at the similar temperature as acetone formation, and was responsible for the large evolution of hydrogen observed. The coincidence of acetone and carboxylate formation further suggests a common reaction pathway existed for the two products. This 'link' was more firmly established by the effects of potassium promotion (chapter 9) and of chlorine treatment (chapter 8) of ZnO, and by the behaviour of 1-PrOH (see the following section), that demonstrated that a reduction in the extent of oxidation, through an effective lowering in the availability of surface oxygen to form the carboxylate, resulted in an increase in the quantity of acetone formed (see chapters 8 and 9). Such a common reaction pathway for dehydrogenation and oxidation has been shown by Miyata et al[109], where IR spectroscopy identified the carboxylate to be formed via the enol after both acetone and 2-PrOH adsorption on ZnO.

In the literature several proposals have been made for the reactive oxygen source in oxidation processes on ZnO. Recent papers by Tarawah et al[94], Roberts et al[27] and Akhter et al[85] propose CO_2, produced after methanol adsorption/decomposition on ZnO, involves surface reduction of lattice oxygen, while the work of Kagel[100,103] proposes the carboxylate to form by reaction of alkoxy with the associated surface hydroxyl formed in the initial dissociation of the alcohol. Nakajima et al[119] have proposed a similar mechanism for

propene oxidation over ZnO, where adsorbed oxygen anneals the surface vacancies created by carboxylate formation. Although the long term stability of the ZnO toward 2-PrOH decomposition indicated the net surface reduction to be low, the results also found the overall water to propene ratio to be less than predicted by the reaction stoichiometry. This pointed toward a consumption of hydroxyl species in annealing oxygen vacancies produced through carboxylate formation.

The mechanism for formation of the carboxylate is proposed to be as follows:

$$(CH_3)_2CHO_{(a)} \rightarrow (CH_3)_2CO_{(a)} + H_{(a)} \quad [21]$$

$$(CH_3)_2CO_{(a)} + O_{(s)} \rightarrow C_2H_6COO_{(a)} + V_o \quad [22]$$

$$(CH_3)_2CO_{(a)} + OH_{(a)} \rightarrow C_2H_6COO_{(a)} + H_{(a)} + V_o \quad [23]$$

$$2H_{(a)} \rightarrow H_2(g) \quad [24]$$

The stoichiometry of the carboxylate could not be determined from the results so its structure has been left indeterminant. The desorption of higher molecular weight compounds (for example, mass 41) points toward a possible structural rearrangement of the methyl groups. Although formation of the acetate (as proposed by Deo et al[112] from 2-PrOH) was possible, since no methane was evolved in the temperature region of carboxylate formation, it shows that only α hydrogen abstraction took place (consistent with the common reaction 'link' with the dehydrogenation process).

Reaction [21] is common to both acetone and carboxylate formation. The selectivity for the subsequent reactions is proposed to be dependent on the availability of an oxygen source; if $OH_{(a)}$ or $O_{(s)}$ is present then the oxidation is favoured, and if not, then dehydrogenation is the preferred pathway. In both cases the oxygen is derived from the lattice since an increased water-derived hydroxyl coverage

was found to decrease carboxylate formation. This will be considered further in section 7.4.3 and chapters 8 and 9.

The anion vacancy is shown to be produced at the stage of carboxylate formation since the vacancy annealing process associated with propene formation as given below, requires the anion vacancies to be formed at low temperature, rather than on CO_2 evolution at high temperature. Previously Gopel et al[69] have shown vacancies to be formed both at low temperature in CO oxidation on ZnO.

After acetone adsorption, no equivalent α hydrogen is available for carboxylate formation as described above. A more direct reaction with surface hydroxyls may have occurred to form the carboxylate in this case (as proposed by Deo et al[112] and Sheppard et al[113]) :

$$(CH_3)_2CO_{(a)} + OH_{(a)} \rightarrow CH_3COO_{(a)} + CH_{4(g)} \quad [25]$$

The higher temperature found for methane release (575 K), compared to that of hydrogen in 2-PrOH carboxylate formation (447 K), is consistent with the greater energy required for C-C bond cleavage compared to C-H cleavage in acetone derived carboxylate formation. As noted above, since an increase in the water derived hydroxyl coverage did not also increase carboxylate formation, the possibility exists that oxidation occurs via a different pathway. The similarity between the temperatures of methane and propene evolution after acetone adsorption also suggests a polymerisation process as an alternative oxidation route:

$$2(CH_3)_2CO_{(a)} \rightarrow CH_3COO_{(a)} + CH_2{=}CHCH_{3(g)} + CH_{4(g)} \quad [26]$$

The formation of polymerised acetone species on ZnO has been reported by Tamaru et al[106,107].

The similarity between the carboxylate decomposition products

(CO_2, hydrogen and methane) and their evolution temperatures from both 2-PrOH and acetone suggests a similarity in stoichiometry of the carboxylate species. However, since no methane was evolved during the oxidation of the alkoxy species, the carboxylate produced from 2-PrOH must have been more 'saturated' with methyl groups than the equivalent acetone derived carboxylate. Athough no calibration factor was available for methane desorption, a comparison of the CO_2 to methane peak area ratios shows almost twice as much methane to be evolved from 2-PrOH carboxylate decomposition as from the acetone carboxylate consistent with this proposal.

A generalised mechanism for the carboxylate decomposition reaction is given as follows (after Davydov et al[118] and Miyata et al[109]):

$$R\text{-}COO_{(a)} \rightarrow CO_2 + H_2 + CH_4 \qquad [27]$$

where R= $(CH_3)_x$, x=1 for acetone and x>1 for 2-PrOH.

The dehydration reaction is proposed to occur by β hydrogen elimination from the alkoxy species, releasing propene into the gas phase and forming an adsorbed hydroxyl group:

$$(CH_3)_2CHOH_{(a)} + O_{(s)} \rightarrow (CH_3)_2CHO_{(a)} + OH_{(a)} \qquad [28]$$

$$(CH_3)_2CHO_{(a)} \rightarrow CH_2{=}CHCH_{3(g)} + OH_{(a)} \qquad [29]$$

There are two possible fates for the hydroxyl species formed. It can either undergo a recombination to produce water:

$$2OH_{(a)} \rightarrow H_2O_{(g)} + O_{(s)} \qquad [30]$$

or it can react with an lattice oxygen vacancy to produce hydrogen and anneal the defect:

$$OH_{(a)} + V_o \rightarrow H_{2(g)} + O_{(s)} \qquad [31]$$

For α propene, shown in the previous section to be associated with the

Zn polar surface, dehydration yielded propene and water almost exclusively, with step [30] not occurring until high temperature due to the strong dehydrating properties of this surface. For β propene, associated with the non-polar surface, both water and hydrogen were produced at a similar temperature to the propene (although hydrogen formation was the minor route). The presence of the larger relative quantity of water is consistent with the weaker adsorption of water on this surface, while the presence of hydrogen is consistent with a significant density of defect sites formed by the oxidation reaction. The small hydrogen to propene ratio is a consequence of the presence of surface hydroxyls, derived from the water impurity in the injected alcohol, annealing most of the defects at the temperature of carboxylate formation according to reaction [31]. The presence of this water was shown by the large low temperature water peak produced from chlorine treated and potassium promoted ZnO (see chapters 8 and 9).

Although the result that propene was also produced following acetone adsorption lended support to a mechanism of the type proposed by Manazec for alcohol dehydration over metal oxides[37] i.e. involving the enol species as a reaction intermediate, this mechanism is unlikely since the initial step of Manazec's scheme (α hydrogen abstraction) would have resulted in the immediate formation of acetone, since the enol formed is unstable at the temperature observed for propene formation.

The requirement of propene formation needing an anion vacancy adjacent to the adsorbed alkoxy, as suggested by Bowker et al[108,115], cannot be correct since suppression of carboxylate formation, and hence anion vacancy formation, by potassium promotion and chlorine treatment (see chapters 8 and 9), did not correspondingly

suppress β propene evolution. (Although both α and γ propene were suppressed, this effect can be ascribed to site blockage- see chapters 8 and 9).

(7.4.3) 1-Propanol

(7.4.3.1) Crystal Face Dependence of the Decomposition Products

The crystal face dependence of the 1-PrOH decomposition products is established in a manner the same as used for 2-PrOH (described in the previous section) i.e on the basis of the information provided by 1-PrOH and water coadsorption, saturation surfaces coverages, and the effects of potassium promotion and chlorine treatment (to be described in chapters 8 and 9).

Compared to 2-PrOH, the face dependence of 1-PrOH decomposition appeared less well defined. An increased hydroxyl coverage after coadsorption of 1-PrOH and water was found to suppress the 481 K and 573 K propene peaks. Although, after the behaviour of 2-PrOH, this suggests both peaks to be associated with the polar crystal surfaces, the effect of chlorine treatment (see chapter 8) was to suppress only the 481 K peak, while only narrowing the 573 K peak width. In view of the very selective polar site poisoning effects of chlorine, this shows the main 573 K peak to be associated with the non-polar surface. Further, the narrowing effect shows this peak is comprised of at least two closely overlapping desorption states. The narrowing appeared to be due to a reduction in the desorption in the high temperature half of this peak, suggesting that this was a contribution from the Zn polar surface.

This result indicates only limited dehydration occurred on the Zn polar surface compared to 2-PrOH. However, since the high temperature water desorption associated with this surface remained limited after 1-PrOH only adsorption (to approximately 50-60 H_2O/cm^2), and did not increase to the maximum number of available cation sites (approximately $150x10^{12}$ cm^{-2}), it points to the other cation sites being occupied by another adsorbed surface species. At low 1-PrOH coverage essentially the only decomposition product produced was CO_2 derived from the carboxylate. Since the Zn polar surface has been shown by water and 2-PrOH to be the most active in decomposition and adsorption at low coverage, this implies that some oxidation to the carboxylate occurred on this surface, in preference to dehydration as shown by 2-PrOH. The formation of multiple hydrogen desorption peaks under conditions of low 1-PrOH coverage also shows possibly greater than one surface site may have been associated with carboxylate formation. This point is discussed further below.

The peak temperature of the 573 K propene was 86 K higher than the equivalent β propene produced from the non-polar surface after 2-PrOH adsorption. Such a temperature increase is consistent with the TPD results of Bowker et al[108,115] and Noller et al[146] who found the 1-PrOH decomposition products to be evolved at higher temperatures than the equivalent 2-PrOH products.

By analogy to 2-PrOH, and in line with the relative desorption temperatures of ZnO single crystal surfaces reported by Lui et al[114], the propene peak at 481 K is assigned to the O polar surface. The coverage in this peak was similar to that of the γ propene formed after 2-PrOH adsorption and also assigned to this surface.

1-PrOH decomposition was characterised by a very high selectivity toward oxidation to form the carboxylate. As noted above, although it appeared that oxidation occurred on the Zn polar surface, the total quantity of CO_2 desorbed was simply too great to be accounted for by the formation of carboxylate on this surface only. Although only a single CO_2 peak was obtained, compared to the peak evolved after 2-PrOH carboxylate decomposition, its width was significantly broader, indicative of a wider spread in surface adsorption strengths, and possibly the involvement of greater than one type of surface oxidation site. The water coadsorption results show a reduction in CO_2 desorption of approximately 80×10^{12} molecules/cm^2 accompanied by a decrease in the peak width on the high temperature edge. Both effects would be consistent with a loss of Zn polar sites to hydroxyl species. The remaining CO_2 coverage (345×10^{12} molecules/cm^2), associated with carboxylate formation on the non-polar surface, gives an approximate 75% coverage of the available cation sites on this surface. Possible reasons for the high oxidation selectivity exhibited by 1-PrOH are further considered in the following section describing the decomposition mechanism.

Assignment of the very low coverage propionaldehyde peak is more uncertain since this peak was almost completely suppressed by the coadsorption of water. In the previous section it has been shown for 2-PrOH that the dehydrogenation reaction is closely linked to the surface oxidation process and that common surface precursors, and therefore sites, exist for both. It seems likely then that propionaldehyde is also produced on the same surface as acetone from 2-PrOH, and as carboxylate from 1-PrOH. Chlorine treatment was found to increase propionaldehyde formation and to decrease carboxylate

formation consistent with this. Although some carboxylate appears to be formed on the Zn polar surface, the effect of chlorine treatement demonstrated the propionaldehyde precursor to be associated essentially with only the non-polar surface.

Coadsorbed water was found not to cause a reduction in the quantity of reversible 1-PrOH desorption which also suggests an association with the non-polar surface. The relatively high coverage of 1-PrOH would then give a 35% coverage of this plane, which when combined with the 75% carboxylate coverage already assigned to this surface, yields a figure of greater than 100% cation site saturation. This 10% error in coverage is well within any errors associated with the estimation of the relative crystal surface distribution and with the calibration factors of the desorption products, showing that full saturation of this surface was achieved.

(7.4.3.2) Decomposition Mechanism on Zinc Oxide

Bowker et al[108] have proposed a decomposition mechanism for 1-PrOH on ZnO that is analogous to the mechanism described in the previous section for 2-PrOH on ZnO and consists of the same adsorption and reaction steps. Rather than repeat the comments made in describing the 2-PrOH mechanism, the previous section should be consulted for details. The reaction steps are also presented in section 2.4.7.

The previous section has presented a decomposition mechanism for 2-PrOH consistent with the TPD results obtained in this study. This section will present an equivalent mechanism for 1-PrOH decomposition containing the same reaction steps, with the apparent differences in the nature of the desorption spectra between the two alcohols explained on the basis of a different relative selectivity for α and β

hydrogen abstraction from the adsorbed alkoxy surface intermediate (see below).

A molecularly adsorbed form of the alcohol, through surface coordination the lone electrons of the alcoholic oxygen, is again proposed to be the initiating step:

$$CH_3CH_2CH_2OH_{(g)} \rightarrow CH_3CH_2CH_2OH_{(a)} \qquad [32]$$

The reverse of this step is likely to have produced the alcohol desorption peak observed at 405 K. Again the similarity of the peak temperature with that 2-PrOH, and with the desorption temperatures of other alcohols from ZnO[25,95,97,99], is evidence for this peak being the reverse of [32], rather than due to alkoxy recombination.

Alkoxy formation subsequently occurs at the adsorption temperature according to:

$$CH_3CH_2CH_2OH_{(a)} + O_{(s)} \rightarrow CH_3CH_2CH_2O_{(a)} + OH_{(a)} \qquad [33]$$

No evidence was again found for the desorption of water and the formation of vacancy sites at this stage as proposed by Bowker et al[108]. Given the high 1-PrOH selectivity toward carboxylate formation, and hence surface oxygen consumption, it seems improbable that lattice oxygen would also be lost at this stage without causing a rapid reduction of the ZnO surface. The reproducibility of the 1-PrOH desorption spectra also shows this not to be the case.

Although Miyata et al[147] have demonstrated the formation of an enol species after propionaldehyde adsorption on ZnO, on the basis of the behaviour shown by acetone and 2-PrOH described in the previous section, such an enol species would also not be expected to be a stable surface intermediate in 1-PrOH decomposition. Although the adsorption of propionaldehyde was not investigated in this study, the

coincident desorption of hydrogen with the propionaldehyde peak at 475 K points to a surface decomposition, rather than a simple enol desorption process. Propionaldehyde is proposed to form by the reaction limited decomposition of the alkoxy species through abstraction of α hydrogen:

$$CH_3CH_2CH_2O_{(a)} \rightarrow C_3H_6O_{(a)} + H_{(a)} \quad [34]$$

$$C_3H_6O_{(a)} \rightarrow CH_3CH_2CHO_{(g)} \quad [35]$$

$$2H_{(a)} \rightarrow H_{2(g)} \quad [36]$$

As for acetone formation, the intermediate $C_3H_6O_{(a)}$ structure may be of an enol structure[150]. However, this is again only speculative since the TPD results give no direct structural information of this nature. The formation of a small amount of water at 475 K points to the occurrence of limited reaction of adsorbed hydrogen with surface hydroxyls:

$$H_{(a)} + OH_{(a)} \rightarrow H_2O_{(g)} \quad [37]$$

Similar to 2-PrOH, the quantity of hydrogen evolved with the dehydrogenation product was far in excess of that predicted by the reaction [34] to [36] stoichiometry. This was particularly evident for 1-PrOH where the quantity of propionaldehyde produced was very low. As for 2-PrOH, the hydrogen desorption is proposed to be due to the oxidation reaction forming the carboxylate species:

$$CH_3CH_2CH_2O_{(a)} \rightarrow C_3H_6O_{(a)} + H_{(a)} \quad [38]$$

$$C_3H_6O_{(a)} + O_{(s)} \rightarrow C_2H_6COO_{(a)} + V_o \quad [39]$$

$$C_3H_6O_{(a)} + OH_{(a)} \rightarrow C_2H_6COO_{(a)} + H_{(a)} + V_o \quad [40]$$

$$2H_{(a)} \rightarrow H_{2(g)} \quad [41]$$

Again, as for carboxylate formed from 2-PrOH, the stoichiometry of the carboxylate could not be determined from the TPD results. However, since only hydrogen desorption was detected at 475 K, only α hydrogen

abstraction can have taken place, consistent with the mechanism of Deo et al[111]. Reaction [38] is common to both propionaldehyde and carboxylate formation, with the high oxidation selectivity exhibited by 1-PrOH showing reactions [39] and [40] to be the preferred reaction pathway over [35]; possible reasons for this are considered below.

Decomposition of the carboxylate occurred at high temperature releasing CO_2, hydrogen and water. Although no methane was evolved, some ethene desorption was detected, possibly due to the decomposition reaction:

$$CH_3CH_2COO_{(a)} \rightarrow CO_{2(g)} + H_{2(g)} + CH_2{=}CH_{2(g)} \quad [42]$$

The formation of the mass 29 desorption peak at 640 K appears to be related to a partial carboxylate decomposition process. This would explain the apparent lack of desorption of a larger hydrocarbon fragment coincident with CO_2 from carboxylate decomposition (methane was obtained for 2-PrOH carboxylate decomposition). The mass 29 mass spectrometer signal is characteristic of the aldehyde CHO mass fragment[98]. The detection of a small quantity of mass 44 with the mass 29 shows it likely that acetaldehyde was produced at this temperature in a reaction leaving a formate-like carboxylate structure that subsequently decomposes to yield hydrogen and CO_2 at the slightly higher temperature of 713 K.

Reactions [28] to [31] previously given for 2-PrOH dehydration are also presumably valid for 1-PrOH, with the formation of propene proceeding according to:

$$CH_3CH_2CH_2OH_{(a)} + O_{(s)} \rightarrow CH_3CH_2CH_2O_{(a)} + OH_{(a)} \quad [43]$$

$$CH_3CH_2CH_2O_{(a)} \rightarrow CH_2{=}CHCH_{3(g)} + OH_{(a)} \quad [44]$$

Again there are two reactions possible for the hydroxyl produced:

$$2OH_{(a)} \rightarrow H_2O_{(g)} + O_{(s)} \quad [45]$$

$$OH_{(a)} + V_o \rightarrow H_{2(g)} + O_{(s)} \quad [46]$$

The release of hydrogen with propene at 573 K according to reaction [46] appeared the more significant route, consistent with the larger consumption of $O_{(s)}$ in carboxylate formation that would produce a greater number of surface oxygen vacancies.

The different decomposition selectivity shown by the two alcohols can be related to differences in the relative rates of β hydrogen elimination, producing propene, compared to α hydrogen abstraction, producing the dehydrogenation and oxidation products. The high dehydration selectivity shown by 2-PrOH, particularly on the Zn polar surface, is proposed to be a consequence of the branched structure of this alcohol increasing the tendency for β hydrogen surface interaction, thereby increasing the activity for abstraction of this hydrogen. For the linear 1-PrOH structure, the rate of β abstraction would be lower since there are fewer equivalent β hydrogen atoms which may be further from the catalyst surface, favouring α hydrogen abstraction as the decomposition route. In addition, the 1-PrOH structure also presents two α hydrogens, compared to the single hydrogen available with 2-PrOH, further increasing the likelihood of α hydrogen abstraction.

CHAPTER 8

EFFECT OF CHLORINE TREATMENT

(8.1) Decomposition on Zinc Oxide Treated with Chlorine

The desorption spectra for 2-PrOH and 1-PrOH presented in the previous chapter differed significantly to those previously reported by Bowker et al[108,115]. Repetition of 2-PrOH and 1-PrOH adsorption using the same ZnO as studied by Bowker et al (ICI low surface area ZnO) found these differences to be reproducible on the apparatus used in this study, with the desorption spectra obtained for both alcohols (to be fully described in section 8.2) almost identical to those of Bowker et al. Although in the case of 2-PrOH, the presence of surface hydroxyls could partially account for some of the spectral differences (see sections 7.1.3 and 7.1.4), the TPD behaviour of ICI low surface area ZnO was not changed by full dehydroxylation before alcohol adsorption (see section 8.2).

XPS measurements were made to determine if the spectral differences were the result to surface contaminants present on the ICI low surface area ZnO (described in Appendix 4). These measurements revealed a high level of chlorine present on the surface of ICI low surface area ZnO. This prompted the investigation of the effect of chlorine pretreatment of ZnO on the adsorption and decomposition of 1-PrOH and 2-PrOH, the results of which are described in this chapter.

Chlorine treatment was carried out by dosing a dehydroxylated ZnO sample at room temperature, positioned in-situ in the reactor, with approximately 1 ml of chlorine gas by injection into the carrier gas flow through a septum. The treated catalyst was then heated to 800 K

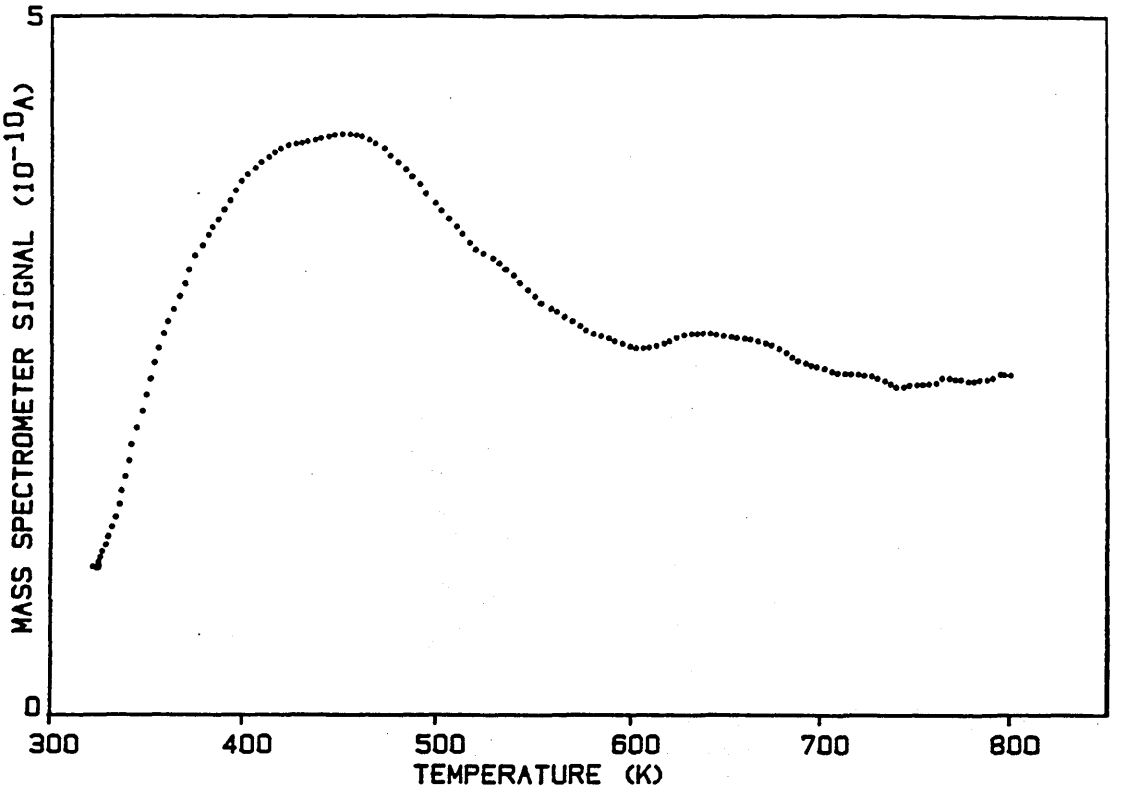

Figure 8.1: The water desorption spectrum after adsorption at 340 K to saturation coverage on chlorine treated zinc oxide.

at 39 K/min before alcohol adsorption was carried out.

(8.1.1) Water

The desorption spectrum of water obtained after adsorption at 320 K to saturation coverage on the chlorine treated ZnO is given in figure 8.1 above. Comparison to the spectrum from untreated ZnO (figure 6.1) showed the presence of chlorine to have caused a reduction water desorption in the high temperature region from the α and β sites previously assigned to adsorption sites on the Zn (0001) and prism surfaces of ZnO (section 6.4). The main water desorption occurred at lower temperature to form a broad desorption peak at 450 K, with a minor peak at 641 K also present. The saturation surface coverage of water was determined to be 411×10^{12} H_2O/cm^2.

(8.1.2) 2-Propanol

The desorption spectrum obtained after the saturation dose of 2-PrOH at 320 K onto chlorine treated ZnO catalyst is shown in figure 8.2. The main desorption product peak temperatures and the surface coverages are summarised in table 8.1. The main effect of the chlorine treatment was to remove the α and γ propene states and to completely suppress any CO_2 desorption. The reduction in desorption of water in the high temperature region was consistent with the result for water adsorption on the same catalyst. This desorption spectrum was close to that found by Bowker et al[115] after 2-PrOH adsorption on ICI low surface area ZnO (see section 8.2), with the exception of the water desorption profile which these workers did not detect.

A comparison of the peak temperatures and surface coverages given in table 7.1, for untreated ZnO, to those of table 8.1, for chlorine treated catalyst showed the following points. Both 2-PrOH and acetone coverages were increased by chlorine adsorption, as were their desorption peak temperatures, with the acetone peak showing a 77 K increase compared to the untreated ZnO peak temperature. Hydrogen desorbed in a peak slightly above the acetone peak temperature and in an underlying broad desorption structure. The quantity of hydrogen in the peak was estimated to be slightly less than the amount of acetone formed, while the contribution in the unstructured desorption was estimated to be a further 120×10^{12} H_2/cm^2.

The surface coverage of the remaining β propene state was reduced from 160 to 122×10^{12} molecules/cm^2 and its peak temperature increased from 487 K to 525 K. A water peak at a similar temperature to propene had an estimated propene to water ratio of 10:1.

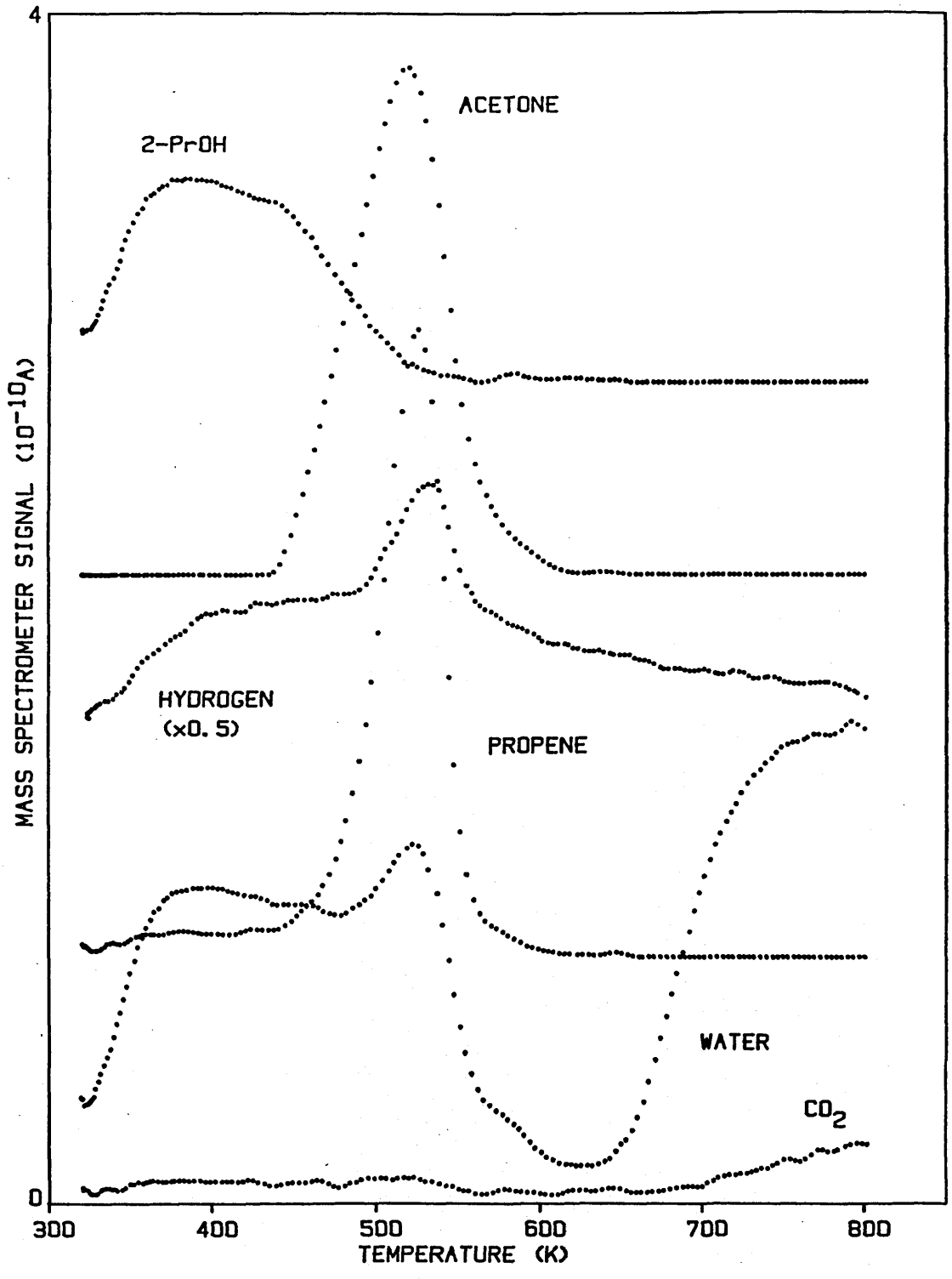

Figure 8.2: The desorption spectrum after adsorption of 2-propanol at 340 K to saturation coverage on chlorine treated zinc oxide.

Table 8.1: The desorption products, peak temperatures and saturation surface coverages following 2-propanol adsorption at 320 K onto chlorine treated zinc oxide.

desorption product		peak temperature (K, ±2)	surface coverage (10^{12}molec/cm^2)
2-propanol	β	385	85
	α	437	
acetone		518	62
propene	γ	-	0
	β	525	122
	α	-	0
CO_2		-	0
water		396	71
		461	11
		521	69
hydrogen		522	36

The complete removal of the CO_2 peak from the spectrum showed that oxidation to the carboxylate species was entirely suppressed by the presence of chlorine.

The total surface coverage, excluding the water desorbed, was found to be 269x10^{12} molecules/cm^2 compared to 570x10^{12} in the absence of chlorine.

(8.1.3) 1-Propanol

The desorption spectrum obtained after the saturation dose of 1-PrOH at 320 K onto chlorine treated ZnO is shown in figure 8.3. Table 8.2 details the main desorption peak temperatures and corresponding

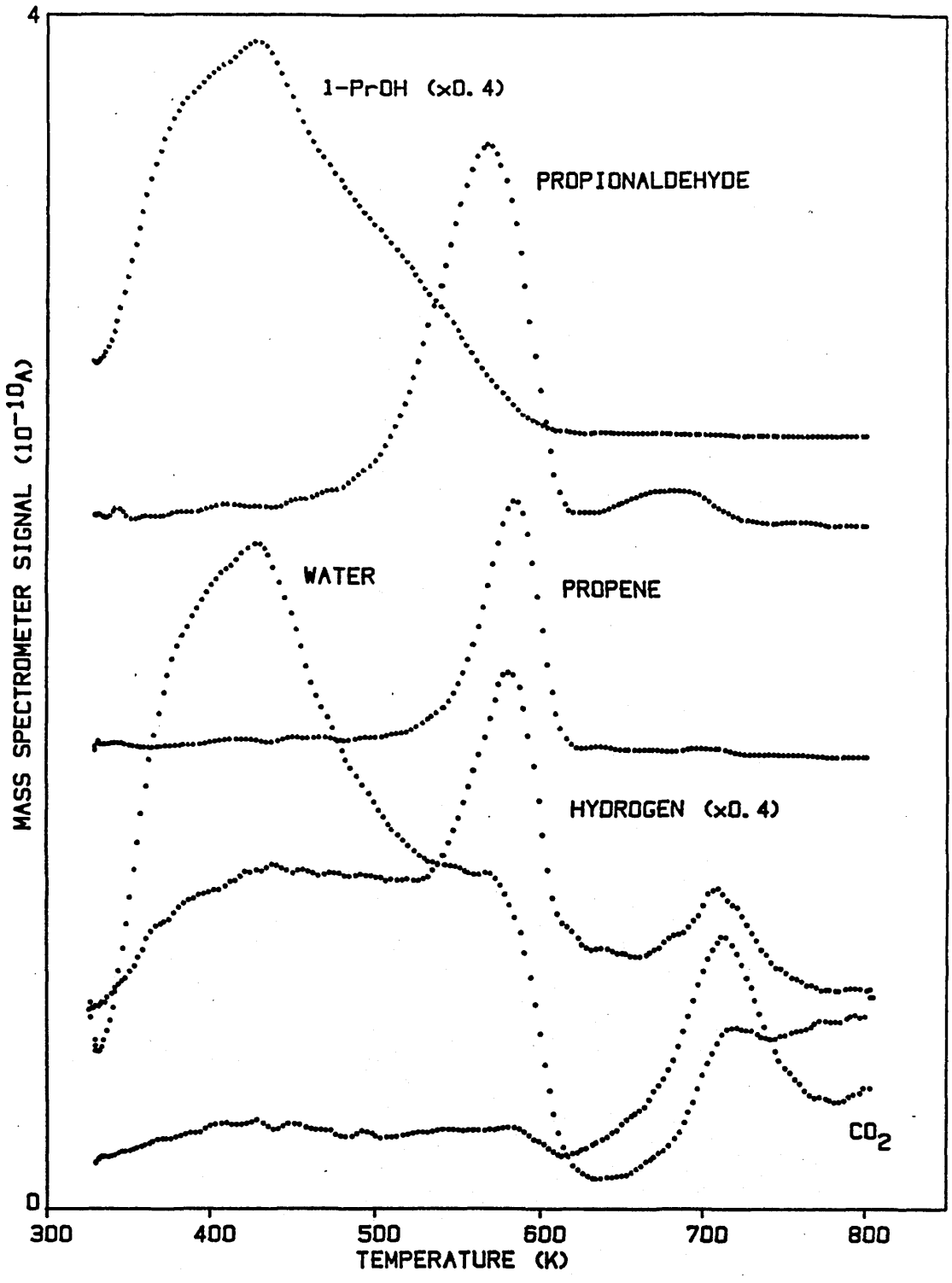

Figure 8.3: The desorption spectrum after adsorption of 1-propanol at 340 K to saturation coverage on chlorine treated zinc oxide.

Table 8.2: The desorption products, peak temperatures and saturation surface coverages following 1-propanol adsorption at 320 K onto chlorine treated zinc oxide.

desorption product	peak temperature (K, ±2)	surface coverage (10^{12}molec/cm^2)
1-propanol	428	283
propionaldehyde	566	59
propene	583	52
mass 29	697	-
CO_2	722	42
water	427	174
	570	10
	718	29
hydrogen	579	75
	708	26

surface coverages. The chlorine treatment caused a large reduction in the CO_2, evidence of a lower carboxylate coverage, although the suppression was not as complete as found for 2-PrOH.

Propene desorption at 583 K was also reduced, with the peak width narrowed compared to propene formed after 1-PrOH adsorption on untreated ZnO. Propionaldehyde formation at 566 K was dramatically enhanced by the chlorine treatment. The treatment also resulted in an increase in reversible 1-PrOH desorption at 428 K. The quantity of the mass 29 desorption product (identified in chapter 7 as being possibly acetaldehyde) was significantly reduced.

Hydrogen was evolved in a broad peak structure roughly coincident with 1-PrOH, while an overlying peak at 570 K similar in temperature

to the propionaldehyde and propene peaks was detected. The hydrogen coverage associated this peak was estimated to be slightly in excess of the propionaldehyde formed.

Water desorbed in a large peak coincident with 1-PrOH and in a further small peak at 579 K in the region of propionaldehyde and propene formation. The estimated propene to water ratio in this small peak was 5:1. Further water desorption occurred at high temperature with a small peak at 708 K.

The total surface coverage was approximately 415×10^{12} molecules /cm^2 compared to the coverage of 686×10^{12} molecules/cm^2 obtained after 1-PrOH adsorption on untreated ZnO.

(8.2) ICI Low Surface Area Zinc Oxide

(8.2.1) Water

(8.2.1.1) Thermal Desorption Spectrum

The thermal desorption spectrum obtained after water adsorption to saturation coverage at 340 K on the ICI low surface area ZnO is given in figure 8.4. Two main water desorption peaks were obtained from a 'fresh' catalyst sample; a large, broad peak at approximately 468 K and a smaller peak at 688 K. The presence of this high temperature peak was dependent on the extent of use of the catalyst since after several desorption experiments it was found to reduce and eventually disappear from the spectrum (as shown in figure 8.4). The lower temperature peak coverage did not appear to change, although the peak temperature was found to decrease slightly with use. The water desorption spectrum from a used catalyst corresponded closely to that obtained from the chlorine treated ZnO described in section 8.1.1.

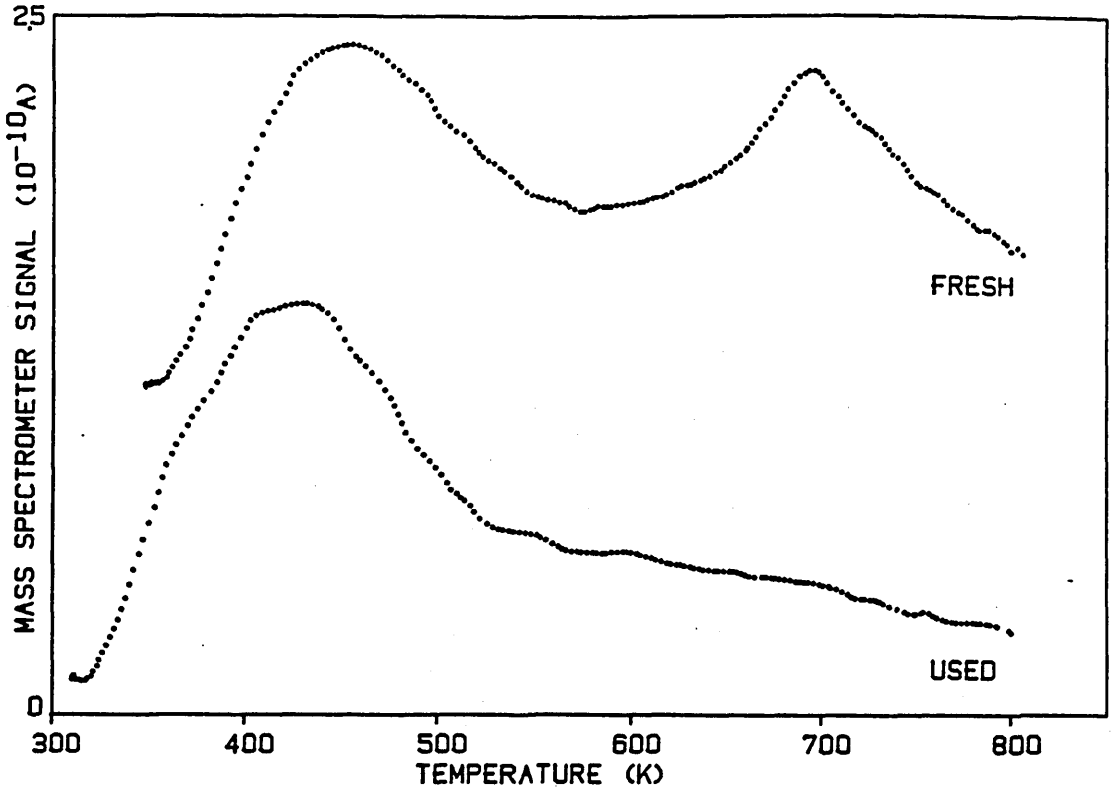

Figure 8.4: The water desorption spectrum after adsorption at 340 K to saturation coverage on ICI low surface area zinc oxide.

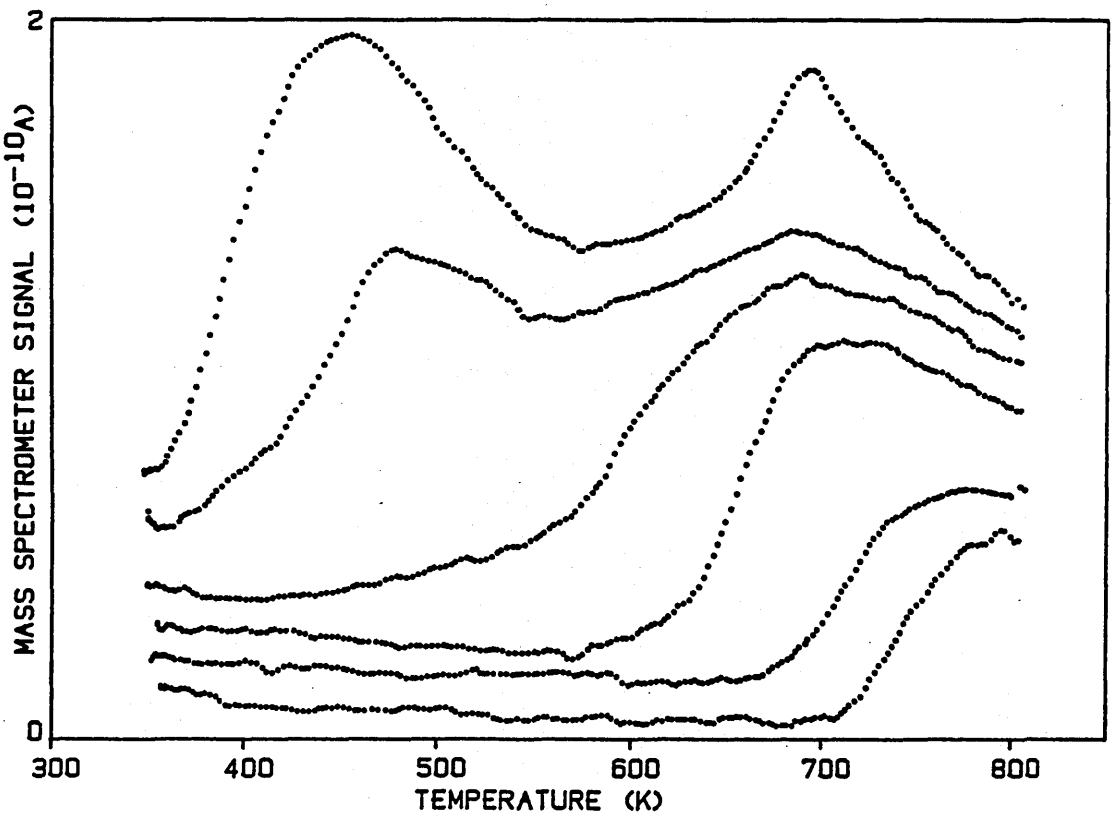

Figure 8.5: The coverage dependence of the water desorption spectrum after adsorption at 340 K on ICI low surface area zinc oxide.

The saturation water coverage (obtained by water pulse injection) on a fresh catalyst sample was determined to be 382×10^{12} H_2O/cm^2 in good agreement with the result obtained for chlorine treated ZnO (section 6.1.1). If saturation was made by subjecting the catalyst to a water saturated He flow for several minutes, a slightly higher coverage of 473×10^{12} H_2O/cm^2 was obtained due to increased coverage in the lower temperature peak. A further slow uptake of water was also noticeable in this state over a longer time period. For example, a pretreated catalyst sample left exposed to the air for two weeks was found to give approximately 3x the coverage in the 468 K peak compared to that obtained after water injection.

Bowker et al[25] studying the same ZnO catalyst were unable to detect any water desorption after exposure of the catalyst to water vapour. This may have been a consequence of poor detection sensitivity in their TPD system.

The coverage dependency of the water desorption is given in figure 8.5. A consistent coverage variation plot was difficult to obtain due to the catalyst aging effect described above which made the spectra less reproducible. The spectra show similar trends to those described earlier for the untreated ZnO (section 6.1.1) i.e. population of the high temperature desorption states occurred first.

(8.2.1.2) Determination of the Heat of Adsorption

The heat of adsorption for the main desorption peak at 468 K was determined in two ways;

(i) the heating rate variation method[24]

(ii) the amplitude variation method[24].

Difficulties were encountered due to the slight peak temperature shift that occurred with 'aging' of the catalyst as described above. This problem was overcome by not heating the catalyst to temperatures above 573 K, with reproducible peak temperatures then obtained for the lower temperature desorption peak, although this precluded determination of the adsorption energy for the high temperature state. Heating rates in the range 14 to 86 K/min were used, with figure 8.6 summarising the resulting shifts in peak temperatures. The linear best fit line to the plot gave a heat of adsorption of 72±10 kJ/mol.

An independent check of this result was made using the peak amplitude information also available at the different heating rates[24]. A plot of peak amplitude against inverse peak temperature (figure 8.7) determined the heat of adsorption to be 88±10 kJ/mol. Within experimental error bounds this result was in agreement with the figure obtained by the heating rate variation method.

(8.2.2) 2-Propanol

(8.2.2.1) Thermal Desorption and Decomposition Spectrum

The desorption spectrum obtained after a saturation dose of 2-PrOH at 340 K onto ICI low surface area ZnO is shown by figure 8.8. The corresponding peak temperatures and surface coverages are given in table 8.3. This spectrum was similar to that previously obtained by Bowker et al[115] after 2-PrOH adsorption on the same ZnO (but again with the exception of the water desorption profile). It was also similar to the spectrum from chlorine treated ZnO described in section 8.1.2 (figure 8.3), with only slight differences in peak temperatures and surface coverages between the two ZnO samples.

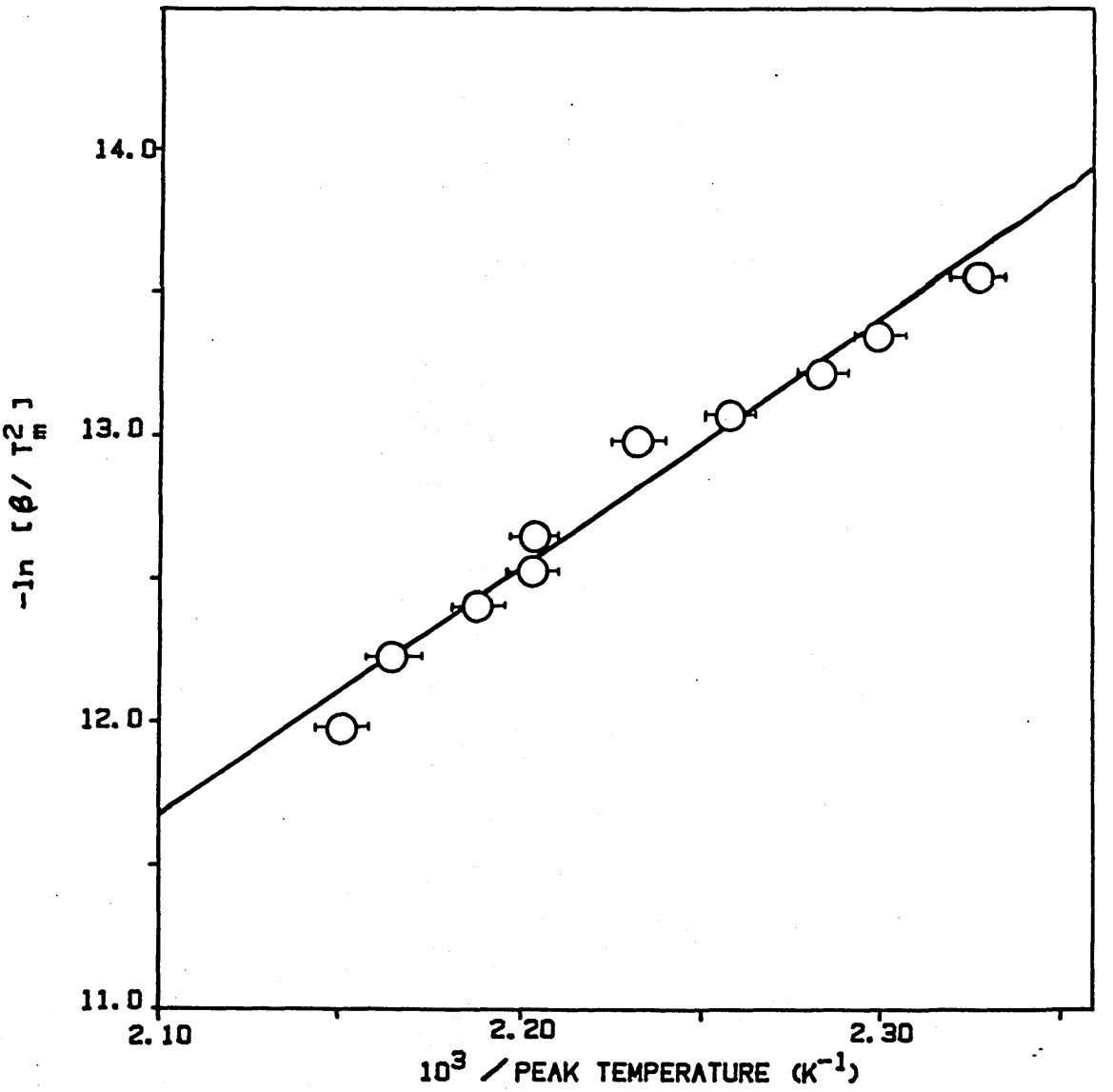

Figure 8.6: Characteristic plot of ln (β/T_m^2) against $1/T_m$ for water desorption from ICI low surface area zinc oxide.

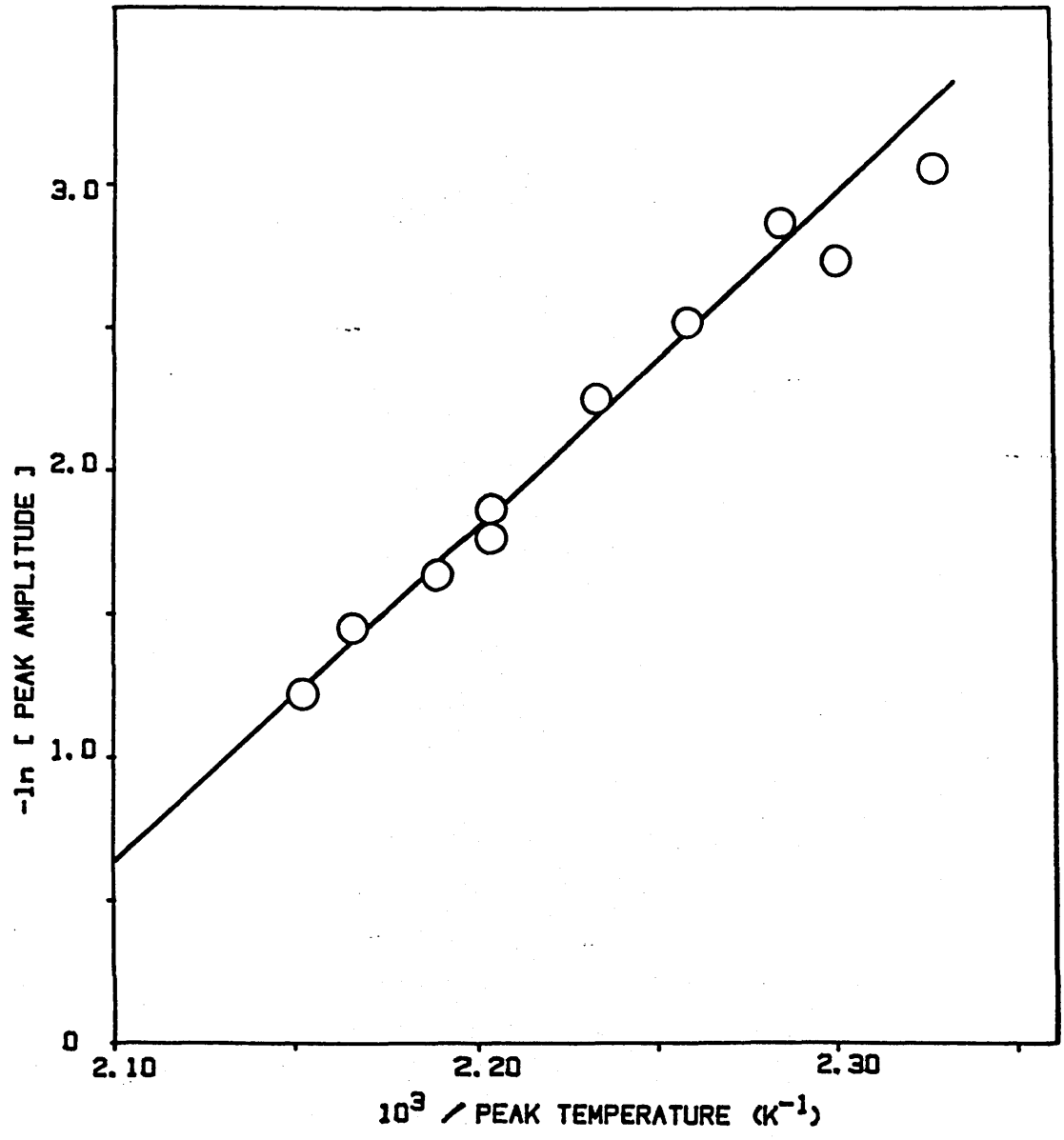

Figure 8.7: Characteristic plot of ln (peak amplitude) against $1/T_m$ for water desorption from ICI low surface area zinc oxide.

Table 8.3: The desorption products, peak temperatures and saturation surface coverages following 2-propanol adsorption at 340 K on ICI low surface area zinc oxide.

desorption product	peak temperature (K, ±2)	surface coverage (10^{12}molec/cm^2)
2-propanol	401	28
acetone	487	60
propene	513	89
water	390	38
	512	18
	728	71
CO_2	751	18
hydrogen	509	78

Both α and γ propene peaks were absent from the spectrum with only the β propene state present. Only small high temperature water and CO_2 desorption peaks were formed.

Hydrogen desorption occurred in a single broad peak coincident in temperature to propene (as previously found by Bowker et al[115]). Although only the single hydrogen peak maximum could be clearly resolved, the peak shape (sloping leading edge with a steep trailing edge) showed that it may have consisted of an envelope of two very closely overlapping hydrogen states. The quantity of hydrogen desorbed was estimated slightly in excess of the acetone formed.

Water desorption at low temperature consisted of a broad peak at approximately 390 K with a smaller overlying peak coincident with the propene. Although the total quantity of water desorbed was in excess

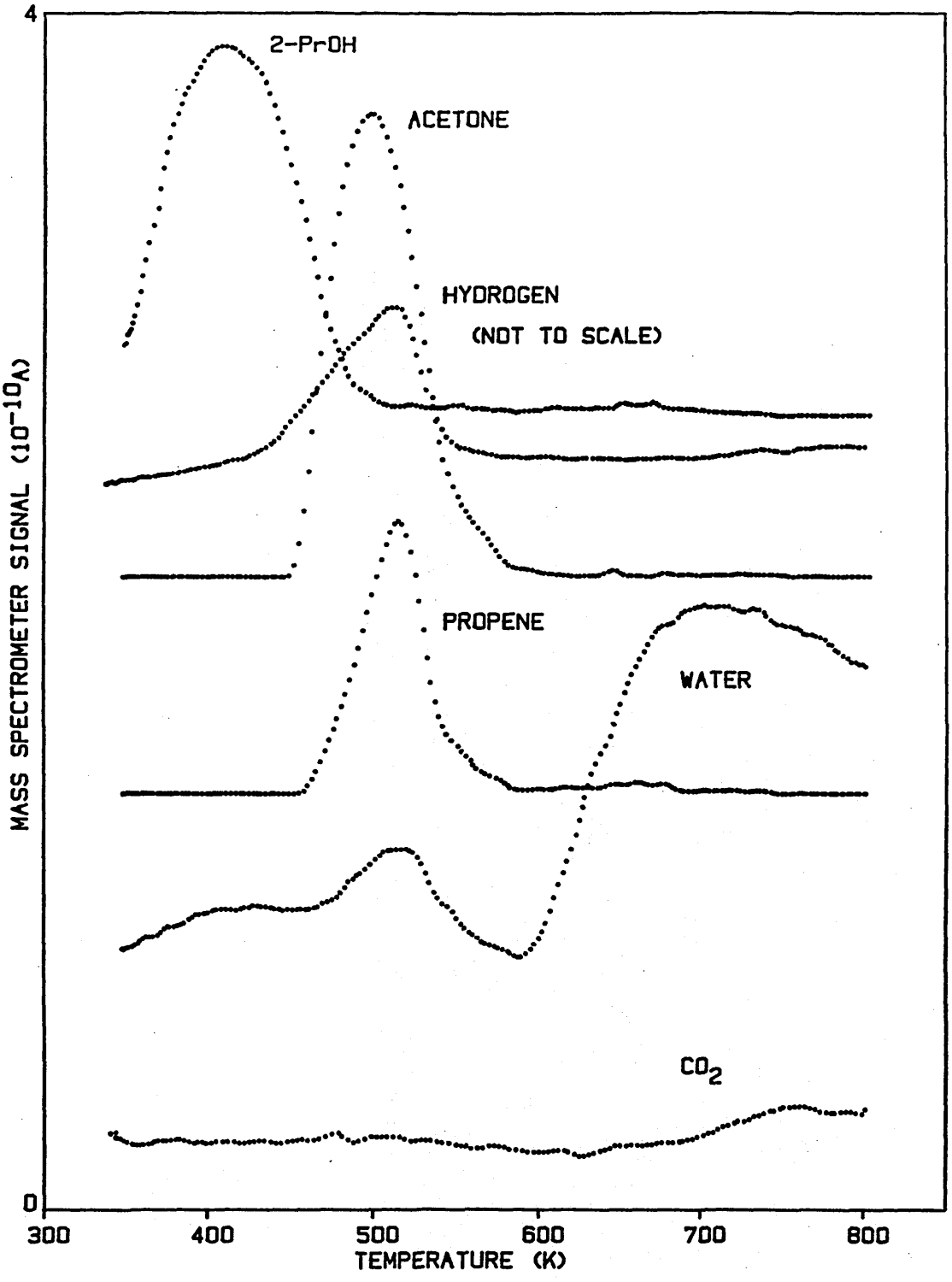

Figure 8.8: The desorption spectrum after adsorption of 2-propanol at 340 K to saturation coverage on ICI low surface area zinc oxide.

of the propene formed, good agreement was obtained between the amount of propene desorbed and sum of the water desorbed at 512 K and at high temperature. The high total water indicated the presence of water impurities in the injected alcohol contributing to the hydroxyl surface coverage. The total coverage obtained, excluding water, was 195×10^{12} molecules/cm^2 in reasonable agreement with Bowker et al[115] who reported a figure of 220×10^{12}.

(8.2.2.2) Coverage Dependence

The coverage dependence of the selectivity of 2-PrOH decomposition on ICI low surface area ZnO was found to follow the same trends as shown by the ZnO catalyst (section 7.1.2). The desorption spectra obtained at low coverage (30% of saturation) and medium coverage (60% of saturation) are given in figures 8.9 and 8.10. The changes in the product surface coverages with 2-PrOH dose are summarised by figure 8.11.

At low 2-PrOH dosage (<30% of saturation) no acetone peak was formed, the only desorption products being propene, water and CO_2 (figure 8.9). (Note that hydrogen was not scanned during this desorption experiment but was almost certainly also desorbed.) A single β propene desorption peak was obtained at all coverages with a constant peak temperature of 513 K. Although a small shoulder was observed on the trailing edge of this peak at some of the lower 2-PrOH doses, no other evidence for either the α or γ propene states was detected. The acetone peak temperature was found to decrease with coverage from an initial 504 K to 488 K at surface saturation.

CO_2 formed a poorly defined peak at approximately 753 K. A lack of a sharp peak maximum at all coverages showed that only limited

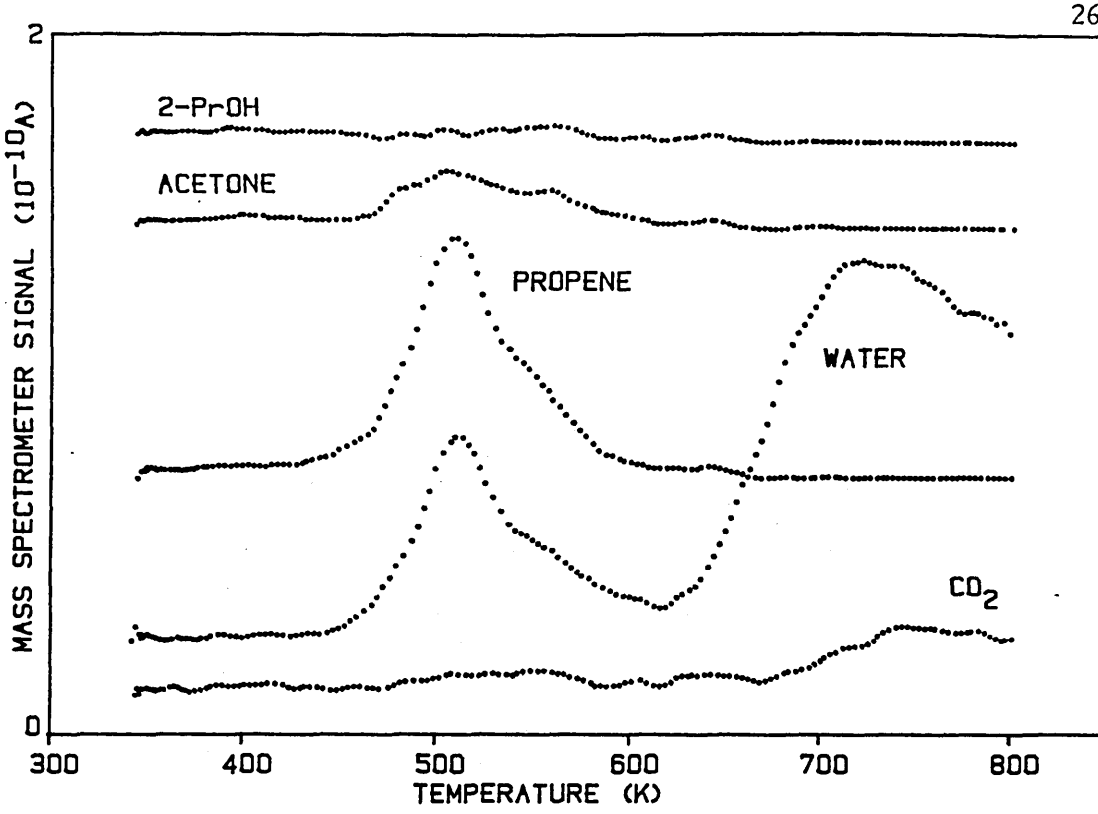

Figure 8.9: The desorption spectrum after adsorption of 2-propanol at 340 K to low coverage on ICI low surface area zinc oxide.

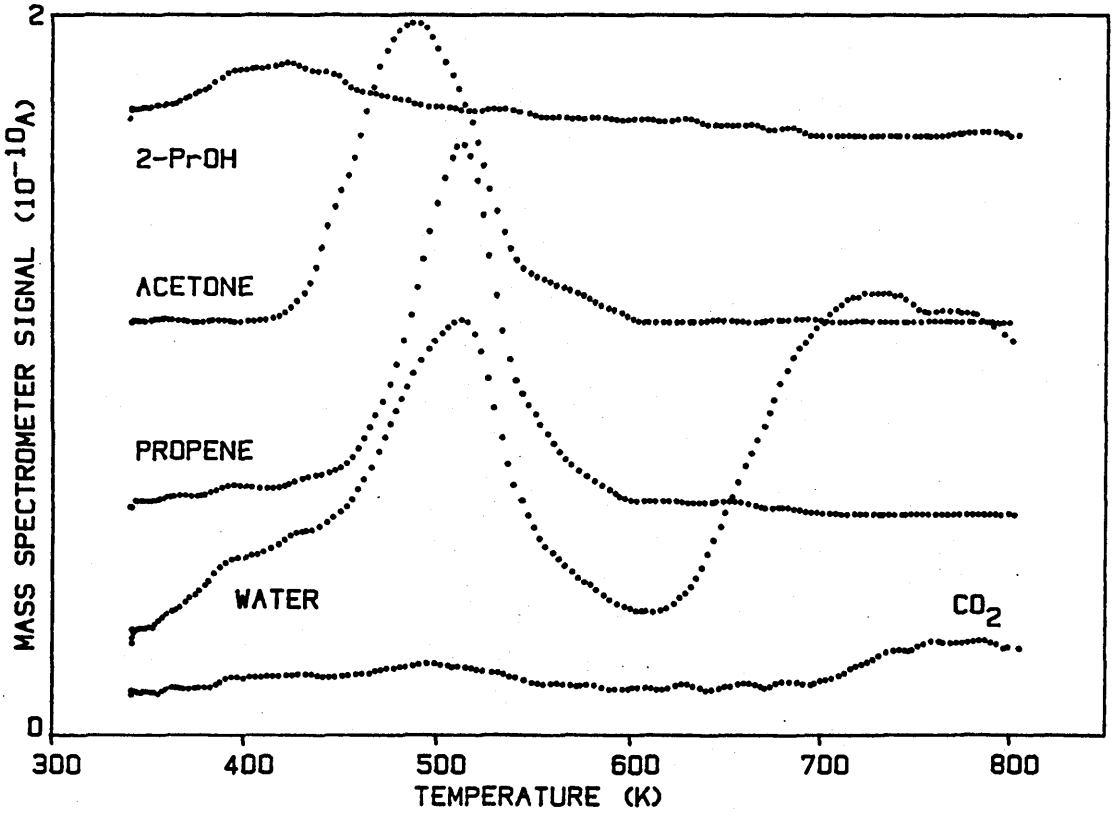

Figure 8.10: The desorption spectrum after adsorption of 2-propanol at 340 K to medium coverage on ICI low surface area zinc oxide.

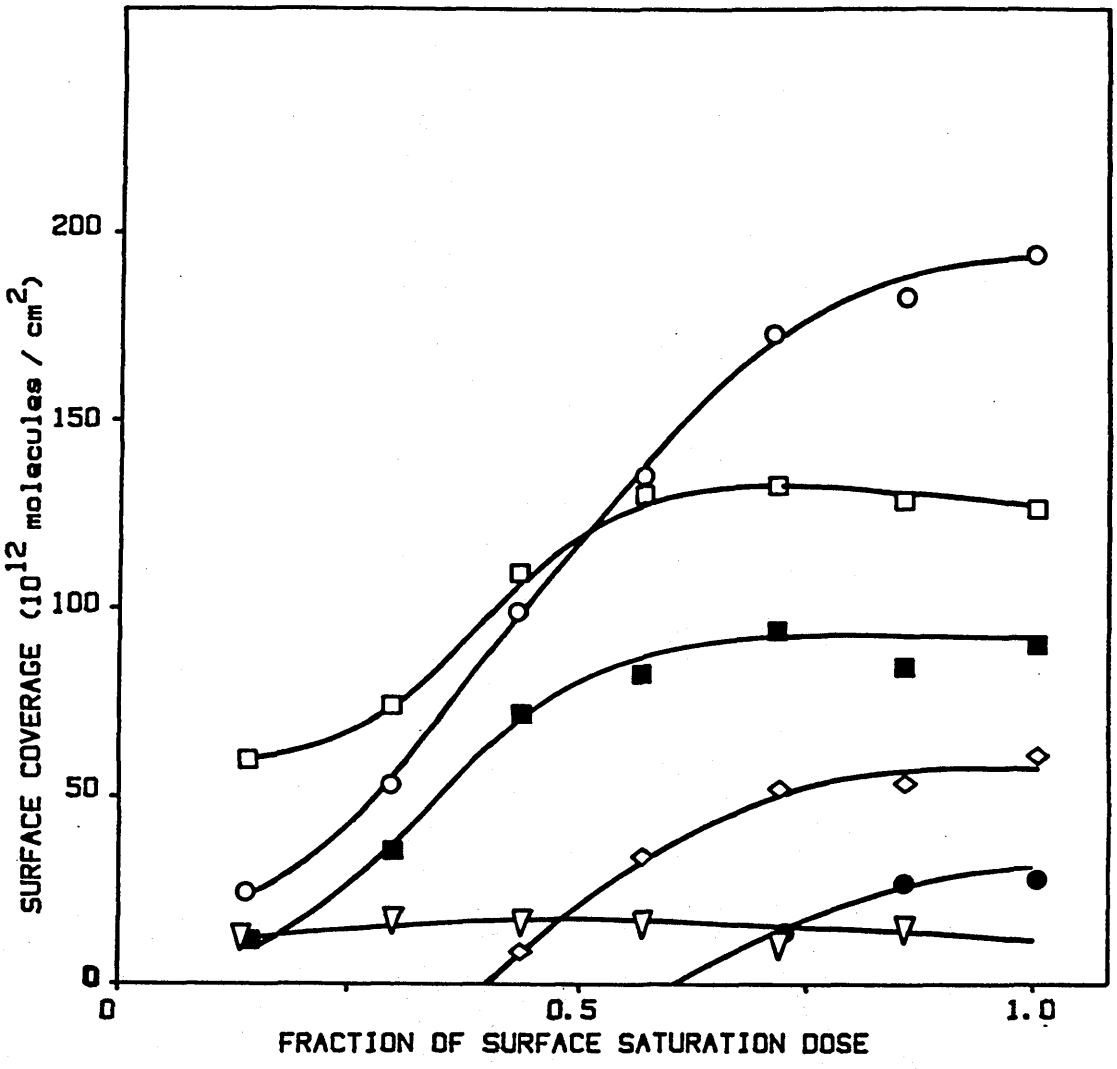

Figure 8.11: Plot of the desorption product surface coverages as a function of 2-propanol surface saturation dose at 340 K on ICI low surface area zinc oxide. ○ total coverage (excluding water); ■ propene; □ water; ▽ CO_2; ● 2-PrOH; ◇ acetone.

oxidation forming the surface carboxylate took place. Full population of the CO_2 peak occurred after a 2-PrOH dose corresponding to 70% of surface saturation. A decrease in the amount of CO_2 desorbed after six experiments appeared related to the aging effect previously described for water desorption on the same catalyst (section 8.2.1). A similar decrease was also found for the propene and total water desorbed.

Reversible 2-PrOH desorption was found to begin after a dose corresponding to 70% of surface saturation (figure 8.11). Only a single desorption peak could be resolved, initially at 420 K but decreasing to 401 K by saturation coverage.

(8.2.3) 1-Propanol

(8.2.3.1) Thermal Desorption and Decomposition Spectrum

The desorption spectrum obtained after a saturation dose of 1-PrOH at 320 K onto the ICI low surface area catalyst is shown in figure 8.12. The main product peak temperatures and their surface coverages are given in table 8.4. The spectrum is similar to that previously reported by Bowker et al[108]. It is also similar to the desorption spectrum obtained from chlorine treated ZnO described in the previous section, except for the amounts of mass 29 and CO_2 desorption that indicated that greater surface oxidation had occurred.

Reversible 1-PrOH desorption occurred in a broad peak at 392 K and a small shoulder at 448 K, with a profile similar to the 1-PrOH peak evolved from chlorine treated ZnO. A propionaldehyde desorption peak formed at 533 K, although the hydrogen did not peak until a higher temperature (562 K). Propene desorption occurred at 571 K at a

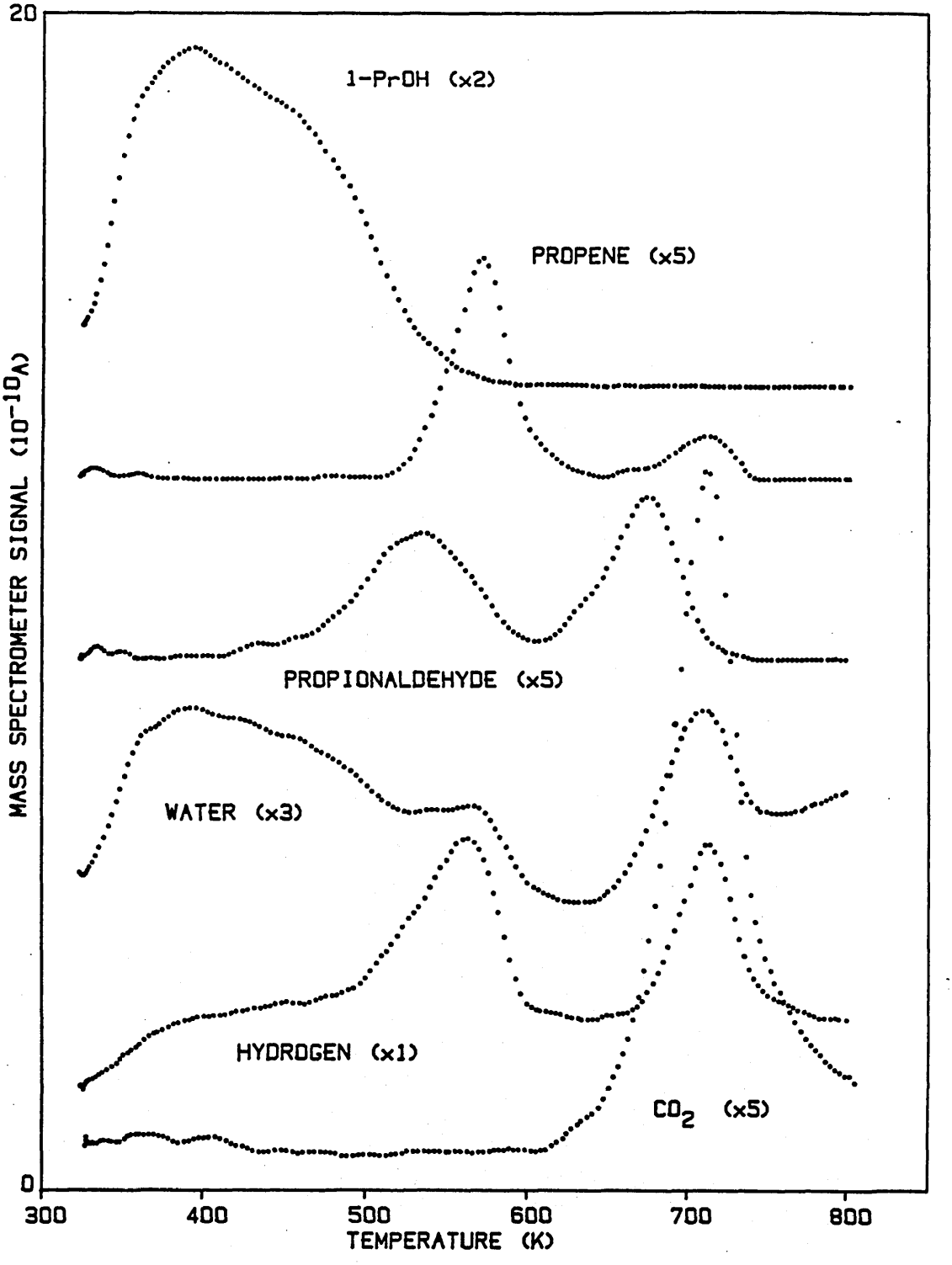

Figure 8.12: The desorption spectrum after adsorption of 1-propanol at 340 K to saturation coverage on ICI low surface area zinc oxide.

Table 8.4: The desorption products, peak temperatures and saturation surface coverages following 1-propanol adsorption at 340 K on ICI low surface area zinc oxide.

desorption product	peak temperature (K, ±2)	surface coverage (10^{12}molec/cm^2)
1-propanol	392,448	370
propionaldehyde	533	30
mass 29	675	-
propene	571	55
water	392	118
	562	7
	711	66
CO_2	712	195
hydrogen	562	203
	711	160

similar temperature to the propene evolved after 1-PrOH adsorption on untreated ZnO. A small amount of water was also evolved at 562 K with the propene (propene to water ratio of 8:1). A CO_2 peak at 712 K, along with coincident hydrogen, was indicative of the carboxylate decomposition reaction. A small mass 27 peak at the same temperature suggested that a small amount of ethene may have also been formed. The mass 29 peak formed at 675 K, also possibly associated with partial carboxylate decomposition.

The total saturation surface coverage, excluding water, was 650×10^{12} molecules/cm^2. This was greater than the 450×10^{12} reported by Bowker et al[108], although if the coverage contribution of the carboxylate (not found by Bowker et al) was neglected then a closer match was obtained.

(8.3) Discussion of Results

LEED and spectroscopic studies previously carried out by Hopkins et al[143,144] have investigated the interaction of chlorine with the Zn (0001) polar, O (000$\bar{1}$) polar and (10$\bar{1}$0) non-polar single crystal surfaces of ZnO (see also Appendix 4 for a further description). Rapid saturation of the Zn polar surface is found to occur to a coverage of 25% of a monolayer, sufficient to satisfy the charge stabilisation criterion for this surface. The O polar and prism surfaces are found to exhibit a much lower reactivity for chlorine. The amount of adsorption on the O polar surface is dependent on the initial surface annealing treatment, and because heat treatment is known to result in the formation of oxygen vacancies on this surface, it is suggested that chlorine occupies oxygen vacancy sites on this surface. On the prism surface an approximate 8% chlorine coverage is achieved, suggested to be due to random adsorption into oxygen vacancy sites. (This uptake is also similar to the defect site densities measured by Gopel et al[82].)

A similar polar surface selective distribution of chlorine is also shown in the earlier IR results of Atherton et al[43] where exposure of ZnO to HCl vapour resulted in the removal of the IR adsorption bands associated with hydroxyl groups assigned to the polar surfaces.

The selective removal of the α and γ propene (attributed to the Zn and O polar surfaces- see section 7.4), but not the acetone, β propene or 2-PrOH desorption peaks (attributed to the prism surface), in the 2-PrOH desorption spectrum from chlorine treated ZnO is consistent with the chlorine surface distribution determined by Hopkins

et al[143,144] and described above i.e selective adsorption onto the polar surfaces. On the O polar surface the oxygen vacancies, proposed as dehydration sites in section 7.4, are also blocked by chlorine for dissociative alcohol adsorption and subsequent dehydration. Similarly, the exposed cations on the Zn polar surface, the sites for the strong adsorption of chlorine [143], are deactivated for 2-PrOH dehydration.

Chlorine treatment was very effective for deactivation of the 2-PrOH oxidation reaction. In chapter 7, the carboxylate reaction sites were attributed to the prism surface, and to be also associated closely with the dehydrogenation sites. However, the effect of chlorine treatment was to enhance, rather than deactivate, the dehydrogenation reaction. From the mechanism presented in section 7.4, this shows that the chlorine cannot have reduced the surface coverage of the common oxidation/dehydrogenation precursor since this would have also resulted in a similar suppression of the dehydrogenation reaction.

Although the mode of chlorine adsorption on the Zn polar surface involves surface cations, this cannot be the case for the non-polar surface, since blockage of cation sites on this surface would have resulted in a suppression of both the dehydrogenation and the dehydration reactions, in addition to the oxidation. As noted above, the dehydrogenation was actually enhanced, while the dehydration, as evidenced by the formation of β propene from 2-PrOH, was not significantly affected. However, since the increase in dehydrogenation product did not match the decrease in CO_2 evolved, some cation deactivation of the dehydrogenation sites is possibly indicated.

Hopkins et al[143,144] have proposed chlorine to adsorb on the non-polar surface in association with the anion vacancy sites.

Although this also probably occurred in the chlorine treatment of the ZnO of this study, the carboxylate coverage (particularly for 1-PrOH) on the non-polar surface, and the extent of its reduction after chlorine treatment, were simply too high for the chlorine surface interaction to be limited to defect sites only.

The mechanism of chapter 7 has proposed carboxylate formation to occur by reaction of an adsorbed acetone species (possibly of the enol structure) with lattice oxygen to produce anion vacancy sites. The effect of chlorine treatment would appear to be to selectively suppress this reaction step in effect by making 'unavailable' the necessary reactive oxygen. It is not clear from the results how this mechanism may operate particularly since chlorine is unlikely to interact directly with lattice oxygen. This suggests that the effect may be at a more fundamental level and involve a number of possibilities including occupancy of step sites, incorporation into the lattice or a change in the electronic properties of the ZnO surface. Without further detailed investigation of chlorine adsorption these can only be regarded as speculation.

The similarities in the desorption spectra obtained after water, 2-PrOH and 1-PrOH adsorption on chlorine treated ZnO, and the spectra from the ICI low surface area ZnO, strongly suggest the differences in the behaviour between the ZnO used in this study and the ICI low surface area ZnO were due to the presence of chlorine, as detected by the XPS measurements i.e. the ICI low surface area ZnO was chlorine contaminated. Consequently, the results of previous thermal desorption and decomposition studies by Bowker et al[25,83,98,99,108,115], based on the ICI low surface area ZnO, should be reinterpreted on the

basis of desorption and decomposition on a chlorine contaminated, rather than a pure, ZnO surface.

The results presented in this chapter have implications in two areas. Firstly, they have shown chlorine to be an excellent selective probe for the polar surfaces of ZnO that can be used to deactivate these surfaces very effectively, while still maintaining the activity of the prism surface cations. Secondly, the results have shown that in the study of metal oxide surfaces it is important to remove any surface impurities as their presence can significantly modify the catalytic properties of the surface. Particular attention should be paid to single crystal oxide surfaces in light of the work of Hopkins et al[143,144] who have shown that the removal of contaminants from crystal surfaces can be extremely difficult.

CHAPTER 9

PROPANOL DECOMPOSITION ON POTASSIUM PROMOTED ZINC OXIDE

(9.1) 2-Propanol

(9.1.1) Thermal Desorption and Decomposition Spectrum

The presence of even small amounts of alkali added to the ZnO had a significant effect on 2-PrOH desorption and decomposition. The desorption spectra obtained at the three alkali loadings studied (0.042, 0.085 and 0.20 wt% K) after a saturation dose of 2-PrOH are shown in figures 9.1 to 9.3. The desorption peak temperatures are summarised in table 9.1.

Desorption in the α 2-PrOH peak was reduced considerably at the 0.042 wt% K loading so that only a shoulder in the 2-PrOH peak was detected. At the higher alkali loadings no desorption from this state was observed. The coverage in the β 2-PrOH state was enhanced by alkali addition reaching approximately 100×10^{12} molecules/cm^2 for the 0.20 wt% K loaded catalyst. Table 9.1 shows the corresponding peak temperature increased from 376 K for the ZnO catalyst to 399 K at the highest alkali loading.

The alkali promotion also resulted in increased acetone production with 90×10^{12} molecules/cm^2 desorbed from the 0.20 wt% K loaded catalyst. The peak temperature also increased from 441 K on the unpromoted catalyst to 470 K for the 0.20 wt% loaded catalyst. Although the acetone peak appeared to be broader for the alkali loaded catalysts compared to unpromoted ZnO, experiments at low 2-PrOH surface coverage detected only a single desorption peak at this

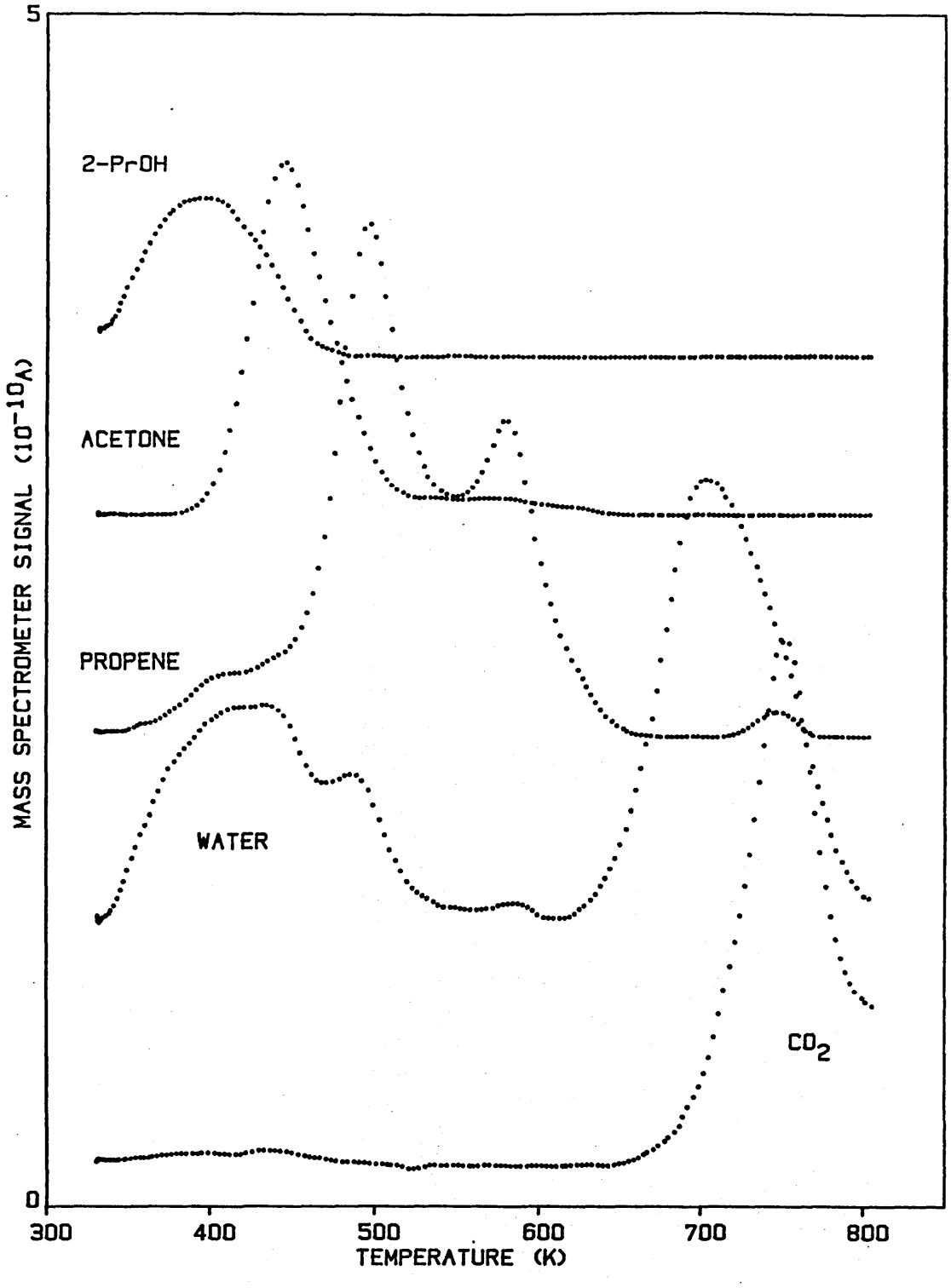

Figure 9.1: The desorption spectrum after adsorption of 2-propanol at 340 K to saturation coverage on 0.042 wt% potassium promoted zinc oxide.

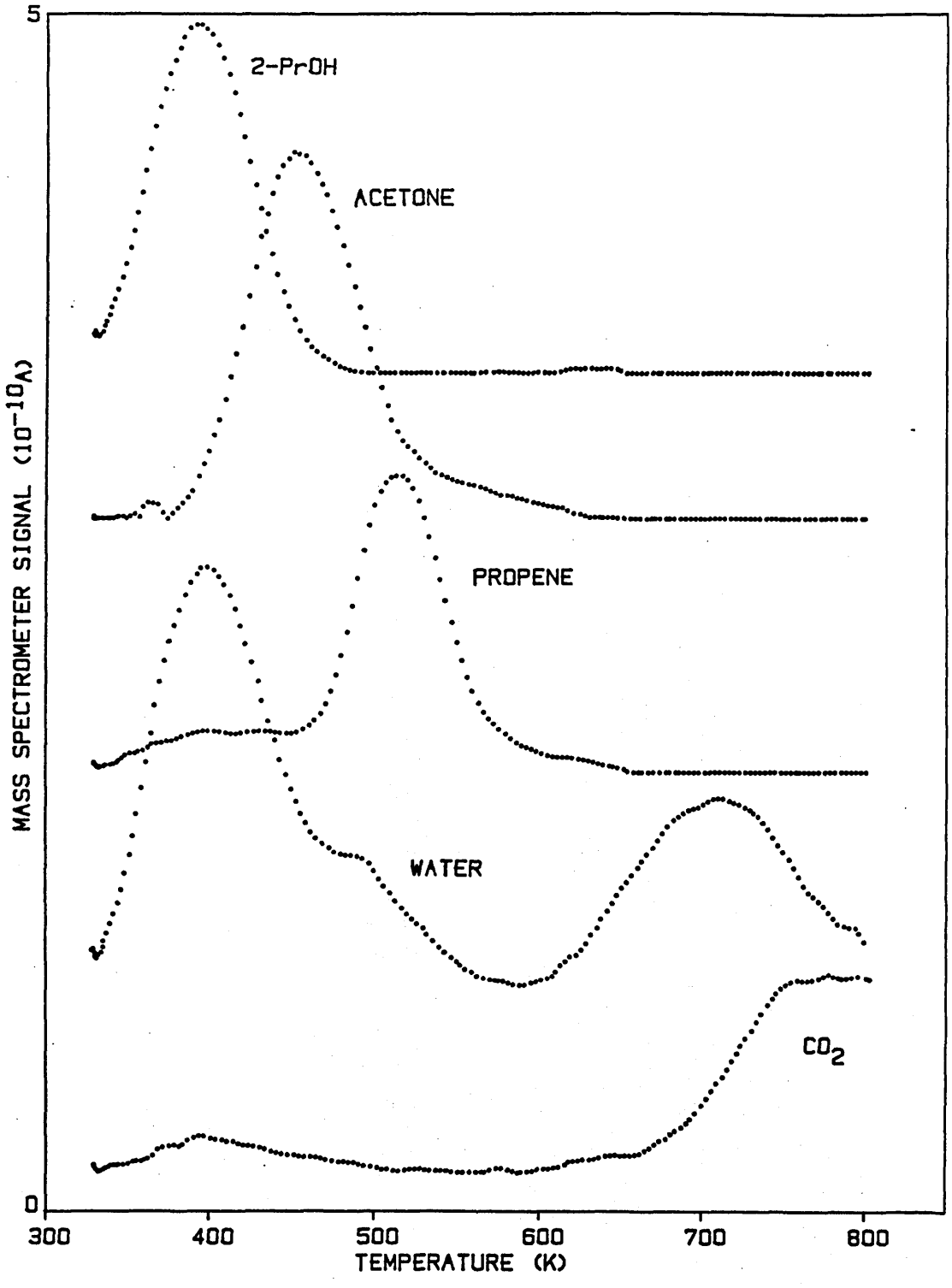

Figure 9.2: The desorption spectrum after adsorption of 2-propanol at 340 K to saturation coverage on 0.085 wt% potassium promoted zinc oxide.

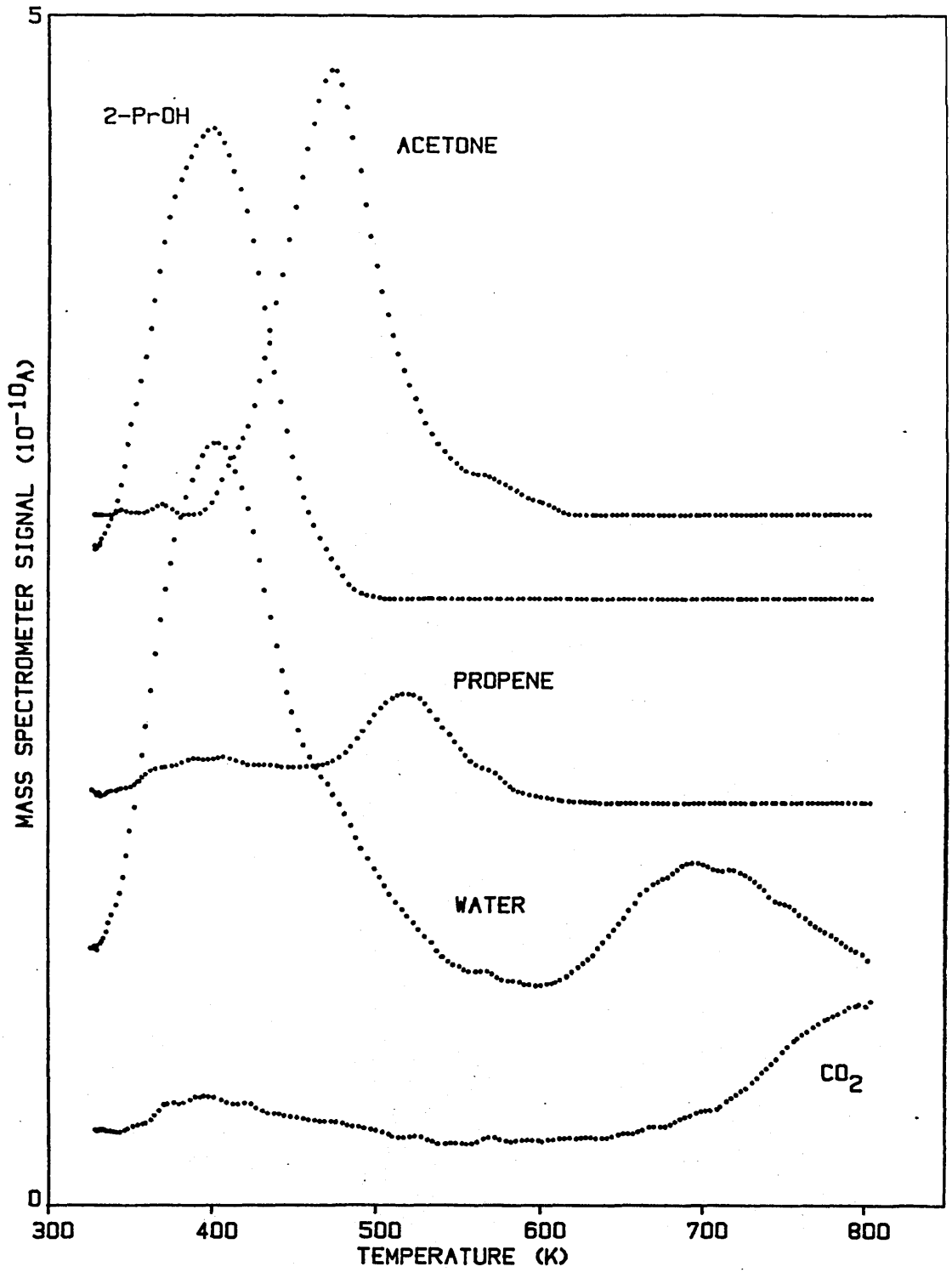

Figure 9.3: The desorption spectrum after adsorption of 2-propanol at 340 K to saturation coverage on 0.20 wt% potassium promoted zinc oxide.

Table 9.1: The effect of potassium promotion on the main product desorption peak temperatures after adsorption of 2-PrOH to saturation coverage at 340 K. The temperatures given in brackets indicate ill-defined or minor desorption states.

desorption product		potassium loading (wt% K)		
		0.042	0.085	0.20
2-PrOH		395	492	399
water		(372),408,433 (484) 583 703	396 (489) - 709	401 (473) - 692
CO_2		478	(485)	-
propene	α	409	-	-
	β	494	512	518
	γ	578	-	-
acetone		441	449	470
hydrogen		(a)	473 753	472 (753)

(a)= not scanned

temperature (see section 7.1.2). As for unpromoted ZnO, there was also a small amount of acetone produced in the range 550-600 K. At the 0.20 wt% K loading, hydrogen desorbed in a single broad peak at approximately 472 K with an estimated coverage of 125×10^{12} H_2/cm^2.

The amount of propene desorbed decreased with increased alkali loading. The α and γ states were progressively and finally completely removed from the desorption spectrum as the alkali loading increased. A significant but less dramatic reduction of the β state also occurred particularly when the alkali loading was increased from 0.085 to 0.20 wt% K. The corresponding β peak temperature followed the same trend shown by the 2-PrOH and acetone peaks by increasing from 487 K on the unpromoted ZnO to 517 K on the 0.20 wt% K loaded catalyst.

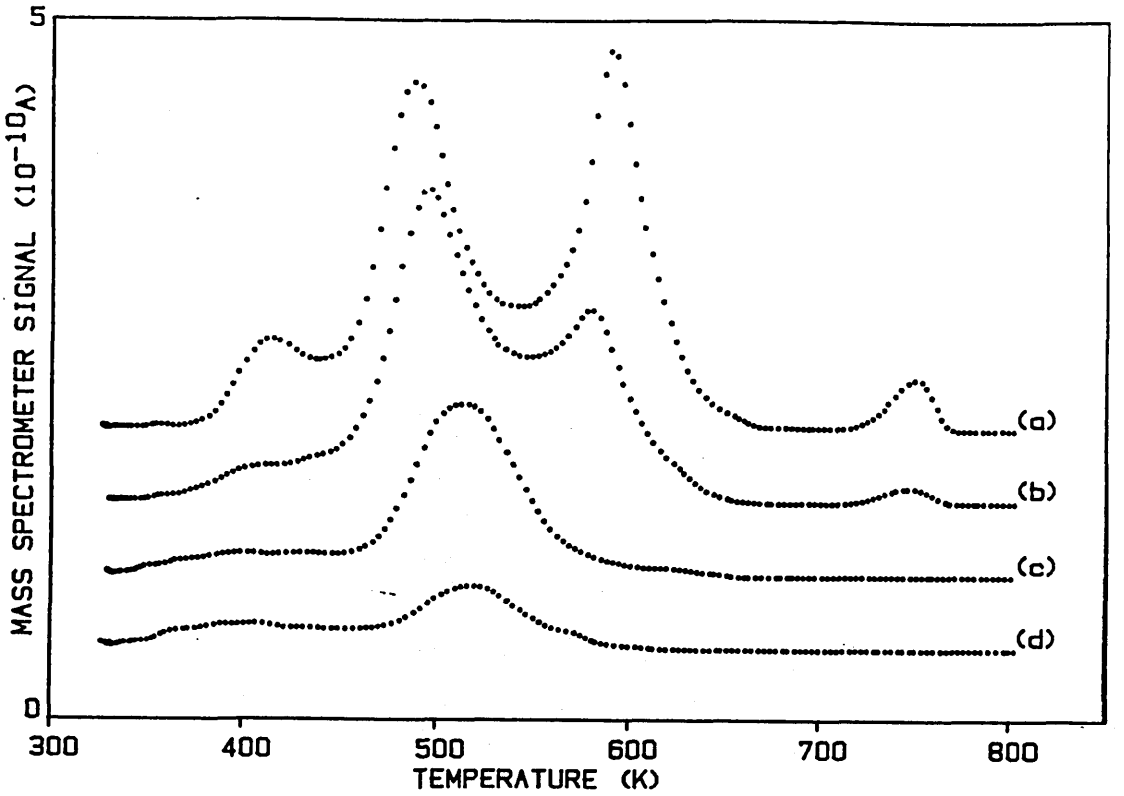

Figure 9.4: The effect of potassium loading on the propene desorption spectrum after adsorption of 2-propanol at 330 K on promoted zinc oxide. (a)= unpromoted ZnO; (b)= 0.042 wt% K; (c)= 0.085 wt% K; (d)= 0.20 wt% K.

These effects are shown more clearly in figure 9.4 given above in which the propene spectra have been extracted from figures 9.1 to 9.3.

The water desorption at high temperature was modified by the presence of the alkali in the same way as that observed after water adsorption onto the same catalysts (see section 6.2.1), i.e. the amount of desorption was progressively reduced with increased alkali loading. In the low temperature region, the water desorption associated with the β propene at 484 K for the unpromoted ZnO was reduced in line with the β propene peak until it was barely observed for the highest loaded catalyst (0.20 wt% K). For the 0.085 wt% and 0.20 wt% K catalysts where only a small amount of water was produced at a similar temperature to the propene, the quantity of water desorbed at high temperature was in reasonable agreement with the propene

coverage. As the alkali loading was increased, a water desorption peak at approximately 393 K was also formed. The similarity in temperature between this and the low temperature desorption peak found after water adsorption onto the same catalysts (section 6.2.1) would suggest that it was due to molecularly adsorbed water rather than being associated with the 2-PrOH desorption peak which occurred at a similar temperature. The total quantity of water desorbed from the alkali promoted catalysts was too high to be accounted for by the dehydration reactions alone (for unpromoted ZnO, the amount of water desorbed has been shown to be less than expected from the propene produced). Since the high temperature water desorption was in approximate agreement with the propene formed (noted above) it would appear that desorption from the weakly adsorbed state at 393 K was due to water present as an impurity in the 2-PrOH.

The oxidation reaction forming the carboxylate was also strongly affected by the presence of the alkali as shown by the large reduction in the amount of CO_2 produced as the alkali loading was increased. However, the rising CO_2 baseline signal obtained at high temperature even for the 0.20 wt% K catalyst raises the possibility of a more strongly bound species remaining on the surface. A similar rise in the baseline was observed after CO_2 adsorption on the same catalysts (section 6.2.2). For the 0.20 wt% K loading a small quantity of hydrogen coincident with CO_2 was evolved at high temperature (15×10^{12} H_2/cm^2).

The variations in surface coverage of the desorption/decomposition products as a function of alkali loading are summarised in figure 9.5. The total surface coverage (excluding water) fell from

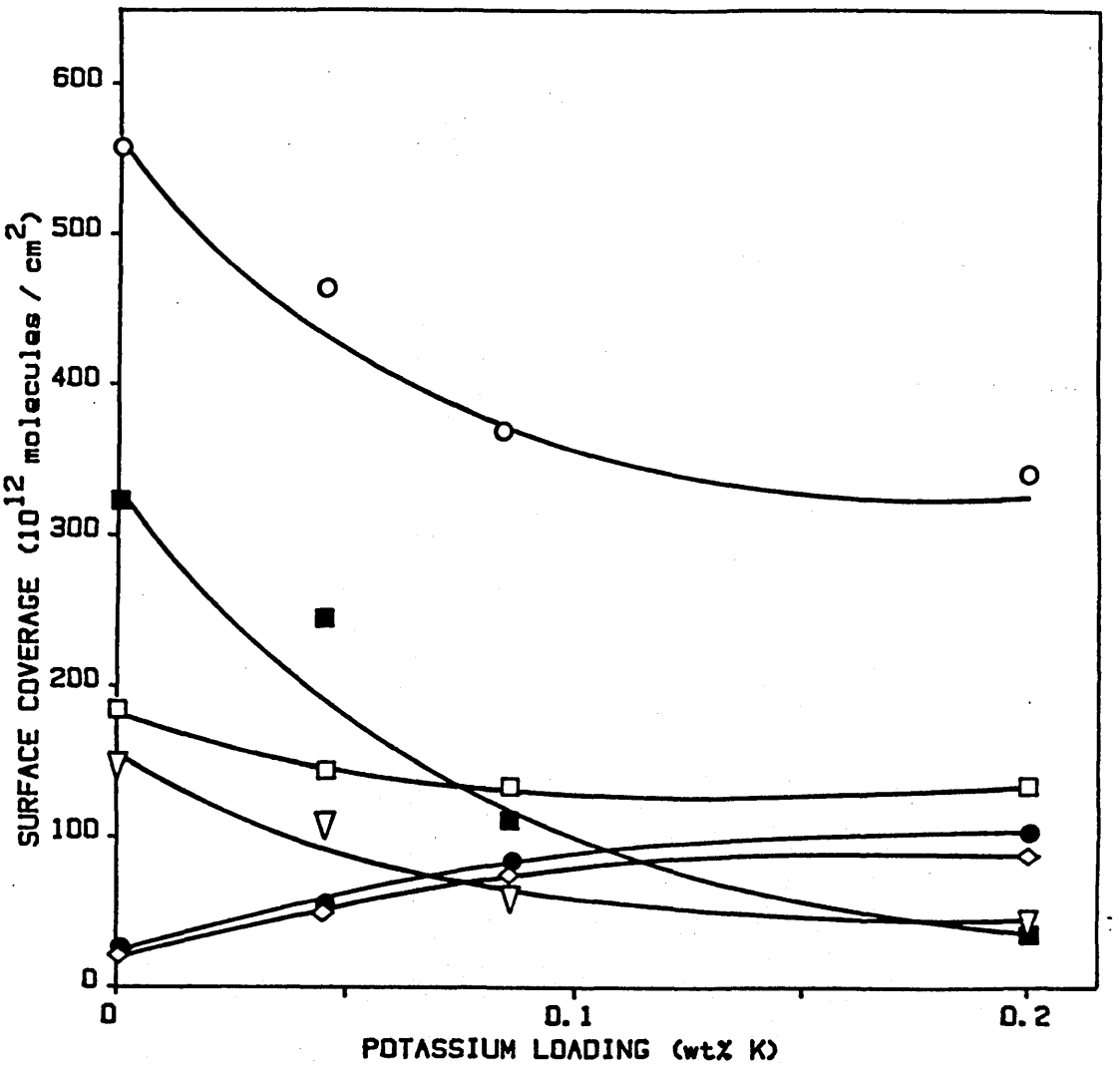

Figure 9.5: The effect of potassium loading on the desorption product surface coverages after adsorption of 2-propanol at 330 K to saturation coverage on promoted zinc oxide. ○ total coverage (excluding water); ■ propene; □ water; ▽ CO_2; ● 2-PrOH; ◇ acetone.

570 molecules/cm^2 for ZnO to approximately 350 molecules/cm^2 at 0.20 wt% K. The fall in the amount of propene and CO_2 produced and the increased evolution of acetone as alkali loading increased are clearly shown in the figure.

(9.1.2) Coverage Dependence

As found for unpromoted ZnO, the selectivity of the 2-PrOH decomposition on promoted ZnO was shown to be coverage dependent. This coverage dependence was investigated for the 0.20 wt% and 0.085 wt% K potassium promoted catalysts. The desorption spectra obtained at low (30% of surface saturation) and medium (70%) surface coverages for these two alkali loadings are shown in figures 9.6 to 9.9, with the changes in surface coverages of the main desorption and decomposition products as a function of alcohol dose summarised in figures 9.10 and 9.11.

On both catalysts only the β propene peak was populated, with the α and γ states suppressed by the presence of the alkali. Although population of the β propene sites continued until full surface saturation for the 0.085 wt% K catalyst, at the higher loading of 0.20 wt% K, saturation of the β sites was quickly reached and no increase in this peak was observed above a 25% of saturation dose. No shift in propene peak temperature with coverage was found for either catalyst although the actual peak position itself was loading dependent (see also table 9.1).

Above a 25% dose for the 0.20 wt% K loading and a 50% dose for the 0.085 wt% K loading (i.e. when the majority of the remaining dehydration sites had been populated) acetone evolution was observed. Only a single desorption peak was formed with its peak temperature

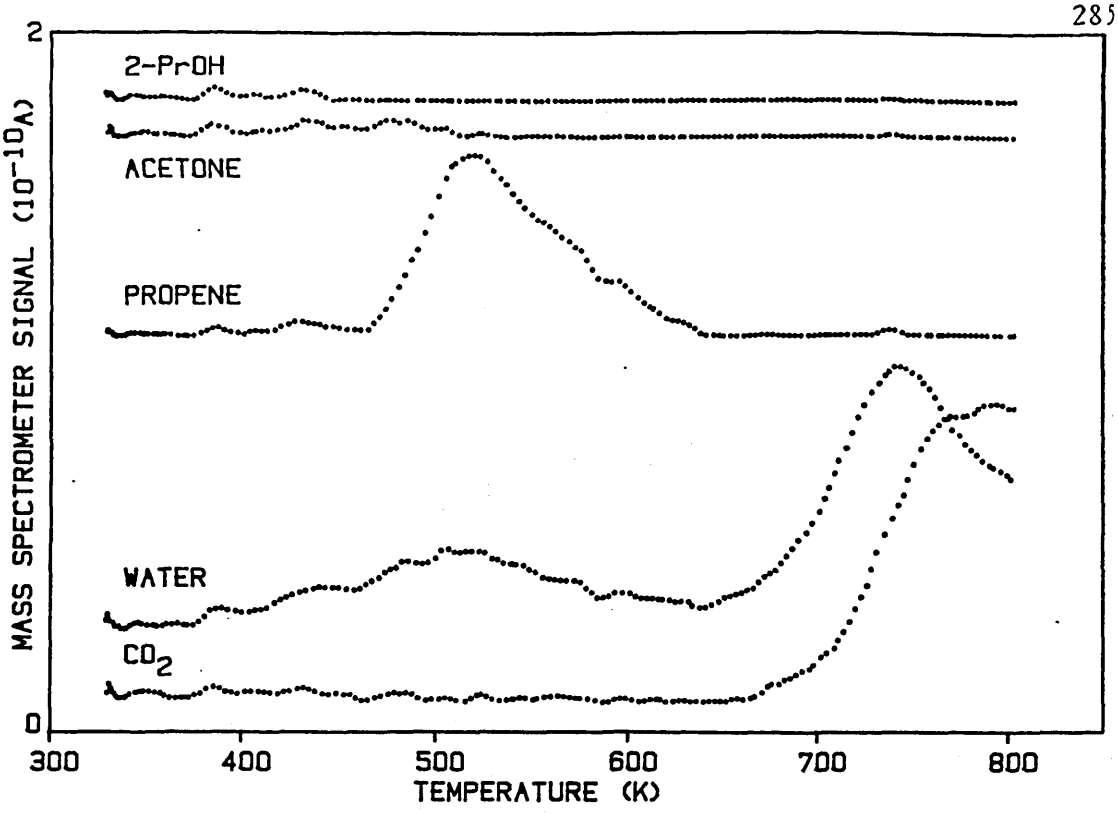

Figure 9.6: The desorption spectrum after adsorption of 2-propanol at 340 K to low coverage on 0.085 wt% potassium promoted zinc oxide.

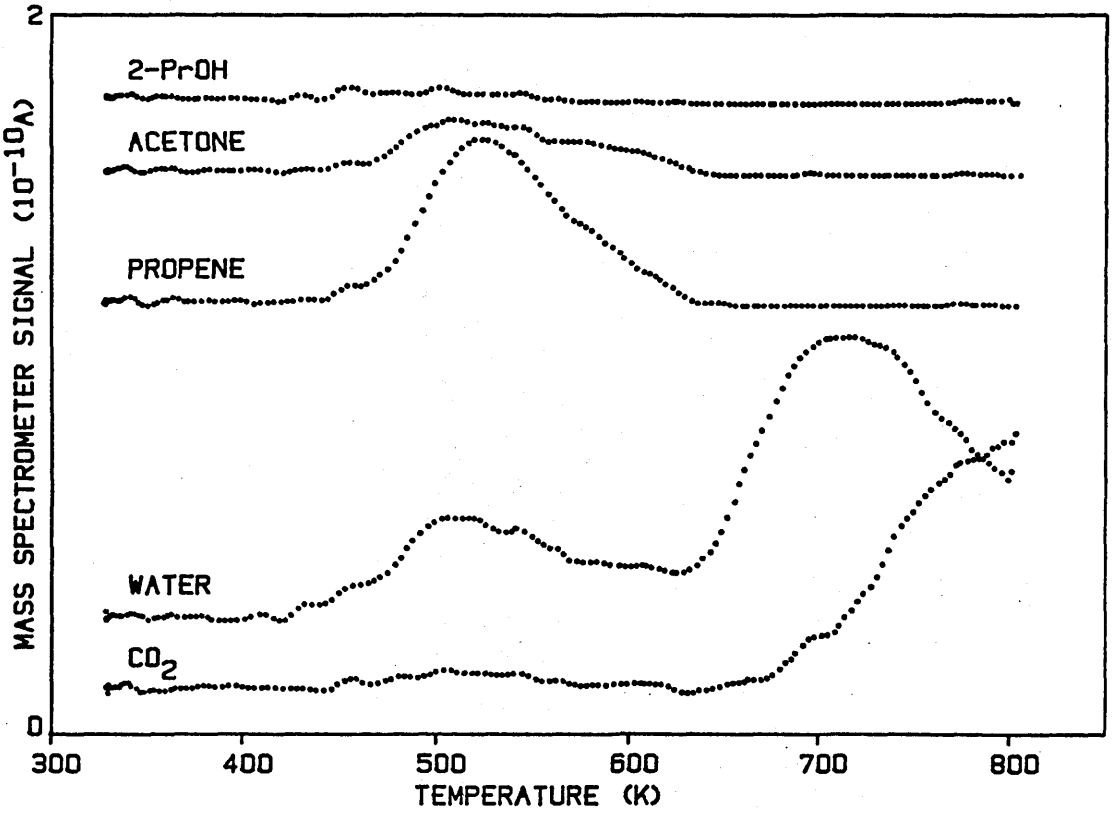

Figure 9.7: The desorption spectrum after adsorption of 2-propanol at 340 K to low coverage on 0.20 wt% potassium promoted zinc oxide.

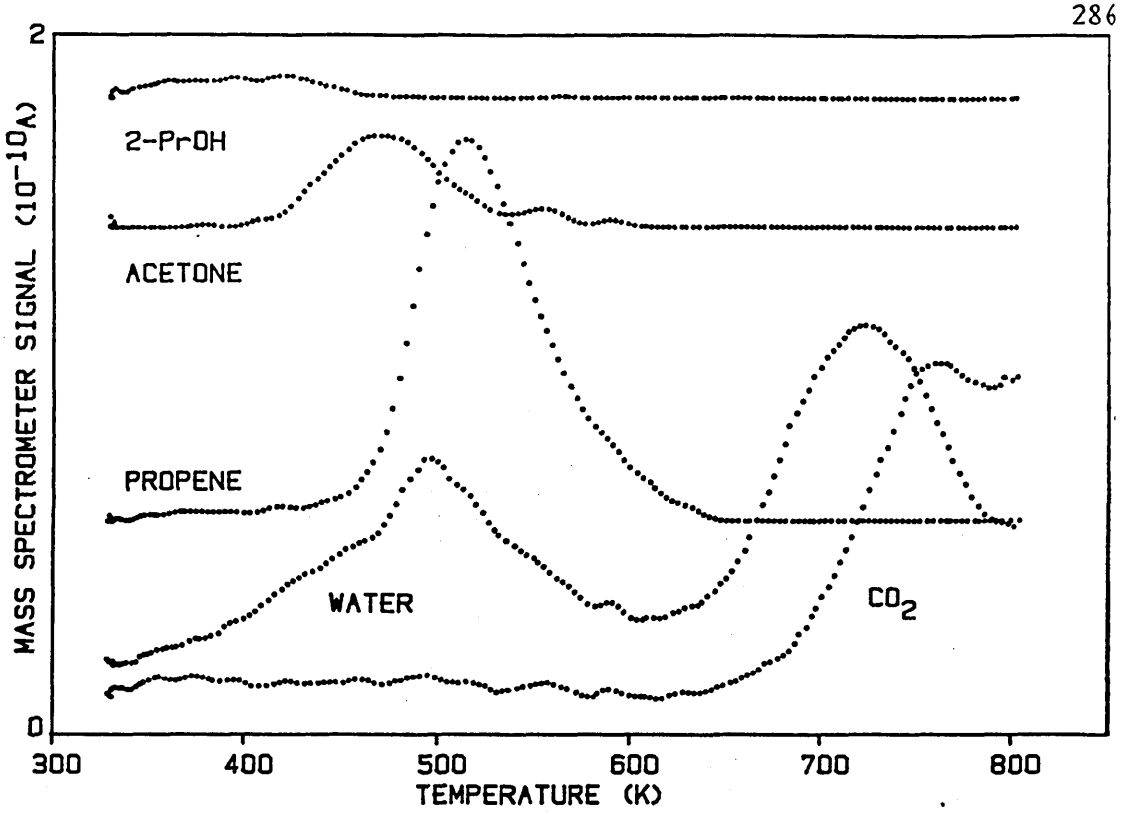

Figure 9.8: The desorption spectrum after adsorption of 2-propanol at 340 K to medium coverage on 0.085 wt% potassium promoted zinc oxide.

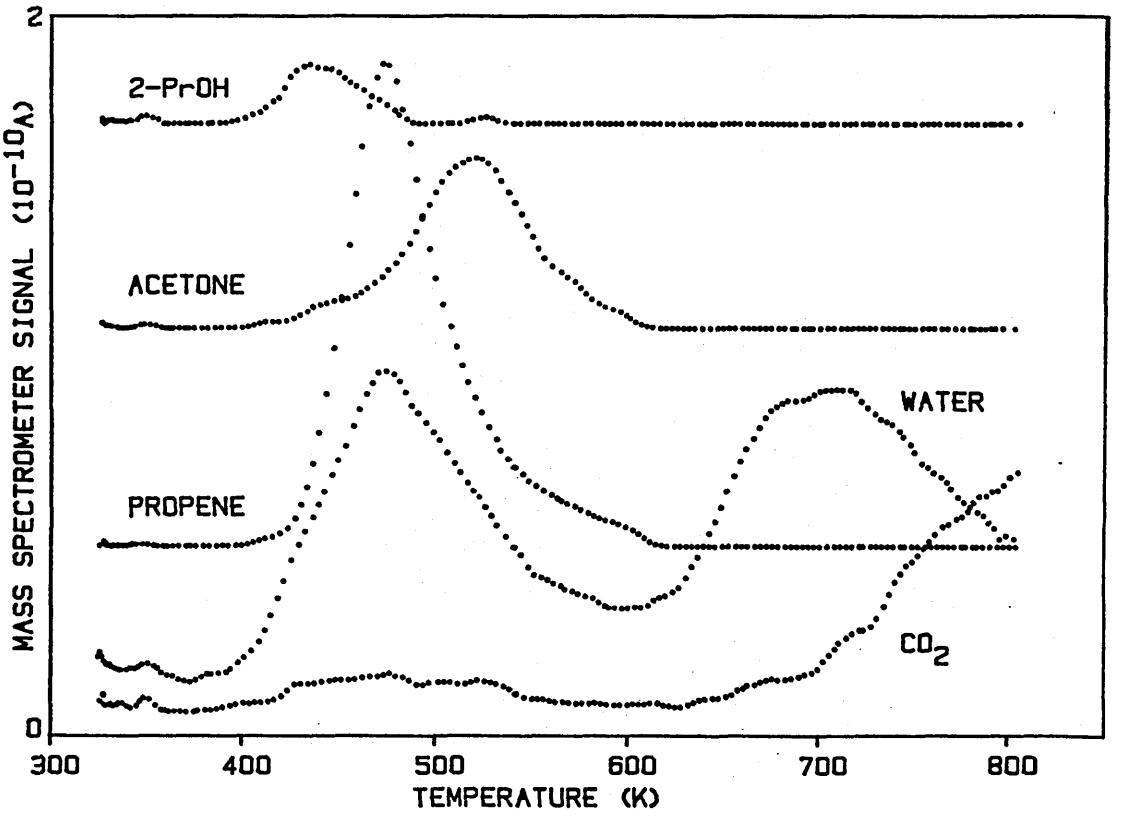

Figure 9.9: The desorption spectrum after adsorption of 2-propanol at 340 K to medium coverage on 0.20 wt% potassium promoted zinc oxide.

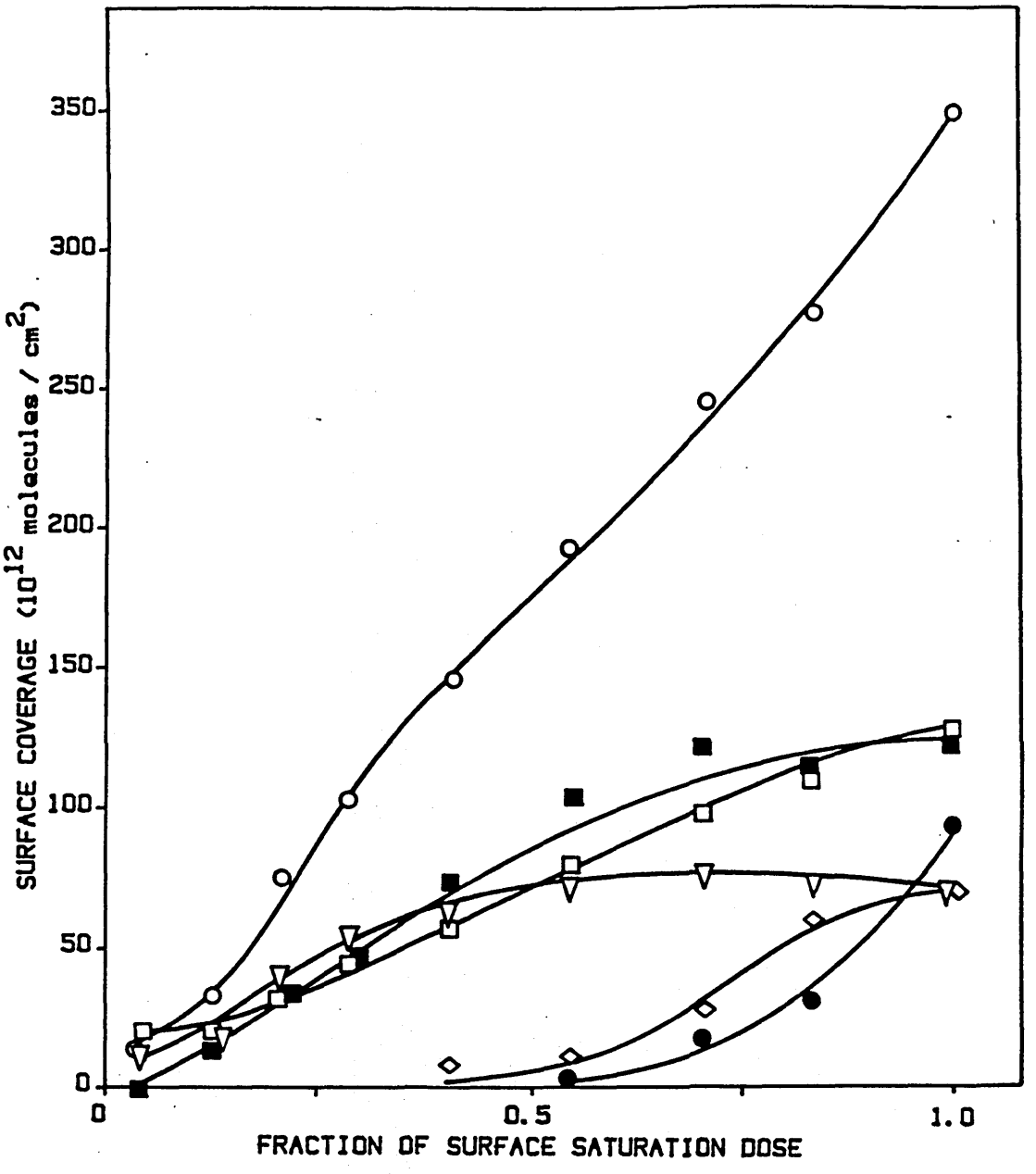

Figure 9.10: Plot of the desorption product surface coverages as a function of 2-propanol surface saturation dose at 340 K on 0.085 wt% potassium promoted zinc oxide. ○ total coverage (excluding water); ■ propene; □ water; ▽ CO_2; ● 2-PrOH; ◇ acetone.

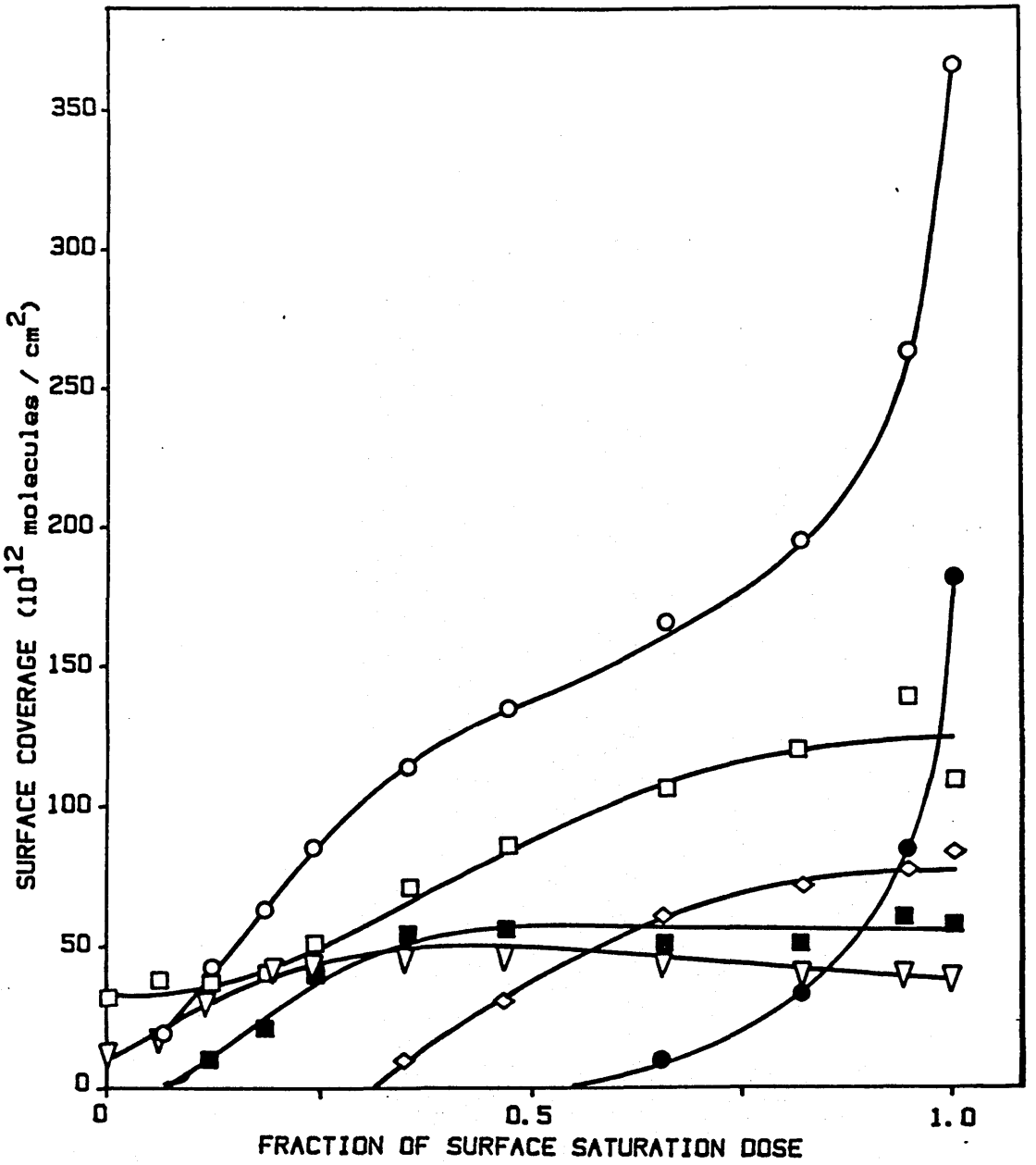

Figure 9.11: Plot of the desorption product surface coverages as a function of 2-propanol surface saturation dose at 340 K on 0.20 wt% potassium promoted zinc oxide. ○ total coverage (excluding water); ■ propene; □ water; ▽ CO_2; ● 2-PrOH; ◇ acetone.

decreasing as coverage increased (470 K to 449 K for 0.085 wt% K and 510 K to 470 K for 0.020 wt% K).

Reversible 2-PrOH desorption occurred for coverages exceeding 60-70% of surface saturation on both catalysts. A coverage dependency in the 2-PrOH peak temperature was found, with a decrease from 420 K to 406 K for the 0.085 wt% K and 433 K to 399 K for the 0.20 wt% K.

At low coverage water desorption occurred only in the high temperature region for both catalysts. As the 2-PrOH dose was increased, lower temperature desorption states were populated until the spectra were dominated by a large peak at approximately 398 K for both alkali loadings. Both catalysts also formed a small water peak at approximately 513 K that decreased in temperature as the coverage increased.

Only a small amount of carboxylate derived CO_2 was evolved from either catalyst. No CO_2 peak was formed with the 0.20 wt% K catalyst and only a rise in the CO_2 baseline signal was obtained that did not significantly alter with coverage (similar to that observed after CO_2 adsorption on the promoted ZnO, see section 6.2.2). The same baseline rise was also observed for the 0.085 wt% K loaded catalyst, although some further desorption in a small peak at 763 K was also present from this catalyst.

(9.2) 1-Propanol

(9.2.1) Thermal Desorption and Decomposition Spectrum

The 1-PrOH desorption spectra obtained at the three potassium promotor loadings (0.042, 0.085 and 0.20 wt% K) after a saturation dose at 340 K are shown in figures 9.12 to 9.14, with the changes in surface coverages of the main desorption products with 1-PrOH dose

summarised in figure 9.15. The desorption peak temperatures are given in table 9.2.

As found for 2-PrOH, the presence of the alkali promoter had a significant effect on the selectivity of 1-PrOH decomposition. Figure 9.15 shows the alkali increased the amount of reversible 1-PrOH desorption, and reduced the extent of alcohol decomposition. The overall surface coverage (excluding the water formed) was initially reduced as a result of the reduction in the quantity of CO_2 desorption (i.e. carboxylate formation) but rapidly increased again as the alkali loading was raised, due to the large increase in reversibly adsorbed alcohol. The coverage of decomposition products, however, continued decreasing as the alkali loading was increased. Reversible desorption accounted for 74% of the desorption products from the 0.020 wt% K ZnO compared to the 23% obtained from unpromoted ZnO. No change in the main 1-PrOH desorption peak temperature (404 K) was found to occur with increasing alkali loading.

In common with the behaviour exhibited by 2-PrOH, 1-PrOH dehydration was also suppressed by the alkali promotion. The 481 K propene peak was removed from the spectra at all three potassium loadings, while the 573 K peak was considerably reduced at the 0.042 wt% K level and only barely detectable at the higher 0.085 wt% loading. At the 0.20 wt% loading no 573 K propene was observed.

The quantity of mass 29 desorption (most probably acetaldehyde- see chapter 7) decreased with the level of potassium promotion, matching the decrease in carboxylate formation (see below). An increase in the desorption peak temperature also occurred with potassium loading (table 9.2).

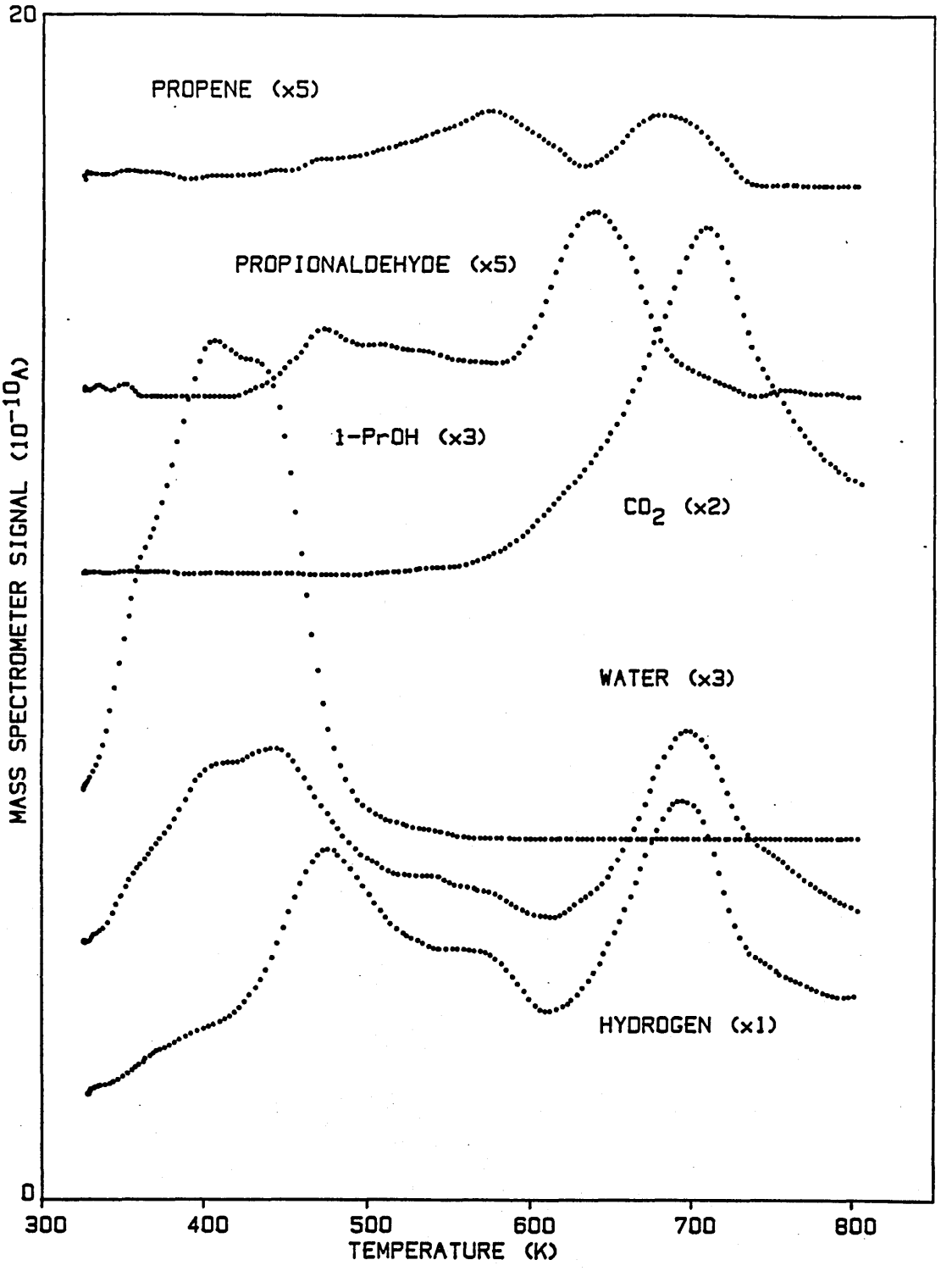

Figure 9.12: The desorption spectrum after adsorption of 1-propanol at 340 K to saturation coverage on 0.042 wt% potassium promoted zinc oxide.

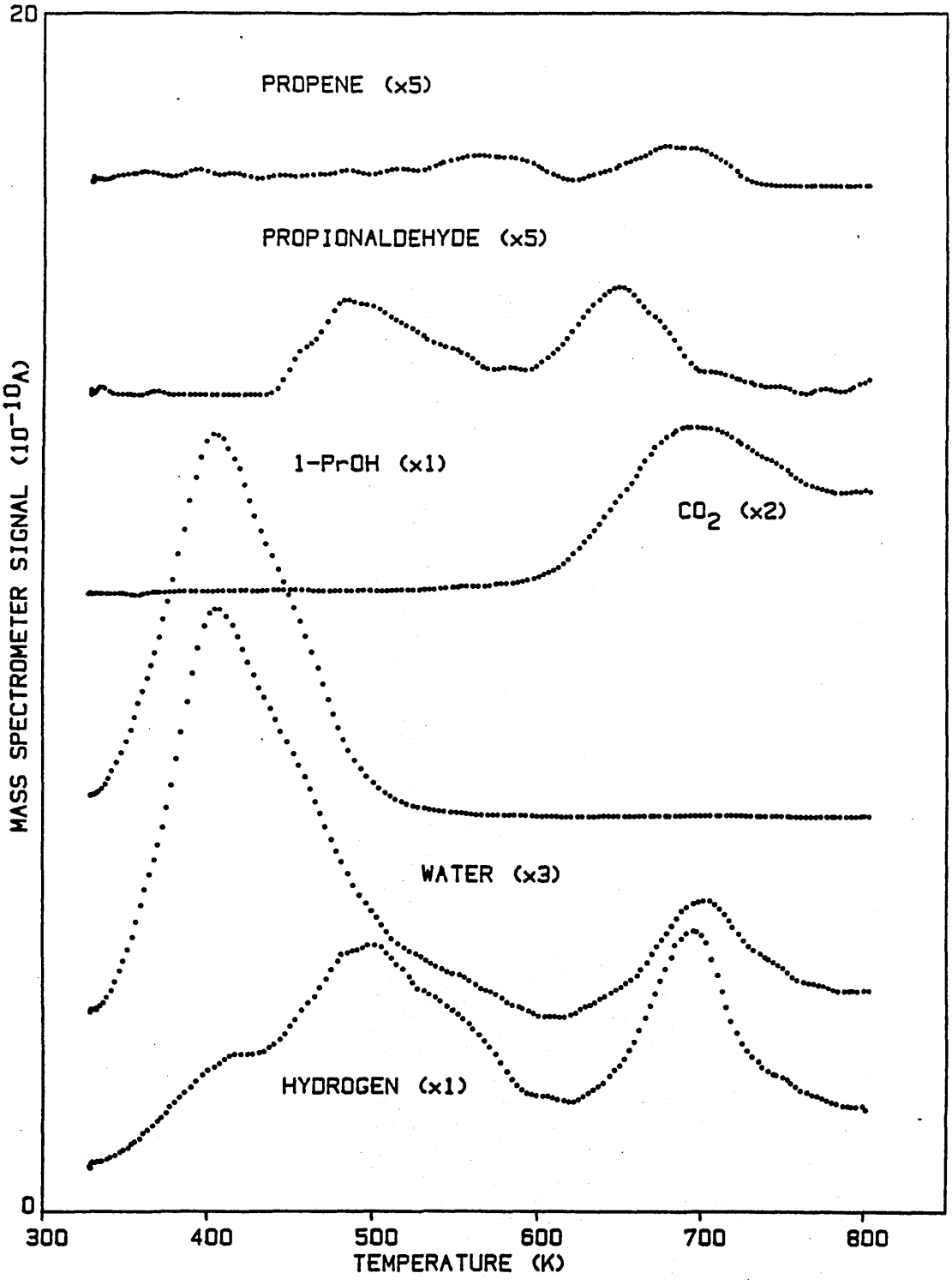

Figure 9.13: The desorption spectrum after adsorption of 1-propanol at 340 K to saturation coverage on 0.085 wt% potassium promoted zinc oxide.

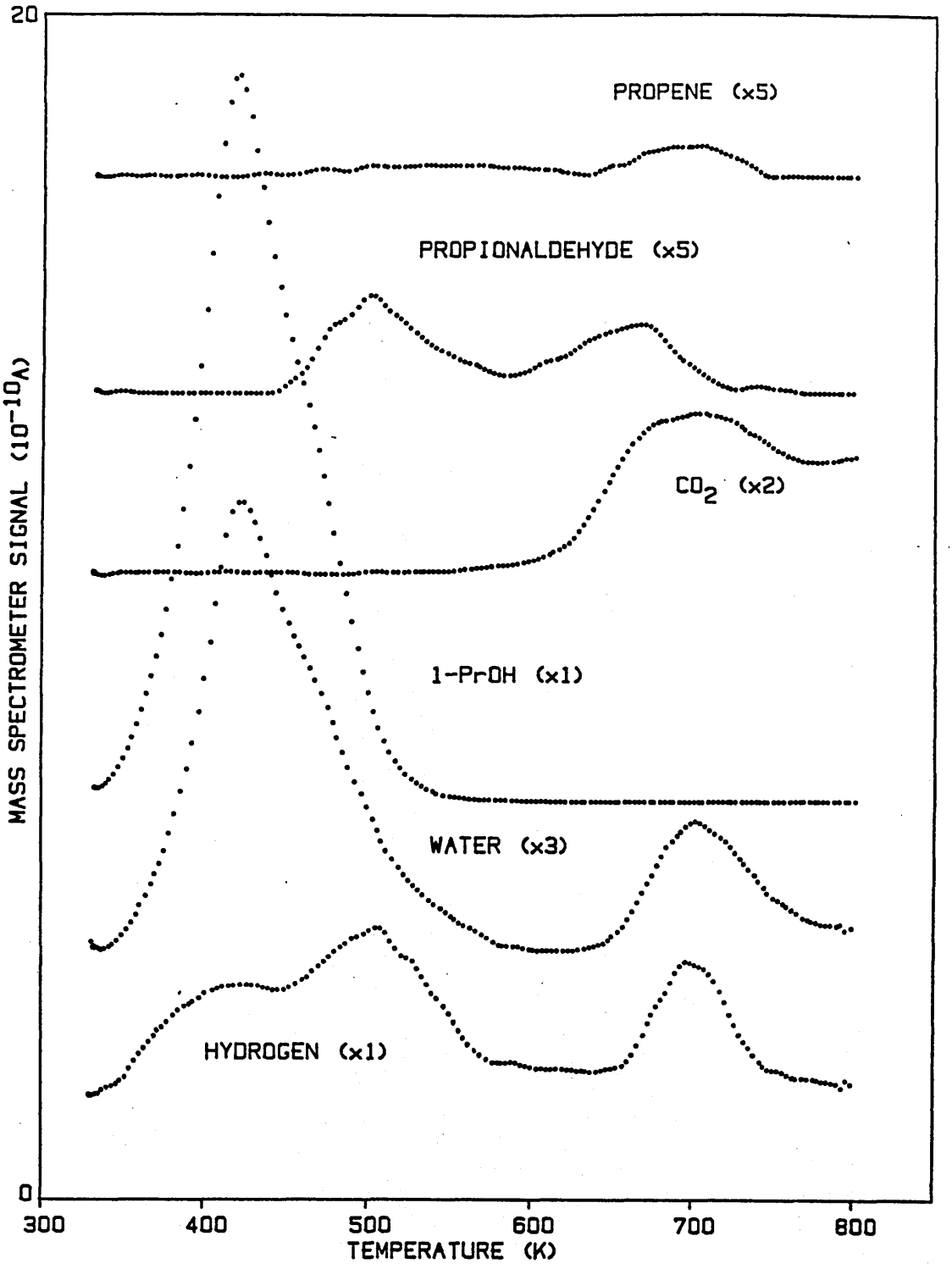

Figure 9.14: The desorption spectrum after adsorption of 1-propanol at 340 K to saturation coverage on 0.20 wt% potassium promoted zinc oxide.

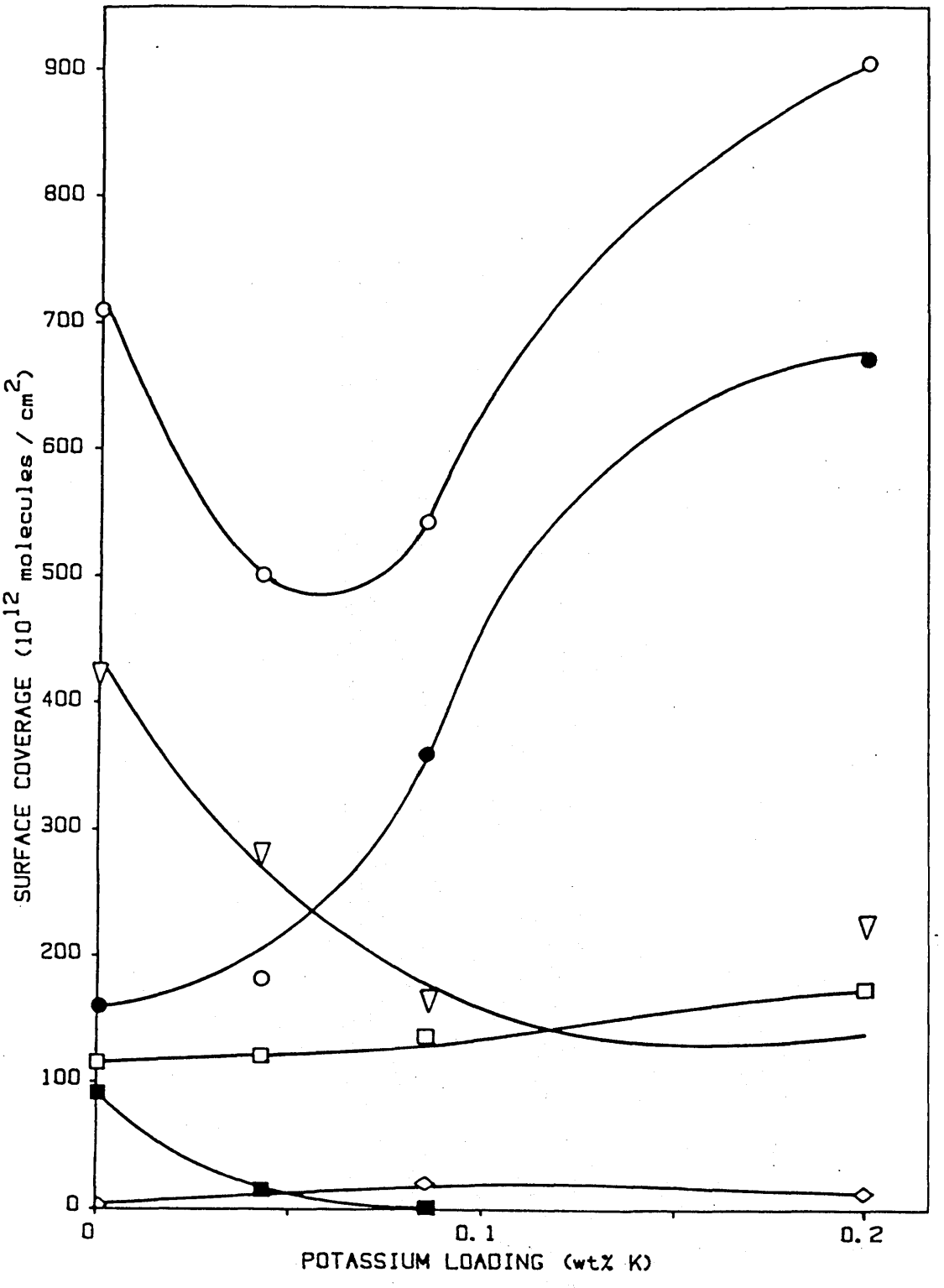

Figure 9.15: The effect of potassium loading on the desorption product surface coverages after adsorption of 1-propanol at 340 K to saturation coverage on promoted zinc oxide. ○ total coverage (excluding water); ■ propene; □ water; ▽ CO_2; ● 1-PrOH; ◇ propionaldehyde.

Table 9.2: The effect of potassium promotion on the main product desorption peak temperatures after adsorption of 1-propanol to saturation coverage at 340 K. The temperatures given in brackets indicate ill-defined or minor desorption states.

desorption product	potassium loading (wt% K)		
	0.042	0.085	0.20
1-PrOH	(357),404,(426)	402	404
water	406,443,(570),695	403,701	404,705
CO_2	710	692	(704)
propene	574	562	-
propionaldehyde	471	481	502
mass 29	637	648	666
hydrogen	475 568 693	499 (540) 694	504 (525) 695

Alkali promotion was found to enhance the propionaldehyde formation in an equivalent manner to that found for acetone after 2-PrOH adsorption on potassium promoted ZnO. The propionaldehyde peak temperature was also found to increase with potassium loading (table 9.2). The quantity of hydrogen desorbed coincident with propionaldehyde decreased with alkali loading consistent with the reduction in carboxylate formation. For the 0.20 wt% K catalyst the amount of hydrogen desorbed at 504 K was approximately 180×10^{12} H_2/cm^2.

The amount of water desorbed in the high temperature region was found to decrease, while an increase was observed in the low temperature peak at 404 K as the alkali loading was increased. This was similar to the behaviour previously described for both 2-PrOH where

the low temperature peak was attributed to the molecular adsorption of the water impurity injected with the alcohol. Also as found for 2-PrOH, the overall quantity of water was too high to be accounted for by the propene formation. However, for the 0.085 wt% amd 0.20 wt% K catalysts, the quantity of water desorbed at high temperature was in excess of the propene formed (although accurate estimation of the quantity of propene evolved was made difficult by the overlap in mass spectrometer cracking pattern with the large 1-PrOH peak). This suggested that some water may have been evolved through the carboxylate decomposition reaction.

Selectivity for oxidation was reduced by alkali promotion although the effect was not as pronounced as for 2-PrOH. This was consistent with the higher oxidation selectivity shown by 1-PrOH on unpromoted ZnO. At the highest loading of 0.20 wt% K, carboxylate formation still occurred as shown by the production of CO_2 and by the evolution of hydrogen in two peaks at 504 K and at 695 K (coincident with CO_2) respectively.

(9.2.2) Coverage Dependence

The coverage dependency of 1-PrOH decomposition selectivity after adsorption onto the promoted catalysts was found to follow the same trends as 2-PrOH adsorption onto the same catalysts i.e population of the remaining dehydration and oxidation sites occurred before the dehydrogenation and reversible adsorption sites. The degree to which the dehydration, dehydrogenation and oxidation reactions occurred and the extent of enhancement in reversible 1-PrOH desorption was dependent on the alkali loading (in a manner shown by the saturation coverage spectra described in the previous section).

The desorption spectra obtained after 1-PrOH adsorption on the 0.042 wt% K catalyst at low coverage (20% of saturation), and at medium coverage (60%), are given in figures 9.16 and 9.17, with the dependence of the surface coverages of the main desorption products with 1-PrOH dose shown in figure 9.18. At low coverage (approximately up to 20% of surface saturation) essentially only oxidation products were obtained, along with water present as an impurity in the injected alcohol. From approximately 30% coverage mass 29 desorption occurred with a peak initially at 657 K but decreasing to 637 K by surface saturation. The water and CO_2 peak temperatures also showed a slight dependence on coverage each decreasing by 10-15 K from low coverage to saturation, while the propene peak formed at 576 K remained at constant temperature with coverage. Propionaldehyde desorption did not occur until a dose of approximately 60-70% of surface saturation.

The corresponding low and medium coverage desorption spectra and the coverage dependency of the main desorption products for the 0.085 wt% K promoted catalyst are shown by figures 9.19 to 9.21. This catalyst behaved in an analogous manner to the 0.042 wt% K catalyst described above, but with decreased selectivities for both oxidation and dehydration, and with enhanced propionaldehyde formation. The lower overall decomposition selectivity was reflected in the appearance of both propionaldehyde and 1-PrOH at a lower fraction surface coverage than found for the 0.042 wt% K loading.

Similarly, the corresponding spectra for the 0.20 wt% K catalyst, along with the dose dependency of the product surface coverages, are given in figures 9.22 to 9.24. Only minor amounts of oxidation and dehydration occurred at all surface coverages on this catalyst, and as

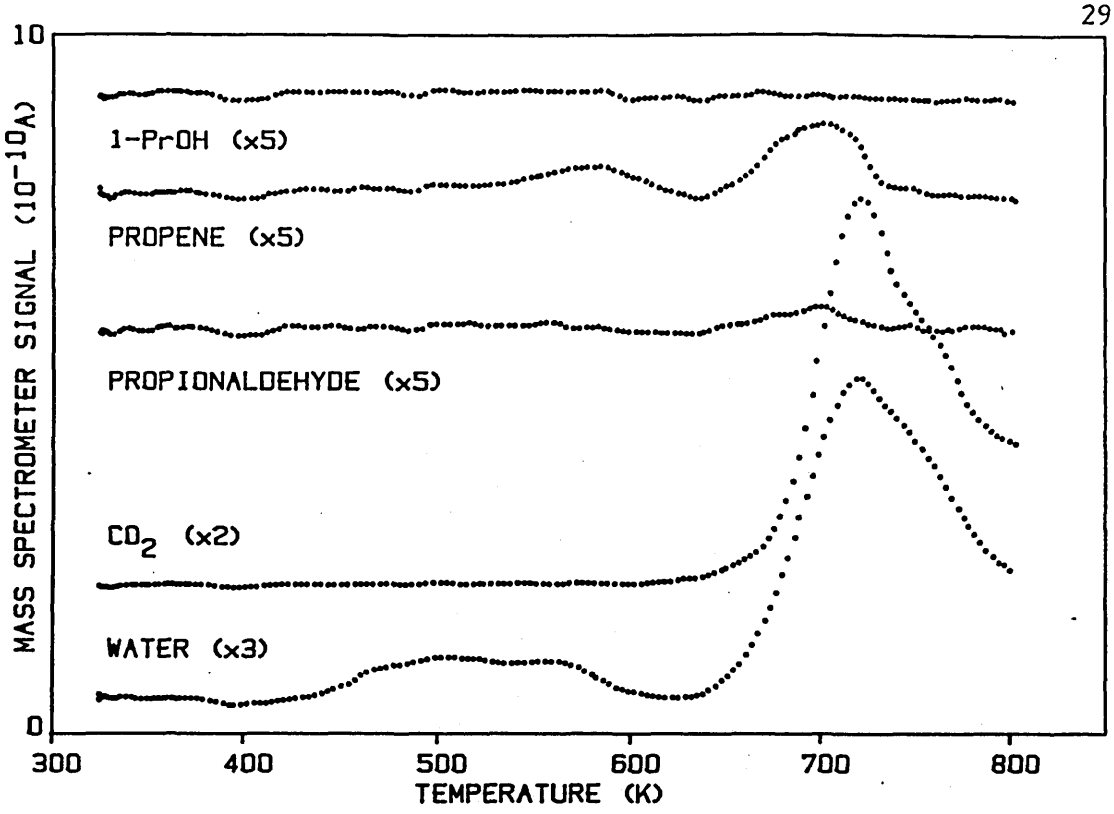

Figure 9.16: The desorption spectrum after adsorption of 1-propanol at 340 K to low coverage on 0.042 wt% potassium promoted zinc oxide.

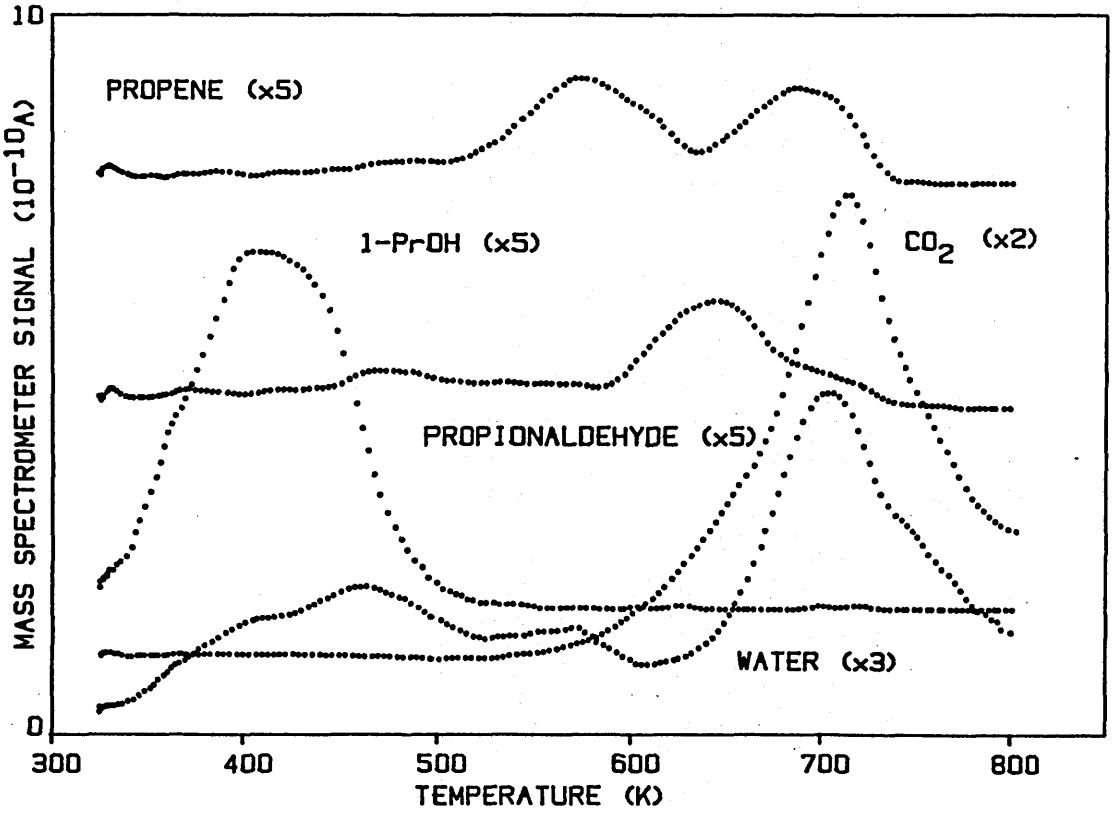

Figure 9.17: The desorption spectrum after adsorption of 1-propanol at 340 K to medium coverage on 0.042 wt% potassium promoted zinc oxide.

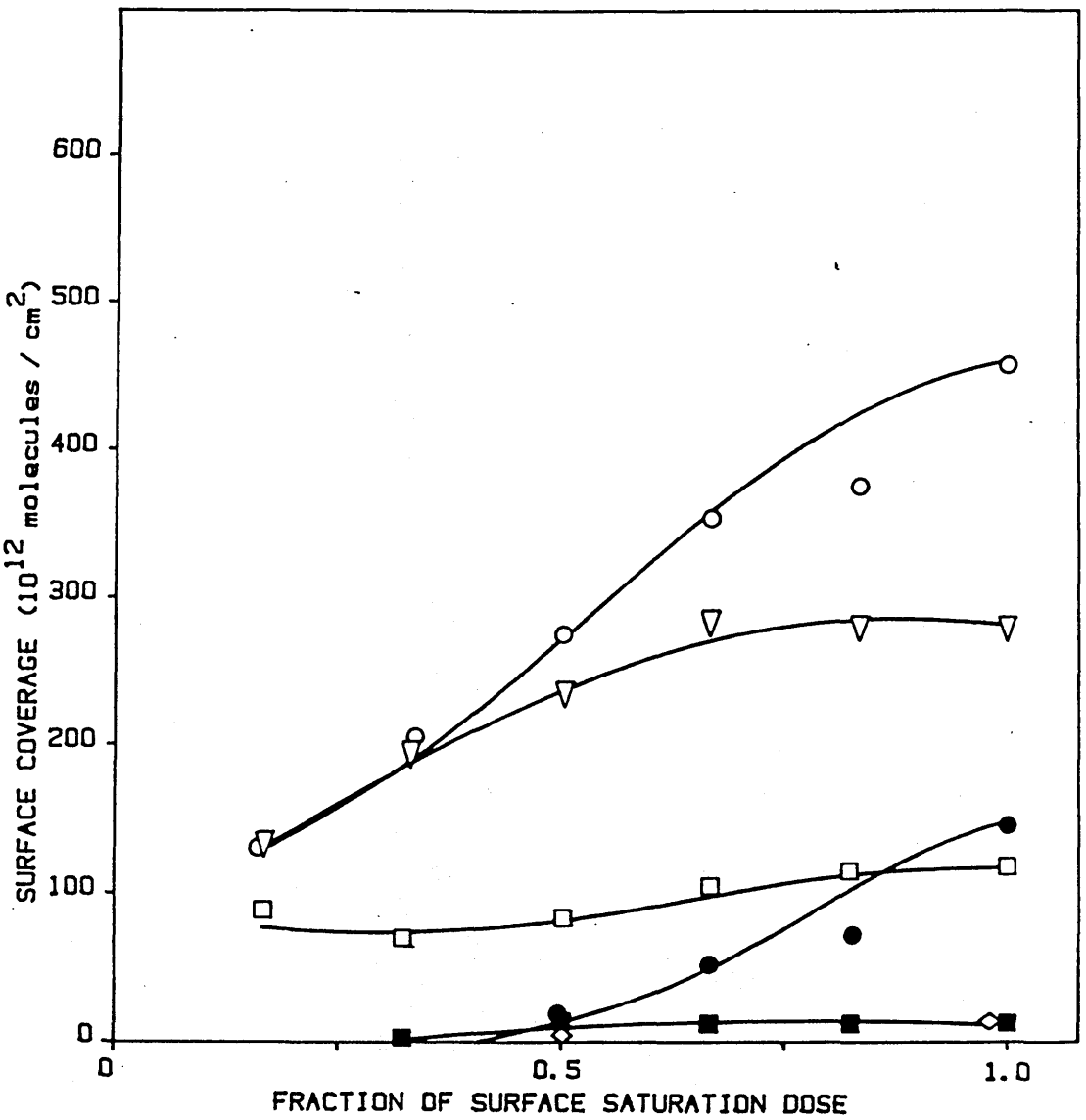

Figure 9.18: Plot of the desorption product surface coverages as a function of 1-propanol surface saturation dose at 340 K on 0.042 wt% potassium promoted zinc oxide. ○ total coverage (excluding water); ■ propene; □ water; ▽ CO_2; ● 1-PrOH; ◇ propionaldehyde.

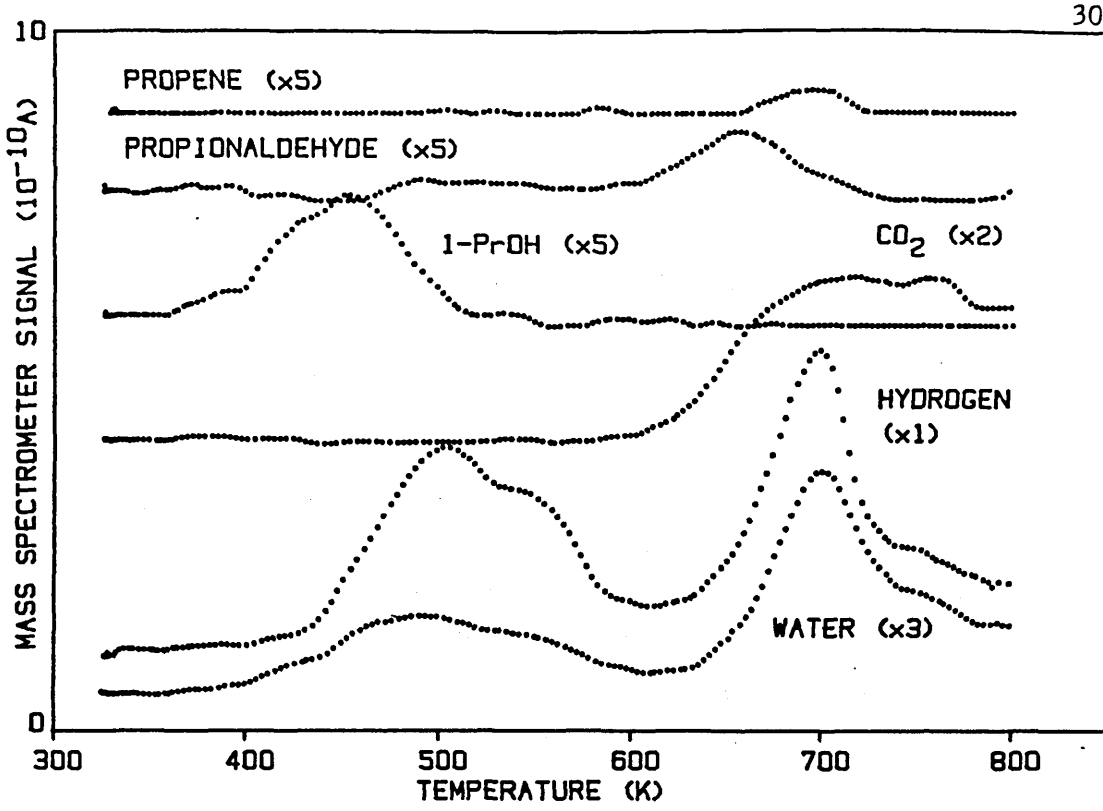

Figure 9.19: The desorption spectrum after adsorption of 1-propanol at 340 K to low coverage on 0.085 wt% potassium promoted zinc oxide.

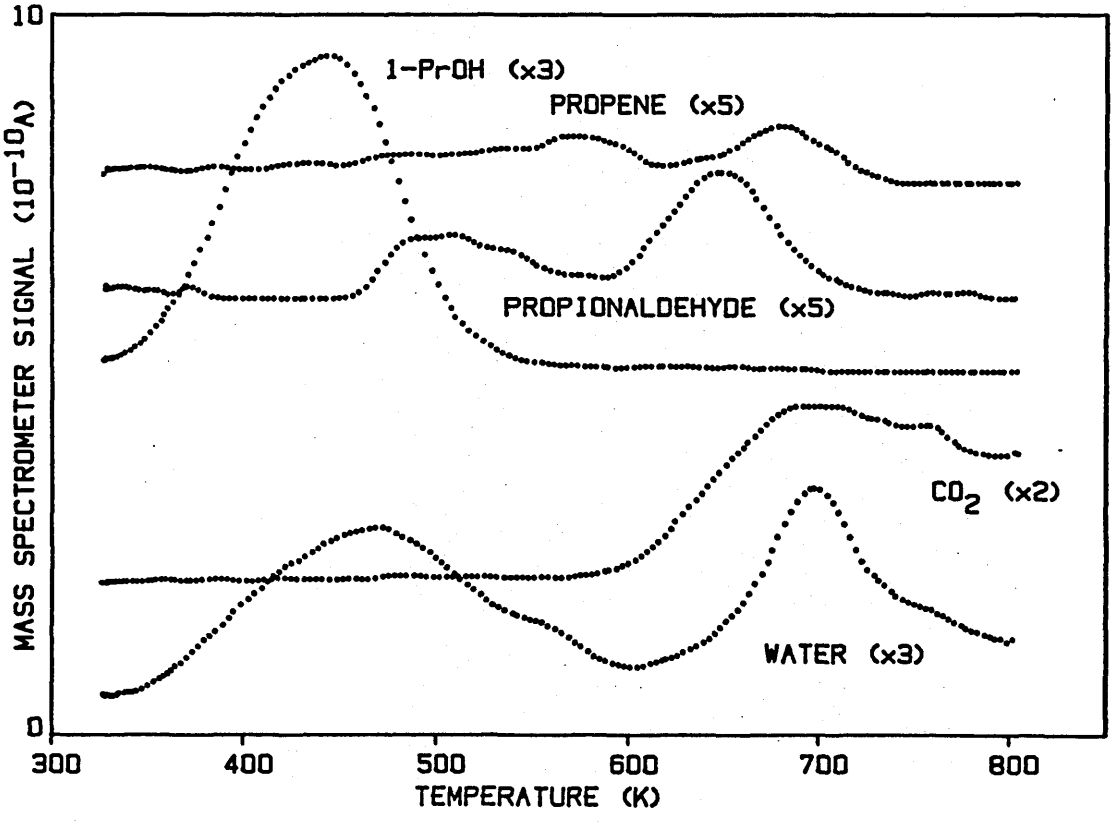

Figure 9.20: The desorption spectrum after adsorption of 1-propanol at 340 K to medium coverage on 0.085 wt% potassium promoted zinc oxide.

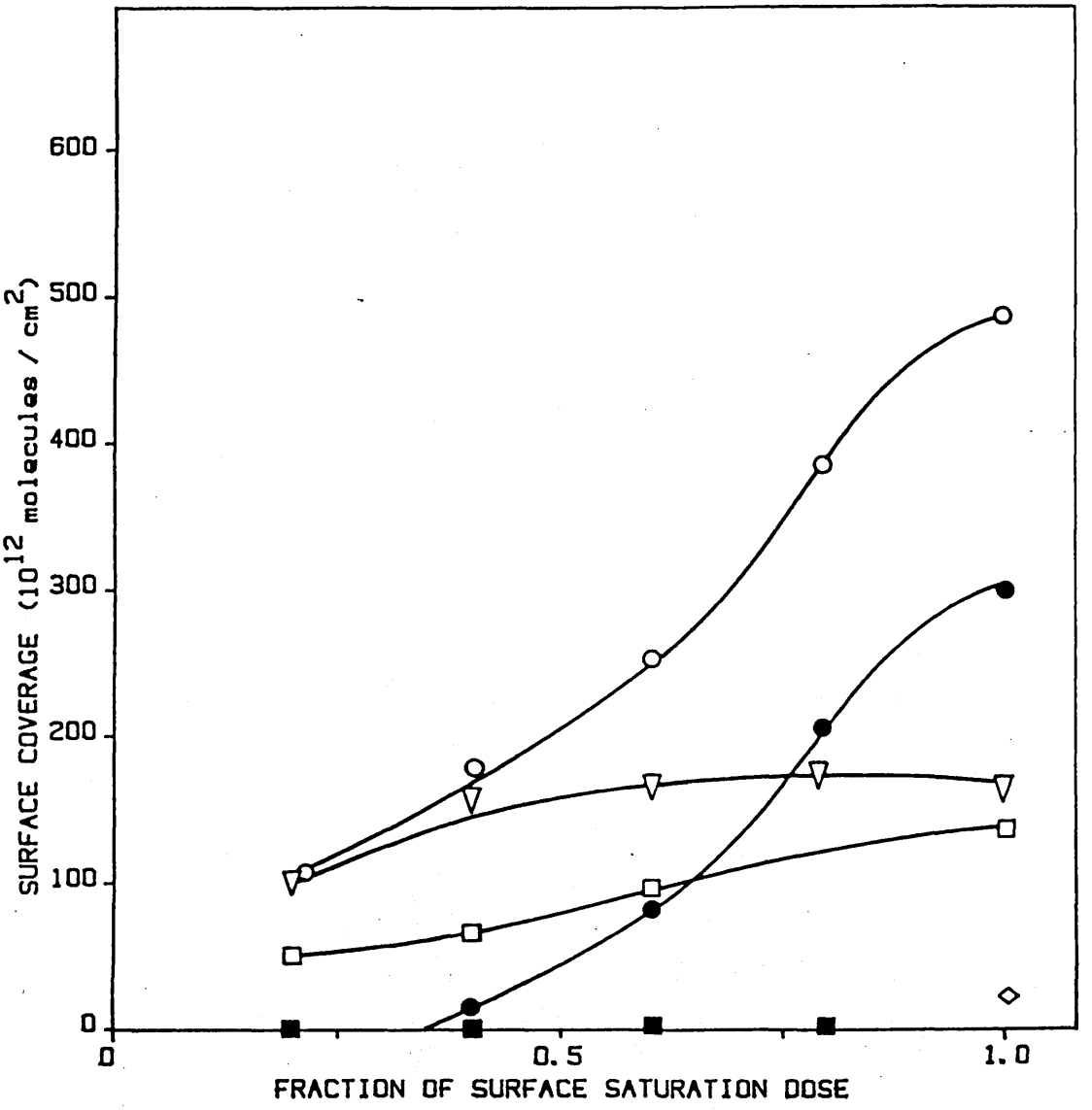

Figure 9.21: Plot of the desorption product surface coverages as a function of 1-propanol surface saturation dose at 340 K on 0.085 wt% potassium promoted zinc oxide. ○ total coverage (excluding water); ■ propene; □ water; ▽ CO_2; ● 1-PrOH; ◇ propionaldehyde.

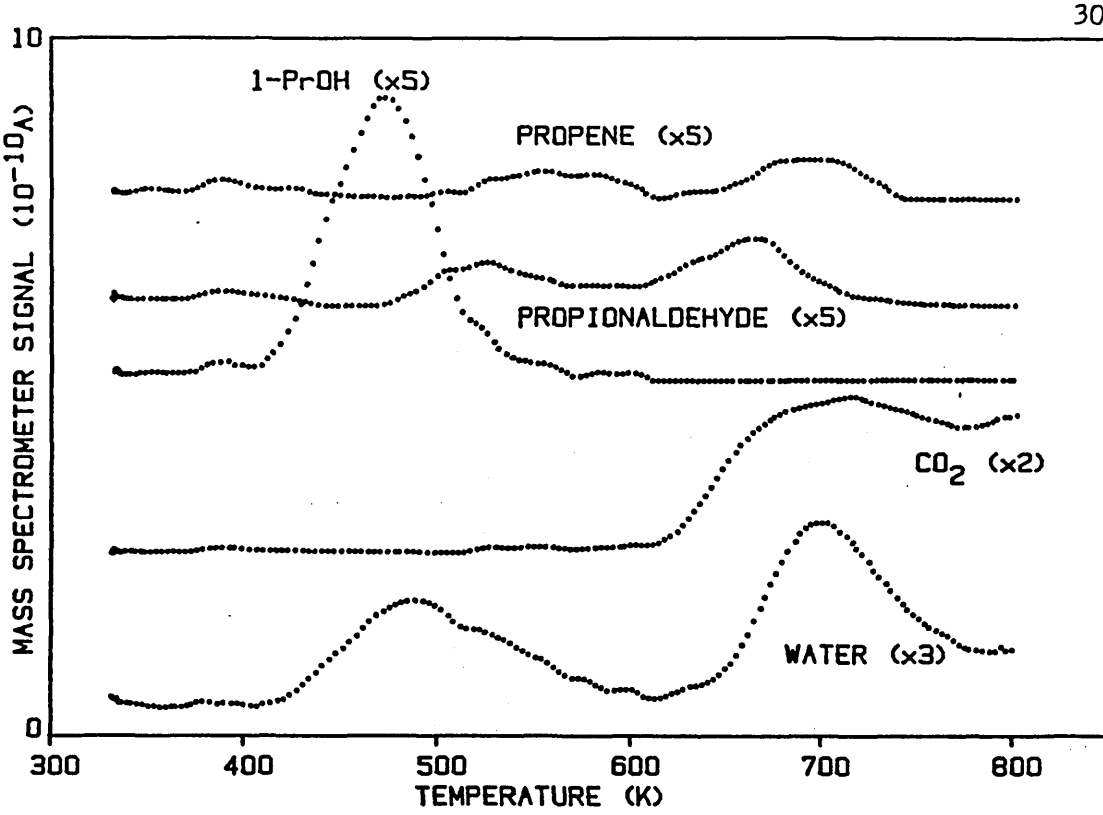

Figure 9.22: The desorption spectrum after adsorption of 1-propanol at 340 K to low coverage on 0.20 wt% potassium promoted zinc oxide.

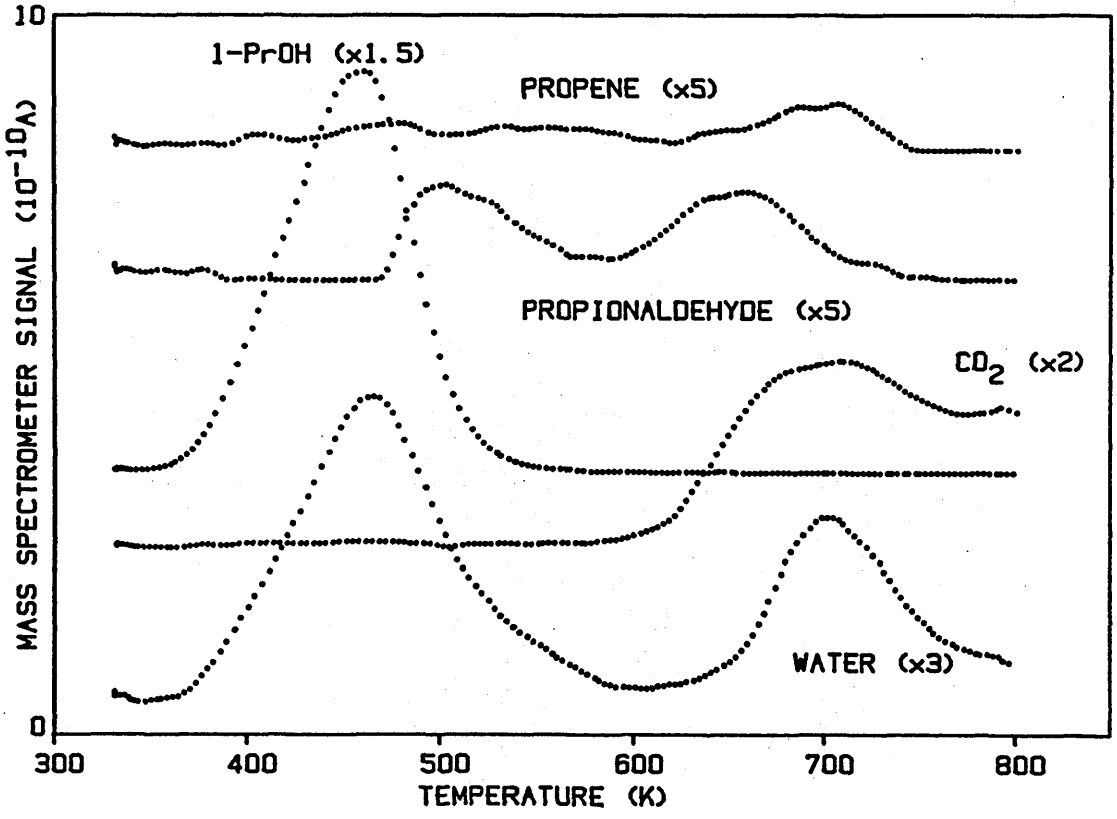

Figure 9.23: The desorption spectrum after adsorption of 1-propanol at 340 K to medium coverage on 0.20 wt% potassium promoted zinc oxide.

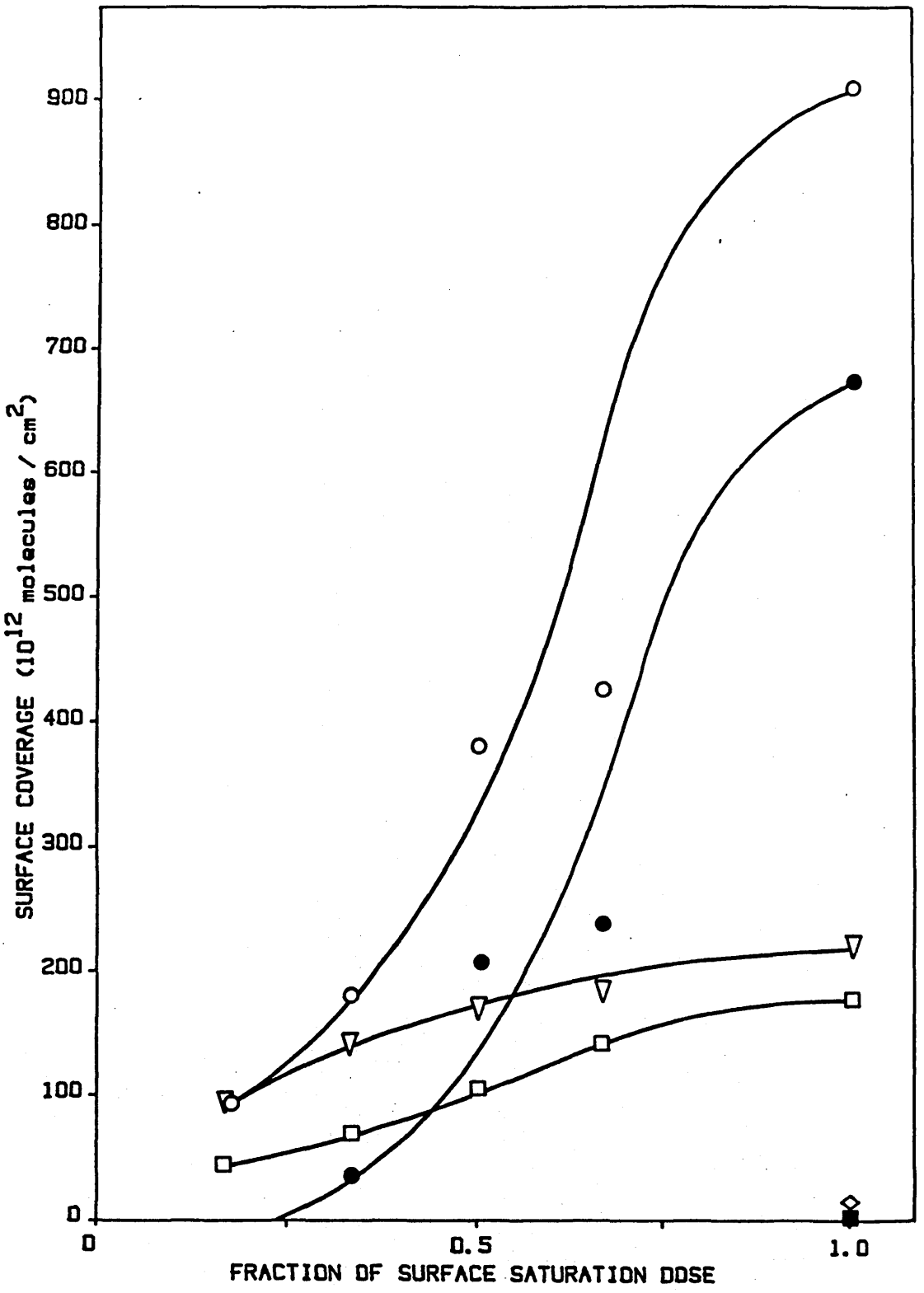

Figure 9.24: Plot of the desorption product surface coverages as a function of 1-propanol surface saturation dose at 340 K on 0.20 wt% potassium promoted zinc oxide. ○ total coverage (excluding water); ■ propene; □ water; ▽ CO_2; ● 1-PrOH; ◇ propionaldehyde.

a result, both propionaldehyde and 1-PrOH desorption peaks were evolved from low 1-PrOH dose. Only limited mass 29 desorption occurred, with the peak temperature not showing a coverage dependency (constant at approximately 663-668 K). Propionaldehyde formation was further enhanced, while the 1-PrOH peak, which dominated the desorption spectra for this catalyst, decreased in temperature with increasing dose from 472 K at low coverage to 404 K at saturation.

(9.3) Acetone

(9.3.1) Thermal Desorption and Decomposition Spectrum

The desorption spectra obtained after saturation doses of acetone at 330 K on the 0.042 wt% and 0.20 wt% K promoted catalysts are given in figures 9.25 and 9.26 respectively. From the 0.042 wt% K catalyst (figure 9.25) a large quantity of acetone was found to be desorbed (coverage approximately 170×10^{12} molecules/cm^2) in two overlapping states at 392 K and 510 K, with a further minor peak at 610 K. The CO_2 peak at 752 K corresponded to a carboxylate surface coverage similar to that obtained after acetone adsorption on unpromoted ZnO (approximately 220×10^{12} molecules/cm^2). A methane peak at 570 K was also evolved as a result of the surface oxidation reaction forming the carboxylate (see chapter 7) and at 770 K due to carboxylate decomposition. A single main propene peak was formed at 490 K (coverage 52×10^{12} molecules/cm^2) and also in an additional minor propene peak at 620 K. Water was produced in small peaks at approximately 408 K and 489 K, and in a larger peak at 712 K.

The desorption spectrum from the 0.20 wt% K catalyst (figure 9.26) gave a single acetone peak at the lower temperature of 367 K,

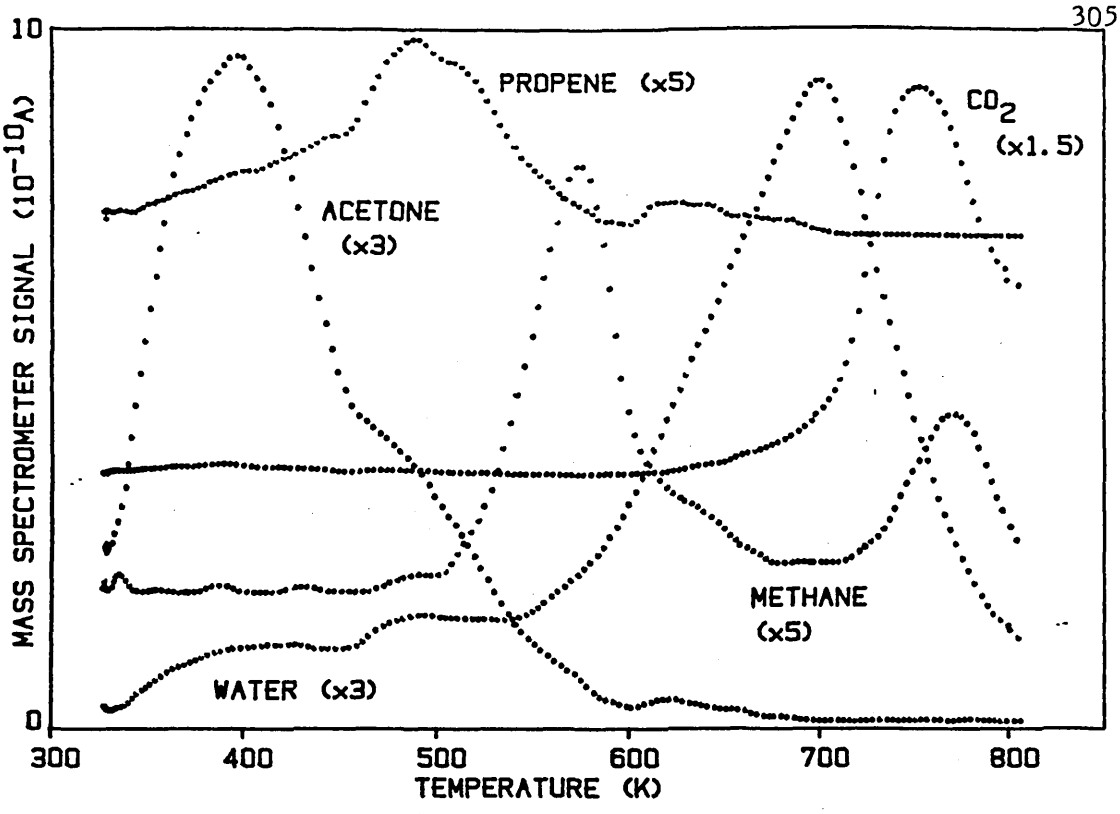

Figure 9.25: The desorption spectrum after adsorption of acetone at 340 K to saturation coverage on 0.042 wt% potassium promoted zinc oxide.

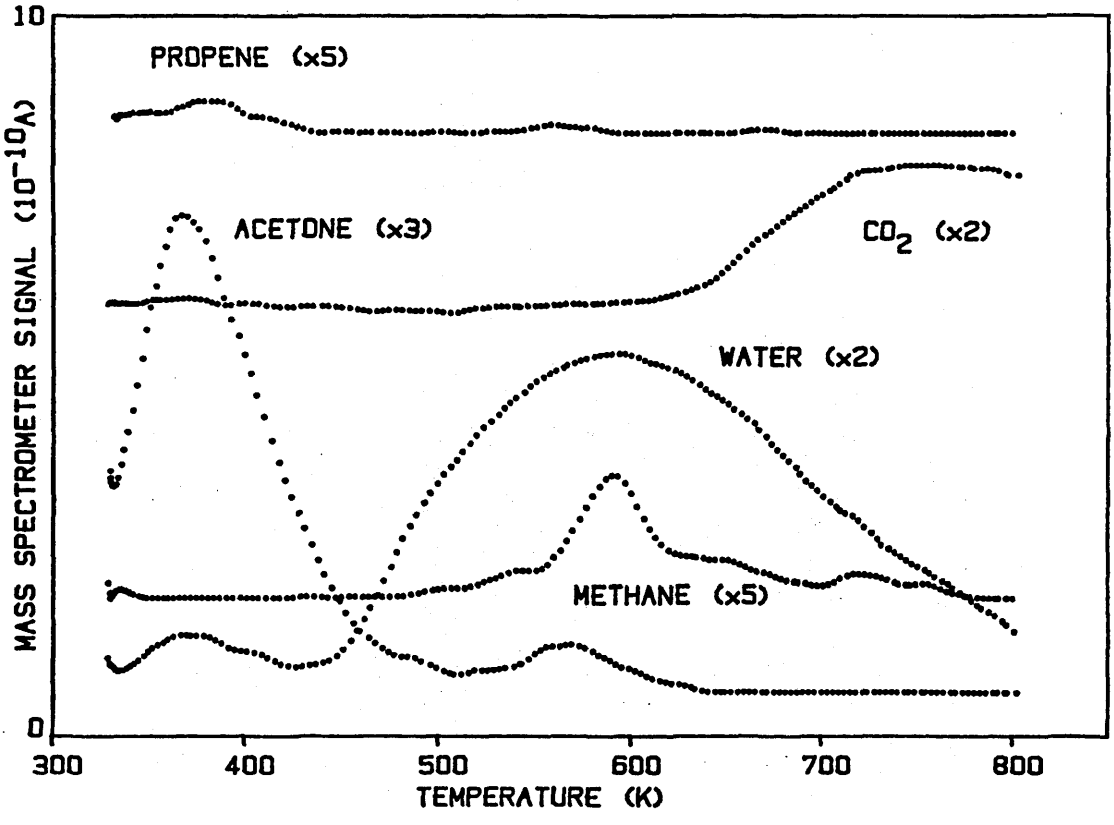

Figure 9.26: The desorption spectrum after adsorption of acetone at 340 K to saturation coverage on 0.20 wt% potassium promoted zinc oxide.

approximately 61 K lower in temperature than the peak obtained after adsorption on ZnO, with a further minor peak at 565 K. Coverage in the main peak was approximately 70×10^{12} molecules/cm^2. A large reduction in the CO_2 peak at 752 K indicated a lower amount of carboxylate was formed, confirmed also by a smaller methane peak at 588 K. No significant propene was evolved, while water was produced in a small peak coincident with acetone and in a large broad peak maximising at approximately 593 K.

(9.4) Discussion of Results

(9.4.1) Introduction

The results presented in this chapter have clearly established the effect of potassium promotion of ZnO with respect to the decomposition of 2-PrOH and 1-PrOH. The addition of potassium has been shown to lead to a suppression of the dehydration and oxidation surface reactions, and a reduction in the ability of the ZnO surface to adsorb water. The yields of dehydrogenation product and reversibly adsorbed alcohol were enhanced by potassium promotion. Points for discussion include the nature and location of the potassium promoter and its effect, if any, on the reaction mechanism.

(9.4.2) 2-Propanol

The principal effect of the potassium promoter is presumably to control the acid-base surface chemistry of the ZnO. The reduction in propene formation is consistent with the addition of potassium producing a more basic surface that suppresses the acid catalysed dehydration reaction. In 2-PrOH and acetone decomposition, only propene

was observed from the polar surfaces of unpromoted ZnO (see chapter 7). On the Zn (0001) surface the amount of propene produced from 2-PrOH is approximately one propene for each Zn^{2+} site, while for the O polar surface it is only 20% of this figure. These observations suggest a site specific effect by the potassium promoter.

As noted in chapter 6, single crystal studies have shown that potassium ions are much more strongly held on the O polar surface than the prism face because of the impurity stabilisation of the former [143]. Furthermore, the potassium ions would not be expected to diffuse into the lattice because of their large effective ionic radius compared to Zn^{2+} [144]. Krupay et al [148] investigating alumina promoted with K_2CO_3 followed the work of Stork and Pott [149] in suggesting that K^+ ions replaced the protons of surface hydroxyls to form OK species. The equivalence between the effects of adsorbed Cl^- (chapter 8) and that of adsorbed potassium can also be interpreted as evidence for the presence of the negatively charged OK^- species. These would be expected to be strongly held on the Zn polar surface of ZnO. In addition, XPS studies on the alkali promoted catalysts (described in Appendix 4) indicated that redistribution of the potassium occurred during decomposition of the K_2CO_3.

It seems likely then that the final alkali distribution, particularly for the lower loadings, may have been weighted towards the polar surfaces. The TPD results obtained after water adsorption on the promoted catalysts (chapter 6) confirmed this since alkali promotion was found to preferentially suppress the high temperature desorption peak attributed to hydroxyls on the Zn polar surface. It was further shown that the 0.085 wt% K catalyst loading corresponded closely to the potassium loading required for saturation of the polar

surfaces and that the water TPD spectrum obtained from this catalyst in fact showed the high temperature desorption peak attributed to the Zn polar surface to be absent. At the same alkali loading the α and γ propene which have been assigned to the Zn and O polar surfaces respectively were also suppressed.

Increased hydroxyl coverage produced by the coadsorption of water and 2-PrOH had an almost identical effect on the α and γ propene. Indeed, there appears to be a near equivalence between the effect of adsorbed hydroxyls and the potassium promoter at the lower loadings with respect to the dehydration to propene. These observations for the 2-PrOH behaviour present a consistent picture of the effect of the potassium promoter. The presence of potassium ions on the O polar face results in impurity stabilisation and a reduction in the number of defect sites, assumed to be oxygen vacancies[143]. Since the Zn^{2+} ions exposed at these oxygen vacancies are probably the sites for hydroxyl adsorption and at which the γ propene is produced, the addition of potassium will decrease the availability of sites for both 2-PrOH dehydration and water adsorption. On the Zn polar surface, the presence of OK groups will effectively prevent the dissociative adsorption of water or 2-PrOH which will again lead to suppression of the dehydration reaction forming propene. Overall, the addition of potassium deactivates the polar surfaces by blocking or removal of adsorption sites.

Assuming that saturation of the polar surfaces with potassium was achieved for the 0.085 wt% K catalyst, then the increased loading of 0.20 wt% K would have given a coverage of approximately 0.5 monolayers on the non-polar surfaces, although the distribution was not likely to

be as sharply defined. The increase in acetone formation attributed to this surface with alkali loading is consistent with the observed decrease in carboxylate formation. In the previous chapter, it was shown that a reduction in the tendency for surface oxidation, as a result of chlorine treatment, caused an increase in the dehydrogenation product yield. This was proposed to be due to the 'removal' of the availability of reactive surface oxygen required in carboxylate formation that led to an enhancement in the dehydrogenation reaction pathway through a common reaction precursor. A similar effect was observed after potassium promotion where carboxylate formation was also suppressed but the acetone yield increased. This suggests that potassium promotion also decreases the availability of reactive surface oxygen. Presumably this is due to a poisoning of surface anion sites through adsorption of K^+. However, compared to the effect of chlorine treatment, the increase in acetone yield was not as marked. Since potassium appears to be able to adsorb as OK^- species[149] (and as evidenced by the deactivation of the Zn polar surface), it is also likely that the adsorption of OK^- onto cations of the non-polar surface took place. As this will also reduce the cation sites available for adsorption of the acetone precursor, the effective acetone yield will be reduced, compared to that obtained after chlorine treatment, where the cation sites on the non-polar surface appear unaffected. Evidence for this loss of cation sites is shown by the reduction in the β propene formation (not found after chlorine treatment).

Although the results for 2-PrOH adsorption on promoted ZnO indicate a change in the selectivity of the resulting decomposition reactions, there did not appear to be a change in the fundamental mechanism of the decomposition. Consequently, the main effect of the

potassium appears to be that of a selective site poison, rather than a true promoter of the surface coverage of any 2-PrOH decomposition product precursor.

The increase in activation energy for 2-PrOH dehydrogenation as alkali loading increases could be attributed to an electronic effect. At first sight this result appears inconsistent with a previous study of potassium promoted ZnO catalyst by Sinha et al[150] who observed a decrease in the activation energy for 2-PrOH dehydrogenation. However, although the potassium loadings used in the present study are lower than those studied by Sinha et al, the effective surface concentration of potassium is probably much higher in the present catalysts. Consequently, the activation energy is observed to increase as described previously for lithium doped ZnO[150,151].

A decrease in the acetone desorption temperature was observed after acetone adsorption on the promoted catalysts compared to acetone desorption from unpromoted ZnO. This may be possibly related to a reduction in acetone adsorption as the enol species (due to a loss of Zn-O pair sites on the non-polar surface, since such sites are required for enol formation[116]) and an enhanced coverage of a more weakly bound form of adsorbed acetone. This is suggested in the result obtained from the 0.042 wt% K catalyst where two overlapping acetone peaks were obtained. The reduced acetone desorption temperature from promoted ZnO further confirms the enol not to be a stable surface species in the 2-PrOH dehydrogenation reaction (since acetone from 2-PrOH was increased on the promoted ZnO).

Lui et al[114] concluded in their single crystal study that the presence of small, but detectable, amounts of surface impurities

including potassium, did not appear to affect the behaviour of their single crystal surfaces toward 2-PrOH decomposition. However, the lack of any observed CO_2 desorption and the low propene to acetone ratios found, combined with the earlier water desorption results of these workers [85], correlate with the results obtained for the alkali promoted catalysts rather than the pure ZnO used in the present study and suggest the crystal surfaces used by Lui et al to be alkali contaminated.

(9.4.3) 1-Propanol

A site specific interpretation of the effect of potassium promotion on 1-PrOH decomposition is less obvious from the 1-PrOH results alone, largely due to the high selectivity toward oxidation shown by 1-PrOH compared to 2-PrOH. Where propene formation from 2-PrOH clearly showed the crystal face dependent effect of the promotion, this was obscured for 1-PrOH where the tendency was for oxidation to occur on both Zn polar and non-polar surfaces. However, although such a site dependent interpretation of potassium promotion is not as clear, the overall effects of promotion on 1-PrOH decomposition can still be seen to be equivalent to the behaviour of 2-PrOH. In particular, the main effects of potassium promotion were to suppress the dehydration and oxidation reactions and to enhance the dehydrogenation yield. The amount of reversibly adsorbed 1-PrOH was also greatly enhanced. These results then allow the effect of alkali promotion toward 1-PrOH decomposition to be interpreted on an equivalent basis to 2-PrOH.

The reduction in overall surface acidity caused by the alkali addition is again seen to lead to a suppression of the acid site catalysed dehydration reactions through site site blockage on the

polar surfaces, and to a lesser extent, of cation sites on the non-polar surface in the manner proposed for 2-PrOH. Also on the non-polar surface, potassium adsorption (as K^+) onto surface anion sites reduces the availability of surface oxygen for participation in carboxylate formation. This has the effect of suppressing the oxidation reaction in favour of the dehydrogenation reaction pathway through the common reaction precursor. The increase in dehydrogenation product is not as marked as found after chlorine treatment, due to the additional loss of cation sites to adsorbed OK^- reducing the availability of dehydrogenation precursor sites.

CHAPTER 10

DESORPTION AND DECOMPOSITION ON ICI HIGH SURFACE AREA ZINC OXIDE

(10.1) Introduction

The ICI high surface area ZnO provided a catalyst sample that was more representative of the type of ZnO currently used as a component of methanol synthesis catalysts. The TPD behaviour of this ZnO was investigated with respect to water adsorption and 2-PrOH decomposition, in order to see if the results could be interpreted in terms of those obtained from the AnalaR grade ZnO studied. The purity specifications of the ICI high surface area ZnO, given previously in table 4.6, showed this catalyst to contain a significant level of sodium (0.12 % Na_2O). As chapters 8 and 9 have demonstrated the TPD behaviour of the lower surface area (AnalaR) ZnO to be very sensitive to the presence of surface contaminants, it was anticipated that the desorption spectra from ICI high surface area ZnO would be influenced by the presence of the alkali. The catalyst was not, however, rigorously investigated with respect to its desorption and decompositional behaviour.

(10.2) Water

(10.2.1) Thermal Desorption Spectrum

The thermal desorption spectrum obtained after a saturation dose of water (by injection) at 340 K onto the ICI high surface area ZnO is shown in figure 10.1. The spectrum was similar to the water desorption spectrum obtained from ZnO (given in section 6.1) in that it was

dominated by desorption at high temperature. The coverage dependence of the spectrum (described below) revealed the high temperature desorption to consist of a sharp peak at 716 K overlapped with a broad underlying peak at approximately 670 K. The coverage in the high temperature peak at 716 K was determined to be 23×10^{18} H_2O/g (with a total saturation coverage of 78×10^{18} H_2O/g). This coverage is expressed on a weight basis since the surface area of this catalyst was found to decrease significantly with use (see section 5.2.1). This was revealed by a reduction in the high temperature peak, and appeared to be more rapid after experiments where larger doses of water had been made.

The spectrum contained three main desorption states at 716 K, 603 K and approximately 402 K. Estimates of the adsorption energies for these states are given in table 10.1, based on the preexponential factor of 5×10^{9} s^{-1} determined for water desorption from ZnO in section 6.1.

If a pretreated ICI high surface area ZnO sample was left exposed to air overnight, adsorption of atmospheric water was found to give the spectrum of figure 10.1, but with the addition of a small desorption peak at 476 K. This indicated that there was some slow water adsorption onto the catalyst surface.

(10.1.2) Coverage Dependence

The coverage dependence of the water desorption spectrum was investigated for doses in the range 10% to 50% of surface saturation. Higher doses were found to cause sintering which resulted in a reduced high temperature desorption peak as noted above. The coverage dependent characteristics of the water spectra were similar to those found

Table 10.1: The water desorption peak temperatures and estimated adsorption energies after water adsorption to saturation coverage at 340 K on ICI high surface area zinc oxide.

peak temperature (K, ±2)	adsorption[(a)] energy (kJ/mol)
716	155
670	145
402	85

(a)= estimated using the Redhead Equation, based on a preexponential factor of 5×10^9 s^{-1}.

for ZnO (section 6.1.1); at low coverage the most stable desorption states were selectively populated, and as the surface coverage was increased, there was gradual population of the lower temperature states. Where previously the α peak temperature from ZnO was found to increase with dose, the similar peak from ICI high surface area ZnO was found to decrease in temperature from approximately 748 K at low coverage to 716 K at saturation.

(10.3) 2-Propanol

(10.3.1) Thermal Desorption and Decomposition Spectrum

The desorption spectrum obtained after a saturation dose of 2-PrOH at 340 K onto ICI high surface area ZnO is given in figure 10.3, with peak temperatures and quantities desorbed given in table 10.2.

2-PrOH was found to desorb in a single peak at 414 K, a similar temperature to the reversible desorption peak previously found from

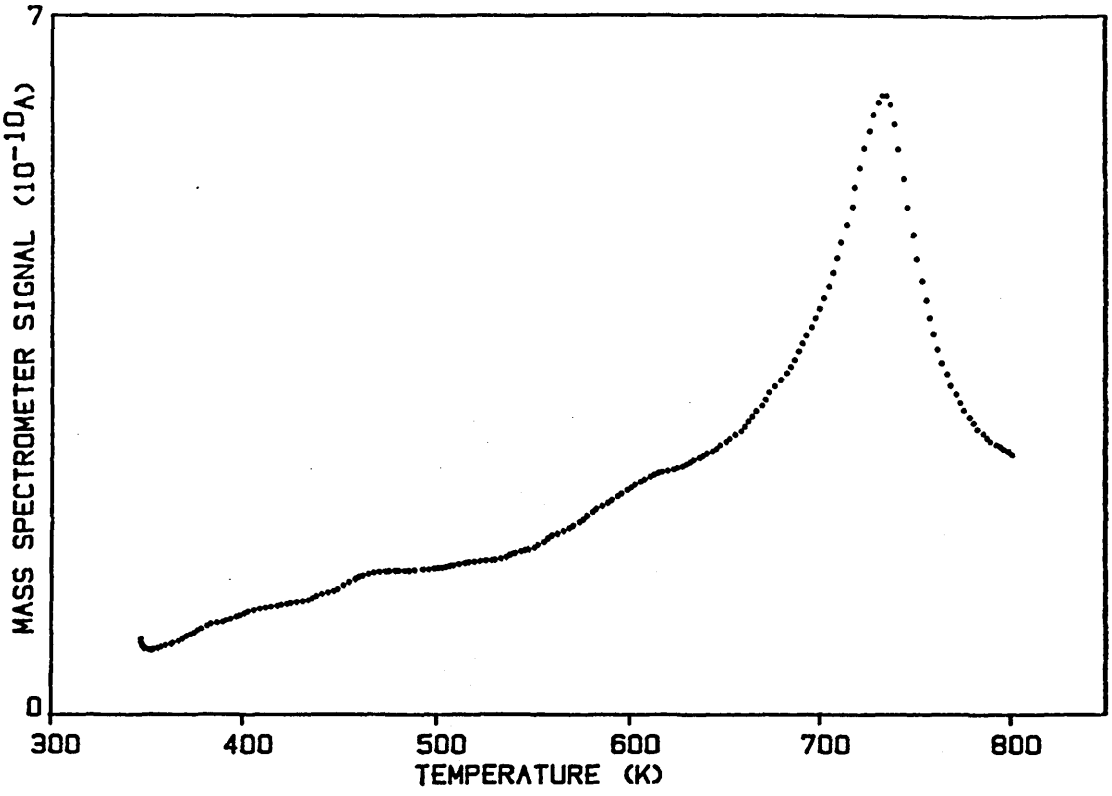

Figure 10.1: The water desorption spectrum after adsorption at 340 K to saturation coverage on ICI high surface area zinc oxide.

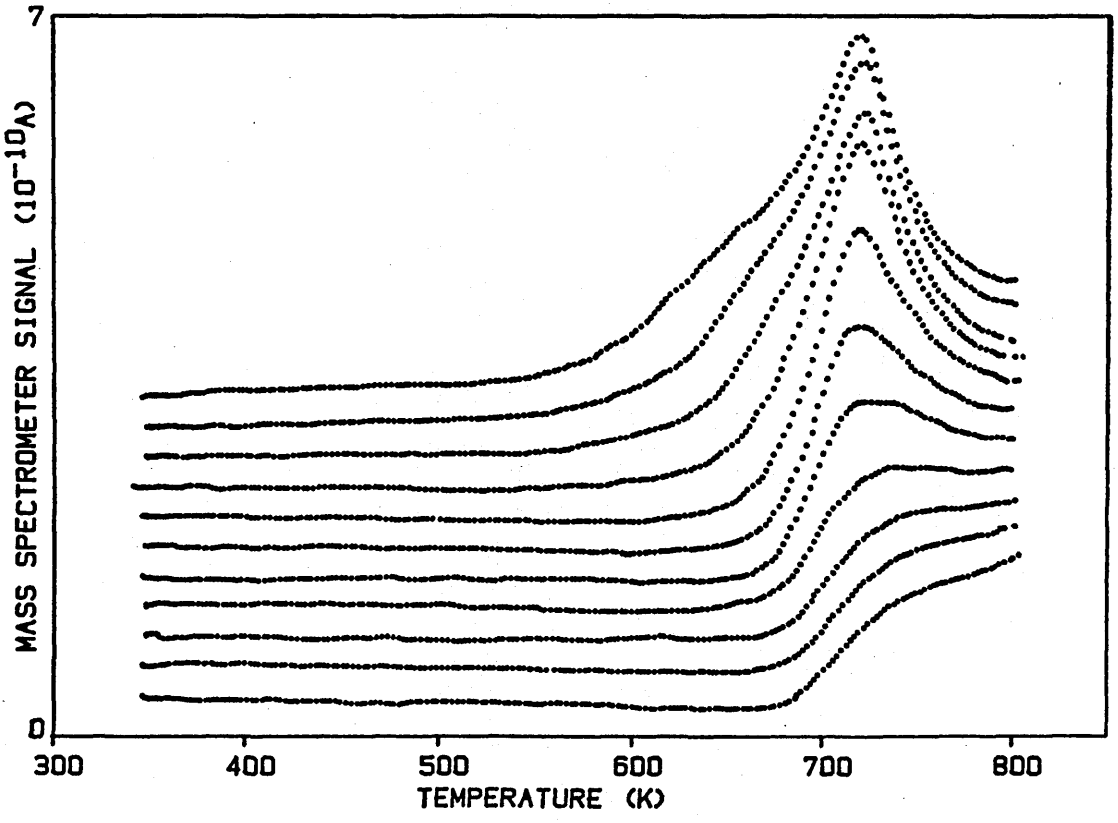

Figure 10.2: The coverage dependence of the water desorption spectrum after adsorption at 340 K on ICI high surface area zinc oxide.

Table 10.2: The desorption products, peak temperatures and saturation surface coverages following 2-propanol adsorption at 340 K on ICI high surface area zinc oxide.

desorption product	peak temperature (K, ±2)	quantity desorbed (10^{18} molecules/g)
2-propanol	414	6.2
acetone	449	6.2
propene	490	19
	554	9.3
CO_2	765	16
water	421	12
	487	1.2
	723	27

ZnO and potassium promoted ZnO. Acetone also desorbed in a single peak at 449 K.

Propene desorbed in two peaks; a main desorption state at 490 K and an overlapping shoulder at 554 K. The effect of a low maximum heating temperature (so that the high temperature water was not desorbed) was to suppress the desorption in the 554 K peak, but not the 490 K peak, consistent with an independence between the propene sites. The site dependence of these peaks is considered further in the discussion.

A broad water peak was formed at a similar temperature to 2-PrOH, with a further minor water peak coincident with propene at 490 K (propene to water ratio approximately 15:1). The bulk of the water, however, did not desorb until high temperature. The total amount of propene desorbed was in agreement with the sum of the water produced

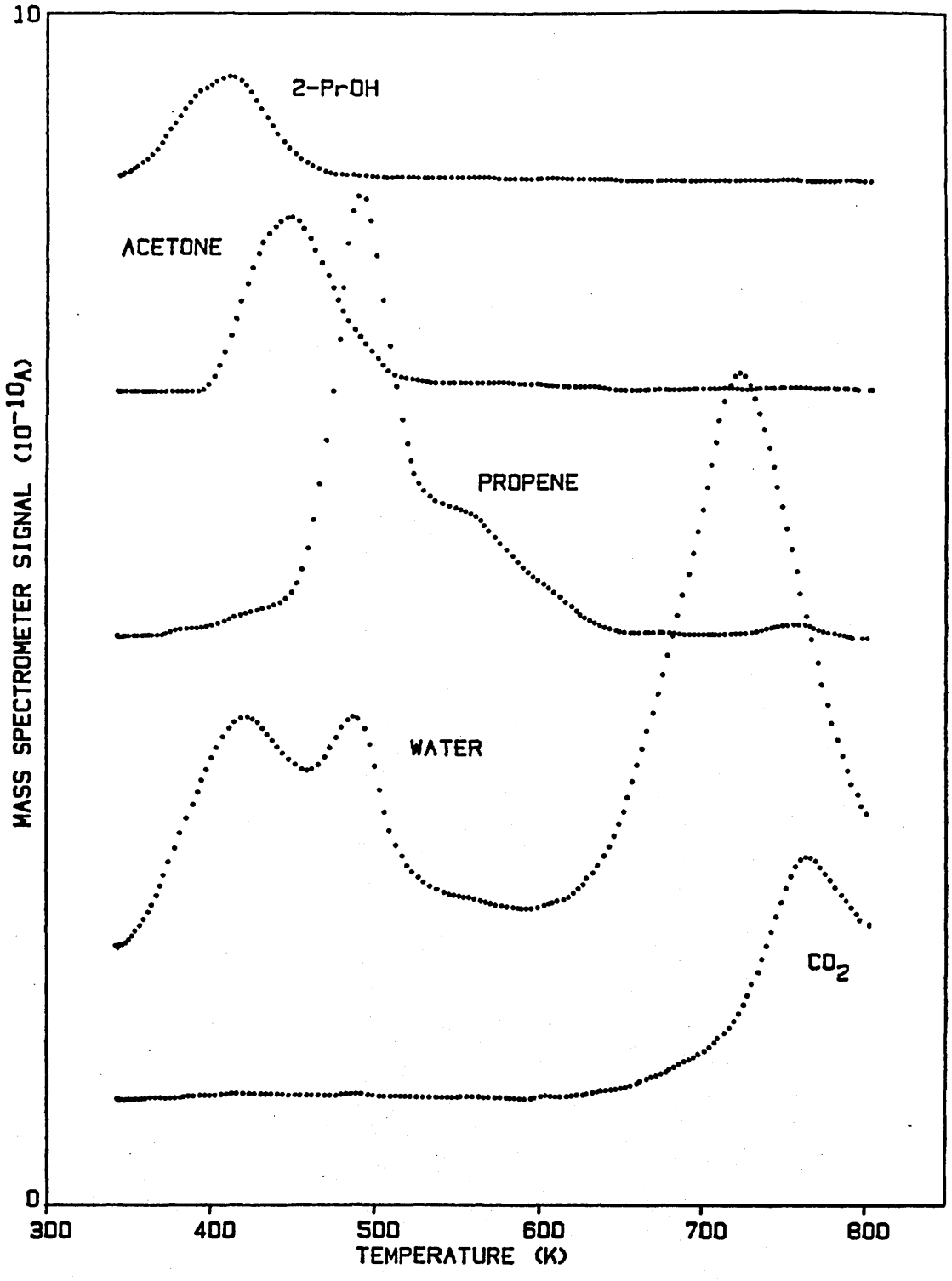

Figure 10.3: The desorption spectrum after adsorption of 2-propanol at 340 K to saturation coverage on ICI high surface area zinc oxide.

in the small peak coincident with the propene and in the high temperature peak.

CO_2, derived from surface carboxylate decomposition, desorbed in a single peak at 765 K, coincident with a small amount of mass 41 desorption (possibly propene). Methane and hydrogen desorption were not monitored during these desorption experiments.

(10.3.2) Coverage Dependence

The 2-PrOH desorption spectrum obtained after a low 2-PrOH dose (approximately 15% of saturation) at 340 K is shown by figure 10.4. This shows the decomposition at low coverage to be selective toward dehydration to propene and oxidation to the carboxylate. Both propene peaks were clearly formed, as was the high temperature water peak and an ill-defined high temperature CO_2 peak. No acetone or 2-PrOH desorption peaks were evolved.

(10.4) Discussion of Results

As noted in the introduction to this chapter, the main purpose of this study of the ICI high surface area ZnO was to determine if the apparent high sodium content evident in the catalyst purity specifications had any influence on the TPD behaviour of this catalyst and, if so, whether this effect could be interpreted on the basis of the results obtained for potassium promotion. The assumption is made that sodium will behave in a similar manner to potassium toward modifying the catalyst TPD behaviour. Although sodium promotion was not specifically investigated to verify this, since the effect of potassium promotion has been shown in chapter 7 to be able to be interpreted largely on the basis of selective site poisoning, it is reasonable to

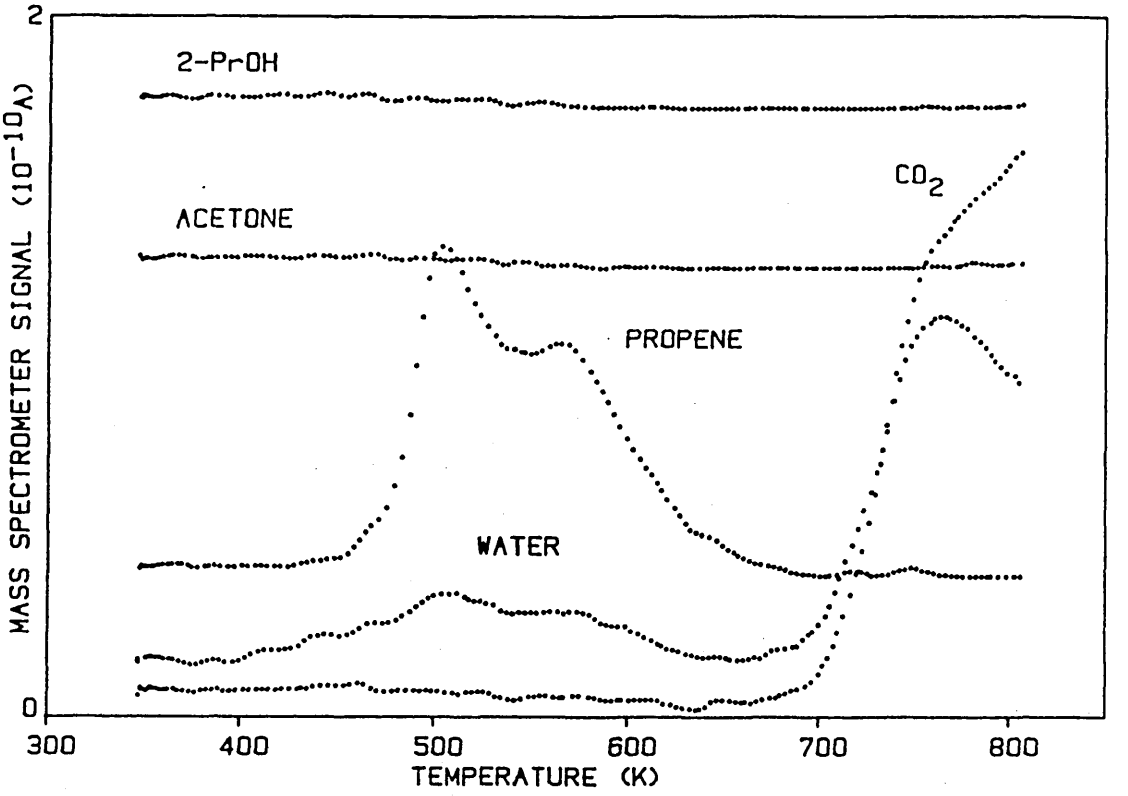

Figure 10.4: The desorption spectrum after adsorption of 2-propanol to low coverage at 340 K on ICI high surface area zinc oxide

assume that since sodium is also an alkali metal, it will act as a site poison which would modify the desorption and decomposition behaviour of the catalyst in a similar way. The effects of sodium promotion of alumina toward alcohol decomposition reported by Deo et al[111,112] further suggest that this would be the case.

The water desorption spectrum showed the quantity of water desorbed in the sharp high temperature state to be approximately 23×10^{18} H_2O/g. On the basis of the behaviour of ZnO described in the previous chapters, this must be associated with the Zn polar surface. Assuming a 10.5 $Å^2$ cross sectional area for the adsorbed hydroxyls[91], this corresponds to an area of 2.4 m^2. Relating this to the total surface area in order to estimate the fraction of the total surface area gives, for a fresh catalyst at 43 m^2/g, a fraction of 6%, while for a 'used' catalyst at 20 m^2/g, the fraction is 12%. These

represent extreme surface area values, so the true result will lie between the two figures.

The fraction of total polar surface for this catalyst has been previously estimated to be 33%[98] (see section 5.2.2), giving a fraction of Zn polar surface of around 17%. However, since the fraction of active Zn polar surface determined from the hydroxyl coverage is significantly lower than this, it shows a significant number of the cation sites appear to be inactive. After the behaviour of potassium on ZnO, this result is consistent with the presence of adsorbed sodium on this surface.

If the measured 23×10^{18} H_2O/g corresponds to adsorption on unblocked cation sites, then the number of 'blocked' Zn polar surface sites is in the range $25\text{-}79 \times 10^{18}$ g^{-1} (for the measured surface area range and assuming a surface ion density of 1.4×10^{15} cm^{-2} [115]). If only sodium is assumed to be causing the site blockage, then this corresponds to the presence of $(240\text{-}750) \times 10^{-6}$ g Na/g or a Na_2O content of 0.03-0.10 wt% (for the 25% Na coverage required to give impurity stabilisation of these cations[143,144]). A value for the Na level of 0.12 wt% Na_2O has been given in table 4.6. Taking into account the approximations used in this calculation, for example, in assuming the fraction of Zn polar surface present, the calculated Na_2O content cannot be anything more than a very approximate estimation. However, what this result does indicate is that a significant fraction of the sodium may be present on the catalyst surface, and that its presence on the Zn polar surface reduces the number of cation sites.

The 2-PrOH TPD spectrum also appears similar to those previously obtained for potassium promoted ZnO given in chapter 9. In

particular, propene formation in the peak at 554 K, equivalent to α propene produced from ZnO (section 7.1) and assigned to the Zn polar surface, has a low coverage showing a reduced number of 2-PrOH dehydration sites to be available compared to the total in the estimated 17% fraction of Zn polar surface. This again is consistent with the presence of adsorbed sodium. The quantity of propene in this peak is lower than in the water peak also associated with the polar surface (described above), although given the possibility of different degrees of sintering between the experimental samples, it is not clear whether this difference is significant. The lack of any propene peak equivalent to γ propene from ZnO, also shows the O polar surface sites to possibly deactivated in a similar manner, as expected from the behaviour shown by potassium on ZnO. The total quantity of water desorbed (excluding the low temperature peak at 414 K associated with 2-PrOH desorption) is in good agreement total amount of propene desorbed. As most of this water is produced at high temperature, it also shows that readsorption of water produced by propene formation at 490 K (equivalent to β propene from ZnO) was significant. The formation of a small high temperature CO_2 peak indicates that only a small amount of oxidation to the carboxylate took place, a result also in line with the presence of the alkali.

Although a more quantitative analysis of the behaviour of this catalyst would require further experimental work, the results demonstrate that the main features of the desorption spectra obtained from the AnalaR grade ZnO, and by the same catalyst promoted with potassium, can be used to interpret the TPD behaviour of ICI high surface area ZnO.

CHAPTER 11

DISCUSSION AND CONCLUSIONS

(11.1) Propanol Decomposition on Zinc Oxide

A mechanism has been proposed for the temperature programmed decomposition of 1-PrOH and 2-PrOH on ZnO based on an interpretation of the experimental results of this study. In this scheme both alcohols adsorb dissociatively to form a surface alkoxy species which undergoes further surface reaction during catalyst heating, leading to the formation of dehydration, dehydrogenation and oxidation products. A common alkoxy intermediate is proposed as a precursor for both the dehydrogenation and oxidation reactions, with selectivity for the two reaction channels determined by the availability of reactive oxygen adjacent to the alkoxy; if this oxygen is present then oxidation forming a carboxylate occurs, and if not, then the alkoxy desorbs as the dehydrogenation product. Although an enol type intermediate was found not to a stable surface species, its presence in the reaction as a short lived intermediate was evidenced by common decomposition pathways for 2-PrOH and acetone.

This reaction mechanism is in agreement with the scheme recently reported by Chan and Griffin[95] for methanol decomposition on ZnO. Chan and Griffin propose a short lived CH_2O surface intermediate as a common precursor in the formation of both the formaldehyde dehydrogenation product, and the surface formate. The reaction selectivity is determined by the availability of O^{2-} anions in an equivalent manner as in the common dehydrogenation/oxidation step proposed for propanol decomposition from this present study. Although Bowker et al[108]

have found methanol decomposition on ZnO to behave in an apparently anomolous way with respect to higher alcohol decomposition, the above conclusion suggests that a single general alcohol decomposition scheme for ZnO can be written.

The overall decomposition selectivity is different for 1-PrOH and 2-PrOH; the dominant decomposition reactions for 2-PrOH are dehydration and oxidation via a surface carboxylate, while for 1-PrOH, the decomposition is highly selective toward oxidation. This difference in selectivity can be interpreted as a measure of the relative rates of α and β hydrogen elimination between the two alcohols and is proposed to be related directly to structural differences.

The crystal face dependence of the decomposition reactions has also been determined. For 2-PrOH, all three decomposition reactions take place on the non-polar surface, but only dehydration occurs on the Zn polar surface. On the O polar surface limited dehydration also occurs in association with oxygen vacancy defect sites. In contrast, for 1-PrOH the main reaction on the Zn polar surface appears to be oxidation, although in common with 2-PrOH, all three 1-PrOH decomposition reactions also appear to take place on the non-polar surface.

ZnO is normally regarded as a highly selective 2-PrOH dehydrogenation catalyst[104]. The present TPD results, however, demonstrate the dehydroxylated ZnO surface to behave primarily as a dehydration catalyst toward 2-PrOH. This is shown to be a direct consequence of the tendency of the Zn polar surface to strongly adsorb hydroxyl groups, so that under normal steady state reaction conditions (with temperatures less than approximately 700 K), the alcohol dehydration sites are effectively blocked. Under TPD experimental conditions, the

presence of adsorbed hydroxyls was shown to shift the overall reaction selectivity toward dehydrogenation as the dehydration sites, and to a lesser extent the oxidation sites, became poisoned by strongly adsorbed hydroxyl species. This result possibly explains the apparent selectivity toward dehydrogenation observed under steady-state alcohol decomposition conditions[106,107]. Under steady-state operating conditions, reaction of gas phase alcohol with the surface species could also occur, as proposed by Tamaru et al[106,107] and Parrott et al[102], and may be an additional factor increasing the dehydrogenation reaction activity. The apparent structural insensitivity for 2-PrOH decomposition on ZnO observed by Djega-Mariadassou et al[152], is likely to be a consequence of only the prism surfaces of ZnO appearing to be active in the decomposition due to the deactivation of the polar surfaces. In addition, the presence of surface impurities (described below) was also found to poison the dehydration and oxidation reactions, but to lead to increased dehydrogenation product yield.

(11.2) Chlorine and Water as Selective Site Probes for Reaction on Zinc Oxide

In this study water and chlorine were used as "selective poisons"[145] toward the alcohol decomposition. The results obtained have established an unambiguous equivalence between the α propene from 2-PrOH and α water surface sites, independent of the interpretation as to the location of these sites.

Treatment of the ZnO with chlorine was found to cause a selective poisoning of the polar surface sites and to reduce the availability of reactive oxygen on the non-polar surface. The cation sites on the non-polar surface appeared to be essentially unaffected. This led to

a selective suppression of the alcohol dehydration and oxidation decomposition reactions on the polar surfaces, and of the oxidation on the non-polar surface. On the non-polar surface the dehydration reaction was essentially unaffected, while dehydrogenation was significantly enhanced due to the effect of reactive surface oxygen removal, thereby suppressing the oxidation reaction channel and causing an enhancement in the dehydrogenation route.

The effect on the Zn polar surface is attributed to the poisoning of cation sites by chlorine which is known to strongly adsorb on this surface to result in charge stabilisation[143,144]. On the non-polar surface, the almost complete lack of carboxylate formation, particularly for 2-PrOH, shows the presence of chlorine only to affect the reactivity of surface anions and not to poison the cation sites. However, it is not clear from the results how this interaction takes place.

The use of water as a site probe also causes a suppression of reaction on the polar faces and to a lesser extent on the non-polar surfaces. In this respect it is equivalent to chlorine although the effects of adsorbed hydroxyls are not as site specific on the non-polar surface compared to chlorine. However, the use of water as a reaction site probe for ZnO has the advantage of being 'non-destructive' in that is easily desorbed from the catalyst surface to restore the original surface condition. Chlorine, however, cannot be removed in a similar manner.

(11.3) The Effect of Potassium Promotion on Alcohol Decomposition on Zinc Oxide

Potassium promotion of ZnO was found to cause a suppression of dehydration and an enhancement in the extent of dehydrogenation and reversible alcohol desorption. These findings are similar to earlier results reported by Deo et al[111,112] who, investigating sodium promotion of alumina toward 1-PrOH and 2-PrOH decomposition, observed a suppression in dehydration activity but an enhancement in dehydrogenation.

At low potassium loading the alkali promoter distribution is proposed to be weighted toward the polar surfaces. On the O polar surface, the presence of the alkali results in electrostatic stabilisation, while on the Zn polar surface strongly bound OK species poison hydroxyl adsorption and dehydration surface sites. At increased potassium loading, a significant fraction of the non-polar surface is also covered by either adsorbed K^+ ions or OK^- species. The main effect of the alkali on this surface is proposed to the effective removal of surface oxygen otherwise available for participation in the oxidation reaction, thereby causing a suppression in the formation of the surface carboxylate (as evidenced by the lack of CO_2 formed).

Apparent promotion effects were observed with an increase in alcohol dehydrogenation product yield and in the quantity of reversibly adsorbed alcohol. However, as previously described, the increase in dehydrogenation is related to the suppression of the oxidation reaction, rather than to be a result of an increase in surface coverage of the dehydrogenation product precursor.

In the Fisher-Tropsch synthesis, where potassium is used as a key catalyst promoter[20], a strengthening in the C-metal bond relative to

the C-O bond is observed for metal catalysts, and has been shown to result in increased CO desorption temperatures[20,21]. In the extreme, however, it can lead to complete dissociation of the C-O bond[20] resulting in a decrease in oxygenate formation in favour of hydrocarbon synthesis[22,23]. However, any electronic effects associated with the presence of adsorbed potassium on ZnO did not appear to be as significant as the selective site blocking effects. This is possibly a consequence of the relatively high potassium surface coverages used, combined with the inability for potassium to diffuse into the ZnO lattice[144]. This suggests that electronic effects may not be the major factor responsible for the promotion of higher alcohol synthesis by alkali metals.

(11.4) The Influence of Surface Impurities on the Catalytic Behaviour of Zinc Oxide

The results have highlighted the important influence that even small coverages of surface impurities, such as alkali metals or chlorine, can have on the reactive behaviour of ZnO. There was a surprising consistency in the way that both electronegative adsorbed species (Cl^-, OK^- and OH^-) and electropositive species (K^+ and Na^+) influenced the decomposition behaviour of the alcohols studied. This is proposed to be related to the manner in which these adsorbed species all behave primarily as selective surface site poisons, particularly on the polar ZnO surfaces.

This finding emphasises the need for careful control of impurity levels in such studies. The results of several published ZnO studies appear to be influenced by the presence of surface contaminants. In particular, it was shown that the ICI low surface area ZnO was

chlorine contaminated and that this has affected the results of previously published studies based on this catalyst[25,83,98,99,108,115].

The effect of the presence of surface contaminants also has important implications with respect to the study of catalytic processes with single crystal surfaces under high vacuum conditions. Kung et al[85,114] has noted the presence of small quantities of alkali contaminants to have no apparent effect on the temperature programmed desorption and decomposition behaviour of ZnO single crystals surfaces. This statement itself is an indication that the results of these workers are likely to have been influenced by surface contaminants since, on the basis of the present TPD results for potassium promotion, a coverage dependent effect should have been found. Further evidence for the TPD results of Kung et al showing the influence of these contaminants is that they can be interpreted on the basis of the results for potassium promoted ZnO from the present study. For example, the lack of CO_2 desorption observed from 2-PrOH decomposition, and the water desorption spectra from the Zn polar crystal surface, correlate well with the behaviour of potassium promoted, rather than unpromoted, ZnO. The results and conclusions of these workers should then be treated carefully and perhaps be reinterpreted on the basis that they are representative of alkali contaminated single crystal surfaces.

(11.5) The Relevance of the Results to the Higher Alcohol Synthesis

The results of this study have a number of implications that are relevant to the higher alcohol synthesis with respect to the site dependency of the reaction mechanism on ZnO, and to the promotion or

poisoning effects of potassium toward alcohol synthesis.

For both unpromoted and potassium promoted ZnO, the active surface for alcohol synthesis appears to be the non-polar surface , since for both forms of ZnO, the polar surfaces will be effectively deactivated under reaction conditions. On unpromoted ZnO this is due to strongly adsorbed hydroxyl species, and on promoted ZnO, to the presence of adsorbed K^+ and OK^- species.

The main effect of alkali promotion in propanol decomposition appears to be that of a selective site poison, rather than a reaction promoter. Although appearing at first sight to behave as a promoter toward the dehydrogenation reaction, the increased dehydrogenation product yield is related to a suppression of the oxidation reaction pathway, rather than due to any true enhancement in the coverage of any precursor surface intermediate. Although not verified experimentally, this suggests that the alkali may behave in a similar manner with respect to alcohol synthesis. In high alcohol synthesis from CO and hydrogen, a similar poisoning effect of alkali promotion has in fact been reported by Natta et al[12] as a reduction of overall catalyst activity, and more recently as a reduction in hydrocarbon formation[153].

This leads to an interpretation of the role of the alkali promoter as being one of a selective site poison that causes suppression of both hydrocarbon formation and any dehydration of oxygenate products to a greater extent than the reactions that form the oxygenate compounds. Similar conclusions have been reached by Chuang et al[22,23] in a study of the effect on alkali promotion on CO hydrogenation on a Rh/TiO_2 catalyst and by McClory et al[21] who have further suggested the electronic effect of alkali promotion with respect to CO hydrog-

enation is secondary to geometric site blocking effects.

Manazec[37] has proposed the difference between 1-PrOH and 2-PrOH alcohol yields in higher alcohol synthesis to be due to differences in stability of the linear, compared to branched, surface enol intermediates, that favour branched alcohol formation (see section 2.2.2). This cannot be correct since both Vedage et al[13] and Smith et al[14] have previously reported the addition of only 1-PrOH (and not 2-PrOH) to a syn-gas feed stream results in an increase in 1-methyl-propanol formation, in contradiction to Manazec's mechanism. The TPD results for 1-PrOH and 2-PrOH decomposition also show the 1-PrOH derived surface intermediates to have higher peak temperatures and therefore to be more stable than the corresponding 2-PrOH intermediates. If the enol is an intermediate in the formation of dehydrogenation and oxidation products (as proposed in the mechanism of chapter 7), then for the Manazec mechanism to be correct, 2-PrOH decomposition should favour the oxidation pathway while 1-PrOH will be selective toward dehydrogenation (since the 1-PrOH intermediate will be less stable so will desorb rather than react with surface oxygen). Experimentally the reverse of this was obtained, showing that although the enol may be an intermediate in the mechanism of higher alcohol synthesis, the relative stabilities of the branched versus linear enol structure appears not to the factor determining the high yield of branched alcohols as proposed by Manazec.

REFERENCES

(1) Hydrocarb Proc, 35, May 1986

(2) M.I. Greene, Chem Eng Prog, 46, Aug 1982

(3) J.L. Keller, Hydrocarb Proc, 127, May 1979

(4) E. Supp and D. Konigsbrugge, Oil Gas- Euro Magazine, 1/85, 31, 1985

(5) J.A. Weiszmann, J.H. D'Auria, F.G. McWilliams and F.M. Hibbs, Hydrocarb Proc, 41, June 1986

(6) J.F. Knifton, R.A. Grigsby and S. Herbstman, Hydrocarb Proc, 111, Jan 1984

(7) Hydrocarb Proc, 17, Aug 1986

(8) Ph. Courty, J.P. Arlie, A. Convers, P. Mikitenko and A. Sugier, Hydrocarb Proc, 105, Nov 1984

(9) R. Malpas, Hydrocarb Proc, 34-A, Aug 1985

(10) U.S. Patent 4 122 110, Oct 24, 1978

(11) J. Haggin, Chem Eng News, 29, Nov 12, 1984

(12) G. Natta, U. Colombo and I. Pasquon, "Catalysis", Reinhold, New York, 5, 131, 1957

(13) G.A. Vedage, P. Himelfarb, G.W. Simmons and K. Klier, Am Chem Soc, Div Pet Chem, Pre Symp, **28**, 1261, 1983

(14) K.J. Smith and R.B Anderson, Canad J Chem Eng, **61**, 40, 1983

(15) G.T. Morgan, D.V.N. Hardy and R.B. Procter, J Chem Soc (Lond), **41**, 1T, 1932

(16) P.K. Frolich and D.S. Cryder, Ind Eng Chem, **22**, 1051, 1930

(17) R.B. Anderson, J. Feldman and H.H. Storch, Ind Eng Chem, **44**, 2418, 1952

(18) K. Klier, Appl Surf Sci, **19**, 267, 1984

(19) W.-D. Mross, Catal Rev Sci Eng, **25**, 591, 1983

(20) M.E. Dry, "Catal Sci Tech", Springer-Verlag, Berlin, **1**, 159

(21) M.M. McClory and R.D. Gonzalez, J Catal, **89**, 392, 1984

(22) S.C. Chuang, J.G. Goodwin and I. Wender, J Catal, **92**, 416, 1985

(23) S.C. Chuang, J.G. Goodwin and I. Wender, J Catal, **95**, 435, 1985

(24) J.L. Falconer and J.A. Schwarz, Catal Rev Sci Eng, **25**, 141, 1983

(25) M. Bowker, H. Houghton, K.C. Waugh, J Chem Soc, Farad Trans I, **77**, 3023, 1981

(26) J.F. Edwards and G.L. Schrader, J Phys Chem, **89**, 782, 1985

(27) D.L. Roberts and G.L. Griffin, J Catal, **101**, 201, 1986

(28) H.H. Kung, Catal Rev Sci Eng, **22**, 235, 1980

(29) G.A. Vedage, R. Pitchai, R.G. Herman and K. Klier, Proc 8th Int Cong Catal (Berlin), **2**, 47, 1984

(30) G. Natta, "Catalysis", Reinhold, New York, **3**, 349, 1955

(31) F. Fischer, Ind Eng Chem, **17**, 574, 1925

(32) P.K. Frolich and W.K. Lewis, Ind Eng Chem, **20**, 354, 1928

(33) R. Taylor, J Chem Soc (Lond), 1429, 1934

(34) G.D. Graves, Ind Eng Chem, **23**, 1381, 1931

(35) M. Di Conca, A. Riva, F. Trifiro, A. Vaccari, G. Del Piero, V. Fattore and F. Pincolini, Proc 8th Int Cong Catal, Berlin, **II**, 173, 1984

(36) K.J. Smith and R.B. Anderson, J Catal, **85**, 428, 1984

(37) T.J. Manazec, J Catal, **98**, 115, 1986

(38) C.S. John, in "Catalysis", **3**, Chem Soc, London, 169, 1980

(39) R.R. Gay, M.H. Nodine, V.E. Heinrich, H.J. Zeiger and E.I. Solomon, J Am Chem Soc, **102**, 6752, 1980

(40) A.L. Dent and R.J. Kokes, J Phys Chem, **73**, 3772, 1969; ibid, **73**, 3781, 1969

(41) G.L. Griffin and J.T. Yates, J Chem Phys, **77**, 3744, 1982; ibid, **77**, 3751, 1982

(42) R. Nosker, P. Mark and J.D. Levine, Surf Sci, **74**, 682, 1978

(43) K. Atherton, G. Newbold and J.A. Hockey, Disc Farad Soc, **52**, 33, 1971

(44) T. Morimoto and M. Nagao, J Phys Chem, **78**, 1116, 1974

(45) A.R. Lubinsky, C.B. Duke, S.C. Chang, B.W. Lee and P. Mark, J Vac Sci Tech, **13**(1), 189, 1976

(46) F. Bocuzzi, E. Garrone, A. Zecchina, A. Bossi and M. Camia, J Catal, **51**, 150, 1978; ibid, **50**, 160, 1978

(47) W. Gopel and U. Lampe, Phys Rev B, **22**, 6447, 1980

(48) P. Esser, R. Feierabend and W. Gopel, Ber Bunsenges Phys Chem, **85**, 447, 1981

(49) W.H. Cheng and H.H. Kung, Surf Sci, **102**, L21, 1981

(50) W.H. Cheng and H.H. Kung, Surf Sci, **122**, 21, 1982

(51) M. Henzler, Appl Phys, **9**, 11, 1976

(52) J. Saussey, J.-C. Lavalley and C. Bovet, J Chem Soc, Farad Trans I, **78**, 1457, 1982

(53) W. Gopel, Surf Sci, **62**, 165, 1977

(54) W. Gopel, J Vac Sci Tech, **15**, 1298, 1978

(55) G.L. Griffin and J.T. Yates, J Catal, **73**, 396, 1982

(56) R.J. Kokes, A.L. Dent, C.C. Chang and L.T. Dixon, J Am Chem Soc, **94**, 4429, 1972

(57) B. Fubini, G. Giamello, G. Della Gatta and G. Venturello, J Chem Soc, Farad Trans I, **78**, 153, 1982

(58) S. Naito, H. Shimizu, E. Hagiwara, T. Onishi and K Tamaru, J Chem Soc, Farad Trans I, **67**, 1519, 1970

(59) A. Baranski and R.J. Cvetanovic, J Phys Chem, **5**, 208, 1971

(60) A. Baranski and J. Gatuska, J Catal, **44**, 259, 1976

(61) C.C. Chang, L.T. Dixon and R.J. Kokes, J Phys Chem, **77**, 2634, 1973

(62) A.L. Dent, Acc Chem Res, **6**, 226, 1973

(63) Y. Kubokawa, Bull Chem Soc Jpn, **33**, 743, 1960

(64) G. Ghiotti, F. Boccuzzi and R. Scala, J Catal, **92**, 79, 1985

(65) J.H. Taylor and C.H. Amberg, Can J Chem, **39**, 535, 1961

(66) Y. Kubokawa and O. Toyama, Bull Chem Soc Jpn, **35**, 1407, 1962

(67) Y. Kubokawa, Bull Chem Soc Jpn, **33**, 555, 1960

(68) C.H. Amberg and D.A. Seanor, Proc 3rd Int Cong Catal, Amsterdam, 450, 1964

(69) W. Hotan, W. Gopel and R. Haul, Surf Sci, **83**, 162, 1979

(70) P.M.G. Hart and F. Sebba, J Chem Soc, Farad Trans I, **56**, 551, 1960

(71) G. Carnisio, F. Garbassi, G. Petrini and G. Parravano, J Catal, **54**, 66, 1978

(72) J.-C. Lavalley, J. Saussey and T. Rais, in Symp Catal React One C Molecs, Bruges, 1982

(73) V.E. Henrich, Prog Surf Sci, **9**, 143, 1978

(74) M.R. McClellan, M. Trenary, N.D. Shinn, M.J. Sayers, K.L. D'Amico, E.I. Solomon and F.R. McFeely, J Chem Phys, **74**, 4726, 1981

(75) M.J. Sayers, M.R. McClellan, R.R. Gay, E.I. Solomon and F.R. McFeely, Chem Phys Lett, **75**, 575, 1980

(76) Matshushita and Nakata, J Chem Phys, **36**, 665, 1962

(77) R.J. Kokes and R. Glemza, J Phys Chem, **69**, 17, 1965

(78) P. Amigues and S.J. Teichner, Disc Farad Soc, **52**, 33, 1971

(79) T. Morimoto and K. Morishige, Bull Chem Soc Jpn, **47**, 92, 1974

(80) T. Morimoto and K. Morishige, J Phys Chem, **79**, 1573, 1975

(81) W. Gopel, R.S. Bauer and G. Hansson, Surf Sci, **99**, 138, 1980

(82) F. Runge and W. Gopel, Z Physik Chemie N.F., **123**, 173, 1980

(83) M. Bowker, H. Houghton, K.C. Waugh, T. Giddings and M. Green, J Catal, **84**, 252, 1983

(84) W.H. Cheng, S. Akhter and H.H. Kung, J Catal, **82**, 341, 1983

(85) S. Akhter, W.H. Cheng, K. Lui and H.H. Kung, J Catal, **85**, 437, 1984

(86) A.A. Tsyganenko and V.N. Filimonov, J Molec Struct, **19**, 579,1973

(87) T. Morimoto, M. Nagao and F. Tokuda, Bull Chem Soc Jpn, **41**, 1533, 1968

(88) M. Nagao and K. Morishige, Bull Chem Soc Jpn, **47**, 2107, 1974

(89) H.S. Taylor and D.V. Sickman, J Am Chem Soc, **54**, 602, 1932

(90) E. Giamello and B. Fubini, J Chem Soc, Farad Trans I, **79**, 1995, 1983

(91) K. Morishige, S. Kittaka and T. Moriyasu, J Chem Soc, Farad Trans I, **76**, 738, 1980

(92) A. Ueno, T. Onishi and K. Tamaru, J Chem Soc, Farad Trans I, **67**, 3585, 1971

(93) D.L. Roberts and G.L. Griffin, J Catal, **95**, 617, 1985

(94) K.M. Tarawah and R.S. Hansen, J Catal, **87**, 305, 1984

(95) L. Chan and G.L. Griffin, Surf Sci, **155**, 400, 1985

(96) S. Tsuchiya and T. Shiba, J Catal, **6**, 270, 1969

(97) W. Mokwa, D. Kohl and G. Heiland, Surf Sci, **117**, 659, 1982

(98) M. Bowker, H. Houghton and K.C. Waugh, J Catal, **79**, 431, 1983

(99) M. Bowker, H. Houghton and K.C. Waugh, J Chem Soc, Farad Trans I, **78**, 2573, 1982

(100) R.O. Kagel and R.G. Greenler, J Chem Phys, **49**, 1638, 1968

(101) N. Takezawa, C. Hanamaki and H. Kobayashi, J Catal, **38**, 101, 1975

(102) S.L. Parrott, J.W. Rogers and J.M. White, Appl Surf Sci, **1**, 443, 1978

(103) R.O. Kagel, J Phys Chem, **71**, 844, 1967

(104) O.V. Krylov, "Catalysis By Nonmetals", 116, Academic Press, London, 1970

(105) D.J. Wheeler, P.W. Darby and C. Kemball, J Chem Soc, **60**, 332, 1960

(106) O. Koga, T. Onishi and K. Tamaru, J Chem Soc, Farad Trans I, **76**, 19, 1980

(107) E. Akiba, M. Soma, T. Onishi and K. Tamaru, Zeit fur Physik Chemie N.F., **119**, 103, 1980

(108) M. Bowker, R.W. Petts and K.C. Waugh, J Catal, **99**, 53, 1986

(109) H. Miyata, K. Hata, T. Nakajima and Y. Kubokawa, Bull Chem Soc Jpn, **53**, 2401, 1980

(110) H. Miyata, M. Wakamiya and Y. Kubokawa, J Catal, **34**, 117, 1974

(111) A.V. Deo and I.G. Dalla Lana, J Phys Chem, **75**, 716, 1969

(112) A.V. Deo, T.T. Chuang and I.G. Dalla Lana, J Phys Chem, **73**, 234, 1971

(113) M.I. Zaki and N. Sheppard, J Catal, **80**, 114, 1983

(114) K. Lui, S. Ahkter and H.H. Kung, ACS Symp Ser, **279** (Solid State Chem Catal), 205, 1985

(115) M. Bowker, R.W. Petts and K.C. Waugh, J Chem Soc, Farad Trans I, **81**, 3073, 1985

(116) K. Nagai, K. Tanaka and K. Miyahara, Bull Chem Soc Jpn, **47**, 2847, 1974

(117) R.J. Kokes and A.L. Dent, Adv Catal, **22**, 1, 1972

(118) A.A. Davydov, A.A. Yefremov, V.G. Mikhalchenko and V.D. Sokolovskii, J Catal, **58**, 1, 1979

(119) T. Nakajima, H. Miyata and Y. Kubokawa, J Chem Soc, Farad Trans I, **81**, 2409, 1985

(120) R.J. Cvetanovic and Y. Amenomiya, Adv Catal, **17**, 103, 1967

(121) R.J. Cvetanovic and Y. Amenomiya, Catal Rev, **6**, 21, 1972

(122) R.J. Gorte, J Catal, **75**, 164, 1982

(123) R.A. Demmin and R.J. Gorte, J Catal, **90**, 32, 1984

(124) P.I. Lee and J.A. Schwarz, J Catal, **73**, 272, 1982

(125) J.S. Rieck and A.T. Bell, J Catal, **85**, 143, 1984

(126) D.M. Jones and G.L. Griffin, **80**, 40, 1983

(127) R.K. Herz, J.B. Keila and S.P. Marin, J Catal **73**, 66, 1982

(128) P.I. Lee, J.A. Schwarz and J.C. Heydweiller, Chem Eng Sci, **40**, 509, 1985

(129) P.A. Redhead, Vacuum, **12**, 203, 1962

(130) A. Brenner and D.A. Hucul, J Catal, **56**, 134, 1979

(131) A. Savitsky and M.J.E. Golay, Anal Chem, **36**, 1627, 1964

(132) C.G. Enke and T.A. Nieman, Anal Chem, **48**, 705A, 1976

(133) H.H. Madden, Anal Chem, **50**, 1383, 1978

(134) R.H. Perry and C.H. Chilton (ed), Chemical Engineers Handbook, 5th Edn, McGraw Hill, Tokyo, 2-8, 1973

(135) M. Bowker, J.N.K. Hyland, H.D. Vandervell and K.C. Waugh, Proc 8th Int Cong Catal, Berlin, **II**, 35, 1984

(136) K.C. Waugh, M. Bowker, R.W. Petts, H.D. Vandervell and P.J.R. O'Malley, Appl Catal, **25**, 121, 1986

(137) F.M. Nelsen and F.T. Eggertsen, Anal Chem, **30**, 1387, 1958

(138) S.J. Gregg and K.S.W. Sing, in "Adsorption, Surface Area and Porosity", Academic Press, London, 44, 1967

(139) V.I. Marshneva and A.A. Davydov, Kin Catal, **21**, 521, 1980

(140) D.G. Rethwisch and J.A. Dumesic, Langmuir, **2**, 73, 1986

(141) S. Akhter, K. Lui and H.H. Kung, J Phys Chem, **89**, 1958, 1985

(142) G. Zwicker and K. Jacobi, Surf Sci, **131**, 179, 1983

(143) B.J. Hopkins, R. Leysen and P.A. Taylor, Surf Sci, **48**, 486, 1975

(144) P.A. Taylor and B.J. Hopkins, J Physics C, **11**, L643, 1978

(145) H. Knozinger, Adv Catal, **25**, 184, 1976

(146) Noller and Ritter, J Chem Soc, Farad Trans I, **80**, 275, 1980

(147) H. Miyata, K. Hata and Y. Kubokawa, J Catal, **49**, 8, 1977

(148) B.W. Krupay and Y. Amenomiya, J Catal, **67**, 362, 1981

(149) W.H. Stork and G.T. Pott, J Phys Chem, **78**, 2496, 1978

(150) R. Sinha, C. Chiranjivi and R.J. Rao, Ind J Tech, **18**, 47, 1980

(151) B. Viswanathan, M.V.C. Sastri and V. Srinivason, Z Phys Chemie, **79**, 216, 1972

(152) G. Djega-Mariadassou and L. Davignon, J Chem Soc, Farad Trans I, **78**, 2447, 1982

(153) A. Riva, F. Trifiro and A. Vaccari, Royal Soc Chem Farad Div Autumn Meeting, Sept 1986, J Chem Soc, Farad Trans I, in press

(154) G. Connell and J.A. Dumesic, J Catal, **92**, 17, 1985

(155) J.G. Van Ommen, W.J. Bolink, J. Prasad and P. Mars, J Catal, **38**, 120, 1975

APPENDICES

Appendix 1: Determination of the Mass Spectrometer Cracking Patterns

The mass spectrometer cracking patterns for CO_2 and the C_3 hydrocarbon and oxygenate compounds were determined by passing a steady stream of helium carrier gas, containing the appropriate compound, through the empty reactor system and monitoring a range of different mass ion signals on the mass spectrometer. The cracking fractions were expressed relative to the largest mass signal for each compound. Table A.1 details the cracking patterns determined for the compounds investigated in this study. In addition, the temperature stabilities of the patterns were checked by linearly ramping the reactor temperature until thermal cracking products (hydrogen and methane) were detected. Table A.2 gives the maximum temperatures found before detection of thermal cracking.

Table A.1: Mass spectrometer cracking patterns.

compound	mass number (amu)	relative ion signal (Amp)
CO_2	44	1000
	28	274
	16	199
2-propanol	45	1000
	43	997
	15	581
	39	287
	41	290
	42	230
	31	147
	2	154

Table A.1 continued..

1-propanol	31	1000
	29	343
	27	272
	28	242
	42	83
	39	70
	2	75
	43	60
acetone	43	1000
	15	518
	58	159
	42	89
	27	82
	39	60
	29	60
	2	59
propene	41	1000
	39	790
	42	637
	27	468
	40	266
	38	180
	37	119
	2	27

Table A.2: Maximum reactor operating temperatures before the onset of detectable thermal cracking in the mass spectrometer cracking pattern.

compound	maximum temperature (K)
1-propanol	593
2-propanol	553
acetone	>800
propene	>800

Appendix 2: Surface Area Calculation Method

Catalyst surface areas were determined by measurement of the physisorption of nitrogen from a 9.74% N_2/He flow at liquid nitrogen temperature and calculated according to the BET equation. The necessary cooling of the catalyst sample was accomplished by replacing the reactor tube with a 6mm OD glass U-tube that could be positioned into a flask of liquid nitrogen.

The BET equation relates the total volume of gas adsorbed onto a surface to the volume adsorbed as a monolayer, according to the following equation[138]:

$$v = \frac{v_m c P}{(P_o-P)[1+(c-1)P/P_o]} \qquad [1]$$

where P= adsorbate pressure

P_o= vapour pressure at the adsorption temperature

v= volume of gas adsorbed

v_m= monolayer volume of adsorbed gas

c= constant characteristic of the gas-solid interaction.

Substituting x, for the adsorbate partial pressure (P/P_o) and rewriting equation [1] gives:

$$\frac{x}{(1-x)v} = \frac{1}{c\, v_m} + \frac{(c-1)x}{c\, v_m} \qquad [2]$$

This equation is valid for x in the range 0.05-0.35[138]. The characteristic BET plot of $x/(1-x)v$ against x is linear of slope= $(c-1)/cv_m$ and intercept= $1/(cv_m)$. Nitrogen typically has a high c value so that for $(c-1)/c \simeq 1$ and $1/(c\, v_m) \simeq 0$. Therfore for high C the BET plot passes through the origin and has slope $1/v_m$. Only one experimental point is then required for determination of the monolayer volume

according to:

$$v_m = v\ (1-x) \qquad [3]$$

A more accurate modification of this single point method uses a correction factor that 'converts' the single point v_m to a true BET v_m:

$$v_m = v\ (1-x)\ [1 + (1-x)/cx] \qquad [4]$$

The specific surface area is calculated from the monolayer volume expressed as the number of molecules adsorbed and using a molecular cross sectional area for N_2 of 16.2 $Å^2$.

A complete adsorption isotherm was measured for the ICI high surface area ZnO catalyst so that the characteristic constant c could be determined. The characteristic BET plot for this catalyst is given in figure A.1. From the plot a value for c was determined to be 125± 60. Although this result was rather imprecise, substitution of the extreme values into the [1 + (1-x)/cx] correction factor gave results of 1.05 and 1.14 respectively. Accordingly a value of 1.1 was used in surface area calculations by equation [4].

Appendix 4: Method for Mass Spectrometer Data Deconvolution

Because of common mass fragments in the desorption product mass spectrometer cracking patterns, it was necessary to account for any overlap contributions in the desorption peaks before analyses of the results in terms of coverages and peak temperatures could be made. This was carried out by correcting the experimental peak data by subtraction of the contribution from any other desorption products with common cracking patterns, scaled according to the cracking patterns given in Appendix 1. For example, the mass 43 acetone

desorption peak was corrected for the contribution from 2-propanol desorption by subtraction of the appropriately scaled 2-propanol mass 45 signal (factor= 99.7) from the acetone data. Computer software was written to accomplish this and the corrected desorption results stored with the original experimental results as binary data in the unused kathrometer data channel space. In this manner the original raw experimental data was always retained rather than being replaced by the deconvoluted data. All data from the alcohol and acetone desorption experiments was treated in this manner.

Appendix 4: XPS Measurements

XPS measurements were conducted on samples of fresh and pretreated potassium promoted ZnO and on the ICI low surface area ZnO in order to provide information on the nature of the potassium distribution and identify any possible surface contaminants.

For the potassium promoted ZnO the K to Zn XPS peak area ratios determined by XPS are plotted in figure A.2. The linear relationship shown for the fresh catalyst samples indicates a reasonably even distribution of undecomposed K_2CO_3 over the catalyst surface or an invariant K_2CO_3 crystallite size. The thermal pretreatment is seen to result in an increase in the K to Zn ratio showing that significant changes in the alkali distribution occurred during carbonate surface decomposition. The increase in the K to Zn ratio indicates a breakdown in the carbonate crystallites, and that the distribution of potassium became more even in the catalyst. Surface diffusion of a potassium promoter has been previously observed during the activation of an ammonia synthesis catalyst[154] so it appeared likely that similar diffusional effects may have been also responsible for the

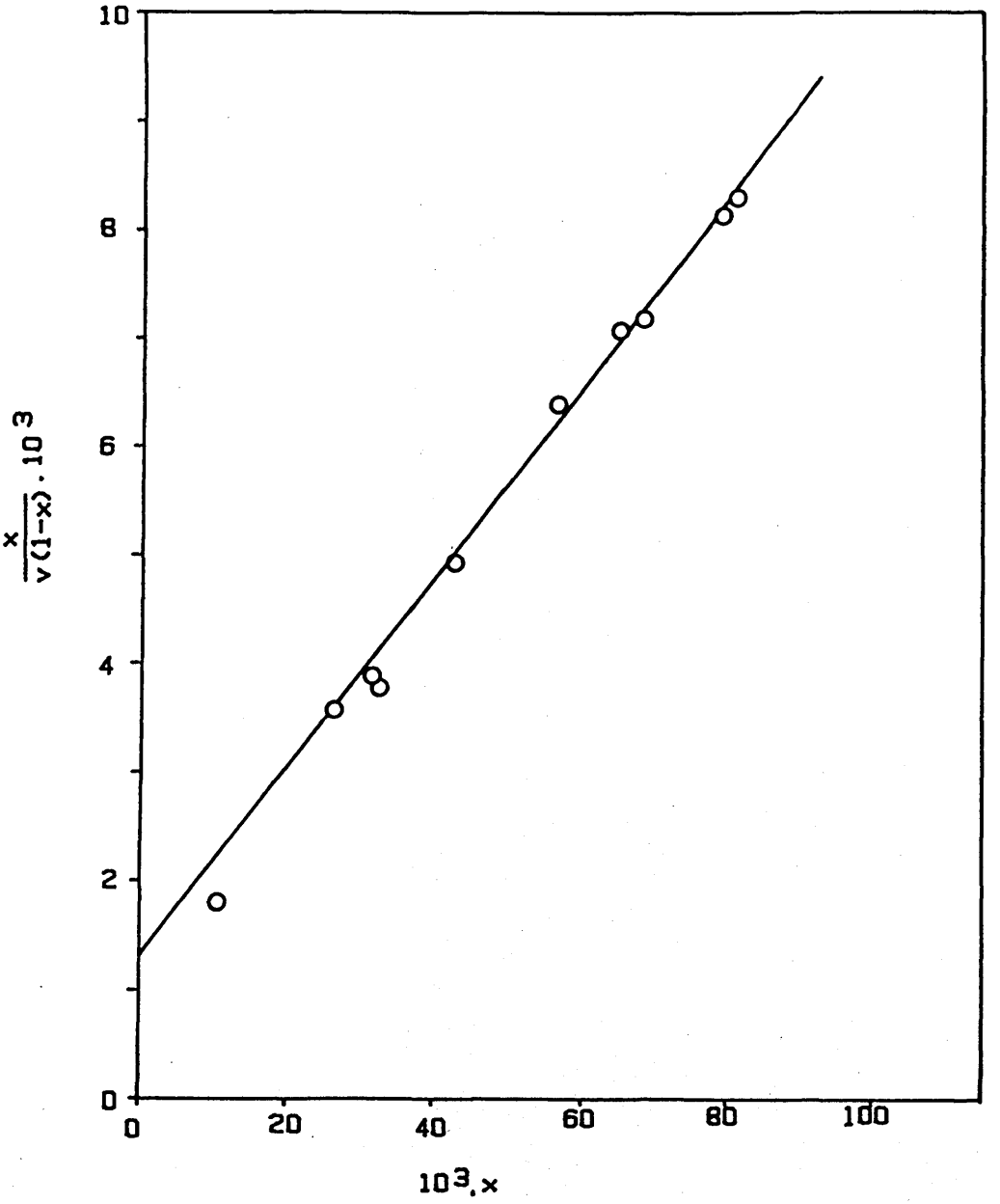

Figure A.1: Characteristic BET plot for ICI high surface area ZnO. x= nitrogen partial pressure; v= volume of nitrogen adsorbed (ml)

observed alkali distribution changes during pretreatment of promoted ZnO. Single crystal studies have shown that potassium ions are more strongly held on the polar surfaces of ZnO than the non-polar[143]. In particular the ions are very strongly bound to the O polar surface where impurity stabilisation effects lead to a one third monolayer coverage as required for charge stabilisation[144]. This suggests that the alkali surface redistribution observed during catalyst pretreatment would lead to a potassium distribution weighted toward the polar surfaces, particularly for the lower alkali loadings. The results of chapters 6 and 9 present results that are consistent with this assumption. Furthermore, potassium ions would not be expected to diffuse into the lattice because of their large effective ionic radius compared to Zn^{2+}[143]. This is also supported by the XPS results.

The form of the adsorbed potassium was not specifically investigated. The presence of traces of water in the carrier gas, although in very low concentration, make it unlikely that the potassium would be present as K_2O since, at water concentrations greater than 10^{-2}ppm, K_2O reacts to form KOH[155].

XPS scanning further revealed a high level of chlorine to be present on ICI low surface area ZnO compared to the AnalaR grade ZnO. Figures A.3 and A.4 give the XPS data for each of the catalysts. From the relative Zn to Cl peak intensities the coverage of chlorine on the surface of ICI low surface was estimated to be approximately 30% of a monolayer (assuming all the Cl^- is at the surface). A trace of chlorine also appears to be present on the surface of AnalaR grade ZnO, but represents only a fraction (approximately 0.1) of the coverage associated with the ICI low surface area ZnO. No other significant surface contaminants were revealed by further scanning.

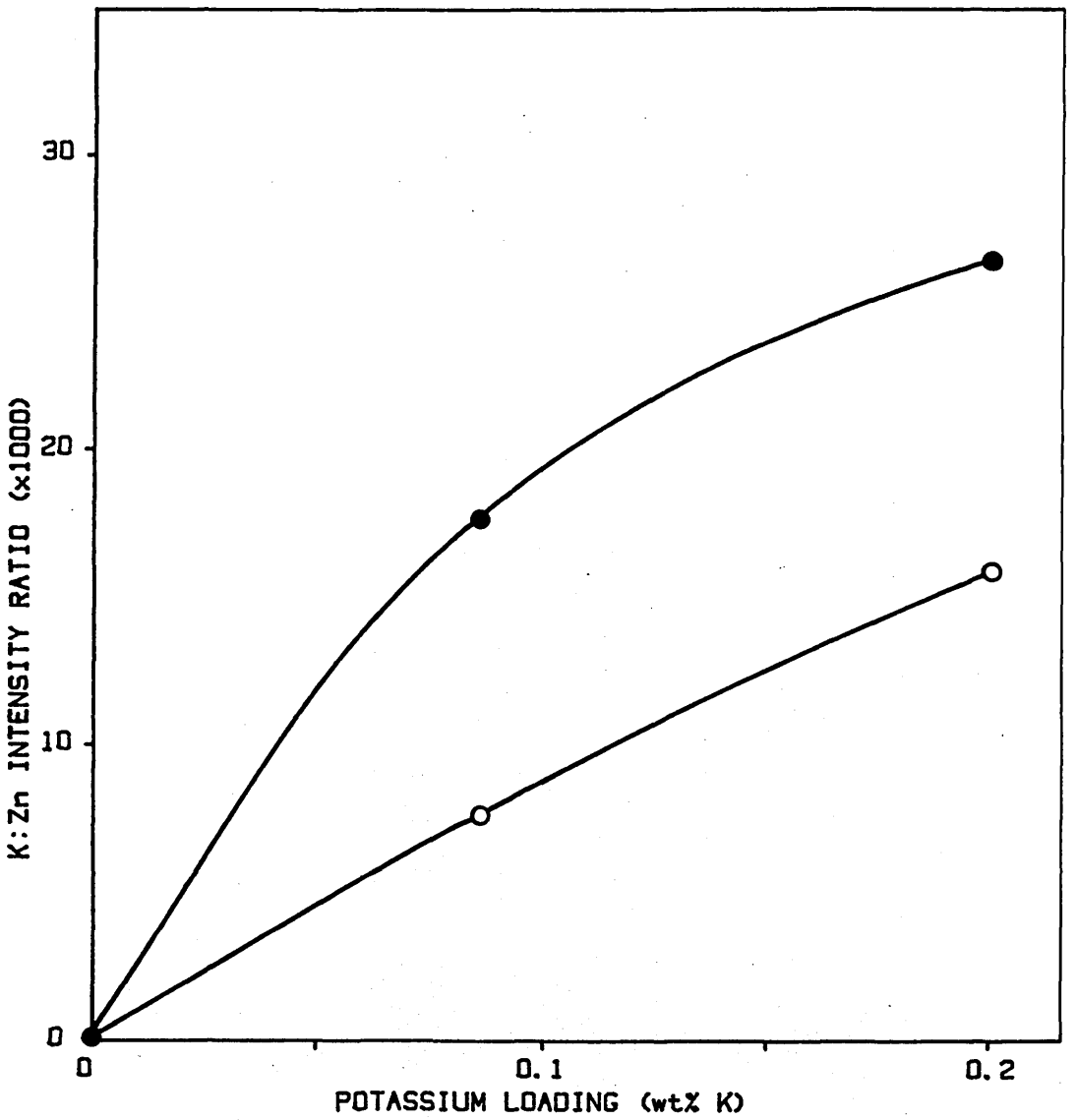

Figure A.2: Plot of the potassium $2p_{3/2}$ to zinc $2p_{3/2}$ XPS intensity ratio as a function of potassium loading for fresh and pretreated unpromoted and promoted zinc oxide. ○=fresh; ●=pretreated

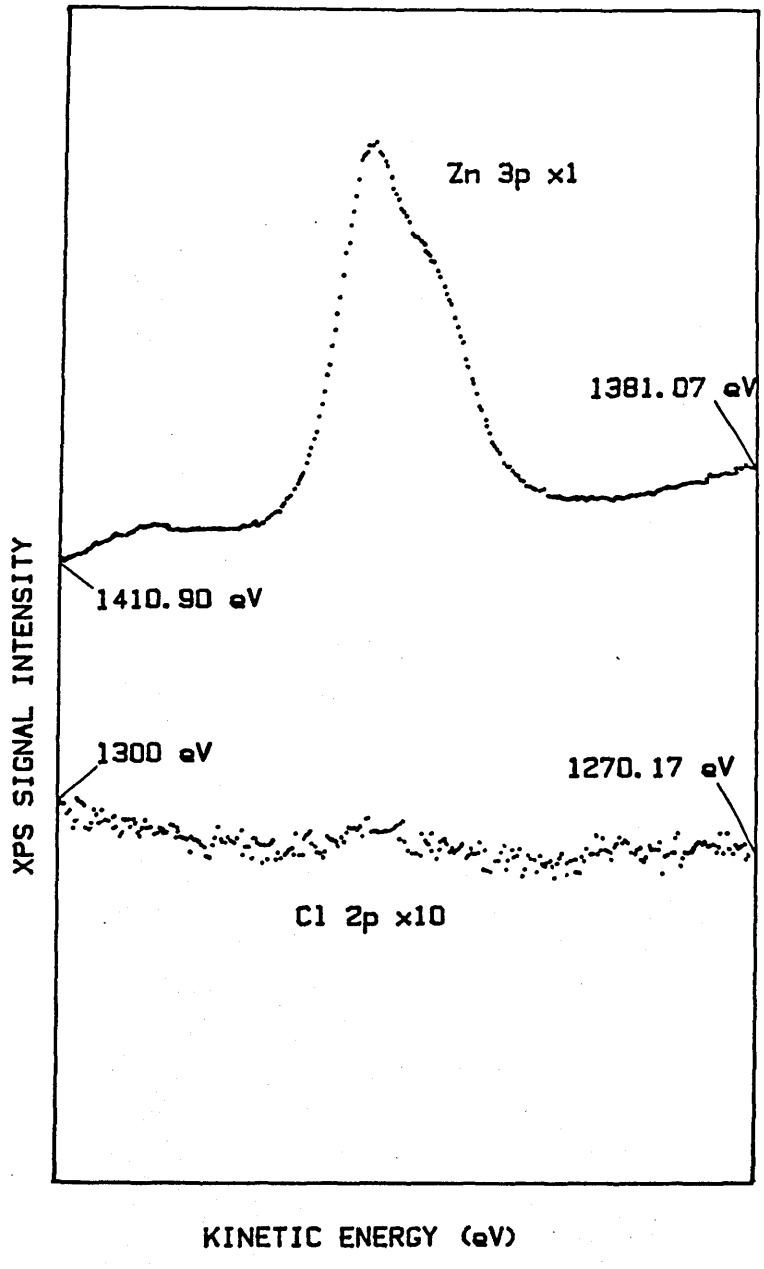

Figure A.3: Zn 3p and Cl 2p XPS peaks from AnalaR grade zinc oxide.

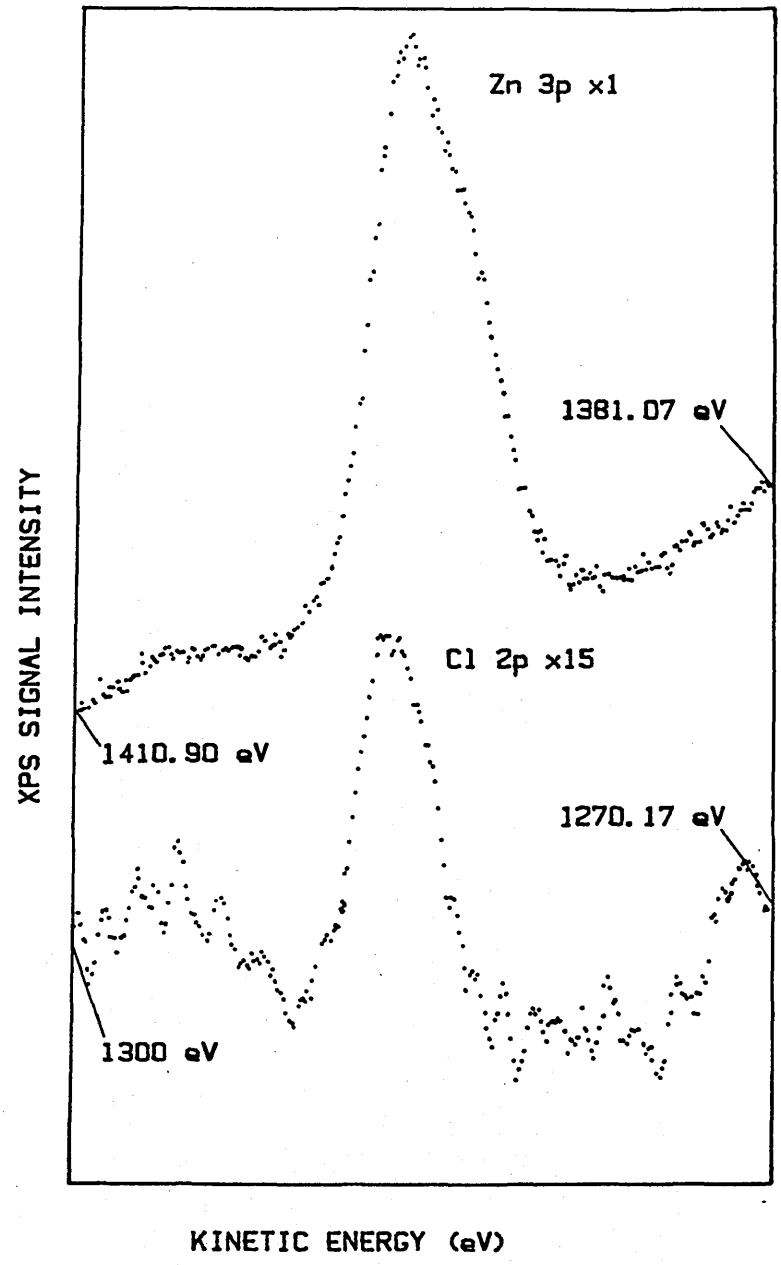

Figure A.4: Zn 3p and Cl 2p XPS peaks from ICI low surface area zinc oxide.